ANALYSIS OF POST-TRANSLATIONAL MODIFICATIONS IN THE REGULATION OF CELL SIGNALING AND BEHAVIOR

A Dissertation
Presented to
The Academic Faculty
By

Shilpa Choudhury

In Partial Fulfillment
Of the Requirements for the Degree
Doctor of Philosophy in Biological Sciences

Georgia Institute of Technology

August, 2018

ANALYSIS OF POST-TRANSLATIONAL MODIFICATIONS IN THE REGULATION OF CELL SIGNALING AND BEHAVIOR

Approved by

Dr. Matthew P. Torres, Advisor
School of Biological Sciences
Georgia Institute of Technology

Dr. Brian Hammer
School of Biological Sciences
Georgia Institute of Technology

Dr. Yury Chernoff
School of Biological Sciences
Georgia Institute of Technology

Dr. Amit Reddi
School of Chemistry and Biochemistry
Georgia Institute of Technology

Dr. John Hepler
Department of Pharmacology
Emory University

Date Approved: 24 July 2018

PREFACE

The central dogma of molecular biology, which states that “DNA makes RNA and RNA makes protein” offers a framework for understanding the sequential transfer for genetic information within a biological system that begets cellular and organismal phenotype. Under this premise, the genome of a cell provides the basic blueprint for the synthesis of proteins needed for cell survival. Although the basic principle of the central dogma has remained unchanged during the past five decades, the complexity has profoundly increased. Indeed, the completion of genome sequencing of several organisms, including human, revealed that the relationship between genes and proteins is far from simple. For example, the human proteome, or collection of all expressed proteins in an organism, is estimated to be nearly five times larger than the number of genes in the human genome. This unexpected gap between genome and proteome size has led to a fundamental question: how can such a small number of genes be sufficient to support the observed cellular and organismal phenotypic complexity?

In general, the wide gap between genome, proteome, and phenotypic complexity can be explained by processes occurring during two distinct phases of information transfer: First, through the transcription and processing of messenger RNA (mRNA) from DNA; and second, through the post-translational modification of protein. Indeed, DNA transcription and RNA processing are well known points of control, through epigenetic DNA and histone modification-based regulation and through mRNA editing and RNA splicing. Likewise, proteins translated from mRNA can undergo significant diversification through the introduction of post-translational modifications (PTMs), which are chemical or proteinaceous modifications to the native structure of an expressed protein. Indeed, the diversity of PTM types and the amino acids on which they can be found provides an

exponentially expansive landscape of possible *proteoforms*, each of which may exhibit a distinctive structural and functional behavior.

An important distinction between both transcriptional and post-translational points of control is in the rate at which they occur, which defines the rate at which they can influence cellular phenotype. Introducing variation through transcription and RNA processing occurs slowly, whereas the formation of unique proteoforms through PTM occurs very rapidly. Moreover, most PTMs are also reversible and can therefore function as a highly versatile switch to dynamically control protein structure, localization and/or function. Furthermore, globally, concurrent PTM of several proteins can also conditionally re-wire cellular networks so as to shape the behavioral and phenotypic traits of an organism. Thus, PTMs represent a form of proteomic control that is fast, dynamic, and highly versatile, and hence, they are often found to regulate many different biological processes including cell signaling pathways, cell adhesion and migration, cellular proliferation and differentiation, and many more.

Currently, more than 200 types of discrete enzymatically-catalyzed PTMs are known that range from covalent addition/removal of chemical entities (such as phosphate-, acetyl-, alkyl-, glycosyl- groups) to a side chain residue in a protein to covalent cleavage of peptide backbones in proteins. Nearly all proteins are modified by either one or multiple types of PTMs, and/or are multiply modified by the same kind of modification. Indeed, technological advances in high-throughput mass spectrometry (MS) have fostered an exponential increase in the rate and precision at which PTMs are discovered, far beyond what could be possible through classical biochemical/biophysical methods. However, due to the much slower rate at which PTMs can be studied for functionality, this exponential increase has led to a major knowledge gap between the existence of a PTM and whether it is biologically important. Therefore, developing tools that prioritize functional relevance of PTMs, is a fundamental challenge of our time.

In an attempt to address the bottleneck between PTM knowledge and PTM function, the Torres lab has developed a computational method - Systematic Analysis of PTM Hotsposts (SAPH-ire) – a quantitative PTM ranking method that enables functional prioritization of PTMs based on a variety of protein features. This model for function potential prediction provides a useful guide for empirical functional studies of PTMs. The net effect of these computational advances and the increasing availability of high throughput MS-derived PTM data represents a key breakthrough for rapid acceleration of the pace of biological research.

My overriding goal in this thesis is to understand PTM-mediated regulation of two diverse, yet extremely important physiological processes - G-protein signaling (primary doctoral project) and extracellular matrix mediated cell adhesion and migration (collaborative project with Dr. Barker). The first part of this thesis will discuss canonical G-protein signaling, for which I have discovered novel regulatory properties of phosphorylation sites in the N-terminal tails of G protein gamma subunits that were initiated through SAPH-ire predictions. This part of the thesis is accentuated by highly mechanistic molecular genetics studies that build on pre-existing models of a canonical G protein signaling pathway. The second part of this thesis will discuss how I have employed MS-based characterization of citrullination, a rare and understudied extracellular PTM that is known to disrupt cell adhesion and migration signaling in humans. My hope is that the discoveries made in this thesis will not only further our understanding of PTM-based regulatory mechanisms that exist in G-protein signaling but will also open avenues for future studies in the field of extracellular matrix biology.

ACKNOWLEDGEMENTS

I would like to express my heartful gratitude to my advisor Dr. Matthew Torres for his guidance and support throughout my graduate career. I joined his lab in 2013 as a naïve and dormant scientist and have grown immensely ever since due to his kind (at times strict) nurturing. I have great respect for his philosophy of science and have found inspiration from his vision time and again. He has and will continue to have a positive influence on my research career.

I would also like to thank my thesis committee members, Dr. Brian Hammer, Dr. Amit Reddi, Dr. Yury Chernoff and Dr. John Hepler. Their feedback, guidance and support has shaped not only my thesis work but my development as a researcher.

My time in graduate school introduced me to some of the finest people. I am thankful to all the current and alumni members of the lab- Zahra, Kuntal, Hyojung, Nolan, Jiani, Alex, Maneesha, Ramya, Rushika, Niveda, Henry, AK, and Parastoo- who have been like a family and made working in lab enjoyable. I would cherish the bond I made with my colleague and friend, Zahra, who is an excellent scientist in-making. I would also like to thank Kuntal, Maneesha, and AK for recreating family environment away from home, especially during festive seasons. I am thankful to my mentees- Matt Tillman, AK, and Parastoo who have helped me at various stages of research work. Special thanks to the bioinformatics group who have been instrumental in the development of SAPH-ire, that laid the foundation of my work. I will miss the endless conversations about science and food I had with these people.

I would like to thank my friends, specially Sai, my sister Shivangi, and my extended family in India for their love and encouragement. I am most grateful to my parents who have supported all my decisions and always shown faith in me. Lastly, I am thankful to my

husband, Shekhar, for his love and patience, and for living the “PhD student life” with me. I am grateful to have him as a life part.

TABLE OF CONTENTS

TABLE OF CONTENTS CONTINUED

TABLE OF CONTENTS CONTINUED

TABLE OF CONTENTS CONTINUED

LIST OF TABLES

LIST OF FIGURES

LIST OF FIGURES CONTINUED

LIST OF SYMBOLS AND ABBREVIATIONS

PTMs	Post Translational Modifications
MS	Mass Spectrometry
GPCRs	G Protein Coupled Receptors
$G\alpha$	G protein alpha subunit
$G\beta\gamma$	G protein beta gamma dimer protein
$G\gamma$	G gamma subunit
$G\gamma$-Nt	N-terminus tail of G gamma subunit
Ste18-Nt	N-terminus tail of G gamma subunit in yeast, Ste18
MAPK	Mitogen Activated Protein Kinase
$Ste5^{FBD}$	Fus3-Binding Domain on the scaffold protein, Ste5
$Ste5^{ND}$	Fus3-Non-Docking mutant of Ste5
CDK	Cyclin Dependent Kinase
Cln	Cyclin
PAD	Peptidyl Arginine Deiminase
Fn	Fibronectin
ECM	Extra-Cellular Matrix
RA	Rheumatoid Arthritis

SUMMARY

Heterotrimeric G proteins, composed of Gα, Gβ, and Gγ subunits, are essential for converting extracellular chemical stimuli into appropriate intracellular responses. The principal mechanism of G protein signal transduction is highly conserved throughout eukaryotes, including yeast. Binding of extracellular signal to cell surface receptors activates G proteins through a well characterized process involving GTP binding on the Gα subunit, dissociation of the heterotrimeric complex into Gα and Gβγ subunits, and activation of downstream effectors that elicit a response to the stimulus. As mediators between transmembrane receptors and intracellular effectors, heterotrimeric G proteins are well positioned to serve as PTM-mediated regulators of G-protein signaling. Indeed, three primary PTMs are essential for G proteins to function: N-terminal myristoylation and palmitoylation of Gα subunits, and C-terminal prenylation of Gγ subunits, all three of which function as a lipid bar code to anchor heterotrimeric G proteins to specialized microdomains in the plasma membrane of cells and also confer functional interaction with other proteins. In this context, while the signaling roles of Gα and Gβ subunits and the PTMs which occur on these subunits are widely identified; Gγ subunits are thought to serve the limited role of a membrane anchor for its obligate partner Gβ and no other regulatory role was known.

This study highlights a previously unknown role of Gγ subunit in the regulation of G-protein signaling mediated through phosphorylation of their N-terminal intrinsically disordered region. Using a yeast model organism, *Saccharomyces cerevisiae*, that harbors a single canonical G-protein signaling system to regulate a yeast mating pathway, we have identified a novel phosphorylation-dependent regulatory role of Gγ subunit in yeast (Ste18). A number of unique discoveries have ensued that provide a foundation for

future studies in mammalian systems, where G protein signaling serves as a major drug target for the treatment of human disease. First, Ste18 is dynamically phosphorylated in response to GPCR activation. Second, this phosphorylation event is dependent on a MAPK (Fus3), which is the ortholog of human Erk2. Third, Ste18 phosphorylation, in conjunction with phosphorylation of a Gβγ effector scaffold protein (Ste5), negatively regulates activation of the yeast mating pathway that is responsible for phosphorylation-based activation of Fus3. Fourth, negative regulation by phosphorylated Ste18/Ste5 is mechanistically achieved by reducing binding affinity between Gβγ/(Ste4/18) and effector Ste5, which results in controlling the bulk rate of active signaling complex formation at the plasma membrane in response to a GPCR stimulus. Fifth, Ste18/Ste5 phosphorylation regulates the sensitivity of the yeast mating process by altering its switch-like behavior. I go on to demonstrate that Ste18 phosphorylation can be promoted by signals other than GPCR stimulation. Specifically, I show that Ste18 phosphorylation is also sensitive to osmotic stress and cell-cycle progression, both of which may represent cross-talk mediated responses that funnel through the aforementioned Ste18/Ste5 regulatory mechanism. Together, these findings reveal that combinatorial phosphorylation of Ste18 and the Gβγ effector protein (Ste5) constitute a dynamic regulatory module that mediates negative regulation of G protein signaling in yeast and provide a foundation for understanding similar mechanisms undergone in mammalian cells.

PART I

PRIMARY THESIS PROJECT

ROLE OF Gγ SUBUNIT AS A NEGATIVE FEEDBACK PHOSPHO-REGULATOR OF G-PROTEIN SIGNALING IN YEAST

CHAPTER 1

INTRODUCTION AND LITERATURE REVIEW

Cells of both unicellular and multicellular organisms communicate with other cells both near and far as well as respond to continuous changes in their environment to perform important physiological processes necessary for survival. This fundamental process is mediated through signal transduction systems which sense and process the dynamic temporal information in the microenvironment of the cell into appropriate cellular response. All signal transduction systems consist of a transmembrane receptor which receives the extracellular signal and subsequently transfers the information to intracellular effector proteins which generates an intracellular signal. During this transduction process, the signal is often amplified before evoking a cellular response. Additionally, feedback pathways regulate the entire signaling process.

G-protein signal transduction system, so called due to the requirement of GTP bound proteins (G-proteins) for signaling, is one of the most extensively studied signaling system, primarily due to their involvement in diverse physiological processes in humans and wide pharmacological relevance (1–8). The first evidence of the GTP dependence of receptor activation of cAMP came from the Martin Rodbell group, suggesting the presence of an unknown GTP-binding transducer protein, which were later discovered by Alfred Gilman in 1979 (reviewed in (9)) Since then the field has immensely benefitted from the advent of powerful recombinant DNA techniques, advances in protein engineering, X-ray crystallography, and mass spectrometry, which together with classical biochemistry expanded the understanding about the key players and the standard model of activation of G-protein signaling system.

1.1. The basic model of G-protein signaling system

The well-established understanding of the standard model of the activation of the G-protein signaling system has stemmed from studies across diverse organisms such as yeast and humans. The basic elements of G-protein signaling system include G-protein coupled receptors (GPCRs), heterotrimeric G-proteins (Gαβγ), G-protein linked effectors, and regulators of G protein signaling (RGS)(10). GPCRs, by virtue of their seven transmembrane-domain helical structure, provide a ligand binding pocket at the extracellular surface and an interaction interface with heterotrimeric G-proteins at the cytoplasmic surface(11).

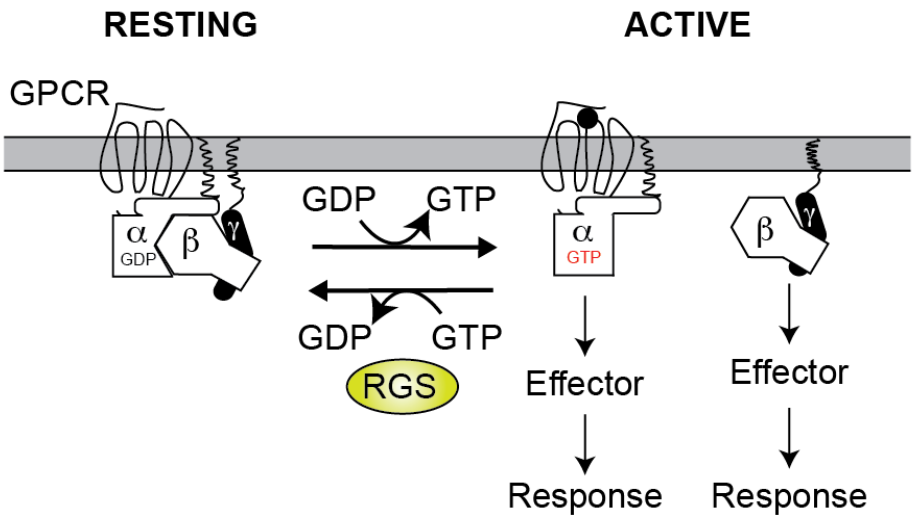

Figure 1.1. Schematic diagram of canonical G-protein signaling system. Activation of the G protein coupled receptor (GPCR) at the cell surface triggers exchange of GDP with GTP on Gα subunit, dissociation of Gα and Gβγ subunit, activation of downstream effectors and finally culminates with appropriate cellular response. The system is deactivated by the hydrolysis of GTP to GDP on Gα subunit, which is accelerated by the regulator of G protein signaling (RGS) protein.

Under resting state, heterotrimeric G-proteins comprising of Gα subunit, and the obligate heterodimer Gβγ subunits, are tightly bound as a closed complex; and the Gα subunit is coupled to GDP. In humans, there are approximately 1000 GPCRs which recognize a structurally diverse repertoire of ligands, such as photons, hormones, chemokines, amino acids, and neurotransmitters (10–12). Activation of GPCRs by binding of a ligand triggers conformational changes in the receptor. Activated GPCRs act as a guanine nucleotide exchange factor (GEF) and catalyze the exchange of GDP for GTP on Gα subunit, leading to the dissociation of Gα and Gβγ subunit. The Gα and Gβγ subunits are then free to transmit the signal by interacting with a variety of downstream effector proteins, eventually generating a physiological response to the stimuli(11,13–15). Conventionally, Gα subunits are viewed as the primary transducers of the signal; whereas Gβγ subunits act as a guanine nucleotide dissociation inhibitor (GDI). However, in recent years the number and variety of effectors that are known to be modulated by Gβγ subunits have increased(4,16). The system is desensitized by the intrinsic GTPase activity of Gα that hydrolyzes the bound GTP to GDP, the rate of which is accelerated by the GTPase accelerating (GAP) activity of RGS proteins (Figure 1.1). The GDP bound Gα has a lower affinity for effectors, but rather re-associates with Gβγ subunits with high affinity to form a closed heterotrimeric complex(17,18).

1.2. The key elements of G-protein signaling system

1.2.1. G-protein coupled receptors (GPCRs) – GPCRs are the largest superfamily of cell surface receptors and are so named as they transmit signal across the membrane by activating the heterotrimeric guanine nucleotide binding proteins (G-proteins) bound to the cytosolic tail of GPCRs, which then activates downstream effectors. In humans, about 1%

of the genome, encodes for approximately 1000 GPCRs with sequence length between 289 and 3312, with most GPCRs consisting of 300–500 amino acid residues (19,20). Together, they mediate cellular responses to a variety of extracellular signals ranging from photons and small molecules to peptides and proteins(10,11). Despite differences in the sequence and ligand sensitivity, the overall structural architecture of these receptors is highly homologous as was revealed by the exponential growth in the crystallography of GPCRs. Currently, there are structural records of 53 unique receptor from over 200 PDB entries spanning a range of conformational states from multiple inactive states, active-intermediate states, and active states in complex with G proteins(reviewed in (21–24)).

All GPCRs share an identical structural topology comprising of seven transmembrane α-helices (7TMH) connected by three extracellular loops (ECL1-3) and three intracellular loops (ICL1-3) (reviewed in (22–24)). Interestingly, the transmembrane helices of GPCRs are frequently tilted with varied tilt and rotation angles that depend not only on the receptor type but also on its activation state. Additionally, the 7TMH structure contains a number of kinks, mostly produced by presence of helix breakers such as cysteine and proline residues, that roughly divide the structure into two regions-extracellular region and intracellular region. While the extracellular region of GPCRs, which includes the N-terminus, ECL 2, and ECL3, is responsible for ligand binding; the intracellular region of GPCRs is involved in interaction with heterotrimeric G-proteins. Moreover, the intracellular region of GPCRs which interacts with G-proteins is subjected to much larger conformational changes upon receptor activation than the extracellular region. These activation-related conformational changes in the helices is accompanied by rotamer changes in highly conserved side chains that stabilize the global movements of helices and help prime the intracellular side of a GPCR to act as a guanine exchange factor (GEF) for the heterotrimeric G-proteins (reviewed in (22–24)).

Activation of a GPCR triggers exchange of GTP for GDP on Gα and subsequent dissociation of Gα and Gβγ subunits. Depending on the type of G protein to which the receptor is coupled, a variety of downstream effectors are activated in a cascade manner (reviewed in (25,26)). The signal is attenuated by receptor phosphorylation and binding of a β-arrestins which mediates internalization of the receptor (27).

1.2.2. Heterotrimeric G-proteins - Heterotrimeric G-proteins comprising of Gα, Gβ and Gγ subunits are intracellular partners of GPCRs that transduce signal from the ligand bound receptor to downstream effector proteins. In their inactive form, GDP bound Gα subunit binds tightly to the obligate heterodimer of Gβγ subunit and is coupled to the C-terminus of GPCR as a closed complex. Ligand binding to the GPCRs promotes exchange of GTP for GDP and the functional dissociation of Gα and Gβγ subunits, each of which is now free to interact with downstream effectors(10,28). Signal is terminated by the intrinsic GTP hydrolysis rate of the Gα subunit and the subsequent reassociation of Gα- GDP and Gβγ subunits. The GTPase action of Gα subunit is regulated by accessory protein, regulator of G-protein signaling (RGS) proteins(17,18). Resolution of crystal structures for inactive, active, and transition-state G-proteins, as well as several biochemical and genetic studies, have provided the framework for understanding the role of heterotrimeric G-proteins as molecular switches or transducers(reviewed in (10,11)).

1.2.2.1. The Gα subunits – There are 23 Gα proteins in the human that can be divided into four families, $G\alpha_s$, $G\alpha_i$ / $G\alpha_o$, $G\alpha_q$ / $G\alpha_{11}$, and $G\alpha_{12}$ / $G\alpha_{13}$. Each family has multiple members that share both sequence and functional similarities (29). The $G\alpha_s$ has two members- the ubiquitously expressed $G\alpha_s$ and the $G\alpha_{olf}$ expressed in olfactory sensory

neurons. When activated, both of these proteins activate adenylyl cyclase and result in increased concentration of intracellular cyclic AMP. On the other hand, $G\alpha_i$ / $G\alpha_o$ class contains $G\alpha_{i1}$, $G\alpha_{i2}$, $G\alpha_{i3}$, $G\alpha_o$, $G\alpha_t$, $G\alpha_g$, and $G\alpha_z$ subunits that are expressed in wide range of cells such as neurons, rods and cone cells of the eye, taste receptor cells, and in platelets. Unlike $G\alpha_s$, members of $G\alpha_i$ / $G\alpha_o$ inhibit cyclic AMP production. The $G\alpha_q$ / $G\alpha_{11}$ has five members, $G\alpha_q$, $G\alpha_{11}$, $G\alpha_{14}$, $G\alpha_{15}$, and $G\alpha_{16}$. While $G\alpha_q$ and $G\alpha_{11}$ are widely expressed in mammalian cells; others are specifically expressed in stromal, epithelial and hematopoietic cells. The $G\alpha_q$ / $G\alpha_{11}$ family of proteins activate the pathway by regulating the β-isotype of phospholipase C (PLC-β) which cleaves phosphoinositol diphosphate into diacylglycerol and inositol triphosphate, which in turn activate protein kinase C and mobilize calcium respectively. The fourth class of $G\alpha$ family has only two members, $G\alpha_{12}$ and $G\alpha_{13}$, which are expressed in most types of cells, and activate Rho GTPase nucleotide exchange factors (RhoGEFs) which in turn activates the small G-protein RhoA that regulates cell shape and mobility (reviewed in (30)).

Crystallography of $G\alpha$ subunits revealed a conserved structure consisting of two domains, namely the Ras-like domain and the α-helical domain. While the Ras-like domain provides essential GTPase and nucleotide exchange activity; the helical domain contributes to the specificity of interaction with GPCRs and effectors. $G\alpha$ subunits also contain an extended N-terminal region that interacts with the $G\beta\gamma$ subunit and with the membrane via myristate and/or palmitate group covalently attached at/near their N-termini, which together stabilize the location of $G\alpha$ subunits at the membrane. Two flexible linkers connect the Ras-like domain and the helical domain, allowing movement of these two domains relative to each other (31,32). Additionally, these domains participate in the formation of a deep cleft for the binding of either the GDP or GTP nucleotide. Three switch regions in the GTPase domain- switch I, II, and III- interacts with the phosphates of the

bound nucleotide and forms an interface with the activated receptor (GEF) as well as the RGS protein (GAP). The cumulative effect of all the interactions between the switch region, nucleotide, and other proteins dictates whether Gα subunit exists in a GDP-bound inactive closed complex or GTP-bound effector-binding active state (reviewed in (10,14)).

1.2.2.2 The Gβγ dimers – The Gβγ heterodimer consists of two obligate partners- Gβ and Gγ subunits- that interact to form the irreversible Gβγ dimer rapidly after synthesis(reviewed in(33)). Currently, 5 distinct members of Gβ family and 13 different members of Gγ family have been identified in human. In the Gβ family, $G\beta_{1-4}$ share 80% amino acid sequence identity compared to the 50% identity for $G\beta_5$; whereas, there is significantly lower identity in Gγ subunits (reviewed in (34)). Most of the different types of Gβ and Gγ subunits can pair to form a large number of potential Gβγ dimers, with few exceptions. For example, $G\beta_1$ can combine with all Gγ subunits, whereas $G\beta_2$ pairs with $G\gamma_2$ but not $G\gamma_1$ subunit (35). Although the functional relevance of the variability in Gβγ dimers is not completely understood, several knockout studies suggest that specific Gβγ subtypes interact with specific GPCRs and are responsible for specificity of pathway activation. For example, studies done in mice where $G\gamma_7$ subunit was genetically deleted, resulted in distinct behavioral changes associated with specific loss of cyclic AMP production in the striatum (36). In another study, deletion of $G\gamma_3$ results in changes in metabolism resulting in resistance to a high fat diet (37). In both of these cases loss of the specific Gγ subunits also resulted in a loss in specific Gα expression, indicating roles for specific Gαβγ combinations in these phenotypes (36,37).

The Gβγ subunits have been crystallized, either alone or in combination with known effectors, all of which generated similar β-propeller structure in Gβ subunits that is

associated with a helical Gγ subunit (38–40). All Gβ subunits contain seven WD-40 repeats, a tryptophan and aspartic acid sequence that repeats every 40 amino acids and forms antiparallel β-strands which fold into a seven bladed β-propeller or torus-like structure. Additionally, the N-terminus of the Gβ subunits form an α-helix structure (38–40). The Gγ subunits folds into two α-helices. The N-terminal α-helix of Gγ is involved in a coiled-coil interaction with the α-helix of Gβ subunits; whereas the C-terminal α-helix of Gγ extensively interacts with the base of the Gβ propeller (38–40). Moreover, the C-terminus of all Gγ subunits contain the CAAX motif (where C is cysteine, a is aliphatic amino acid, and X is any amino acid); the cysteine residue of which is subjected to prenylation, a lipid modification critical for the membrane localization of the Gβγ dimer (41,42). In this process of prenylation, the last three amino acids (-AAX) is proteolytically removed and the newly generated C-terminal cysteine is carboxymethylated (41,42). Dissociation of the Gβγ subunits from the heterotrimer complex does not trigger massive conformational changes in Gβγ dimer, rather it exposes the residues required for binding and activation of the effectors (39).

1.2.3. G-protein linked effectors-

1.2.3.1 Gα effectors – Currently, the effectors of all four classes of Gα subunits are well established. Adenylyl cyclase was the first effector to be discovered by Sutherland and Rall(43). These enzymes are large membrane bound proteins responsible for the production of cAMP and are activated by the GTP- bound $G\alpha_s$ class of subunits. There are 9 isoforms of adenylyl cyclase that are generally widely expressed, although type I and type II are primarily restricted to neurons. Similarly, type III adenylyl cyclase are specifically expressed in olfactory cells. Despite the difference in expression, all isoforms of adenylyl cyclase are activated by $G\alpha_s$ subunits. Interestingly, some isoforms of adenylyl

cyclase are inhibited by Gα subunits. These Gα subunits belong to the $G\alpha_i$ class (where i = inhibitor), and can directly inhibit the types I, V, and VI adenylyl cyclase (reviewed in (10)). Unlike adenylyl cyclase which is activated or inhibited by direct interaction with $G\alpha_s$ or $G\alpha_i$ respectively, the Ca^{2+}, Na^+, and Cl^- ion channels in cardiac cells are regulated by $G\alpha_s$ and $G\alpha_i$ by an unknown mechanism (reviewed in (10)). The retinal $G\alpha_t$ mediates regulation of cGMP phosphodiesterase by photon activated rhodopsin. The enzyme cGMP phosphodiesterase catalyzes the hydrolysis of cGMP, causing closure of cGMP-gated cation channels and in hyperpolarization of the cell membrane. The $G\alpha_q$ class of proteins activate phosphoinositide-specific phospholipase C-β type (PLC-β), which hydrolyzes the phosphoester bond of the plasma membrane lipid phosphatidylinositol 4,5-biphosphate into the calcium mobilizing second messenger inositol 1,4,5- trisphosphate (IP_3) and the protein kinase C-activating second messenger diacylglycerol (DAG). Additionally the activities of a broad range of membrane, cytoskeletal, and cytosolic proteins also are directly regulated by PLC-mediated changes in membrane concentrations of PtdIns(4,5)P2 (reviewed in (10)). Comparatively less is known about the $G\alpha_{12/13}$ family, but few studies have shown that activated $G\alpha_{12}$ or $G\alpha_{13}$ interact with Rho-family guanine nucleotide exchange factors (RhoGEFs), which in turn activate small G-protein RhoA which plays a key role in the regulation of the actin cytoskeleton, cell shape, cell polarity, cell migration and cell growth. (reviewed in (10)).

1.2.3.2 Gβγ effectors - In recent years, the roles of Gβγ subunits have expanded from being just a negative regulator (as a GDI) for Gα subunits to a more central participant in G-protein signaling. Gβγ subunits are now known to interact with Gα subunits, GPCRs, and several downstream effector proteins(16).

As a negative regulator of Gα signaling, Gβγ subunits prevent the spontaneous activation of Gα subunits in the absence of receptor stimulation (reviewed in (44)). Interaction of Gβγ dimer with Gα subunit induces multiple changes in Gα subunits including conformational changes that stabilizes the switch regions I and II of Gα, decrease the dissociation rate of GDP from Gα, and simultaneously increasing the rate of dissociation of GTP from Gα. Thus, Gβγ subunits act as a guanine dissociation inhibitor (GDI) of Gα by facilitating increased affinity of Gα for GDP which favors heterotrimeric complex formation (reviewed in (16)).

The Gβγ subunits also enhance coupling of heterotrimeric complex to its appropriate receptor. This effect is independent of the enhanced stability of heterotrimeric complex at the membrane, compared to the stability of Gα and Gβγ subunits post-disassociation from the heterotrimeric form (reviewed in (16)). The ability of Gβγ subunits to bind to receptors is influenced by the type of Gγ subunit in the dimer. For example, $G\beta_1$ when paired with $G\gamma_1$ subunit facilitates binding of $G\alpha_t$ to rhodopsin, but not when $G\beta_1$ pairs with $G\gamma_2$ subunit (35). However, the site on Gγ subunits which confers this ability to bind to receptors is currently not known.

Although Gβγ subunits were primarily considered as a GDI for Gα subunits, a large body of work revealed that free Gβγ subunits can activate a large number of its own downstream effectors (reviewed in (4,10,34)). The first evidence of such a direct effector of Gβγ in humans were the G-protein regulated inward rectifier K+ channels (GIRK). GIRKs are expressed in various tissues such as heart, pancreas, and brain; and has a homotetramer structure, wherein the N- terminus of one subunit folds with the C-terminus of the adjacent subunit. Additionally, GIRK has multiple Gβγ binding sites, one on the N-terminus and two on the C-terminus of each subunit. The binding sites on N- and C-terminus of adjacent subunits are brought close in proximity in the holochannel and is

recognized by one Gβγ subunit. Different receptor/GIRK combinations are recognized by different Gβγ dimers. The presence of multiple binding site allows for graded activation of the channel which leads to increasing hyperpolarization of the cells (reviewed in (4,10)).

Voltage-gated Ca^{2+} channels localized in the presynaptic terminal of neurons mediate calcium ion influx across plasma membrane and is inhibited by Gβγ subunit in response to norepinephrine. Voltage-gated Ca^{2+} channels are oligomeric complex of three different subunits- α_1 subunit, β subunit, and $\alpha_2\delta$ subunit. Much like the subunits in GIRK channel, α_1 subunit of voltage-gated Ca^{2+} channels contain three Gβγ binding sites, one each in the N-terminus, C-terminus, and intracellular loop connecting transmembrane domains. However, in contrast to multiple Gβγ binding to GIRK, only a single Gβγ occupies the binding sites per Ca^{2+}channel, as the multiple binding sites fold into proximity in the native structure of the channel. While the involvement of $G\beta_1$ and $G\beta_3$ have been shown in this process, much less is known about the specificity of Gγ or the mechanism by which the binding of Gβγ inhibits the channel (reviewed in (4,16,34)).

Adenylyl cyclase is another well studied effector of Gβγ. In humans, there are 9 isoforms of adenylyl cyclase, all of which are activated by GTP-bound active $G\alpha_s$, but only a subset of them are directly regulated by Gβγ. While type I adenylyl cyclase is inhibited by Gβγ, types II, IV, V, and VI adenylyl cyclases are stimulated by Gβγ. The structure of all AC isoforms includes a highly variable N terminus (NT) and two well conserved catalytic domains (C1, C2). While the C1/C2 domains form the catalytic pocket for cAMP production, the NT harbors one or more regulatory binding sites for Gβγ and/or other regulatory proteins such as Gα. However, it was later determined that interactions between Gβγ and the regulatory sites in the NT of adenylyl cyclase has little role in the stimulation of adenylyl cyclase. Instead, recent study showed that Gβγ also interacts with

the catalytic domains (C1, C2) of isotypes V and VI of adenylyl cyclase; and this interaction is necessary for activation of adenylyl cyclase. On the other hand, inhibition of type I adenylyl cyclase by $G\beta\gamma$ is comparatively less well understood. It was observed that $G\beta\gamma$ released from $G\alpha_s$-coupled receptors, but not $G\alpha_i$- coupled receptors, mediate inhibition of type I adenylyl cyclase. However, the detailed mechanism underlying the inhibition of type I adenylyl cyclase is not completely understood (4,45).

Another effector of $G\beta\gamma$ is phospholipase-C (PLC) which cleaves phosphoinositol diphosphate into diacylglycerol and inositol triphosphate. The two end products in turn regulate important cellular processes- diacylglycerol directly activates phospholipase kinase C while inositol triphosphate diffuses to the endoplasmic reticulum and mobilizes intracellular calcium stores. Of the 13 currently known isoforms of PLC, only the β, ε, and η-isoforms are regulated by $G\beta\gamma$ mediated by direct interactions between the PH and catalytic domains of PLC. The magnitude of PLC activation was dependent on the $G\beta\gamma$ combination ($G\beta_1\gamma_2$ being the most efficient) and on the isoform of PLC (reviewed in (4,16,34)).

Direct interaction between $G\beta\gamma$ and phosphoinositide 3-kinases (PI3K) activates the latter and triggers the phosphorylation of phosphatidylinositols at the position 3-hydroxyl group of the inositol ring, producing phosphatidylinositol 3,4,5-triphosphate (PIP_3). This, in turn, recruits and activates cytosolic effectors with PIP_3-binding pleckstrin homology (PH) domains, thereby controlling important cellular functions such as proliferation, survival, or chemotaxis. Like other effectors, PI3Ks demonstrate $G\beta\gamma$ specificity, with combinations of $G\beta_{1\text{-}4}$ with $G\gamma_2$ stimulating PI3Ks to equivalent levels, whereas dimer of $G\beta_5$ and $G\gamma_2$ is unable to activate PI3K (reviewed in (4,16,34))

G-protein coupled receptor kinases (GRKs) are serine/threonine protein kinases that phosphorylate numerous GPCRs and are activated by free $G\beta\gamma$. Phosphorylation of

GPCRs by GRKs promotes the recruitment of β-arrestins which subsequently leads to receptor internalization and desensitization. Unlike many other kinases, GRKs do not need to be phosphorylated to achieve an activation state. Instead, docking of GRKs with ligand bound receptor leads to activation of GRKs. This docking is mediated by direct interaction between the carboxyl terminal of the kinase and the membrane-localized free Gβγ dimer which serves to target this enzyme to its membrane-incorporated receptor substrate (46,47). Once activated, GRKs phosphorylate the intracellular loops and the carboxyl terminal of GPCRs which facilitates the receptor's binding to β-arrestins with high affinity. This binding event both physically prohibits receptors from further coupling to heterotrimeric G-proteins and targets the receptors to clathrin-coated pits, where receptor endocytosis occurs. Thus, resulting in receptor desensitization (46,48).

1.2.4. Regulator of G-protein signaling (RGS) – RGS proteins are a family of 30 members that negatively regulate G-protein signaling via GTPase accelerating activity of their RGS homology (RH) domain (17). The first RGS protein was discovered in *Saccharomyces cerevisae*, wherein the G-protein signaling pathway mediates response to mating pheromone (49). The study revealed that loss of Sst2 (yeast RGS protein) rendered the yeast supersensitive to pheromone and was later shown to interact directly with and negatively regulate Gpa1 (yeast Gα subunit) (49). Multiple homologs of Sst2 were later discovered, including the first mammalian homolog BL34 (later renamed as RGS1) in B-lymphocytes (50). Each of these RGS proteins consist of the conserved RH domain of 130 amino acids that folds in to a bundle of nine helices. The RH domain interacts with the switch III region of Gα subunits, and the RH/switch interface primarily dictates the selectivity for the Gα subunit (50). For example, RGS2 demonstrates a stronger selectivity for $G\alpha_q$, but not other classes of Gα subunits ($G\alpha_s$, $G\alpha_i$, $G\alpha_{12/13}$) (51).

This interaction promotes the transition state for GTP hydrolysis within the nucleotide binding domain and thus facilitate deactivation of $G\alpha$ (52). Moreover, RGS proteins can physically block the interaction between certain G-proteins and its effectors, such as in the case of RGS4 which binds to $G\alpha_q$ and inhibits interaction with the effector protein, PLC-β1 (53)

The modular nature of G-protein signaling system with multiple components enables cells to assemble vast combinations of complex signaling units that allow different cells to respond adequately to different extracellular signals. Furthermore, it allows for an expanded protein repertoire that can be targeted by pharmaceutical agents in case of a malfunction.

1.3 Pharmacological significance of G-protein signaling

Components of the G-protein signaling system, most prominently GPCRs, have been of long-standing interest as drug targets, as they regulate numerous diverse physiological processes. Indeed, abnormalities in G-protein signaling system have been implicated in various metabolic, immunological, and neurodegenerative diseases, along with cancer(1,2,4,5,8,54–58). Although the underlying physiology of any disorder is often complex and multifactorial, several GPCRs that play a key role in the pathophysiology have been identified and are employed as drug targets. In fact, currently, 475 drugs (approximately 34% of all marketable drug targets approved by FDA) act on 108 unique GPCRs and account for a global sales volume of over 180 billion US dollars annually(59–61). Examples of major GPCR pharmacological targets include angiotensin II receptor (cardiovascular disease)(62), glucagon receptor (type 2 diabetes)(63), serotonin receptor (Alzheimer's disease)(63), CXCR2 and CXCR4 (cancer)(64,65), to name a few.

Moreover, additional 321 pharmacological agents are currently under clinical trials, of which approximately 20% target novel 66 GPCRs(61,62,66,67). However, GPCRs targeted by drugs show genetic variation in their functional regions such as drug- and effector-binding sites in the human population, thus, leading to altered or adverse drug response(68). Increased understanding of the system has fostered the development of alternative drugs which target and inhibit the RGS proteins, or heterotrimeric G-proteins as an approach to treat certain pathologies(4,69,70).

Targeting RGS proteins presents a unique and challenging paradigm to modulate the pathway output downstream of GPCR activation. Thus, a lot of effort has been given to the discovery of peptides or small molecules that can physically block the RGS/Gα protein-protein interaction or alter the expression levels or localization of an RGS protein within a cell (69). To date the common approach toward modulating RGS protein function has focused on disrupting the protein-protein interaction between the RGS proteins and their Gα subunit partners. These efforts have resulted in the identification of both peptide and small molecules that disrupt RGS activity at Gα proteins. For example, Wang et al. identified a unique peptide sequence P17 (Val-Arg-His-Val-Ala-Val-Glu-Val-Gly-Gly-Val-Val-Val-Val-Gly) that blocked the interaction between RGS4 and Gα_{i1}, with specificity over RGS7, and functionally inhibited RGS4 action (71). The N-terminal Arg as well as the C-terminal Val-Gly were essential for the inhibitory action of the peptide (71). Other examples of peptide inhibitors include YJ34 (72) and P2 (73). Additionally, small molecules such as the pyrido [1,2-a] pyrimidine derivatives CCG-63802 and CCG-63808 which prevent association between RGS4 and Gα_o have also been identified (3).

Positioned between activated GPCRs and downstream effectors, heterotrimeric G proteins play the pivotal role of a transducer in G-protein signaling signaling; and thus, have been obvious targets for drug development (11,16). Indeed, several small molecules

that target either Gα or Gβγ subunits have been developed (4,70). These molecules bind the different G protein subunits and primarily modulate the activation/deactivation cycle of heterotrimeric complex. For example, suramin and its analogues (NF449 and NF503) is a polysulfonated naphthylamine-benzamide derivative that bind specifically to $G\alpha_s$ subunit. This binding inhibits GPCR promoted GDP release followed by GDP/GTP exchange as well as the interaction of $G\alpha_s$ with its effector, adenylyl cyclase (reviewed in (70)). Other examples of small molecules which target Gα subunits are BIM-46175 ($G\alpha_s$), YM-254890 ($G\alpha_s$), YM-280193 ($G\alpha_s$), and FR-900359 ($G\alpha_s$) hinder GDP/GTP exchange as well as Gα - Gβγ dissociation (reviewed in (70)). Additionally, Gβγ subunits have recently been investigated as a potential drug target. Indeed, many small molecule inhibitors have been identified that prevent interaction of Gβγ subunits with specific downstream effectors. The inhibitor peptide GRK2ct (βARKct) consisting of a C-terminal 194 amino-acid peptide of GRK2 is one of the most famous Gβγ binder and modulator (74). This peptide is known to interfere with GRK2 activity through disrupting its Gβγ -mediated membrane translocation (74). Additionally, various non-peptide inhibitor molecules have been developed by Smrcka and group. Among these molecules, M119 was one of the most potent compounds with high apparent affinity for $G\beta_1\gamma_2$. This small molecule inhibits the activation of Gβγ effectors, PLC-β and PI3K, and their related cell response including neutrophil chemotaxis and inflammation, in a concentration dependent manner (reviewed in (4)). However, M119 had no effect on Ca2+ release, thus nicely illustrating the specificity of M119 on Gβγ dependent responses (reviewed in (4)). Other small molecules, such as M119B, M158C, and M201, have also been identified to differentially inhibit Gβγ effectors (reviewed in (4)).

Though GPCRs continue to be the major drug target, there is a strong drive for innovation in the pharmaceutical industry for discovery of new protein targets and new

binding sites within known targets. Enhanced understanding of the mechanism and regulation of the G-protein signaling system continues to provide further opportunities for the development of new and improved targeted therapeutics.

1.4 Post-translational regulation of G-protein signaling

G-protein signal transduction, like other cellular processes, relies heavily on reversible post-translational protein modifications (PTMs) for fine tuning the signaling output. All key components of the pathway, including GPCRs, heterotrimeric G proteins ($G\alpha\beta\gamma$), effector proteins, and RGS are subject to a variety of covalent modifications, which occur both in normal and pathological contexts (56,75–93). Most of these PTMs are added or removed in a highly dynamic manner, which allows for rapid reprogramming of the pathway. The most prominent PTMs which occur on members of G-protein signaling pathway are lipid modification, phosphorylation, and ubiquitination (56,75–93). Lipid modifications to proteins include prenylation, myristolyation, and palmitoylation. Prenylation consists of farnesylation or geranylgeranylation of cysteine residues of target proteins; whereas myristoylation occurs on N-terminal glycine residues of a target protein. Both prenylation and myristoylation are irreversible PTMs. On the other hand, palmitoylation is a reversible lipid modification which occurs by thioesterification of cysteine residues and covalent attachment of palmitic acid on target proteins. These lipid modifications regulate the localization of the protein at the membrane, and hence activation of some proteins (reviewed in (94)).

Phosphorylation is the addition of phosphate moiety to either serine, threonine, or tyrosine residue of a protein, and primarily regulates the activation state of the protein, protein-protein interaction profile, or primes the protein for degradation (reviewed in (94)).

Ubiquitination is a highly dynamic, coordinated, and enzymatically catalyzed covalent attachment of a small regulatory protein, ubiquitin, to proteins which are then targeted for degradation and recycling (reviewed in (94)).

Together, these modifications regulate various components of the G-protein signaling pathway, and hence provide another layer of dynamic regulation of the pathway output (56,75–93).

1.4.1. Post-translational modifications of GPCRs- GPCRs are heptahelical integral plasma membrane proteins that contain seven membrane-spanning domains, and thus, lipid modifications seem unlikely to contribute to the localization of the receptor protein at the membrane. Nevertheless, many examples of GPCRs that are subject to lipid modification wherein palmitate is attached to one or more cysteine residues exist in literature. Rhodopsin was the first GPCR to be identified as a target for palmitoylation, and it was suggested that the attached palmitate might be incorporated into the plasma membrane bilayer, thereby creating an additional intracellular loop (95). The palmitoylated cysteine were found in the cytoplasmic tail of the protein, positioned 10-14 amino acids downstream of the last transmembrane domain (95). Later many GPCRs including the β2-adrenergic receptor (96), human somatostatin receptor (97), human thyrotropin receptor (98) and others, were shown to possess cysteine residues in the C-terminus at an analogues position to that in rhodopsin. Site-directed mutagenesis of these cysteine residues which block palmitoylation of the receptor affects GPCR trafficking in some cases, while in others affects the receptors ability to couple to G-proteins. Mutation of palmitoylation sites in δ-opiod receptor, H_2 histamine receptor, chemokine CCR5 receptor, and vasopressin V2 receptor, resulted in intracellular accumulation of the receptors. While receptors like β2-adrenergic receptor and endothelin receptor are uncoupled from their

corresponding G-protein, through a less understood mechanism, upon elimination of palmitoylation (reviewed in (99)).

Almost all GPCRs are regulated by phosphorylation which leads to receptor desensitization (100). Phosphorylation occurs on the C-terminal tail and the intracellular loops of GPCRs which contain multiple serine and threonine residues clusters that get unmasked due to agonist-induced conformational changes. These sites are primarily phosphorylated by GRKs which promotes interaction with β-arrestin at higher affinity (reviewed in (82)). This was illustrated in the case of rhodopsin which bound β-arrestins at 10-fold higher affinity when phosphorylated (101). This increase in affinity of phosphorylated receptors for β-arrestins is not universal for all GPCRs, with some receptor phosphorylation mediating no or small change in affinity for β-arrestins (reviewed in (82)). Interestingly, GPCRs are multiply phosphorylated in a sequential manner with the precise location of phosphorylation depending on the ligand type and concentration as well as the cell type (reviewed in (76)). While it has been suggested that the receptor- β-arrestin interaction is dependent on the bulk negative charge rather than the precise location of phosphorylation; the phosphorylation pattern dictates the heterogeneity in the affinity and type of interaction between β-arrestin and receptor (reviewed in (76,82)). Furthermore, it was suggested that multi-site phosphorylation of GPCRs likely reflects action of multiple kinases. Indeed, increasing evidences have shown other kinases such as PKA and PKC to phosphorylate GPCRs, such β1 -adrenergic receptor (102) and D2-dopamine receptor (103), and mediate desensitization, albeit through an unclear mechanism.

In addition to palmitoylation and phosphorylation, many GPCRs are subject to ubiquitination in which either a single ubiquitin moiety is added to one or several lysine residues (monoubiquitination or multi-monoubiquitination), or a chain of ubiquitin is added to K48 residue. The best characterized role of ubiquitination on GPCRs is to function as a

lysosomal sorting signal (reviewed in (56,77)). Indeed, studies done in yeast *Saccharomyces cerevisae* and in mammals showed that Ste2 (yeast GPCR) (104) as well as many mammalian GPCR (most prominently the chemokine CXCR4 receptor) (105) get mono ubiquitinated and internalized into lysosome after chronic stimulation. Ubiquitination of receptors is required for the interaction with ESCRT (endosomal sorting complex required for transportation) machinery which is responsible for trafficking ubquitinated receptors from early endosomes to late endosomes where receptors are degraded in the lumen of lysosome (reviewed in (56,77)). In contrast, non-ligand mediated or basal ubiquitination of GPCRs, such as chemokine CXCR7 receptor and protease activated receptor PAR1, is essential for retention of the receptor at the plasma membrane. In these cases, ubiquitination of lysine inhibits the constitutive internalization of the receptor by precluding binding of clathrin adaptor protein to the receptor (reviewed in (56,77)). The density of functional receptors at the plasma membrane is also regulated by polyubiquitination of GPCRs, which marks the misfolded GPCRs in endoplasmic reticulum for degradation. This has been illustrated for δ- and μ- opiod receptors as well as many other GPCRs (reviewed in (56,77)). Thus, post translational modification of GPCRs is essential for proper receptor signaling and appropriate cellular response.

1.4.2 Post-translational modifications of heterotrimeric G proteins- Heterotrimeric G proteins ($G\alpha\beta\gamma$) must be stably anchored at the plasma membrane to transmit signal. Lipid modifications that occur on $G\alpha$ and $G\gamma$ subunits serve as hydrophobic anchors (reviewed in (89,99)).

All $G\alpha$ subunits have a myristate and/or palmitate group covalently attached at or near their N-termini. While myristoylation occurs exclusively on $G\alpha$ of the $G\alpha_i$ family; all mammalian $G\alpha$ subunits (except $G\alpha_t$) undergo palmitoylation. N- myristoylation involves

addition of 14-carbon fatty acid myristate through an irreversible amide bond to a glycine residue at the extreme N-terminus (after the initiating methionine has been cleaved). The reaction is catalyzed by N-myristoyl transferase, and enzyme with strict requirement for N-terminal glycine, followed usually by a serine or threonine (regulation of G-protein by covalent modification by C Chen). Thus, $G\alpha_s$ subunits which have a N-terminal glycine but lack the serine or threonine are not subject to myristoylation. Palmitoylation represents attachment of a 16-carbon fatty acid palmitate through a thioester bond to a cysteine residue within the first 20 N-terminal amino acids of $G\alpha$ subunits. Unlike the case for myristoylation, the biochemistry of palmitoylation is not well understood (reviewed in (89,93,99)).

The G protein γ subunits are covalently modified by the 20-carbon isoprenoid geranylgeranyl, or in the case of $G\gamma_1$, $G\gamma_9$, and $G\gamma_{11}$ by the 15-carbon farnesyl moiety. These modifications occur on a C-terminal cysteine in the CAAX motif, in which cysteine is followed by two aliphatic amino acids and the X amino acid is any amino acid that specifies recognition by geranylgeranyl transferase or farnesyl transferase. Following prenylation $G\gamma$ subunits undergo two consecutive modifications, that is proteolytic removal of the last three amino acids (-AAX) and caboxy methylation of the cysteine; however, the exact role of these two subsequent modifications are still not clear (reviewed in (89,99)).

Lipid modification of G proteins is essential for their signaling function. Indeed, numerous site-directed mutagenesis studies have shown that elimination of lipid modification prevents G-proteins from localizing at the membrane and result in signaling defects (reviewed in (89,99)).

Several $G\alpha$ subunits have been shown to be phosphorylated at serine/threonine or tyrosine residues, with phosphorylation of $G\alpha_z$ in human platelets being the first to be identified (reviewed in (93)). This phosphorylation reaction was catalyzed by protein

kinase C; and occurred on serine-27 and to a lesser extent on serine-16 in the N-terminus of $G\alpha_z$ subunit, preferentially for the GDP bound form. PKC also mediates phosphorylation of $G\alpha_{12}$ subunit which is present endogenously in human platelets. The phosphorylation occurs within the N terminal 50 residues but haven't been mapped further. In both the cases, $G\alpha_z$ and $G\alpha_{12}$ when phosphorylated showed reduced interaction with $G\beta\gamma$ subunit. Phosphorylation of $G\alpha_z$ also inhibits its interaction with RGS proteins, thus prolonging the activation of $G\alpha_z$ (reviewed in (93)). Additionally, $G\alpha_z$ is a substrate for phosphorylation by the p21 activated kinase (PAK1). Much like the PKC mediated phosphorylation, PAK1 phosphorylates a serine residue in the N-terminus of $G\alpha_z$ and inhibits its interaction with $G\beta\gamma$ subunit. In contrast, $G\alpha_t$ is phosphorylated on serine by PKC and on tyrosine residues by the insulin receptor kinase with the physiological significance still unknown (reviewed in (106)). Additionally, $G\alpha_s$ subunits have been reported to be phosphorylated by the kinase pp60 which belongs to the tyrosine protein kinase Src family. This phosphorylation event moderately increased the steady state GTP hydrolysis rate of $G\alpha_s$ subunit (reviewed in (106)).

Among $G\gamma$ subunits, only $G\gamma_{12}$ is reported to be phosphorylated on a serine residue in the N-terminus by PKC. Phosphorylation increased the affinity of $G\beta\gamma_{12}$ for $G\alpha_{i,}$ thus promoting the formation of a more stable heterotrimer (reviewed in (93)). Phosphorylation of $G\beta\gamma_{12}$ was also reported to have an inhibitory effect on interaction with the effector protein, adenylyl cyclase but had no impact on the activation of PLC- β, indicating selectivity in the effect of phosphorylation on effector activation by $G\beta\gamma_{12}$ (reviewed in (93)).

Among mammalian G proteins, $G\alpha_s$, $G\alpha_q$, and $G\alpha_{i2}$ have been shown to be polyubiquitinated and targeted for degradation by the proteasomal pathway (107–109). Furthermore, it has been shown that this ubiquitination of $G\alpha$ subunits is inhibited by the guanine nucleotide exchange factor, Ric-8, through a lesser known mechanism. However,

the importance of the interaction between the C-terminal of Gα subunits and Ric-8 for the suppression of polyubiquitination of Gα subunits is well established (109).

1.4.3 Post-translational modifications of RGS proteins – Much like GPCRs and heterotrimeric G proteins, RGS proteins undergo modifications such as palmitoylation and phosphorylation. Although most RGS proteins do not contain consensus motifs for the covalent addition of either myristate or isoprenoids, but they do contain exposed cysteine residues undergo palmitoylation. Indeed, several RGS proteins, such as RGS4, RGS7, RGS10, RGS16, and RGS19 have been shown to be palmitoylated. Palmitoylation of RGS proteins regulates the localization as well as protein interactions of RGS. For example, abrogation of palmitoylation of RGS16 dampens its ability to interact with $G\alpha_i$ and $G\alpha_q$ subunits (reviewed in (110)).

RGS proteins also undergo phosphorylation which can either enhance or inhibit GAP activity, based on the RGS and kinase involved. For example, RGS2 phosphorylation by protein kinase C (PKC) reduces its GAP activity, thus resulting in the increase of Gq/11 signals (111). Similarly, phosphorylation of RGS16 by an unknown kinase reduced its GAP activity (112). These examples of phosphorylation represent a positive feedback loop to enhance receptor signals. On the other hand, the GAP activity of RGS-19 is increased by ERK-mediated phosphorylation, resulting in negative feedback regulation of ERK activation (113). Phosphorylation along with ubiquitination can also change the stability of RGS protein. This is evident for RGS7 which is subject to ubiquitination mediated proteasomal degradation and has a short half-life. However, phosphorylation of a p38-recognition motif on RGS7 dampens its proteolysis, probably due to the stabilizing effect provided by an interacting partner (reviewed in (110)).

Thus, PTMs offer alternate regulatory mechanisms for G protein signaling; continued search and understanding of which can have important implications in the successful development of therapeutic targets. Indeed, constant addition of new PTMs from studies done in humans as well as model organisms, using traditional biochemical techniques as well as modern techniques such as mass spectrometry, have enormously contributed to the field.

1.5 Yeast as a model organism

The budding yeast, *Saccharomyces cerevisae,* is a powerful model organism for studying fundamental aspects of eukaryotic cell biology, including the G-protein signaling system responsible for the mating process(114). Indeed, the studies done in yeast played a significant role in establishing many signaling landmarks and paradigms, including the prototype RGS protein, Sst2(49,92,115,116). Furthermore, *Saccharomyces cerevisae* has been instrumental in understanding the roles of many PTM-based regulators including phosphorylation mediated regulation (117–119). Several aspects of yeast make it an attractive model to study G protein signaling system- (1) The G protein signaling pathway in yeast is very well characterized. Importantly, the pathway activation can be easily monitored with long established assays that probe into various steps in the pathway. (2) Many of the yeast proteins including G proteins have mammalian orthologs, which broadens the relevance of studies done in yeast to humans. (3) The yeast genome is fully sequenced and annotated. (4) The ease of genetic manipulation of yeast facilitates analysis of gene knockouts and point mutants. (5) Yeast can be used for large- scale protein expression and purification that facilitates proteomic studies(120).

1.5.1 The yeast mating pathway as a model for G protein signaling- The G-protein signaling system in yeast mediates the mating response, wherein the two mating types - MAT**a** and MATα, fuse to form a diploid cell. This process is triggered by the binding of pheromones - a-factor and α-factor secreted by MAT**a** and MATα respectively - to its specific GPCRs. The α-factor binds to Ste2 expressed only on Mat**a** cells; whereas a-factor binds to Ste3 expressed only on Matα cells(121). As with other G protein systems, receptor activation upon binding of a ligand (pheromone) stimulates the exchange of GDP to GTP on Gα (Gpa1) and dissociation of Gα (Gpa1) and Gβγ (Ste4/Ste18). The dissociated Gβγ (Ste4/Ste18) interact with multiple effector proteins, of which three key effectors are (i) the scaffold protein, Ste5 (ii) the p21-activated kinase Ste20, and (iii) the Cdc24/Cdc42/Far1 complex. Together, these interactions lead to the flow of information via the sequential activation of the four-tiered kinase cascade to nuclear transcription factors and other targets. The process culminates in the expression of about 200 mating-specific genes (about 3% of the genome), arrest in the G1 phase of the cell-cycle, oriented growth (shmoos) towards the mating partner, and eventually fusion of the two mating cells. This entire process is well regulated and takes about 4h(121,122).

Upon pheromone stimulation, the free Ste4/Ste18 interacts with Cdc24, the GEF for the small Ras like protein Cdc42. This interaction is abridged by a scaffold protein Far1(123,124). Both Far1 and Cdc24 shuttle between the nucleus and cytosol; and are sequestered in the nucleus in the absence of pheromone. On pheromone stimulation, Far1-Cdc24 accumulates in the cytosol and localize at the shmoo tip along with Ste4/Ste18; serving as a landmark for orienting the cytoskeleton during the polarized growth, presumably by generating a highly localized GTP-bound Cdc42(125–127). The exchange of GDP to GTP on Cdc42 facilitates its interaction with Ste20, which serves the dual role of localizing Ste20 to the membrane and activating the kinase(128). Moreover,

the direct interaction between Ste20 and Ste4/Ste18 also aids the localization of Ste20 to the membrane(129,130). Activation of the Ste20 triggers sequential activation of Ste11(MAPKKK), Ste7(MAPKK), Fus3(MAPK), and Kss1(MAPK). This three-tiered signal transduction module known as MAPK cascade, which is conserved throughout the eukaryotes, was first discovered in yeast. In yeast, a significant fraction of the pool of Ste11, Ste7, and Fus3 are bound to the scaffold protein, Ste5. Like Far1, Ste5 is present in the nucleus in the absence of pheromone stimulus and is exported to the cytosol after exposure to pheromone(115,131–133). Physical interaction between the RING domain of Ste5 and Ste4/Ste18, along with the interaction of PM and PH domains with the plasma membrane, localizes Ste5 to the membrane(134–136). This localization brings the MAPK cascade module in close vicinity to Ste20, thus, facilitating the sequential flow of activation from Ste20 to Ste11, Ste7 and finally to the mating-specific MAPK, Fus3 as well as the unscaffolded MAPK, Kss1. Fully-activated Fus3 is phosphorylated at two sites, T180 and Y182 (referred to here as di-phosphorylated or activated Fus3); and drives the mating process by phosphorylating many downstream effectors, primarily the transcription factor, Ste12 and the scaffold protein, Far1 (137). Ste12 induces the transcription of genes required for mating, whereas Far1 enables cell-cycle arrest and proper shmoo formation. Upon phosphorylation by Fus3, Far1 acts as a cyclin-dependent kinase (CDK) inhibitor and blocks exit from G1 phase of the cell cycle(138,139). The arrest of cells in G1 ensures all cells have only one copy of their genetic material prior to conjugation, thereby preventing aneuploidy. In parallel, the pheromone-dependent localization Far1 to the membrane, where the Ste4/Ste18-Far1-Cdc24-Cdc42 complex establishes a site for polarized growth by recruiting polarity proteins(124,127). All these events are highly coordinated and regulated at various levels. Several proteins and PTM-based regulators participate in the regulation of the G-protein signaling system, including a secreted protease (Bar1) that destroys α-factor pheromone(140,141), enzymes that modify

(ubiquitinate, phosphorylate) the pheromone receptors and promote their internalization(142,143), GAPs for both Gpa1Gα (Sst2) (49) and Cdc42 (Bem3, Rga1, Rga2)(144), and phosphatases (Msg5, Ptp2, Ptp3) that deactivate Fus3(145,146).

Recent studies have also uncovered the unexpected role of the scaffold protein, Ste5, in restricting the mating pathway output. This inhibition is mediated by a partially phosphorylated form of Fus3, which is allosterically auto-phosphorylated at Y182 upon binding to the Fus3 binding domain (FBD) of Ste5(147). Additionally, Ste5 harbors four MAPK sites (T267, S276, T287, and S329), very close to a Fus3 binding domain (FBD) and proximal to the RING domain which binds to Ste4/Ste18. When phosphorylated by the mono-phosphorylated Fus3, these sites negatively regulate full activation of Fus3 and the pheromone response(148). Inhibitory phosphorylation at these sites is presumably short lived as the phosphatase, Ptc1, competes with Fus3 for access and de-phosphorylates the inhibitory sites, enabling complete pathway activation(149) (Figure 1.2). However, the exact mechanism by which Ste5 phosphorylation mediates the negative regulation is still unknown.

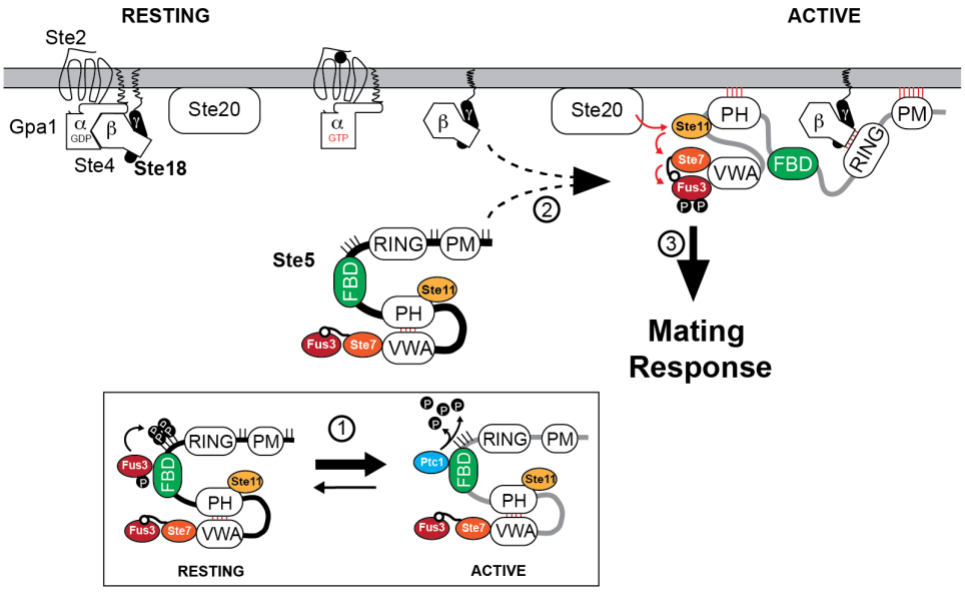

Figure 1.2 Working model of the mating pathway of *Saccharomyces cerevisae*. To facilitate clarity, a contemporary model of the pheromone pathway is shown here, which is inferred from prior studies described in the text. The mating pathway of *Saccharomyces cerevisae* is triggered in response to pheromone-dependent activation of the G protein coupled receptor, Ste2 and subsequent recruitment of Ste5 to the plasma membrane (PM), mediated by $Ste5^{PM}$ and $Ste5^{PH}$ domains as well as the $Ste5^{RING}$ domain that binds directly to free Gβ/Ste4. Under resting conditions, Ste5/PM association and MAPK activation is disfavored due to hyper-phosphorylation at positions surrounding $Ste5^{PM}$ (sites marked as sticks), auto-inhibition of the $Ste5^{PH}$ domain through a competitive interaction with $Ste5^{VWA}$, and the lack of free Gβ/Ste4 that is sequestered by GDP-bound Gα/Gpa1. Pathway activation is also inhibited by the $Ste5^{FBD}$, which allosterically activates Fus3 to promote phosphorylation of $Ste5^{T287}$ and three other phosphosites proximal to $Ste5^{FBD}$ and $Ste5^{RING}$ (P-lollipops). Upon pheromone stimulation, cascade activation of MAP kinases relies on PM recruitment and stable association of Ste5 that is concomitant with several state changes including (but not limited to): (1) up-regulated expression of the phosphatase Ptc1, which competes with Fus3 for binding to $Ste5^{FBD}$ and promotes Ste5 de-phosphorylation; (2) a large conformational change in Ste5 accompanied by de-inhibition of $Ste5^{VWA}$; and (3) MAPK cascade activation of Fus3 and Kss1. For simplicity, interactions involving proteins such as Ste20, Far1, Cdc42, Cdc24 and many more involved in shmoo formation are not shown. Central components of the model discussed extensively here as a framework for this work include the $Ste5^{FBD}$ and phosphoregulatory control by Fus3 and Ptc1 captured in part by (116,147,149), conformational dynamics and PM association of Ste5 captured in part by (150,151), and the role of Gβγ/$Ste5^{RING}$ as an essential feature for Ste5/PM association captured in part by (134). Several more contributions have been cited in the main text.

1.5.2. Co-ordination between the mating pathway and other pathways- Yeast live in a dynamic environment and must coordinate multiple external and internal cues to make proper cell fate decisions. While stress conditions, such as an increase in external osmolarity (referred to as hyperosmotic stress), or depletion of glucose (nutrient stress) are common external stimuli; the phase of the cell cycle is an important internal clue. Both the stress signals and the cell-cycle cues are often co-integrated with mating signals. Thus, the yeast mating pathway serves as a unique model to study signal integration and cross-talk with other pathways (88,127,139,152,153).

One such pathway is the HOG pathway which responds to hypersosmotic stress, and is composed of two independent branches, *SHO1* and *SLN1*. Both of these branches converge on the MAPKK, Pbs2, which also serves as a scaffold for the upstream

MAPKKKs and the downstream MAPK, Hog1. Like the mating pathway, the HOG pathway employs a three-tiered kinase cascade consisting of sequential activation of Ste11 (MAPKKK), Pbs2 (MAPKK) and finally Hog1 (MAPK)(154,155). Activated Hog1 phosphorylates several cytoplasmic and nuclear targets to ensure rapid adaptation to hyperosmotic conditions, including the activation of a glycolytic enzyme Pfk26 that is involved in the production of glycerol precursors. In fact, glycerol accounts for 95% of the solute accumulated during stress recovery(155,156). On the other hand, yeast adapts to nutrient limitation by adopting an altered morphological growth pattern referred to as filamentation(157). Interestingly, several components are shared between the HOG, filamentation, and the mating pathway; despite which the fidelity of the signal transduction pathway is maintained(154). Alternatively, cross-talk between these pathways ensures that stress response takes priority over mating during co-stimulation, by inhibiting the mating pathway via phosphorylation of key proteins in the signaling cascade. For instance, activated Hog1 inhibits the mating response by phosphorylating a protein kinase Rck2 and the adaptor protein Ste50, thereby inhibiting pheromone induced protein translation and dampening Fus3 (mating specific MAPK) activation(118,119).

The mating signal is also integrated with the cell division status of individual cells. Indeed, mating pheromones induce a growth arrest at the G1 phase of the cell cycle only. Whereas, cells that have already passed the G1/S or “start” checkpoint, are refractory to pheromone arrest. While the inhibitory action of Far1 on Cdc28 is responsible for the growth arrest(138,158); the repression of pheromone signaling relies on the degradation of Far1 in a G1-cyclin (Cln1/2) dependent manner(159). Additionally, the G1/CDK activity phosphorylates a cluster of sites flanking the PM (plasma membrane binding) domain of Ste5, thereby disrupting the localization of Ste5 at the membrane, which is otherwise

critical for activation of the mating pathway(158). The Gα subunit, Gpa1, is also phosphorylated and ubiquitinated in response to cell cycle changes(88).

Thus, stress response pathways as well as cell-cycle delay mating under suboptimal conditions, primarily through mediating post-translational modifications of multiple pathway components, identification of which continues to add insight into the mechanism.

1.6. Overview of the dissertation

In Dewhurst et.al., SAPH-ire (our in-house PTM-prioritization tool) was employed to reveal novel PTM regulatory elements in discrete protein families including the heterotrimeric G-proteins (160). This study revealed that N-terminal tail (Nt) of G protein gamma (Gγ) subunits contain phosphorylation hotspots which have a high likelihood to have regulatory/impactful biological function (160). However, any correlation of these phosphorylation sites with a biological function was missing.

1.6.1. State-of-knowledge of the Gγ subunits (prior to this work) - In comparison to the precisely ascribed signaling roles of Gα subunits, those of Gβ and Gγ are rarely distinguished independently due to their obligate heterodimeric interaction. Within this context, Gγ subunits have essential functionality as membrane anchors for Gβ subunits, mediated through prenylation of cysteine residues in their C-terminal tails(35,161,162). Beyond this role, any additional signaling attributes of Gγ subunits have remained somewhat elusive. Moreover, the structure of Gγ subunits is significantly disordered (between 15% - 40%), and therefore unresolved by x-ray crystallography studies(160).

The vast majority of intrinsic disorder in Gγ subunits is contained within the N-terminal region of all Gγ subunits throughout eukarya(160). Intrinsically disordered regions are often hotspots for PTMs, and PTM-dependent regulation is essential for G protein signaling. Structural analysis of PTM hotspots observed across all eukaryotic members of the Gγ protein family recently revealed that Gγ subunits, including yeast Ste18, exhibit PTM loads (number of PTMs observed relative to the residue length of the protein) 2-fold greater than any other signaling component, including GPCRs, RGS proteins, Gα and Gβ subunits. Furthermore, nearly half of all Gγ PTMs (41%) are condensed within the N-terminal tail, which harbors 5-fold greater PTM load compared to the rest of the protein. Phosphorylation is the predominant modification in Gγ subunits, nearly 60% of which are also found in the N-terminal tail. Finally, all Gγ subunits harbor at least 2 serine or threonine residues in the tail region. However, the functional significance of the phosphorylation on the N-terminal tail of Gγ subunits is unknown(160).

1.6.2 Hypothesis and overview of main dissertation - This dissertation is founded on the broad hypothesis that the unstructured N-terminal tails of Gγ subunits act as a phospho-regulator of G protein signaling. We tested this hypothesis in the eukaryotic model organism, *Saccharomyces cerevisae*, which harbors a single canonical G-protein signaling system that controls mating(121). As one of the most well-studied signaling pathway, the yeast mating pathway has been and continues to be instrumental in the discovery of various regulatory elements including the RGS protein and several PTM-based regulators(80,87,88,92,163,164).

The study presented in chapter 2 interrogates the role of Gγ subunit N-terminal tail, Ste18-Nt, in the feedback regulation of the mating pathway. We show that Ste18-Nt is dynamically and rapidly phosphorylated in response to GPCR activation in a Fus3-

dependent manner. Furthermore, we show that the phosphorylated Ste18-Nt, together with the inhibitory phosphorylation of the scaffold protein, Ste5, constitute a negative regulatory system that synergistically controls the activation of the MAPKs, Fus3 and Kss1. Moreover, phosphorylation of Ste18 and Ste5, weaken the binding between $G\beta\gamma$ and Ste5 and also prevent rapid and stable association of Ste5 at the plasma membrane. Elimination of this phosphor-inhibitory complex via point mutations on Ste18 and Ste5 results in ultra-rapid and robust Fus3 activation and Ste5/PM recruitment. These results provide support for the broad hypothesis that $G\gamma$ N-terminal tails function as intrinsically disordered PTM regulatory elements in G protein signaling systems, and also further resolve the underlying mechanism of feedback inhibition of the pathway.

In chapter 3, we explore the possible role of phosphorylated Ste18-Nt in regulating cross-talk with stress-response pathways, such as osmotic and glucose stress. Here we show that Ste18-Nt undergoes phosphorylation in response to multiple independent stimuli such osmotic stress, and cell-cycle progression, including the previously described GPCR activation. Moreover, unlike the pheromone stimulated phosphorylation of Ste18-Nt, the phosphorylation events in response to osmotic stress and cell-cycle were independent of Fus3. However, no effect of glucose deprivation was seen on Ste18 phosphorylation. Extrapolating from the evidence for the inhibitory phosphorylation of Ste18, we propose a model in which phosphorylation of the intrinsically disordered N-terminal tail of Ste18 inhibits premature activation of the mating pathway in conditions of osmotic stress and inappropriate cell-cycle stage.

CHAPTER 2

NEGATIVE FEEDBACK PHOSPHORYLATION OF Gγ SUBUNIT STE18 AND THE STE5 SCAFFOLD SYNERGISTICALLY REGULATES MAPK ACTIVATION IN YEAST

2.1 ABSTRACT

Heterotrimeric G proteins (Gαβγ) are essential transducers in G protein signaling systems in all eukaryotes. In yeast, G protein signaling differentially activates mitogen-activated protein kinases (MAPKs) – Fus3 and Kss1 – a phenomenon controlled by plasma membrane (PM) association of the scaffold protein Ste5. Here we show that phosphorylation of the yeast Gγ subunit (Ste18), together with Fus3 docking on Ste5, control the rate and stability of Ste5/PM association. Disruption of either element alone by point mutation has mild but reciprocal effects on MAPK activation. Disabling both elements results in ultra-fast and stable bulk Ste5/PM localization and Fus3 activation that is 6-times faster and 4-times amplified compared to wild type cells. These results further resolve the mechanism by which MAPK negative feedback phosphorylation controls pathway activation and provides compelling evidence that Gγ subunits can serve as intrinsic regulators of G protein signaling.

2.2 INTRODUCTION

Canonical G protein signaling systems – including 7-transmembrane G-protein coupled receptors (GPCRs), heterotrimeric G-proteins (Gαβγ) and diverse effector proteins – comprise a highly conserved system enabling the transduction of extracellular

signaling molecules such as hormones, neurotransmitters, and chemokines (11,165). As one of the primary signal transduction mechanisms in eukaryotes, G protein signaling pathways control a wide range of processes in both single-cell and multi-cellular organisms such as yeast and humans (166–170). Owing to their high degree of structural conservation, fundamental mechanisms underlying the regulation of G protein signaling have emerged from empirical studies conducted across widely diverse organisms from yeast to human. Such attributes have also helped to solidify their prominent role as pharmaceutical targets for the treatment of human disease (171).

The yeast model system for G protein signaling remains one of the most well-characterized signaling pathways in history, and has been instrumental in the discovery of G protein regulatory mechanisms including regulators of G-protein signaling (RGS) proteins, and post-translational modification (PTM) based regulators (49,87,172–179). In budding yeast *Saccharomyces cerevisiae*, a single canonical G protein signaling pathway controls the process of mating, wherein two yeast of opposite and complementary mating type, *MAT**a*** and *MAT*α, fuse to form an **a**/α diploid cell (180). As in the case of multicellular organisms including mammals, G protein signaling in yeast is initiated by agonist-dependent activation of a GPCR at the cell surface (180). In *MAT**a*** cells, a single peptide mating pheromone (α factor) serves as the agonist of the pheromone GPCR, Ste2, and upon binding promotes the exchange of GDP for GTP on the Gα subunit (Gpa1). GTP binding stabilizes a conformational change in Gα and dissociation of the heterotrimer into Gα and G$\beta\gamma$ (Ste4/Ste18) components (173,181). In yeast, G$\beta\gamma$ serves as the primary activator of the mating pathway whereas Gα serves primarily to sequester G$\beta\gamma$ (180). When not sequestered, G$\beta\gamma$ nucleates the formation of a protein complex at the plasma membrane that includes a p21-activated protein kinase (PAK; Ste20); a protein scaffold (Ste5) in complex with a MAPKKK (Ste11), MAPKK (Ste7), MAPK (Fus3), as well as

additional proteins important for cell polarization (182,183). Activation of the pheromone response pathway through this process drives a phosphorylation cascade resulting in double phosphorylation (referred to here as di-phosphorylation or activation) of $Kss1^{T183,Y185}$ and $Fus3^{T180,Y182}$ – highly conserved orthologs of the human MAPKs Erk1 and Erk2 – which phosphorylate several targets necessary for a complete mating response. Once activated, Fus3 translocates to the nucleus wherein it phosphorylates the transcription factor Ste12 and other proteins necessary to drive a gene transcription program resulting in morphological change, cell cycle arrest, and eventual mating (137,184). Signaling is terminated by hydrolysis of GTP to GDP on the $G\alpha$ subunit and re-association of the heterotrimeric complex, a process that is accelerated by the RGS protein (Sst2) (49).

Several aspects of pheromone pathway behavior – such as switch-like vs graded dose-responsiveness and differential activation of MAPKs Fus3 and Kss1 – have been linked directly to the Ste5 scaffold, which plays a major role in nearly all aspects of pathway control. Ste5 contains multiple domains that effectively tune the pheromone activation profile of Fus3, which binds to Ste5, distinctly from Kss1, which does not (Figure 1.2 in Chapter 1). The Fus3 binding domain (FBD) plays a critical role in this process by allosterically activating the autophosphorylation of $Fus3^{Y182}$ (referred to here as mono-phosphorylation) in a manner independent of pheromone stimulation (147). Mono-phosphorylated Fus3 phosphorylates $Ste5^{T287}$ and three other phosphosites proximal to the RING domain, which functions to inhibit full activation of Fus3 and the mating pathway (185). Inhibition is relieved in part by the action of the pheromone dependent phosphatase, Ptc1, which competes with Fus3 for FBD binding and dephosphorylates Ste5, failure of which (*ptc1Δ*) prevents activation of Fus3 (149).

Within the context of G protein signaling, Gγ subunits have been largely understood as membrane anchors for Gβ subunits, and rarely have been studied in any other context. Phosphorylation of Gγ12 has been shown to enhance the affinity of Gβγ for Gα subunits in vitro (186); and impact the activity of the Gβγ12 dimers toward specific effectors (187). Recently, we showed that Gγ subunits across all eukaryotes harbor at least 2 phosphorylation sites in their intrinsically disordered N-terminal tails, many of which have also been observed as phosphorylated in high throughput proteomics screens (188). Here, we show that the N-terminal tail of the yeast Gγ subunit, Ste18, together with the Fus3/Ste5^{FBD} docking interaction, constitute a negative regulatory system that synergistically controls the activation of Fus3 and Kss1 through a dynamic phospho-inhibitory mechanism that prevents rapid and stable association of bulk Ste5 at the plasma membrane. Disruption of either side alone (by point mutation of Ste18^{Nt} or Ste5^{FBD}) results in minor but significant and reciprocal changes to the rate and amplitude of Fus3 activation and Ste5/PM recruitment, whereas combined disruption of both elements results in ultra-rapid and robust Fus3 activation and Ste5/PM recruitment. We show that negative regulation is facilitated by weakened binding between Gβγ and Ste5 when both proteins are phosphorylated – a mechanism that may have emerged through co-evolution of the two distinct phospho-regulatory elements. Taken together, these data reveal a new way in which Gβγ/effector binding can be modulated to control signaling output through post-translational modification.

2.3 RESULTS

2.3.1 The N-terminal tail of Ste18 is rapidly phosphorylated in response to GPCR activation

Like other Gγ subunits throughout Eukarya, the terminal ends of Ste18, representing 20% of its residue content, are intrinsically disordered – most of which correspond to the N-terminal tail ($Ste18^{Nt}$). This region in Ste18 (residues 1-13) harbors phosphorylation sites at Thr-2, Ser-3, and Ser-7, specifically (188,189). Phosphorylation of $Ste18^{Nt}$ produces a distinctive electrophoretic mobility shift in response to pheromone stimulation, which can be detected by SDS-PAGE and immunoblotting (188). Treatment with alkaline phosphatase eliminates the mobility shift in a manner that depends on the presence or absence of phosphatase inhibitors (Figure A.S1A). Moreover, phospho-null mutations ($Ste18^{T2A,\ S3A,\ S7A}$; referred to here as $Ste18^{3A}$) and phospho-mimic mutations ($Ste18^{T2E,\ S3E,\ S7E}$; referred to here as $Ste18^{3E}$) eliminate or restore the mobility shift, respectively (188). To determine a precise estimate of phosphorylation kinetics early and late after receptor activation, we surveyed the phosphorylation-dependent mobility shift of Ste18 in both long and short time course experiments (Figure 2.1A, A.S1B). We found that phosphorylation occurs almost instantaneously after receptor activation and is readily detectable within 30 seconds (Figure 2.1B, A.S1B). Maximum phosphorylation is achieved at ~80% of total Ste18 levels within 3 minutes with a $t_{1/2}$ of 1.25 minutes (Figure 2.1B, inset). Phosphorylation remains stable for the duration of pheromone exposure up to 90 minutes. Activation profiles for Fus3 and Kss1 MAPKs were consistent with their expected patterns of activation at 3μM pheromone concentrations (Figure 2.1C) (190).

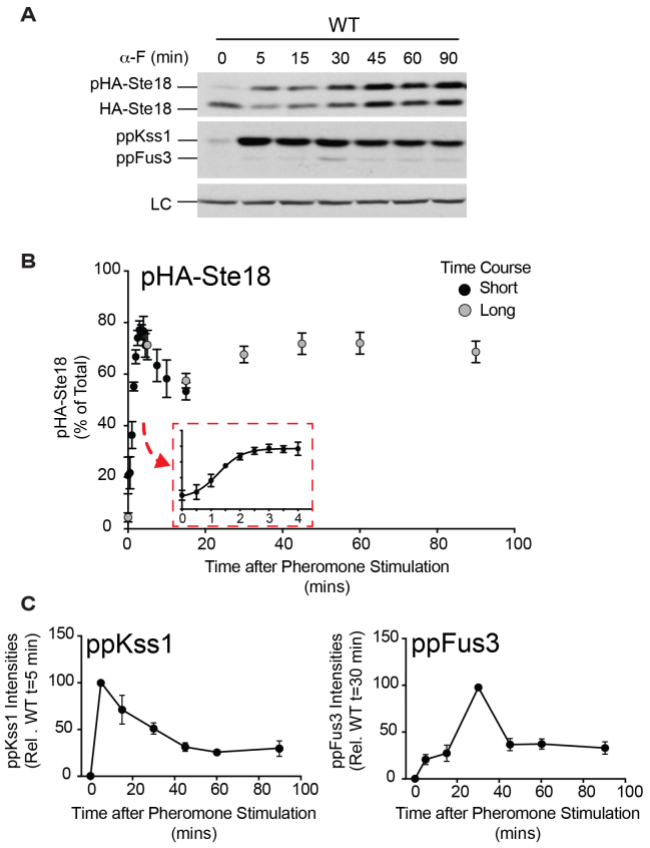

Figure 2.1. Ste18^{Nt} is rapidly phosphorylated in response to GPCR activation. (A) Immunoblots of HA-Ste18, activated MAPKs (ppKss1 and ppFus3), and a protein loading control (LC) in wild type cells treated with 3μM pheromone (α-F) for the indicated time (long time course). (B) Quantification of pHA-Ste18 over short (black circles) and long (grey circles) time course periods in wild type cells. Data correspond to the percent abundance of phosphorylated HA-Ste18-Nt (pHA-Ste18) relative to total HA-Ste18 (mean ± S.D.; n=12). Short- and long-time course data were normalized to each other at 5 minutes. (C) MAPK activation profile in wild type cells from the long-time course experiment shown in A.

Surmising that Ste18 phosphorylation may depend on a kinase within the pheromone pathway, we monitored Ste18 phosphorylation in cells lacking single components of the pathway including: Ste20, Ste11, Ste7, Fus3, Kss1, in addition to the MAPK scaffold Ste5. We found that all kinases upstream of and including the scaffolded MAPK complex were necessary for robust phosphorylation of Ste18^{Nt} in response to

pheromone (Figure A.S1C, D). Kss1, which is rapidly phosphorylated after receptor activation but is not scaffolded by Ste5, is not required for pheromone-dependent Ste18 phosphorylation. Since Ste18 phosphorylation should not be lost in *fus3Δ* cells if MAPKs upstream of Fus3 are responsible for phosphorylation, these data suggest that Fus3, but not upstream MAPKs are necessary. Other genes involved in the pheromone pathway that either regulate pheromone dependent kinase activation or are themselves pheromone-activated kinases had little to no effect when deleted from the genome (Figure A.S2). Taken together, these data demonstrate that Ste18 is rapidly phosphorylated in response to GPCR activation in a manner that requires Fus3.

2.3.2 Phosphorylation of $Ste18^{Nt}$ and Ste5 function synergistically to delay Fus3 peak activation in response to pheromone

Considering that Ste18 is rapidly phosphorylated within seconds of receptor stimulation, we hypothesized that it must be a pre-requisite for proper pathway activation. Consistent with this hypothesis, we found that preventing phosphorylation of Ste18 ($Ste18^{3A}$) resulted in a significant shift in peak activation of Fus3, which occurred twice as fast (15 minutes earlier) than in wild type cells (Figure A.S3 A,C). In contrast, activation of Fus3 and Kss1 in cells harboring the phosphomimic form, $Ste18^{3E}$, was no different from wild type cells, as would be expected if phosphorylation is a prerequisite feature required for normal pathway activation (Figure A.S3 A, B). Thus, Ste18 phosphorylation is required for delayed peak activation of the scaffolded MAPK Fus3 but has no effect on the activation of the un-scaffolded MAPK, Kss1.

Negative feedback phosphorylation of Ste5, like phosphorylation of Ste18, occurs early/before the mating response and also requires Fus3. Therefore, we hypothesized that both elements may function in concert to delay Fus3 peak activation. This hypothesis was inspired, in part, by two points of indirect evidence that converge on Fus3 as a negative

regulator of the pheromone response. First, rapid receptor-activated phosphorylation of $Ste18^{Nt}$ requires Fus3 (Figure A.S1), and activated Fus3 has been previously shown to counteract the stability of Ste5/PM association during the pheromone response (191). Second, Fus3-mediated negative feedback phosphorylation on Ste5 dampens the intensity of Fus3 di-activation in response to pheromone (190,192,193). Additionally, we considered as further evidence that stable Ste5/PM association is facilitated in part by the interaction of the $Ste5^{RING}$ domain ($Ste5^{138-214}$) with residues in Ste4 ($Ste4^{49-65}$) that are located in the coiled-coil structure formed by both Gβ (Ste4) and Gγ (Ste18) subunits and in very close proximity to where phosphorylation occurs in $Ste18^{Nt}$ (193).

To test the hypothesis, we monitored phosphorylation of Ste18, Kss1, and Fus3 in cells that endogenously express different combinations of Ste18 phosphosite and $Ste5^{FBD}$ docking site mutants. Precise mutation of multiple sites within two essential binding surfaces (A and B) in the $Ste5^{FBD}$ (a.k.a. $Ste5^{ND}$) prevents Fus3 docking, allosteric activation, and negative feedback phosphorylation of Ste5 (147). Interestingly, phosphorylation of $Ste18^{Nt}$ was unaffected by $Ste5^{ND}$, suggesting that Fus3 docking to Ste5 is not necessary for Ste18 phosphorylation (Figure 2.2. A, B). As observed in previous experiments, peak activation of Fus3 occurred significantly early in $Ste18^{3A}$ compared to $Ste18^{3E}$ or wild type cells (Figure 2.2. C, E), whereas Kss1 activation was unaffected (Figure 2.2. C, D). In contrast, we found that peak activation of Fus3 (at 30 min) and Kss1 (between 5-30 min) was significantly elevated but not early in $Ste5^{ND}$ cells harboring the wild type form of Ste18, an observation that is nearly identical with previously reported evidence (Figure 2.2. C-E) (190).

We made several unique observations with yeast harboring both Ste18 and Ste5 mutations in combination. First, peak activation of Fus3 occurs rapidly in $Ste18^{3A}$/$Ste5^{ND}$ cells, wherein neither protein can be phosphorylated (Figure 2.2. E, Table A.S2). Significantly, this response was 25 minutes earlier and nearly 1.5-fold greater in amplitude

than observed for Ste5ND alone and 3.6-fold greater than the response in wild type cells (Figure 2.2. E, Table A.S2). Neither this nor any other mutant showed abrupt differences in the pattern of pheromone-dependent Fus3 expression level compared to wild type cells, suggesting that differences in the intensity of activated Fus3 at early time points is due to Fus3 phosphorylation and independent of Fus3 expression (Figure A.S4A). Interestingly, Ste18^{3A}/Ste5ND, but not other cell types also exhibited morphological defects in the absence of pheromone, showing pronounced elongation in multiple cases (Figure A.S4B). Second, in cells harboring the combination of Ste18^{3E} and Ste5ND, Fus3 peak activation occurs early (15 min) and with no change in amplitude – nearly identical to the response in Ste18^{3A}/Ste5^{WT} cells and indicative that phosphorylation restricted to either Ste18 or Ste5 is sufficient to elicit an equivalent outcome in Fus3 peak activation (Figure 2.2. E, Table A.S2). Complementary phos-tag analysis of Fus3 phosphorylation further suggest that either Ste18^{Nt} phosphorylation or Ste5 phosphorylation (controlled by Fus3 docking on Ste5), can effectively inhibit the aberrant di-phosphorylation of Fus3 in the absence of pheromone (Figure A.S5). Moreover, preventing such control on both proteins together results in aberrant Fus3 di-phosphorylation in the absence of pheromone. Unexpectedly, activation of Kss1 was also affected by combined disruption of Ste18/Ste5. However, in contrast to Fus3, Kss1 becomes hyper-activated in Ste18^{3E}/Ste5ND cells (Figure 2.2. D). Further confirmation of these results was achieved by endpoint immunoblot assays conducted within the first 15 minutes of pheromone stimulation (Figure A.S4C-E).

Evidence from MAPK activation analysis suggested that Ste18 and Ste5 phosphorylation behave synergistically such that the combined effect of both produces an effect that is greater than the sum of their separate effects. Indeed, a quantitative test for synergy revealed that phosphorylated Ste18/Ste5 are synergistic in their control of Fus3 peak activation time, but additive in their control of Fus3 peak amplitude, with an overall synergistic impact that is ~4x greater than the sum of effects contributed by Ste18 or Ste5

alone (Table A.S2). Taken together, these data suggest that phosphorylation of Ste18 and MAPK docking/phosphorylation of Ste5 (heretofore referred to as the Ste18/Ste5 phospho-inhibitory system) synergize to delay the activation and repress the amplitude of Fus3 activation in response to pheromone.

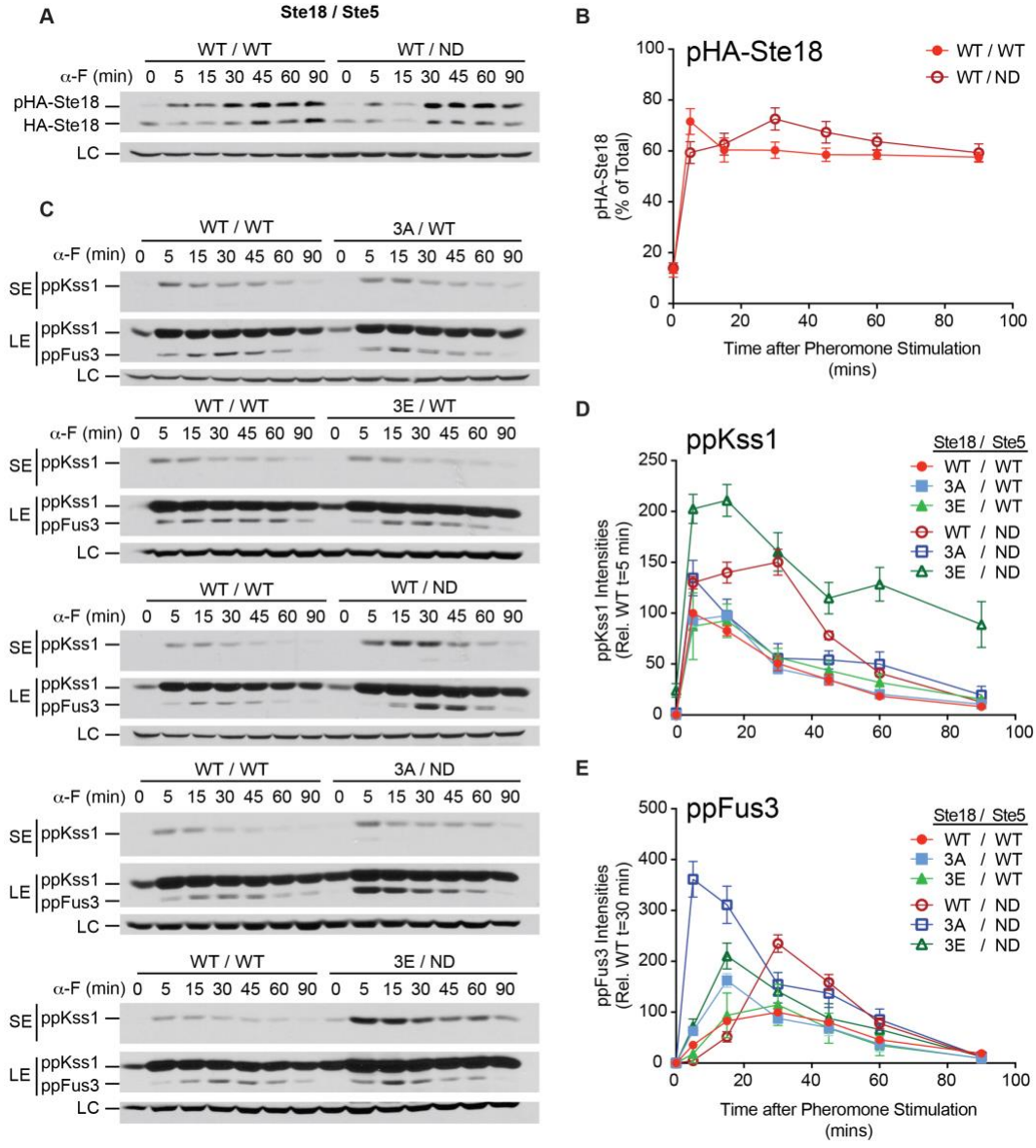

Figure 2.2. Phosphorylation on Ste18 and Ste5 cooperate to prevent early and maximal Fus3 activation. Cells harboring the indicated combination of wild type or mutant versions of Ste18 and Ste5 were stimulated with 3μM α-F followed by quantitative immunoblot analysis of HA-Ste18 or activated Fus3 and Kss1. (A) HA-Ste18 immunoblot in cells harboring wild type (WT/WT) or $Ste5^{ND}$ (WT/ ND). (B) Quantitative comparison of pHA-Ste18 from A (n=4) (C) Representative immunoblot for activated Kss1 and Fus3. (D) Quantitative comparison of activated Kss1 relative to wild type peak activation at 5 minutes from immunoblots shown in C. (E) Quantitative comparison of activated Fus3 relative to wild type peak activation at 30 minutes from immunoblots shown in C. (Mean ± S.D., n=12) (SE: short exposure, LE: long exposure, LC: loading control)

2.3.3 Together, Ste18/Ste5 phosphorylation delays bulk recruitment rate and reduces the duration of Ste5/PM association

Activation of Fus3 requires recruitment and stable association of Ste5 with the plasma membrane, and consequently, mutations that disrupt or enhance Ste5/PM association should be reflected by the kinetics and amplitude of Fus3 activation. To test this hypothesis, we monitored Ste5/PM association by fluorescence microscopy before, during, and after pheromone stimulation of yeast cells. We were unable to detect Ste5-GFP at the PM in any cell that was not treated with pheromone (Figure 2.3. A, top). However, in as few as 23-26 minutes after pheromone stimulation, we observed robust PM accumulation of Ste5-GFP in all cell types – most noticeably in $Ste18^{3A}$/$Ste5^{ND}$ cells (Figure 2.3. A, bottom). Consistent with our hypothesis, preventing phosphorylation on both Ste18 and Ste5 ($Ste18^{3A}$/$Ste5^{ND}$) resulted in robust accumulation of Ste5-GFP at the PM after 25 minutes of pheromone stimulation, reaching a level nearly 7-fold greater than that of wild type cells measured at the same time (Figure 2.3. B). However, no differences were observed in the protein levels of Ste5-GFP (Figure A.S6). Thus, the Ste5-GFP signal at the membrane reflects altered Ste5/PM accumulation rather than protein stability. Furthermore, these data suggest that the bulk recruitment rate of Ste5 to the PM – reflected in the number of Ste5-GFP molecules that accumulate at the PM per unit time

(i.e. total fluorescence intensity/time) – is significantly faster when phosphorylation on both proteins is prevented.

To compare the relative rates and stability of Ste5-GFP/PM accumulation at the population level, we quantified the percentage of the cell population with Ste5-GFP localized at the PM as a function of time. Measured in this way, Ste5/PM accumulation data is more comparable to MAPK activation data, which is a population-based analysis. Preventing phosphorylation on both Ste18 and Ste5 ($Ste18^{3A}/Ste5^{ND}$) significantly enhanced the rate at which the population of cells exhibited Ste5-GFP/PM accumulation, where 100% of the cells were responsive by 14 minutes (Figure 2.3. C, D). This effect was reverted to a wild type state in $Ste18^{3E}/Ste5^{ND}$ cells, mimicking the effects of reciprocal mutations on MAPK activation seen earlier. In contrast, $Ste5^{ND}$ cells exhibited an intermediate phenotype. As expected, mutations to Ste18 alone had mild average effects on Ste5-GFP/PM accumulation.

Lastly, we also observed that Ste5/PM association was noticeably more stable in $Ste18^{3A}/Ste5^{ND}$ cells compared to all other strains, whereby the population of $Ste18^{3A}/Ste5^{ND}$ cells had maximal association for the longest time (141 minutes) compared to that of wild type or $Ste18^{3E}/Ste5^{ND}$ cells (Figure 2.3. E). In support of the hypothesis that this is promoted by more stable association between Ste4/18 and Ste5, co-immunoprecipitation (co-ip) experiments revealed significantly more (2-5x) Ste18 immunoprecipitated with Ste5-GFP in $Ste18^{3A}/Ste5^{ND}$ cells compared to all other cell types (Figure 2.3. F, G). We conclude that rapid bulk recruitment of Ste5 to the PM and subsequent Fus3 activation in $Ste18^{3A}/Ste5^{ND}$ cells can be attributed in part to greater physical association between the two proteins in their non-phosphorylated states, and support evidence that phosphorylation of $Ste18^{Nt}$ and Ste5 together control bulk rate and stability of Ste5/PM association and MAPK activation.

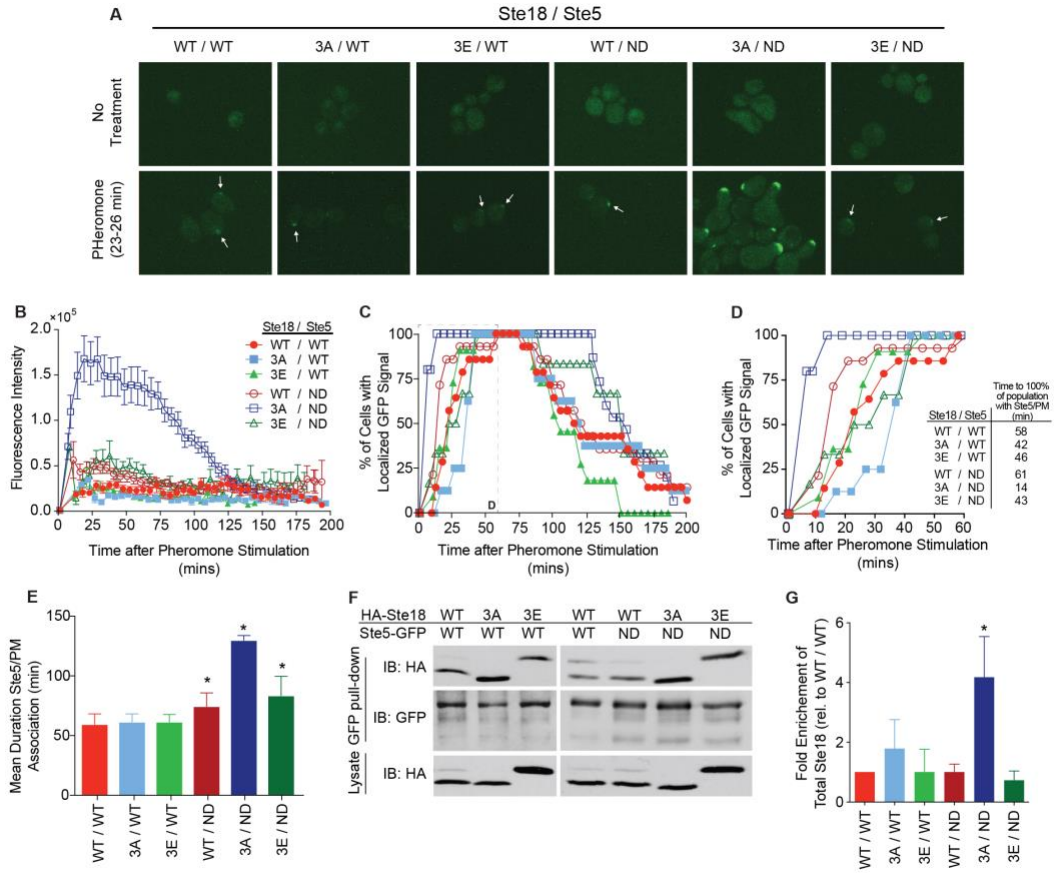

Figure 2.3. Phosphorylation on Ste18/Ste5 regulates the rate and duration of Ste5 association at the plasma membrane. Cells expressing phosphorylation mutants of Ste18 with either Ste5-GFP or Ste5ND-GFP were treated with α-factor to examine Ste5 localization by fluorescence microscopy (see Experimental procedures). (A) Representative fluorescent images showing cells with localized GFP signal at the membrane before (top) or 23-26 min post-pheromone treatment (bottom). (B) Quantification of total Ste5-GFP fluorescence at the shmoo tip in cells treated with pheromone. (C) Time-resolved percentage of the cell population with Ste5-GFP localized at the plasma membrane in response to pheromone stimulation. (D) Zoomed view of the first 60 minutes from panel C. (inset) Time required before 100% of all cells display Ste5-GFP at the shmoo tip. (E) Mean duration of Ste5-GFP/PM association (at the site of an emerging or extant mating projection). (F) Immunoblot showing co-immunoprecipitation of HA-Ste18 with Ste5-GFP from pheromone treated cells. The lysate shown is 4% of the total lysate used for co-ip (see Experimental Procedures). (G) Quantitative analysis of immunoblots from co-ip in F. Bars represent fold-enrichment of total HA-Ste18 relative to wild-type (Mean ± S.D., n=3). All microscopy data represents GFP signal scored in 8-14 cells with error bars depicting SEM in panel B.

2.3.4 Ste18^{3E} partially restores a switch-like mating response in Ste5ND cells

Ste5 has been shown previously to be an important control point for the switch-like morphological response, which in wild type cells is controlled by competitive Ste5^{FBD} docking by Fus3 and the phosphatase Ptc1 (149). Consequently, non-docking Ste5ND mutants, which cannot bind to either Fus3 or Ptc1, exhibit a graded morphological dose-response. We hypothesized that Ste18 phosphorylation might also be involved in controlling the switch-like mating decision. To test this hypothesis, we performed microscopy-based dose-response experiments to quantify shmoo formation as a function of pheromone dose. Modeling the data with a sigmoidal dose-response curve with variable slope, we confirmed that wild type cells exhibit switch-like dose-responsiveness with a hill slope well above 1 (n_H^{WT} = 6.2) (Figure 2.4. A & Table A.S3). Similarly, Ste18^{3A} and Ste18^{3E} cells were also switch-like (n_H^{3A} = 6.3; n_H^{3E} = 3.7). We observed that Ste5ND cells are graded rather than switch-like (n_H^{ND} = 0.97), consistent with previous reports (116,149) (Figure 2.4 B & Table A.S3). Disabling both regulatory elements (Ste18^{3A}/Ste5ND) produced a slightly more graded response ($n_H^{3A/ND}$ = 0.85), exhibiting a hillslope lower than Ste5ND. Not surprisingly, Ste18^{3A}/Ste5ND cells also exhibited an elevated basal response that was ~3-fold greater than that of wild type cells, consistent with earlier results showing elevated Fus3 activation in these cells (Figures 2.2, A.S4B,C, A.S5). Expression of the phosphomimic form of Ste18 in the Ste5ND background (Ste18^{3E}/Ste5ND) resulted in a reversion of the analogue response in Ste5ND cells back to a switch-like state ($n_H^{3E/ND}$ = 2.7) (Figure 2.4. B & Table A.S3). Taken together, these data suggest that phosphorylation on Ste18 regulates the morphological mating switch in cells when Ste5 is incapable of docking with Fus3. Furthermore, these data suggest that Ste18/Ste5 phosphorylation regulates the switch-like mating decision in yeast.

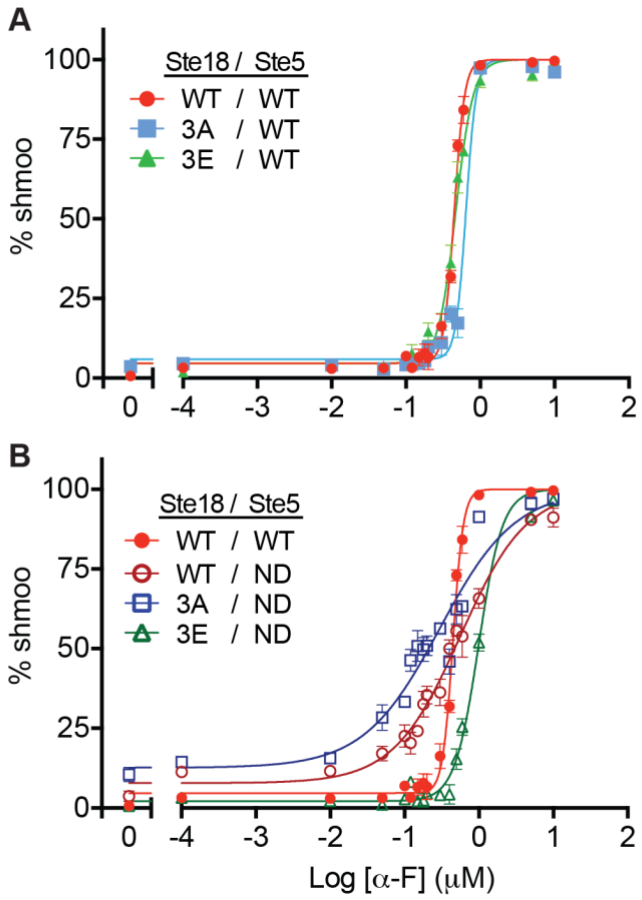

Figure 2.4. The switch-like morphological response to pheromone is regulated by Ste18-Nt phosphorylation when Fus3 cannot bind to Ste5. The morphological dose-response to mating pheromone represented by the cellular formation of a mating projection (i.e. shmoo) was quantified as a percentage of total cells in a population by DIC microscopy. Data were fit to a sigmodal dose-response curve with variable slope. (A) Effect of individual $Ste18^{Nt}$ phosphorylation mutations on the mating response. (B) Effect of $Ste18^{Nt}$ phosphorylation mutations in strains exclusively expressing the Fus3 non-docking mutant $Ste5^{ND}$. Error bars represent SEM across ≥ 200 cells per experiment.

2.3.5 Phosphorylation of the Gγ subunit and MAPK docking on Ste5 appear simultaneously in the phylogeny of yeasts

Recent phylogenetic and experimental evidence has revealed that the Ste5 FBD domain arose ~130 million years ago and is almost exclusively found in the clad to which *Saccharomyces cerevisiae* belongs, but is also partially extant in *V. polyspora* species, which contain a partial FBD that is moderately active (116). Having determined that the phosphorylation of the N-terminal tail of Ste18 and the Ste5^{FBD} function synergistically to control signaling, we asked whether these two structural elements may have co-evolved. Comparison of the phylogeny of Ste18 and Ste5 fungal orthologs revealed compelling evidence in support of this hypothesis. Indeed, the appearance of the phosphorylation sites in the Ste18 intrinsically disordered region (phospho-IDR) coincides with the appearance of Ste5^{FBD} (Figure 2.5 A, A.S7A). Furthermore, all extant members of the clad retain nearly 100% identity for sites of phosphorylation and MAPK binding that are essential to either element (Figure 2.5 B). A somewhat similar putative phospho-IDR was also found in the Ste18 ortholog from *S. castellii* and the distantly related *Y. lipolytica*, both species of which harbor 2 of the 3 phosphosites observed in *S. cerevisiae*, but exhibit dramatically different N-terminal IDR lengths (Figure A.S7B). When looking strictly within the phylogeny of Ste5-containing yeast species (excluding *A. gossypii*, which harbors an extraordinarily long N-terminal IDR), we observed a progressive lengthening over time of the N-terminal IDRs of Ste18 orthologs, culminating in a dramatic increase of 8-10 amino acid residues that appeared coincidently with the Ste5^{FBD} (Figure A.S7C). Taken together, these data suggest that Ste18 and Ste5 phospho-regulatory elements arose at similar times and appear only once in the evolution of budding yeast.

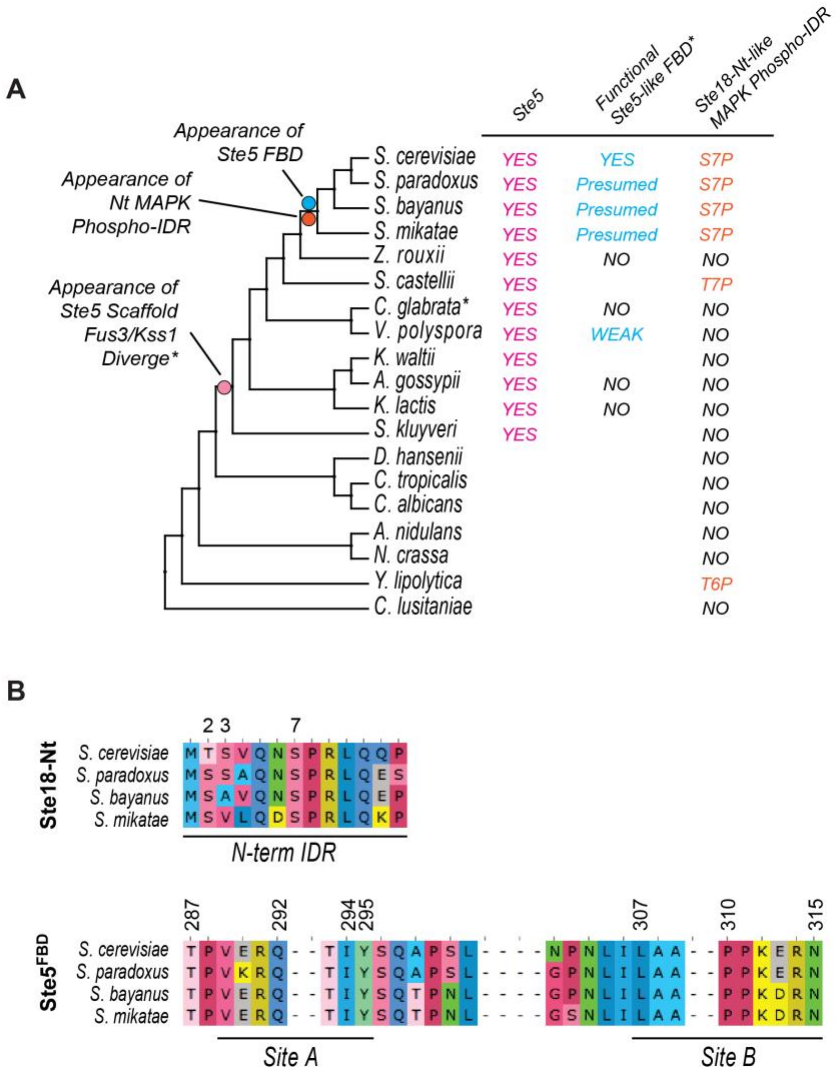

Figure 2.5. Coordinated phospho-regulation of Ste18 and Ste5 evolved at the same time. (A) Bootstrapped phylogenetic tree of Ste18 orthologs from the Ascomycota phylum showing the evolutionary co-occurrence of regulatory phosphorylation sites on the N-terminal tail of the Gγ subunit and the FBD of orthologous Ste5 scaffolds. The presence of Ste5 orthologous proteins, functional Ste5-like FBDs, and N-terminal Gγ phospho-regulatory intrinsically disordered regions (IDRs) are shown next to yeast species harboring each element. (B) Species that contain the synergistic regulatory element ($Ste18^{Nt}$ and $Ste5^{FBD}$) are nearly 100% identical at phosphorylation site alignment positions in Ste18 and MAPK binding sites reported previously in Ste5 (Coyle et al., 2013).

2.4 DISCUSSION

Gγ subunits are recognized as having limited function as membrane anchors for Gβ subunits in heterotrimeric G protein signaling systems (35,161,162). As such, their role in signal transduction beyond this function is generally perceived as benign. We previously revealed that Gγ N-terminal tails are prominent targets of phosphorylation, indicating that they might also possibly be important signal regulators (188). Here we have demonstrated that phosphorylation of the Gγ subunit in yeast regulates G protein signaling through a feedback phosphorylation mechanism that synergizes with MAPK docking-dependent phosphorylation on the protein scaffold Ste5.

2.4.1 New insights into the regulation of Ste5/PM association and MAPK activation.

For good reason, understanding the mechanism by which Ste5 coordinates mating pathway output has been a longstanding endeavor with many revisions over the last 10-15 years. The primary function of Ste5 is to properly translate stimulus dose to MAPK response signals – a function that is facilitated by scaffolding of the MAPK cascade module (MAPKKK Ste11, MAPK Ste7, and MAPK Fus3). In resting cells, Ste5/MAPK and Ste5 inter-domain interactions as well as phosphorylation prevent signaling from occurring spontaneously. Under such conditions Ste5 is distributed between the cytoplasm and the nucleus – a phenotype that is cell cycle regulated in part (194,195). Cytoplasmic Ste5 can still interact with all three components of the MAPK cascade module (151). However, Ste5 is incapable of facilitating MAPK activation in this state due to inter-domain binding between $Ste5^{PH}$ and $Ste5^{VWA}$ domains (150) as well as inhibitory phosphorylation mediated by Fus3 and $Ste5^{FBD}$ interactions (147). Relief of inter-domain binding inhibition is mediated by pheromone-dependent accumulation of PIP_2 in the PM, which, when

stimulated, promotes $Ste5^{PH}$/PM association and de-inhibition of $Ste5^{VWA}$ allows for a 3-fold increase in Fus3 phosphorylation over the inhibited state in vitro (150).

Our evidence suggests that Ste5/PM association is also modulated by phosphorylation on Ste18 in addition to Ste5, both of which function synergistically to control Fus3 activation output. In a wild type cell, phosphorylation of both proteins slows the rate and restricts the amplitude of Fus3 activation, resulting in 30 minute peak activation ($Ste18^{WT}$/$Ste5^{WT}$). Engaging either only one element ($Ste18^{3E}$/$Ste5^{ND}$) or the other ($Ste18^{3A}$/$Ste5^{WT}$) produces an equivalent enhancement in peak activation and amplitude that is 2 times faster and 1.5 to 2 times more intense than in wild type cells (Figure 2.2. E). Disabling both elements ($Ste18^{3A}$/$Ste5^{ND}$) results in ultra-fast and intense Fus3 activation that is 6 times faster and 3-4 times greater than the wild type response. We show further that the response in MAPK activation for these mutants correlates very well with the bulk rate and duration of Ste5/PM association, indicating that it is the dominant control factor for Fus3 activation profiles observed in each mutant.

Considering our body of evidence in light of previous work by others, we propose a model in which the activation/deactivation of the Ste18/Ste5 phospho-inhibitory system is regulated differentially (Figure 2.6A). In a pre-stimulated state, Fus3 is mono-phosphorylated and in this state is capable of phosphorylating Ste5 at up to 4 positions near $Ste5^{FBD}$ (Figure A.S5) (149), while Ste18 is also basally phosphorylated (Figure 2.1. & A.S1). This suggests that inhibition is partially engaged even before a pheromone stimulus. Upon addition of pheromone, the Ste18/Ste5 inhibitory elements become fully activated as both Ste18 and Ste5 become hyper-phosphorylated – demonstrated herein directly for Ste18 (Figure 2.1.), and presumed by an in vitro Fus3 kinase assay with Ste5 (see supplemental figure 9 in (149)). We propose that this constitutes the fully activated inhibitory element that is responsible for bulk inhibition of Ste5/PM association early in the pheromone response, as determined from the relative amounts of Ste5-GFP/PM

accumulation observed in Ste18^{3A}/Ste5ND compared to other cells (Figure 2.3.). Simultaneously, pheromone stimulates recruitment of Ptc1 phosphatase to Ste5^{FBD}, which outcompetes Fus3 binding within 2 minutes post-stimulus and dephosphorylates the inhibitory feedback phosphosites on Ste5 (see supplemental figure 18 in (149)). Since as few as one occupied Ste5 phosphosite leads to inhibition of Fus3 di-phosphorylation (149), it is presumed that all four sites must be completely dephosphorylated. We propose that this constitutes a release by *partial de-inhibition* of the Ste18/Ste5 inhibitory element, which leaves the Ste18 element in-tact (phosphorylated), as can be seen by the fact that Ste18 phosphorylation remains unchanged during this time (Figure 2.2. B). We propose that as a consequence of having one phospho-inhibitory element still intact (phospho-Ste18), the bulk recruitment of Ste5 to the membrane is permitted but relatively slow and the activation of Fus3 is delayed – not reaching peak amplitude until ~30 minutes post-stimulus (Figure 2.1. C, 2.2. E, 2.3). This *half-activated* state of the Ste18/Ste5 system also controls the degree to which Ste18 co-immunoprecipitates with Ste5 and the degree to which Ste5/PM association occurs (Figure 2.3. G) – observations that correlate very well with Fus3 activation.

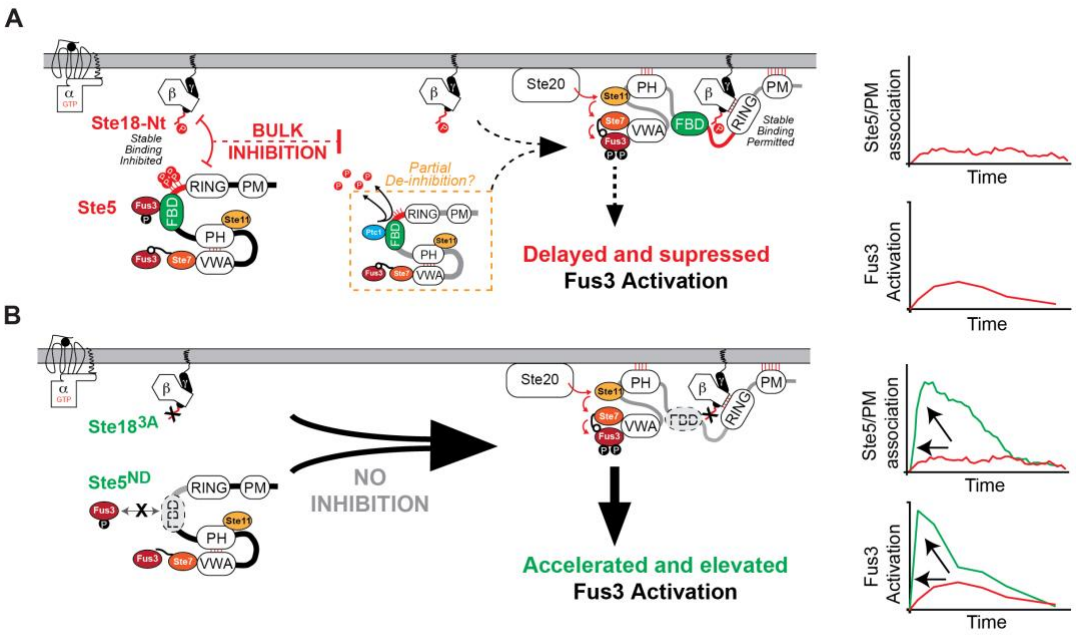

Figure 2.6. Phosphorylated Ste18^{Nt} and Ste5^{FBD} constitute a dynamic phosphoregulatory system for pheromone signaling. (A) In response to pheromone, Ste18 is rapidly phosphorylated at its N-terminal tail (P-lollipop). Ste5 is simultaneously phosphorylated via negative feedback controlled by Fus3/Ste5^{FBD} docking (P-lollipops). Together, this constitutes a phospho-inhibitory system that prevents otherwise rapid Ste5/PM association. While not shown outright here, previous work implicates pheromone-stimulated expression of Ptc1 phosphatase and removal of inhibitory phosphorylation on Ste5 as the inhibition release (149) (dashed orange box). Consequently, the mating pathway is activated with a kinetic delay as evident by the slower rate of Ste5 association at the membrane and delayed peak activation of Fus3. (B) Cells engineered to prevent activation of the Ste18/Ste5 system (Ste18^{3A}/Ste5ND) respond ~6 times faster with ~4 times greater intensity than observed in wild type cells – a response that demonstrates synergy between the two phospho-regulatory elements (phosphorylated Ste18 and Ste5) in the system.

In preventing phosphorylation on Ste18 and Ste5 (Ste18^{3A}/Ste5ND), we show that this system is necessary to delay what is otherwise ultra-fast and intense Fus3 activation (Figure 2.6. B). Consequently, Fus3 activation in this state appears to match the profile of Kss1 activation, which is not scaffolded (Figure 2.2. D/E). Again, the rapid bulk recruitment of Ste5 under these conditions (Figure 2.3), can explain this effect since rapid Ste5/PM

association is known to drive rapid de-inhibition of the $Ste5^{VWA}$ domain by promoting the association of $Ste5^{PH}$ with the plasma membrane – a mechanism that has been demonstrated previously by the Lim lab as an essential step to drive phosphorylation of Fus3 by Ste7 (150). Switch-like behavior of the pathway is also modulated in part by the Ste18/Ste5 phospho-inhibitory system, which controls Ste5/PM association – an observation that is consistent with previous reports demonstrating that $Ste5^{FBD}$ and Ste5/PM association regulate hillslope (116,151).

Several pieces of evidence, both from our work and others, suggest that Fus3 is the major (if not primary) kinase for activating the phospho-inhibitory system. Fus3 phosphorylates proline +1 sites on Ste5 (147), and on $Ste18^{Nt}$ (Figure. A.S3 C,D) – both sites of which emerged at the same time in the evolution of budding yeast (Figure 2.5). Second, Ste5/PM association is enhanced in *fus3Δ* compared to *FUS3* cells treated with pheromone (196) – a phenotype that we also observe for the phospho-null mutant $Ste18^{3A}$/$Ste5^{ND}$ (Figure 2.3). Third, inhibition of an analog-sensitive form of Fus3 (*fus3-as2*) serves to stabilize Ste5/PM association upon pheromone stimulation (191). Consequently, a Fus3-specific phosphatase such as Msg5, which has been suggested to synergize with Ste5 to repress Fus3 activation (197), will alter the ability of Fus3 to function as an activator of the system. Indeed, deletion of the Msg5 phosphatase in $Ste5^{ND}$ cells ($Ste5^{ND}$/*msg5Δ*) results in more intense, but not faster, Fus3 activation compared to wild type or either mutation alone (197), consistent with longstanding evidence that deletion of Fus3-specific phosphatases permits intense and prolonged Fus3 activation (198). Thus, modulation of Fus3 activity necessarily imparts both positive (gene transcription) and negative (Ste18/Ste5) feedback on the pheromone pathway, which will be affected by inhibition or deletion of the kinase.

2.4.2 Gγ N-terminal tails as regulators of G protein signaling – from yeast to humans

Our data reveal the potential for Gγ subunits to play more intricate roles in regulating G protein signaling – affective through PTM-altered protein interactions. As stated earlier, most eukaryotic Gγ subunits are phosphorylated in their N-terminal tails, and all Gγ subunits have the potential to be phosphorylated since serine and threonine are ubiquitous in eukaryotic Gγ subunit N-terminal tails (based on data curated and reviewed by UniProt) (188). In yeast, we find that phosphorylation plays a major role in effector recruitment, but we do not observe evidence that it impacts heterotrimer association, which can be sensitively detected by monitoring Fus3 activation in yeast. This is consistent with previous reports that negative feedback by Fus3 does not impact heterotrimeric G protein dissociation (191). Thus, functional, GPCR-activated phosphorylation of Gγ N-terminal tails is not a process restricted to yeast, and as we have shown here, can regulate G protein signaling output by modulating Gβγ effector binding.

2.5 EXPERIMENTAL PROCEDURES

Yeast strains and plasmids – Standard methods for cell growth, maintenance, and transformation of yeast, and for the manipulation of DNA were used throughout. Strain *BY4741* (*MATa leu2Δ met15Δ his3Δ ura3Δ*) and *BY4741*-derived mutants were used. Details of strainsused are listed in Table A.S1. Strains were constructed using the two-step dellitto perfetto mutagenesis method (199) and confirmed by dideoxy sequencing. LRB341 and LRB345 strains harboring *yck1Δ* and temperature-sensitive *yck2*^{ts} alleles were graciously provided by Dr. Lucy Robinson (200). Plasmids used in this study for kinase deletion screening (pRS316-*CUP1-HA-STE18*), were graciously provided (gift from

T. Chernova). Detailed method of strain construction is provided as Supplemental Information.

Yeast cell culture and treatments – Yeast Strains were grown in YPD growth medium (Yeast Extract, Peptone, 2% Dextrose media) unless otherwise noted. All experiments were conducted with log phase cells between OD600 0.75-0.85 and stimulated with α-factor peptide hormone (Genscript) at 3μM final concentration, if required. Cells were harvested with trichloroacetic acid (5% final vol/vol) and frozen at -80C.

For kinase screening, deletion strains carrying the pRS316-*CUP1-HA-STE18* plasmid were grown in synthetic media lacking uracil and other appropriate amino acids as necessary. Expression of *HA-STE18* was induced by 100μM copper sulfate and cells were stimulated as described earlier. Detailed procedure is provided as Supplemental Information.

Cell extracts and immunoblotting – Proteins were extracted by glass bead lysis in TCA as previously described (201). Protein concentration was determined by DC protein assay (Bio-Rad Laboratories). Protein extracts were resolved by 7.5% or 12.5% SDSPAGE and immunoblotted with epitope-specific antibodies (see entire list in Supplemental Information). Note that the current lot of Phospho-p44/42 MAPK antibody (Cell Signaling Technologies Cat # 9101) exhibits reduced detection sensitivity for activated Fus3 compared to activated Kss1, which affects the ability to detect Fus3 activation in the very early stages of a pheromone response (i.e. before 1 minute). HRP conjugated secondary antibodies (goat-anti-rabbit, goat-anti-mouse or rabbit-anti-goat) were used for detection of reactant bands by chemiluminescence with ECL reagent (Perkin Elmer Cat #NEL 104001EA). Immunoblots were quantified by high-resolution scanning and pixel densitometry using Image J software (202).

Morphological response assay – The morphological response of *STE18/STE5* mutants to α-factor was measured as described previously (116,149) and detailed in Supplemental

Information. The morphology of the cells was determined, 3h post- pheromone stimulation, by differential interface contrast (DIC) confocal microscopy using a PerkinElmer UltraVIEW spinning disk confocal microscope. Number of cells with mating projections were counted as a percentage of total.

Ste5-GFP localization assay – Live cells endogenously expressing either Ste5-GFP or $Ste5^{ND}$-GFP were visualized by microscopy. To ensure visibility across all strains, we exposed cells to 10 μM α-factor followed immediately by deposition onto agar pads saturated with 30μM α-factor. Once deposited, cells were monitored by PerkinElmer Ultraview VoX spinning disk confocal microscope. Detailed procedure for image acquisition and quantification is provided as Supplemental Information.

Co-immunoprecipitation – Cells endogenously expressing different combinations of wild type or mutant HA-STE18 and STE5-GFP were treated with 10μM pheromone for 20 mins followed by cell lysis and co-ip using anti-GFP mAb-agarose (MBL, #D153-8). Eluted proteins were separated by SDS-PAGE and immunoblotting with anti-GFP (Invitrogen, A11122) and anti-HA (Supplemental Information).

Phylogenetic analysis – Ascomycota protein sequences were retrieved from the Broad Institute Fungal Orthogroups Respository (https://portals.broadinstitute.org/regev/orthogroups/). Multiple sequence alignments were achieved using MUSCLE with default parameters (203), 2004). Phylogenetic and graphical analysis of Ste18 and Ste5 sequence alignments were achieved using Unipro UGENE software (204). Bootstrap consensus trees were prepared using 100 (shown) and 500 (not shown) iterations. Presence or absence of Ste5 or the $Ste5^{FBD}$ were determined from a combination of sequence alignment homology as well as previous phylogenetic analyses of Ste5 (Coyle et al., 2013).

Statistical analysis – Statistical analysis for quantifying immunoblots and microscopy data was achieved using Prism software version 6/7 (GraphPad Software Inc.). Statistical significance was determined by ANOVA tests.

Supplemental Information in Appendix A

Document S1. Supplemental Results, Discussion and Experimental Procedures; Table A.S1-A.S3 and Figures A.S1-A.S7.

Acknowledgements
We'd like to give special thanks to Aaron Lifland and the GT EBB1 microscopy core facility for support with confocal microscopy experiments; Prof. Kirill Lobachev and Ziwei Sheng for graciously providing yeast deletion strains; Joseph Lachance for guidance in phylogenetic analysis; and Dr. Tatiana Chernova for the *CUP1* yeast expression plasmid. This work was supported by NIH R01GM117400 to M.T., R00GM094533 to M.T., and startup funds to M.T. provided by the Georgia Institute of Technology.

CHAPTER 3

Interrogating phosphorylation of the N-terminal tail of the G protein gamma subunit, Ste18, in response to multiple conditions

Running title: Identification of Ste18 as a potential phospho-regulatory module for cross-talk between signaling pathways

3.1 ABSTRACT

Ste18 is the G gamma subunit of the heterotrimeric G proteins in yeast *Saccharomyces cerevisae* and is critical for the mating pathway. Like mammalian Gγ subunits, Ste18 is commonly thought to have limited functionality as a membrane anchor for its obligate heterodimer partner, Ste4 (yeast Gβ subunit). Previously, we demonstrated a novel role of Ste18 in the regulation of G protein signaling. In this role, Ste18 required phosphorylation of the unstructured N-terminal tail of Ste18 (Ste18-Nt), a disordered region conserved in all Gγ subunits. Phosphorylated Ste18-Nt along with Fus3 docking on the scaffold protein Ste5, mediated the negative feedback regulation of the mating pathway activation kinetics. Here, we show that Ste18-Nt is phosphorylated under two independent conditions including cell-cycle progression, and osmotic stress- suggesting the role of multiple kinases. Interestingly, the dynamics of phosphorylation were distinct for each stimulus, and had no resemblance to the previously described GPCR activation dependent phosphorylation of Ste18-Nt (Chapter 2; (205)). These results suggest that Ste18-Nt may serve as a communication node between the mating pathway, cell cycle regulation, and osmotic stress; and may prevent activation of the mating pathway under sub-optimal conditions, probably through the Ste18/Ste5 inhibitory module described previously (Chapter 2; (205)). More broadly, these data provide additional evidence that

Gγ subunits – and their intrinsically disordered N-terminal tails – serve as PTM regulatory elements in G protein signaling systems.

3.2 INTRODUCTION

Heterotrimeric G-proteins composed of Gα, Gβ, and Gγ protein subunits are a family of signal transducing proteins that couple an enormous number of G-protein coupled receptors (GPCRs) to intracellular effector proteins (11). Together these proteins mediate a vast number of physiological responses, and dysregulation of these pathways contributes to many diseases, including blindness, cardiac disease, endocrine disorders, and cancer (2,5,54,55,206). G-protein signaling is initiated by the binding of an extracellular agonist such as neurotransmitters, hormones, chemokines, lipids and many more to GPCRs (11,12). Agonist-bound GPCRs act as guanine nucleotide exchange factors (GEF) that promotes the release of bound GDP by Gα subunit. The nucleotide free Gα-subunit then binds GTP, undergoes conformational changes within its switch region, and subsequently dissociates from the Gβγ-dimer, enabling both molecular entities to regulate the activity of their specific effectors. The intrinsic GTPase action of Gα subunit coverts GTP to GDP, facilitating the reassociation of Gα and Gβγ subunits, and subsequent deactivation of the G-protein signaling pathway(11,207). Regulators of G-protein signaling (RGS) proteins accelerate inactivation by increasing the rate of Gα-catalyzed GTP hydrolysis (208,209).

Although the classical paradigm of G-protein signaling pathway is rather linear and sequential, accumulating evidences have revealed signaling via GPCRs is coupled with many other cellular pathways. These interconnections allow the cell to integrate multiple signals and generate appropriate response based on the net status of the pathway (210–

212). This pathway interaction is called cross-talk and is crucial for shaping the controllability of the signaling networks. Misregulation of cross-talk between signaling pathways can lead to various diseases, such as Alzheimer's disease (213,214), head and neck squamous cell carcinoma (215), and cardiac arrhythmia (216,217), to name a few.

A prototypic experimental model used for studying cross-talk between signaling pathways is *Saccharomyces cerevisae*, specifically between the mating pathway, and stress-response pathways such as high osmolarity glycerol (HOG) pathway, filamentous growth pathway, as well as cell-cycle phase (88,139,218,219). Mating is the process by which two opposite mating types-MAT**a** and MATα, fuse to form an **a**/α diploid cell and is controlled by G-protein signaling system (173). As in mammalian cells, receptor activation by the binding of stimuli (pheromone) causes dissociation of Gα (Gpa1) and G$\beta\gamma$ (Ste4/Ste18) subunits. In yeast, free Gpa1 serves to sequester Ste4/Ste18, which is responsible for activating a scaffolded protein kinase cascade consisting of Ste20 (p21 activated kinase, PAK), Ste11 (MAPKKK), Ste7 (MAPKK), Fus3 (MAPK), and Kss1 (MAPK) (173). Direct interaction between Ste4/Ste18 and the MAPK scaffold protein Ste5 organizes each kinase into a protein complex that drives the phosphorylation cascade (220,221) culminating in dual phosphorylation and activation of Fus3 – a highly conserved ortholog of the human MAPK Erk1/2, and the primary pheromone-responsive MAPK in yeast. Full scale activation is switch-like in its response, due in part to the interaction of Fus3 at two distinct positions on Ste5: a productive but weak binding site distal to the G$\beta\gamma$ binding surface that enables full activation of the MAPK; and a non-productive strong binding site, proximal to the G$\beta\gamma$ binding surface (147,185). Recently, we discovered that Fus3-dependent phosphorylation of Gγ (Ste18) at its N-terminal tail and of Ste5 at 4 MAPK phosphorylation sites near the proximal binding site synergistically controls the rate at which the Ste4/Ste18/Ste5 complex is formed at the plasma membrane. Thus, unearthing

a novel role of phosphorylated Gγ in negative feedback inhibition of the pathway (Chapter 2; (205)).

Yeast in which cell cycle progression is un-coupled from pheromone signaling results in aneuploidy, and strongly favors the fusion of cells during G1 phase when a single copy of each haploid genome is present (139). Similarly, yeast in which the hyperosmotic stress and pheromone pathways have been un-coupled undergo fewer successful mating events, illustrating the evolved capacity of yeast to avoid energy expenditure towards mating when they encounter stressful environments (118,222). Indeed, mechanisms that coordinate the mating pathway with the cell cycle have been discovered previously, including the cell cycle-dependent nuclear export and protein stability of the Ste5 scaffold (132), the phosphorylation-dependent ubiquitination of Gpa1 (88), the phosphorylation and activation of Ste20 (PAK) (219,223) and the prominent effect of cell cycle arrest at START by the cyclin-dependent kinase (CDK) inhibitor, Far1, itself a cell cycle-regulated protein (139,153). Likewise, an altogether separate mechanism prevents yeast mating in the presence of hyperosmotic stress, whereby the osmo-sensitive MAPK, Hog1, phosphorylates Ste50, a MAPKKK-interacting protein, that blocks the pheromone-dependent phosphorylation cascade necessary for a mating response (118,119). Yet another pathway coordinates mating with nutrient stress, promoting pseudohyphal or invasive growth that may serve as a way for starving yeast to forage for a food source (157,222). In all cases, these stress response pathways mediate the phosphorylation of several components in the mating and other pathways, which prevent yeast cells from mating under sub-optimal conditions.

As with the GPCRs, the heterotrimeric G-proteins represent an ancient protein family that has been highly conserved over evolution. 23 Gα, 5 Gβ, and 13 Gγ protein subunits have been identified in humans, resulting in large number of potential

heterotrimeric G protein complexes(30). While the signaling roles of Gα subunits are precisely ascribed, those of Gβ and Gγ are rarely distinguished independently due to their obligate heterodimeric interaction (16,224–227). Gβ and Gγ subunits form an obligate heterodimer and act as a stable structural and functional monomer (16,228). The structure of Gβγ shows that Gβ forms a seven bladed propeller structure consisting of seven WD40 repeats, while the N-terminus forms an α-helix; Gγ subunit consists of two α-helices that extensively interacts with the α-helix as well as several of the WD40 repeats of Gβ subunit. The protein-protein interactions that drive Gβγ function are thought to be primarily provided by Gβ subunits (123,130,193,229–231). In contrast, the primary function of Gγ subunits is to anchor Gβ subunits to the plasma membrane (232). Indeed, all eukaryotic Gγ subunits are prenylated at their C-terminus, which is essential for membrane anchoring of the Gβγ heterodimer (161,162), but has also been shown to be involved in controlling the interaction of Gβγ with Gα subunits (233), GPCRs (35,234), and downstream effectors (227). Beyond this role, any additional signaling attributes of Gγ subunits have remained somewhat elusive.

We recently revealed that all proteins in the Gγ subunit family, including the yeast Gγ subunit Ste18, contain an intrinsic disordered region (IDR) through the first 8-15 residues of their N-termini (Gγ-Nt) (188). Much like the C-terminal IDRs of GPCR C-terminal or histone N-terminal tails (235–237), Gγ-Nt is a predominant site of PTMs. Indeed, 41% of all Gγ PTMs, 56% of which correspond to phosphorylation, are clustered within Gγ-Nt (188). In Choudhury et. a. 2018, we showed that phosphorylation of Gγ-Nt coupled with phosphorylation of Gβγ effectors can prevent binding and inhibit MAPK signaling in the eukaryotic model organism, *Saccharomyces cerevisae* (Chapter 2; (205)). Thus, Gγ subunits, besides acting as anchors for their obligate Gβ subunits by virtue of

their C-terminal prenylation, also mediates negative feedback regulation of G protein signaling via phosphorylation of its N-terminal tail (Chapter 2; (205)).

Phosphorylation events which occur on intrinsically disordered regions of proteins often serve as hubs in the signal flow allowing a rapid method for signaling pathways to cross-talk with each other and have functional consequences on downstream signaling (238). Thus, identification of phosphorylation on proteins with the potential to regulate integration of multiple stimuli or cross-talk between signaling pathways is critical. Here, we investigated whether the N-terminal tail of yeast Gγ, Ste18, is phosphorylated in response to stress conditions such as nutrient stress and osmotic stress, as well as cell cycle phase; and thus, could potentially act as hub for cross-talk mediated regulation of G-protein signaling. We show that Ste18 is indeed phosphorylated within its N-terminal IDR in response to multiple independent stimuli such as cell-cycle progression and osmotic stress. Surprisingly, a systematic screen for phosphorylation-deficient genetic mutants revealed that Hog1 and other kinases in the osmotic pathway are dispensable for phosphorylation of Ste18-Nt under osmotic stress. Thus, further work is required to identify the underlying osmotic stress kinase and cell cycle regulated kinase. Taken together with evidence for the synergistic inhibitory phosphorylation of Ste5 and Ste18 that mediates negative feedback regulation of G-protein signaling (Chapter 2; (205)), we propose a similar mode of action for cross-talk mediated regulation.

3.3 Results

3.3.1 The N-terminal tail of Ste18 is transiently phosphorylated in response to osmotic stress but not nutrient stress

Like other Gγ subunits throughout Eukarya, the terminal ends of Ste18, representing 20% of its residue content, are intrinsically disordered – most of which correspond to the N-terminal tail (Ste18-Nt). This region in Ste18 (residues 1-13) also harbors phosphorylation sites at Thr-2, Ser-3, and Ser-7, specifically (188). We demonstrated previously that phosphorylation of Ste18-Nt produces an electrophoretic mobility shift in Ste18, which can be detected by SDS-PAGE and immunoblotting (Chapter 2; (205)). Previously, we observed that rapid and prolonged phosphorylation of Ste18-Nt is stimulated in response to α-factor pheromone GPCR activation (Chapter 2; (205)). Here we show that phosphorylation of Ste18-Nt occurs in response to osmotic stress but is insensitive to glucose limitation stress (Figure 3.1). Whereas the phosphorylation response to pheromone is prolonged (Chapter 2; (205)), the response to osmotic stress is robust but short-lived – nearly matching the kinetic profile of high osmolarity glycerol (HOG) pathway activation of the p38 MAPK ortholog, Hog1 (Figure 3.1 A-C). Interestingly, the phosphorylation of Ste18-Nt was independent of Hog1(Figure B.S1), which is the key kinase reported to inhibit cross-talk between HOG pathway and mating pathway (117–119). Indeed, elimination of any of the kinase directly involved in the pathway were dispensable for Ste18 phosphorylation (Figure B.S1). Thus, further work is required to determine the kinase involved in osmotic stress mediated Ste18 phosphorylation.

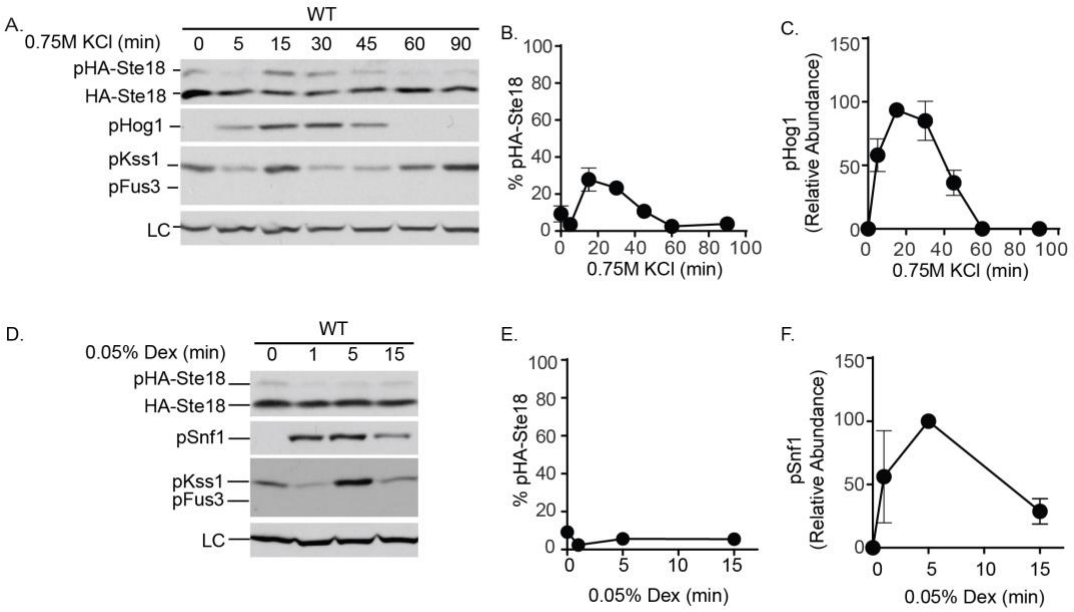

Figure 3.1. Ste18-Nt is phosphorylated in response to osmotic stress. Cells were exposed to either 0.75M KCl (A-C), or 0.05% dextrose (D-F) for the indicated times. (A) Representative immunoblots of HA-Ste18, activated MAPKs (pKss1, pFus3 and pHog1), and a protein loading control in response to osmotic stress. (B, C) Averages and standard deviations of HA-Ste18 phosphorylation percentage (%pHA-Ste18) and activated MAPKs (relative to maximum), representing three independent colonies/experiments quantified from (A). (D- F) Immunoblots and quantitative graphs showing the phosphorylation of Ste18 in response to glucose depletion.

3.3.2 Cell-cycle dependent phosphorylation of Ste18-Nt

We next asked whether phosphorylation could be promoted by cell cycle dependent transitions in the absence of pheromone. We synchronized cells in G_2/M phase with nocodazole and monitored phosphorylation of Ste18-Nt after release into fresh medium. To validate the arrest and release protocol, we monitored the abundance of the mitotic cyclin Clb2, which exhibits peak expression in G2/M phase and is rapidly degraded by the anaphase-promoting complex upon exit into G1 phase (239). Consistent with the hypothesis, we observed a slow, cell cycle-dependent increase in Ste18-Nt phosphorylation, reaching a maximum level at 75 minutes post-release and gradually

decrease thence after (Figure 3.2). This trend was inversely related to Clb2 abundance, suggesting that phosphorylation is maintained only during G1 phase.

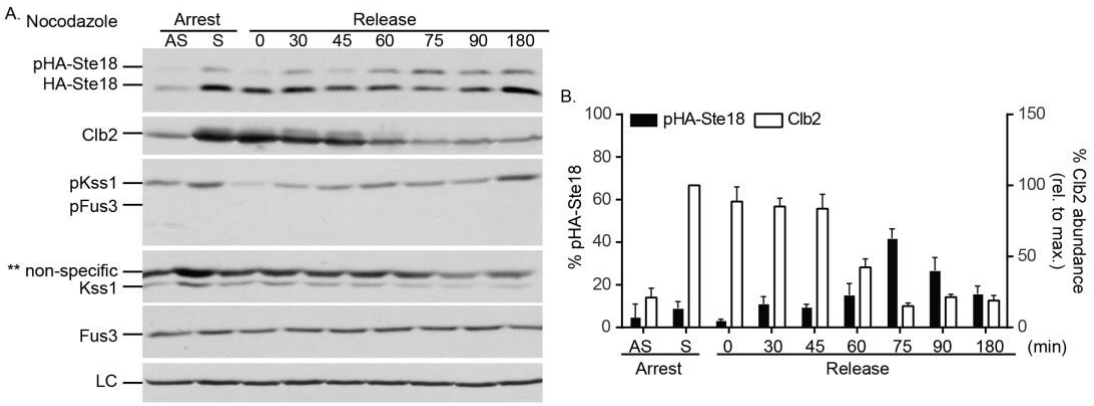

Figure 3.2. Ste18-Nt phosphorylation is cell cycle regulated and G1-phase specific. Cells were synchronized in G2/M phase by treatment with Nocodazole followed by release into fresh medium and time course sampling for 3 hours. (A) Representative immunoblots showing the phosphorylation of HA-Ste18-Nt in asynchronous log-phase cells (AS), nocodazole-synchronized cells (S), and at different time points after release. Each sample was also blotted for Clb2, activated MAPKs pKss1 and pFus3, total Kss1 and Fus3, and loading control (LC). (B) Quantification from three independent experiments showing the average and standard deviation of pHA-Ste18 phosphorylation percentage (left axis) in each sample. Clb2 abundance is shown as a percentage relative to the maximum signal achieved in the synchronous cell culture (right axis).

As expected, neither Kss1 nor Fus3 MAPKs were activated as a consequence of the arrest or release conditions (Figure 3.2), and are therefore unnecessary for cell cycle dependent phosphorylation of Ste18-Nt.

3.4 Discussion

Despite their essential role in G-protein signaling, Gγ subunits have been largely overlooked for their potential to regulate G protein signaling. While considerable evidence

supports the functional significance of PTMs on Gα and Gβ subunits (174,175,177–179), Gγ subunits are recognized as having limited function as membrane anchors for Gβ subunits (161,162). We previously demonstrated that all eukaryotic Gγ subunits contain a structurally conserved, intrinsically disordered N-terminal tail (Gγ-Nt) that is enriched with phosphorylation hotspots predicted to have a high probability of biological impact on G protein signaling (188). Using yeast as a model organism, we further showed that phosphorylation in the intrinsically disordered region of Gγ subunit (Ste18) participates in the negative feedback regulation of G-protein signaling. In this role, Ste18-Nt and the scaffold protein, Ste5, is phosphorylated by the MAPK, Fus3. Together, phosphorylated Ste18-Nt and Ste5, synergistically inhibit G-protein signaling (Chapter 2; (205)). In this study, we extend the array of stimuli that regulate Ste18-Nt phosphorylation Taken together, we propose that the N-terminal tails of Gγ subunits are likely to have regulatory function in mammals and other eukaryotic G-protein signaling systems.

3.4.1 N-terminal tail of yeast Gγ, Ste18 is phosphorylated under multiple conditions

We have found that phosphorylation of Ste18-Nt is regulated under three independent conditions, (i) GPCR activation (Chapter 2; (205)), (ii) cell cycle progression (G1 phase), (Figure 3.2) and (iii) hyperosmotic stress (Figure 3.1A, B). Previously we had shown that the GPCR activation mediated phosphorylation of Ste18 required Fus3 (see Figure A.S1 C-D in Chapter 2; (205)). However, phosphorylation of Ste18-Nt observed in hyperosmotic stress conditions and in G1 phase of the cell-cycle, despite the evident absence of activated Fus3 kinase (Figure 3.1A and 3.2), highly suggests the role of conditionally-dependent multiple kinases. In yeast, the cyclin-dependent kinase Cdc28 is the central coordinator of cell-cycle progression. It does so by associating with specific cyclins at different cell-cycle phase, including Cln1/2 at G1 phase of cell-cycle (240). In

fact two proteins in the mating pathway, Ste20 and Ste5, are phosphorylated by Cdc28 only when it is associated with G1 specific cyclins Cln1/2 (152,194,241). This cyclin specificity is conferred by the presence of Cln1/2 docking motif LxxPϕxϕ (where x is any amino acid and ϕ is a hydrophobic amino acid) on both Ste20 and Ste5 (241). Interestingly, survey of the primary sequence of Ste18 highlighted the presence of a stretch of amino acids in the N-terminus region which partly resembled the Cln1/2 docking motif. This stretch of 16 residues (LQQPQEQQQQQQLSL) has the LxxP and the ϕxϕ (LSL) residues interrupted by a stretch of hydrophilic residues. Although sequence variability in the docking motif has been previously shown in the case of Ste20, Ste5 as well as other Cdc28 substrates, such as Sic1, Bem3 to name a few (241), whether the sequence in Ste18 binds Cln1/2 needs to be experimentally determined. Based on this reasoning, we speculate the cell-cycle dependent phosphorylation of Ste18-Nt to be mediated by the Cdc28, though the specificity for Cln1/2 is uncertain.

In conditions of hyperosmotic stress, we found the kinases involved in the activation of the HOG pathway dispensable for Ste18-Nt phosphorylation (Figure B.S1). This is in contrast to previous studies that have shown components of G-protein signaling pathway, such as Ste50 and Gpa1, to be phosphorylated in a Hog1-dependent manner, either directly or indirectly (117–119). However, many physiological changes including glycerol production, cell-cycle pause, changes in cell wall integrity, and a pause in protein translation occurs within seconds after exposure to hyperosmotic shock (242–245). Kinases involved in such processes could potentially play a role in phosphorylating Ste18-Nt. Further screening of the yeast kinome deletion is required to determine the putative kinases of Ste18-Nt.

In yeast, the mating pathway is well coordinated with other cellular events such as cell cycle (139,153,159,246,247) and hyperosmotic stress response (118). Indeed,

several components in the mating pathway are known to be phosphorylated in response to stress conditions and cell-cycle stage, providing a mechanism for pathway regulation(88,118,175,219,223,248,249). Consequently, we envision that the dynamic phosphorylation of N-terminal tail of Ste18 under various conditions, serves to coordinate the mating, cell-cycle, and osmotic stress pathways. Indeed, post-translationally modified intrinsically disordered tails acting as regulatory hub for various pathways is a common theme in cellular signaling and regulation (235,236). The ability to interact with different PTM "writers" (kinases in this case) is yet another characteristic of intrinsic disordered tails that serve as "regulatory handle", further reinforcing the regulatory relevance of the N - terminal tail of Ste18 (235,236).

3.4. 2 Phosphorylation of Ste18 may serve an inhibitory function to delay G-protein signaling under suboptimal condition.

Earlier we had shown that phosphorylation of Ste18-Nt and Ste5 synergistically inhibit the mating pathway. Ste5 harbors four MAPK sites (T267, S276, T287, and S329) that are phosphorylated by Fus3, very close to a Fus3 binding site and proximal to the binding site for G$\beta\gamma$[Ste4/18] (147). The inhibitory phosphorylation at Ste5 is presumably short lived due to the action of the phosphatase, Ptc1, which competes with Fus3 for access and de-phosphorylates the inhibitory sites, enabling complete pathway activation (149). Similarly, Ste18-Nt is phosphorylated in a Fus3-dependent manner. However, unlike Ste5, Ste18 phosphorylation is retained during this time and is therefore not likely the target of de-phosphorylation. When both substrates are phosphorylated, productive association of the scaffolding MAPK complex with the G$\beta\gamma$ subunit at the plasma membrane is disfavored due to charge repulsion (Chapter 2; (205)). The inhibition presumably remains unless Ste5 is dephosphorylated by Ptc1 to relieve charge repulsion.

The osmoregulatory or HOG pathway represses activation of the mating pathway and this repression requires the catalytic activity of Hog1 (117–119). Costimulation of yeast cells with pheromone and osmolyte (0.75M KCl) results in a delayed and dampened (i) activation of the mating pathway specific MAPK (Fus3), (ii) transcription of mating related genes, and (iii) morphological response such as shmoo formation (118). This Hog1- dependent repression of mating pathway occurs through two mechanisms. One way is by the negative feedback phosphorylation of Ste50, a shared component between HOG and mating pathway, required for activation of Ste11 (118,119). As a consequence of Ste50 phosphorylation, the activation of MAPKs in the mating pathway (Fus3 and Kss1) is attenuated (118). Additionally, cross-inhibition of mating pathway by Hog1 is mediated through phosphorylation and activation of Rck2, the negative regulator of translation. Activated Rck2 phosphorylates the yeast elongation factor EF2, and thus transiently represses translation (118). Interestingly, the function of Hog1 in limiting the mating pathway were only seen at later time points (30 mins onward) of co-stimulation; whereas the repression at early time points was Hog1-independent (see Figure 4 in (118)), hinting at the presence of another repression mechanism which operates at early time points.

Here, we observed that Ste18-Nt is phosphorylated rapidly after salt stress, with phosphorylation of Ste18-Nt peaking at 15 minutes post osmotic stress. Although the kinetic of Ste18-Nt phosphorylation mimicked Hog1 activation, surprisingly Ste18-Nt phosphorylation was independent of Hog1. Thus, it could be possible that the Hog1-independent repressive effect of salt seen at early time points (5 and 15 min) could be mediated through Ste18-Nt. Whether Ste5 participates in this inhibition is unknown. If the Ste18/Ste5 phospho-inhibitory mechanism (described earlier in chapter 2; (205)) did exist under stress condition, it will be short-lived since Ptc1 is expressed during osmoadaptation to prevent hyperactivation of Hog1 (250). The Ptc1 expressed during osmoadaptation

could also mediate de-phosphorylation and hence removal of inhibition from Ste5. However, these speculations will require further validation.

3.4.3 Phosphorylated Ste18 may serve as a node to integrates pheromone and cell-cycle cues.

We have shown that Ste18 is a target of cell cycle dependent phosphorylation in G1 phase – independent of pheromone stimulation. Similar observations have been made for Ste5, as well as Ste20, both of which harbor cyclin docking sites that are essential for phosphorylation by the primary CDK in yeast, Cdc28 (241). In particular, Ste5 harbors 8 CDK sites at its N-terminus, which flank a plasma membrane targeting domain that is essential for regulating the proximity of Ste5 to the G proteins and for activation of the pathway (194,251). Phosphorylation of these sites depends on G1 cyclin and occurs independently of MAPK binding to Ste5 (194). Phosphorylation at these sites disrupts Ste5 membrane localization and restricts pheromone arrest to G1 cells; thus preventing inappropriate mating pathway activation in cells that have passed the Start check-point (158).

Ste18 is also a target of G1 cyclin-dependent CDK phosphorylation and could potentially participate in cell cycle-regulated signaling competence in the presence and absence of other regulatory phosphorylation events on Ste5 and Ste20. An attractive but speculative possibility is that Ste5 is potentially phosphorylated at the 4 MAPK/Cdk sites proximal to the RING domain (currently unknown), which along with phosphorylation of Ste18 disrupts (Ste4/Ste18)/Ste5 binding. This inhibitory mechanism could synergize with the previously known inhibition mediated via phosphorylation of 8 sites flanking the PM domain, resulting in substantial accumulation of negative charge which is unconducive for Ste5/plasma membrane association (71). Interestingly, the Cdc28 docking site on Ste5 shares multiple similarities with FBD- both Cdc28 docking motif and FBD lie in the same

interdomain region of Ste5, are proximal to the four inhibitory phosphorylation sites (T267, S276, T287, and S329), and show competitive binding with Ptc1 (72). However, cell-cycle regulated phosphorylation at these sites, even though these have the S/T-P Cdc28 consensus sequence, needs to be determined for this speculation to hold true. Other possibilities include (i) inhibition of the (Ste4/Ste18)/Ste5 binding due to steric hindrance mediated by the docking of Cln1/2-Cdc28 on Ste5 in close proximity to the RING domain, and consequent inhibition of Ste5/plasma membrane association, or (ii) phosphorylated Ste18 may act in conjugation with phosphorylation of the 8 sites in the N-terminus region of Ste5 to prevent mating pathway activation. Further work is required to determine the precise role of phosphorylated Ste18 in cell-cycle regulation of the mating pathway.

In conclusion, we have demonstrated multi-conditional phosphorylation of the N-terminal tail of Gγ subunit - a well conserved, but previously overlooked region of Gγ. Previously, we had reported that phosphorylated Gγ is inhibitory for mating pathway activation (Chapter 2; (205)). Here, we propose that the intrinsically disordered N-terminal tail of Gγ subunit could potentially act as a phospho-regulatory hub for cross-talk between G-protein signaling pathway, stress response pathway and cell-cycle regulation. Thus, expanding the functional significance of Gγ subunits in G-protein signaling, besides its well-known critical role as a membrane anchor for Gβγ subunit. Recent studies have also implicated the deletion of specific Gγ subunits with various diseases (37,252–255). Thus, the identification of new pathway regulators in yeast, which affect the basal activation and/or agonist efficacy, could not only facilitate our understanding of G protein signaling in mammalian cells but also reveal potential new drug targets.

3.5 EXPERIMETAL PROCEDURES

Yeast strains and plasmids- Standard methods for cell growth, maintenance and transformation of yeast and for the manipulation of DNA were used throughout. Previously described BY4741 (MAT**a** *leu2*Δ *met15*Δ *his3*Δ *ura3*Δ) -derived mutant strain YMT 235 endogenously expressing HA-Ste18^{WT} was used. pRS316-CUP1-HA-STE18 and yeast knock-out (YKO) collection from open biosystems used for kinase deletion screen was graciously provided by Dr. Tatiana Chernova and Dr. Kirill Lobachev, respectively.

Yeast cell culture and treatments - Yeast Strains were grown in YPD growth medium (Yeast Extract, Peptone, 2% Dextrose media) unless otherwise noted. Cells were grown at 30C with shaking at 250 rpm and cell culture density was determined by absorbance at 600 nm. All experiments were conducted with log phase cells at OD 0.8-1. Cells were then treated as per experimental requirement. 10 ml aliquots of treated cells were harvested with 0.5 ml trichloroacetic acid (TCA) on ice and centrifuged at 3724 x g in Allegra X-14R Beckman Coulter Centrifuge. Cells were then washed with 10 ml Mili-Q water, followed by transfer to microcentifuge tubes that were immediately frozen at -80C. Treatment conditions- GPCR activation- In order to activate the G protein signaling system, log-phase cells were treated with α-factor peptide hormone (Genscript) at 3μM final concentration. Cells were harvested as per standard protocol.

Synchronization of cells with nocodazole- Log phase yeast cells were pre-treated with 1% dimethyl sulfoxide (DMSO) for 30 min at 30C. Nocodazole (100X stock solution- 1.5mg/ml in DMSO) was then added to the cells at 15 μg/ml final concentration. Cells were allowed to synchronize at G_2/M phase for 3 h. The synchronized cells were then released by washing the cells twice with MiliQ-water followed by resuspension in fresh medium to an *A*600 nm of 0.7 and growth at 30C (256).

Nutrient Stress- Log-phase cells grown in YPD containing 2% (w/v) D-glucose were centrifuged. Nutrient stress was achieved by washing the cells with YP medium containing 0.05% (w/v) D-glucose and resuspending in 0.05% glucose medium for 15 min (175).

Osmotic Stress- Cells were grown in synthetic complete media with 2% w/v D-glucose till *A*600 nm of 0.8-1. Osmotic stress was achieved by centrifuging the cells and resuspending in synthetic complete media with 0.75M KCl for the desired amount of time (118).

Cell extracts and immunoblotting- Proteins were extracted by glass bead lysis in TCA as previously described (257). Protein concentration was determined by DC protein assay (Bio-Rad Laboratories). Protein extracts were resolved by 7.5% or 12.5% SDS-PAGE and immunoblotting with HA antibodies (Cell Signaling Technology, Cat # 3724) at 1:5000, Phospho-p44/42 MAPK antibodies (Cell Signaling Technology, Cat # 9101) at 1:500, Fus3 antibodies (Santa Cruz Biotechnology, Inc., Cat # sc-6773) at 1:500, Kss1 antibodies (Santa Cruz Biotechnology, Inc., Cat # sc-28547) at 1:1000, phospho-p38 MAPK antibodies (Cell Signaling Technology, Cat # 9216) at 1:500, Clb2 antibodies (Santa Cruz Biotechnology, Inc., Cat # sc9071) at 1:350, Phospho-AMPK alpha (Snf1) antibodies (Santa Cruz Biotechnology, Inc., Cat # 4188) at 1:2000, and glucose-6-phosphate dehydrogenase (G6PDH) antibodies (Sigma-Aldrich, Cat #A9521) at 1:50,000. HRP conjugated secondary antibodies (goat-anti-rabbit, goat anti mouse or rabbit anti goat) were used for chemiluminescent detection using ECL reagent (Perkin Elmer Cat # NEL 104001EA). Immunoblots were quantified by high-resolution scanning and pixel densitometry using Image J software (202).

Statistical analysis- Statistical analysis for quantifying immunoblots was achieved using GraphPad Prism software version 6.

Supplemental Information in Appendix B

Figures B.S1-B.S2. Results of ongoing screen of deletion strains of genes expressing specific non-essential kinase.

CHAPTER 4

CONCLUSIONS AND FUTURE DIRECTIONS

4.1 CONCLUSIONS

G-protein signaling system composed of G-protein coupled receptors (GPCRs), heterotrimeric G proteins (G$\alpha\beta\gamma$), and downstream effectors mediate response to a tremendous variety of stimuli, such as light, hormones, neurotransmitters and many more (11,165,258). Aberration in G-protein signaling has been associated with a number of malignancies; and components of this pathway, especially GPCRs, represent the most important targets in modern pharmacology (1,3–6,259,260). Thus, G-protein signaling is one of the most exhaustively studied cellular process, with increasing efforts made to understand the intricate regulation of the G-protein signaling system through various mechanisms, including post-translational modifications (PTMs).

As G-protein signaling system is conserved among species, molecular and systems-biology studies of this process in yeast have great relevance to human biology. Indeed, the baker's yeast, *Saccharomyces cerevisae*, have had a long history of success for finding new pathway regulators, including regulators of G-protein signaling (RGS) and many PTM-based regulators (49,80,87,163,174,256,261).

In yeast, mating pheromones activate G-protein signaling by initiating dissociation of the heterotrimeric G proteins (G$\alpha\beta\gamma$) to Gα (Gpa1) and G$\beta\gamma$ (Ste4/Ste18), and transduction of signal from the released G$\beta\gamma$ (Ste4/Ste18) to downstream effector proteins (reviewed in (173)). The G$\beta\gamma$ effector protein, Ste5, which scaffolds the three members of the MAPK cascade – MAPKKK Ste11, MAPKK Ste7, and MAPK Fus3, but not MAPK Kss1- is an important factor in mediating signaling efficiency and specificity (185,262–264). Upon pheromone stimulation, Ste5 is recruited to the plasma membrane through

collective stabilizing effect of three interactions- binding of Ste4/Ste18 to the RING domain of Ste5 (134,135,265–267), association of the N-terminal basic PM domain with the acidic phosphoinositides at the plasma membrane (158), and interaction of PH domain with PIP_2 in the membrane (136)- resulting in conformational activation of the VWA domain, a phenomenon that positively regulates cascade activation. Consequently, the activated Fus3 translocate to the nucleus where it activates the transcription factor, Ste12, that triggers the expression of mating specific genes, which leads to cell-cycle arrest and eventually mating (reviewed in (173)).

Full-scale activation of the mating pathway is switch-like in its response and is regulated by another domain of Ste5- Fus3 binding domain (FBD). This domain is also involved in the inhibition of mating pathway activation (147,149,185). $Ste5^{FBD}$ allosterically mediates autophosphorylation of Fus3 to a monophosphorylated form (pFus3), which promotes Ste5 phosphorylation at four sites proximal to the RING domain, and through a previously unknown mechanism decreases the pathway output (147,185,268). Additionally, the phosphatase Ptc1, competes with Fus3 for binding to FBD domain, thereby regulating the overall phosphorylation status of Ste5 at the four sites (149). Interestingly, this Fus3-Ste5-Ptc1 circuit also regulates the switch-like mating process, wherein “non-docking” mutations of Ste5 which abrogate Fus3 binding to the FBD domain confers a graded mating response (149). However, the molecular mechanism underlying the negative feedback regulatory role of Ste5 was unknown.

Similarly, little is known about the function of Ste18 ($G\gamma$ subunit in yeast), besides its role as an anchor for Ste4 ($G\beta$) by virtue of prenylation of the C-terminal region of Ste18 (41). This scarce understanding about the functional relevance of $G\gamma$ subunit is not restricted to yeast $G\gamma$ but is the case with all eukaryotic $G\gamma$ subunits, including the ones in human. Recently, we had showed that all eukaryotic $G\gamma$ subunits possess an intrinsically

disordered N-terminal tail which harbors at least two phosphorylation sites (160). Moreover, the analytical component of our in-house PTM prioritization tool, SAPH-ire, had highly ranked these phosphorylation sites to have a potential function (160). However, the functional significance of these phosphorylation sites was still a mystery.

This study aimed to determine the role of the phosphorylated Gγ subunit in the regulation of G-protein signaling (if any). Using a yeast model system, this study demonstrates that the MAPK Fus3 phosphorylates Ste18 in a rapid and robust manner in response to GPCR activation, and this phosphorylation occurs in the N-terminal tail of Ste18. Interestingly, genetic mutants in which phosphorylation of Ste18-Nt was prevented (phospho-null Ste18, $Ste18^{3A}$) showed earlier activation of Fus3. Thus, phosphorylated Ste18 served as a negative feedback regulator of Fus3. This study further shows that the phosphorylated Ste18 acts in synergy with phosphorylated Ste5 to regulate G protein signaling. Several findings corroborated this conclusion. First, mutants in which phosphorylation on both Ste18 and Ste5 was abolished (a dual mutant expressing phospho-null Ste18, $Ste18^{3A}$ with the "non-docking" Ste5, $Ste5^{ND}$), i.e. $Ste18^{3A}/Ste5^{ND}$, showed augmented Fus3 activation which peaked 6 times faster and 4 times higher. Whereas, disruption of either inhibitory element alone ($Ste18^{3A}/Ste5^{WT}$ or $Ste18^{3E}/Ste5^{ND}$) relieves partial inhibition resulting in minor change in the rate and amplitude of Fus3 activation. Second, removal of phosphorylation from Ste18 and Ste5, through genetic mutations, led to greater interaction between Ste4/Ste18 and Ste5 as depicted by co-immunoprecipitation assay. Third, as a consequence of the stronger interaction between Ste4/Ste18 and Ste5, yeast cells expressing $Ste18^{3A}/Ste5^{ND}$ displayed rapid and stable association of bulk Ste5 at the plasma membrane. Fourth, phylogenetic analyses of Ste18 and Ste5 fungal orthologs revealed that the two phospho-regulatory elements (phospho-Ste18 and phospho-Ste5) have co-evolved. Additionally, data presented in this work showed that this Ste18/Ste5 module controls the switch-like mating response to increasing

concentration of pheromone as well as the differential activation of Kss1. In conclusion, this study provides insights into the mechanism involved in feedback regulation of G-protein signaling which proceed via synergy between the inhibitory phosphorylation of the N-terminal tail of Ste18 with the previously identified inhibitory phosphorylation of Ste5.

Besides feedback mediated regulation of G-protein signaling, mating pathway in yeast is also subject to cross-inhibition during stress conditions and inappropriate cell-cycle phase (117,118,127,158,159,219,222,249,256,269–273). Environmental stresses, such as high osmolarity and depletion of glucose to name a few, inhibit activation of the mating pathway in response to pheromone until the cell has adapted to stress (117–119,222,271,272,274). Similarly, mating is prohibited in cells that have passed the START check-point (127,158,159,219,256,269,270,273). Several components of the mating pathway, including Ste50 (118,249), Rck2 (118), and Gpa1 (117) is phosphorylated during osmotic stress; while Ste20 (219), Far1 (153), and Ste5 (158) is phosphorylated in a cell-cycle dependent manner. These phosphorylation events serve to inhibit activation of the mating pathway. In this study, we have identified Ste18-Nt as a target of cross-inhibition mediated phosphorylation during osmotic stress and G1 cell-cycle phase, but not during glucose depletion. We further speculate that the phosphorylated Ste18 could mediate inhibition of the mating pathway under sub-optimal conditions through a similar phosphorylated Ste18/Ste5 regulatory mechanism described above.

Together, this study shed light on the previously unknown regulatory role of Gγ subunits in G-protein signaling. In this role, the N-terminal intrinsically disordered tail of Gγ acts as a PTM-based regulator to modulate the Gβγ/effector binding, consequently controlling the pathway output. Thus, the work done in this study has successfully expanded the relevance of Gγ subunits in G-protein signaling, beyond its most appreciated role as an anchor for its obligate partner, Gβ subunit (41). In fact, prior to this work,

functional attributes of Gβ and Gγ subunits were rarely distinguished independently; instead in most cases either Gβγ was considered as a functional monomer or Gβ subunit was suggested to be the key player amongst the two proteins (4,275). Furthermore, this work suggests that the intrinsically disordered tail of Gγ subunit could potentially act as a node for cross-talk between G-protein signaling pathway and other pathways.

The conclusion from this study have been summarized below.

1. Gγ subunit in yeast, Ste18, is phosphorylated in response to GPCR activation by mating pheromone. This phosphorylation occurs in the intrinsically disordered N-terminal tail of Ste18.
2. The mating-specific MAPK, Fus3, is necessary for pheromone-dependent Ste18 phosphorylation.
3. Phosphorylation of Ste18, together with phosphorylation of the scaffold protein Ste5, synergistically mediate negative feedback regulation of Fus3 activation.
4. The inhibitory effect of Ste18/Ste5 regulatory module is mediated through regulation of the rate and stability of Ste5 at the plasma membrane.
5. The Ste18/Ste5 phospho-inhibitory module also regulates the switch-like morphological response to increasing concentration of pheromone.
6. The Ste18/Ste5 phospho-inhibitory module co-evolved in fungal phylogeny.
7. Ste18-Nt is phosphorylated in Fus3 and Hog1-independent manner when yeasts cells are exposed to osmotic stress.
8. In the absence of pheromone, Ste18-Nt, like Ste5, is phosphorylated in cell-cycle dependent manner, with maximum phosphorylation seen at G1 cell-cycle phase. Activated Fus3 is dispensable for this cell-cycle dependent phosphorylation.

9. Since the presence of an intrinsically disordered N-terminal tail with at least two phosphorylation sites is a conserved trait in all eukaryotic Gγ subunits, this work can serve as a pioneer study for similar mechanisms in higher eukaryotes.

4.2 FUTURE DIRECTIONS

This study has provided an insight into the novel role of Gγ subunit as a phosphorylation-dependent regulator of the G-protein signaling. Simultaneously, several research directions that might further our in-depth understanding of this novel regulatory unit, have opened up as a consequence of this study. Few of such questions have been discussed below.

What is the design of Ste18-Nt phosphorylation? How does it affect the impact of the regulatory element?

The intrinsically disordered N-terminal tail yeast Gγ subunit, Ste18-Nt, harbors three phosphorylation sites (T-2, S-3, and S-7); thus, may exist in one of the 2^3 phosphoforms, each corresponding to a particular pattern of phosphorylated sites. Moreover, the scope of regulation provided by each site may not be equal. Thus, identification of the phosphorylation site(s) is important to understand its mechanistic impact on the protein behavior.

Analysis of the primary sequence of Ste18 revealed that S-7 but not T-2 and S-3 has the signatory sequence S/T-P which promotes phosphorylation by MAPK/CDK. Using a genetic approach, our preliminary data shows that pheromone-dependent phosphorylation of Ste18-Nt occurs at a single site, S-7 (data not shown). Furthermore, the mobility shift of phospho-Ste18-Nt triggered in response to osmotic stress and cell-

cycle phase is equivalent to the pheromone-dependent electrophoretic profile of Ste18. Thus, we propose that Ste18 is phosphorylated on serine-7 under these conditions as well; although experimental validation is still needed. Since, all eukaryotic Gγ subunits contain two phosphorylation sites in their N-terminal region (160), an interesting question is whether T2 and/or S3 sites are amenable to phosphorylation in other (currently untested) condition(s)? Furthermore, investigating the contribution of each phospho-site in the regulatory mechanism depicted in this study might further our understanding of the regulatory role of Ste18.

Does phosphorylated Ste18-Nt participate in cross-talk mediated inhibition of the mating pathway?

It is well established that the mating process in yeast is coordinated with extracellular cues such as hyperosmotic stress, as well as intracellular cues such as cell cycle phase (118,119,222,271–273). Several components of the mating pathway are phosphorylated to limit the activation of the mating pathway when conditions are unfavorable (117,118,158,219,249,256). This work laid the foundation for the N-terminal tail of Ste18 as a phospho-regulator of G protein signaling. In this role, phosphorylated Ste18 synergizes with the scaffold protein, Ste5 to mediate negative feedback regulation of MAPK activation. In this study, we determined that Ste18 is phosphorylated in a cell-cycle dependent manner and in response to osmotic stress. However, whether and how Ste18 phosphorylation contributes to the regulation of cross-inhibition of the signaling dynamics of the mating pathway in the presence of osmotic stress and G1 phase is yet to be determined.

Does similar phosphorylation dependent Gγ/effector regulatory system occur in higher eukaryotes?

The G-protein signaling system is one of the main signaling pathways in eukaryotes, ranging from the simplest eukaryotic organisms, such as the budding yeast *S. cerevisiae*, to much more complex eukaryotes, such as human (reviewed in (276)). The overall build of the system is similar, consisting of GPCRs, heterotrimeric G proteins, effector proteins and RGS proteins (reviewed in (276)). Both yeast and human utilize G proteins to respond to ligand binding by receptors that detect environmental cues. However, compared to yeast, which employs a single heterotrimeric G protein complex to transduce pheromone-dependent signals through a scaffolded MAPK complex (reviewed in (180)), G-protein signaling in humans, in which there are approximately 800 GPCRs, 23 Gα, 5 Gβ,13 Gγ, multiple effectors, and 30 RGS proteins encoded by the genome, is much more complex (reviewed in (276)). Moreover, unlike in yeast, where Gβγ is the primary transducer of signal; both Gα and Gβγ are important transducers of signal in human (reviewed in (276)). As a result, discovering molecular mechanisms of G protein signaling and regulation is a comparatively simpler endeavor in the yeast model system; and the translation of such discoveries to other organisms may be more challenging in some cases and require special attention.

Using yeast as a model organism, I discovered a novel regulatory role of Gγ subunit in G-protein signaling. In this role, phosphorylated Gγ (Ste18 in yeast) together with the phosphorylated Gβγ effector protein (Ste5) mediates inhibitory regulation of the activation kinetic of the MAPK (Fus3). The inhibition of MAPK activation is accomplished by disrupting the interaction between Gβγ (Ste4/Ste18) and a Gβγ effector (Ste5), by phosphorylation that occurs proximal to the binding sites on both proteins. Specifically, Ste18 is phosphorylated in its N-terminal intrinsically disordered tail, a region close to the

helical region of Gγ which forms a coiled-coil structure with Gβ that participates in the interaction between Ste4/18 and Ste5. Simultaneously, Ste5 is phosphorylated close to the RING domain serves as a Gβγ binding site. As a result of the reduced interaction between Ste4/Ste18 and Ste5, bulk recruitment of Ste5 to the plasma membrane is hampered, which leads to diminished and delayed Fus3 activation. **At a fundamental level, I have identified a phosphorylation dependent Gγ/effector regulatory system that inhibits pathway output in yeast.** Hence, the most intriguing question that remains unexplored is whether a similar phospho-regulatory system exists in humans, wherein both Gγ and effector protein phosphorylation inhibits/regulates G-protein signaling.

In humans, multiple isoforms of Gβ and Gγ subunits combine to form specific combinations of Gβγ that associate with different Gα subunits and receptors, which in turn dictates the specificity of effector interaction and activation (277,278). The unique propeller structure of Gβ confers interaction with various effector proteins such as adenylyl cyclase (isotypes I, II, IV, V, and VI), phospholipase C- β (PLC-β), G-protein regulated inward rectifier K+ channels (GIRK), voltage gated calcium channels, and many more (reviewed in (4,275)). Besides the binding site on the propeller structure of Gβ, other secondary binding sites have been suggested to occur on Gβγ that are used by certain effectors (reviewed in (4,275)). For example, the N-terminal region of Gβγ is one such secondary site important for interaction with adenylyl cyclase isotype II, GIRK1, and PLC-β2 (279,280). Thus, it is possible that phosphorylation of the N-terminus of Gγ impacts activation of effectors. In fact, human $G\gamma_{12}$ subunit when phosphorylated in its N-terminal region by protein kinase C negatively regulates activation of adenylyl cyclase II and cAMP production (91,187). This observation suggests that phospho-regulation of Gγ-Nt is not restricted to the yeast G protein system. Furthermore, since most eukaryotic Gγ subunits have the potential to be phosphorylated in at least two phosphorylation sites in their N-

terminal tails (160), the phospho-regulatory role of Gγ subunit could be a general rule which holds true in both yeast and humans.

Several important questions should be explored to fully comprehend the role of Gγ phosphorylation in humans. First, is to ask what are the dynamics of phosphorylation of G gamma isotypes in humans? Of the 13 isotypes of Gγ, phosphorylation has been reported at one or more serine and/or threonine residues in the N-termini of Gγ 2, 3, 4, 5, 7, 10, and 12 (281–287). These phosphorylation sites were identified by high-throughput mass-spectrometry based phospho-proteomic studies done in melanoma cell line (Gγ2, 5, and 10) (282), neurodegenerated brain (Gγ3) (281), breast cancer cells (Gγ5, and 10) (284), pancreatic and lung cancer cells (Gγ12) (285,286), and in human epithelial cells treated with angiotensin (Gγ12) (287). However, whether or not these Gγ isotypes are phosphorylated in a GPCR activation dependent manner is yet to be determined. Additionally, the time and condition dependent dynamics of Gγ phosphorylation as well as the underlying kinases should also be explored. For example, the phosphorylation dynamics of Gγ12 can be determined in response to a time course stimulation of human endothelial cell lines expressing the angiotensin sensitive GPCR, such as the Mas. Additionally, *in vivo* strategies that employ screening of a deletion library of kinase to identify the kinase, followed by *in vitro* confirmation of the sufficiency of the kinase can be utilized to determine the kinase. As protein kinase C has previously been shown to phosphorylate Gγ12 *in vitro* (187), any role of protein kinase C in the angiotensin dependent Gγ12 phosphorylation can be investigated.

The second major question to be explored should be, how does Gγ phosphorylation affect interaction with other proteins? Gγ subunits participate in either direct or indirect interactions with receptors, Gα subunit, Gβ subunit, and effector proteins

(278–280,288–290). As an obligate partner of Gβ, Gγ interacts extensively to form the heterodimer Gβγ, wherein the N-terminal α-helix of Gγ is involved in a coiled-coil interaction with the N-terminal α-helix of Gβ and the C-terminal α-helix of Gγ extensively interacts with the base of the Gβ propeller structure (reviewed in (4,275)). The N-terminal region of Gγ also impart specificity to effector interactions (278–280,288,290). Moreover, specific Gγ interaction with receptors also regulates guanine nucleotide exchange in the Gα subunit (289). Thus, phosphorylation of the N-termini of Gγ subunits could affect the specificity and strength of interaction with receptors, Gα subunits, and effector proteins, and may also regulate conformational changes in the interacting proteins. Indeed, phosphorylation of the N-terminus of Gγ12 has been reported to negatively control adenyl cyclase II (187). Thus, it will be interesting to test by an immunoprecipitation experiment, *in vitro* binding assay, and/or FRET based assay whether phosphorylation of Gγ12 affects interaction with adenylyl cyclase II Interestingly, the activation of certain isotypes of adenylyl cyclase, such as type III and V, are inhibited in a phosphorylation dependent manner (291,292). Moreover, phosphorylation of human adenylyl cyclase type II has been demonstrated through high-throughput proteomic studies done in tumor samples (283,284,293), and has been implied to be phosphorylated by protein kinase C in rat (294). However, the regulatory effect of phosphorylation on the activation of adenylyl cyclase is unknown. Interestingly, three phosphorylation sites (Y452, S472, Y584) lie in the catalytic domain of adenylyl cyclase type II; and are close to the region (amino acid region 493-509) that is important for interaction with Gβγ (295). Thus, another interesting question to probe is whether adenylyl cyclase type II is phosphorylated in a GPCR activation dependent manner in humans; and if so, whether it regulates binding and activation by Gβγ (similar to our findings in yeast).

A third major question to be explored is whether Gγ phosphorylation affects G-protein signaling pathway output in mammals? The most important question is whether phosphorylation of Gγ has any regulatory effect on the pathway output. Additionally, since G-protein signaling has major implications in health and disease (8,54,55,57) and phosphorylation of many Gγ isotypes were identified in cancer cells or diseased cells (281–286); identification of the regulatory role of Gγ (if any) in G-protein signaling can offer scope for new druggable targets. For example, angiotensin mediated activation of the GPCR, Mas, has important biological role in the pathophysiology of renal inflammation (296). Additionally, Gγ12 has been shown to be phosphorylated in endothelial cells treated with angiotensin (287). Thus, it will be interesting to test if there is any regulatory effect of phosphorylated Gγ12 in the activation of the pathway and eventually on renal inflammation.

The fact that an intrinsically disordered structure has been retained throughout the evolution of Gγ subunits further suggests that this feature is beneficial not only for yeast but also for other organisms. Intrinsically disordered regions (IDR) have continued to emerge as an important structural feature of N and C-terminal PTM regulatory elements, with classic examples such as the N-terminal tails of histones as well as the C-terminal tails of GPCRs, tubulin, and others (297–301). Further experimental evidence will help to determine whether not only the structure, but also aspects of function are conserved in G protein signaling systems in other organisms – for which there is considerable experimental evidence of phosphorylation but virtually no evidence for its role in signaling.

PART II

Mapping global citrullination pattern of human plasma fibronectin to cell behavior and extracellular matrix memory

Collaborative project with Victoria L. Stefanelli and Professor Thomas Barker, University of Virginia

(Publication: Stefanelli VL, Choudhury S, Yeh V, Chambers DM, Pesson K, Torres MP, Barker TH. In submission.)

CHAPTER 5

Mapping global citrullination pattern of human plasma fibronectin to cell behavior and extracellular matrix memory

5.1 ABSTRACT

Posttranslational modifications (PTMs) are covalent modifications of proteins following protein biosynthesis. One such modification, citrullination – deimination of arginine to citrulline by peptidyl arginine deiminases (PADs) - has recently received significant interest in biomedicine. Indeed, citrullination of the extracellular matrix (ECM) protein, fibronectin (Fn), is a common hallmark for the pathogenesis and detection of rheumatoid arthritis (RA), fibrosis and cancer metastasis. Nevertheless, the fundamental characterization of citrullination sites on Fn and its implication on physiological cell behaviors such as adhesion, migration and differentiation remain ill-defined. Here, we used high-resolution mass spectrometry to determine the site-specific citrullination status of Fn, catalyzed *in vitro* by PAD isotypes 2 and 4 – the most prevalent PADs in the pathophysiology of RA and fibrosis. We successfully identified 24 citrullination sites spanning the entire length of Fn, with maximum citrullination (7 sites) observed in the primary cell-attachment regions of the protein. Citrullination was specific in varying degree to the enzymatic activity of individual PADs. Interestingly, five citrullination sites (R1410, R1434, R1479, R1476, R1452) were in or near the canonical sites responsible for integrin binding (RGD and PHSRN). Additionally, cellular and biochemical analysis conducted by Stefanelli et.al. revealed that citrullination of Fn enhanced cell attachment and migration. This change in cell behavior was due to altered Fn-integrin binding dynamics, a switch in the integrin profile of a cell, and concomitant change in the activation of FAK-Src and ILK-GSK signaling. Furthermore, they showed that citrullination of Fn represents a significant

means for recording inflammatory memories. Together, our collaborative effort has not only highlighted the impact of citrullination on cell behavior; but as the most comprehensive report of identification of citrullination sites in Fn, our study provides a valuable resource for functional studies of site-specific and/or global citrullination of fibronectin.

5.2 INTRODUCTION

Posttranslational modifications (PTMs) are covalent and enzymatic modifications of amino acid side chains or termini of proteins, resulting in a change in the function, localization, and/or interaction profile of proteins. Thus, by altering various properties of proteins, PTMs play central role in cellular physiology- an area of research that is becoming increasingly appreciated (reviewed in (302–304)). Indeed, the global analysis of type, dynamics, and function of PTMs of proteins are important goals in cell biology.

Among different approaches to study PTMs, mass spectrometry (MS) – an analytical technique that accurately measures the masses within an ionized sample based on their mass-to-charge ratio- has been extensively used in the past few decades to identify proteins modified by a particular PTM (305–308). In particular, tandem mass spectrometry (MS/MS), which involves multiple steps of mass spectrometry selection and fragmentation of selected ionized samples, is used to determine the identity of modified residue. The traditional approach to detect PTMs is by measuring the mass of peptides derived from the proteolytic digestion of proteins (“bottom-up MS”), rather than of the entire protein (“top-down MS”) as mass differences between modified and unmodified forms of large proteins are difficult to measure. Broadly, a typical workflow consists of separation of protein on a SDS-PAGE gel, excision of gel pieces corresponding to unique protein bands, and subjecting the protein in the gel pieces to a series of chemical reactions,

including cleavage of disulfide bonds by a reducing agent, the capping of free thiol groups by an alkylating reagent, and finally the enzymatic cleavage of peptide bonds to generate peptides (309). The peptides mixture then undergoes high throughput liquid chromatographic separation and subsequent MS analysis (LC-MS). Characteristic mass shifts in fragmentation MS/MS spectra often allows specific detection of the post-translationally modified amino acid residues. Indeed, recent advances in bottom-up MS have dramatically propelled the identification of PTM sites on large number of proteins, with phosphorylation being the most widely identified PTM (305–308). In contrast, citrullination of arginine residues, a PTM catalyzed by the enzymatic action of peptidyl deiminase (PAD), is far less characterized.

Citrullination involves removal of the positively charged imino moiety from the side chain of arginine and converting arginine to an uncommon amino acid, citrulline (reviewed in(310,311)). As a consequence of the hydrolytic reaction, the resulting citrulline shows 1Da reduction in mass and is a neutral amino acid. The enzyme, PADs, which catalyze the deimination reaction, exist in 5 isoforms- PAD1, PAD2, PAD3, PAD4, and PAD6 and are expressed in a tissue-specific manner. Under physiological conditions, PADs function in gene regulation by citrullinating histone proteins. Additionally, PADs 2 and 4 are involved in apoptosis and inflammatory immune responses, such as rheumatoid arthritis (RA) and fibrosis. Since citrulline is not a natural amino acid in proteins, it creates novel epitopes which provoke an autoimmune response (reviewed in (310,311)). Indeed, the presence of antibodies generated against citrullinated fibronectin, is a common hallmark of RA and fibrosis (312).

Fibronectin (Fn) is a large glycoprotein found in body fluids, cell surfaces and extracellular matrix (ECM). It functions as the key link between cells and ECM and is involved in a range of physiological processes such as cell adhesion, cell migration and signaling; events that are critical for embryogenesis, wound healing, haemostasis, and

thrombosis (reviewed in (313–315)). In body fluid including blood plasma and saliva, Fn is present as a soluble disulfide-linked protein and is responsible for mediating blood coagulation through its affinity for fibrin and platelets(316). On the other hand, cellular Fn found in ECM is multimer and fibrous, and interacts with cell receptors to promote cellular adhesion and cytoskeleton organization(313,315,317–319). While plasma Fn is expressed by hepatocytes, cellular Fn is secreted by a wide range of cells. Furthermore, several splice variants of Fn which differ in their cell-adhesive, ligand-binding, and solubility properties are expressed in a cell-type specific manner. This allows cells to modulate their ECM in a developmental and tissue-specific manner (reviewed in (313–315)).

Structurally, each monomer of Fn has a multi-domain architecture with three types of repeating units or modules (type I-III). There are 12 type I, 2 type II, and depending on the splice variant 15-18 type III units in a Fn monomeric protein. Compared to type III unit which is 90-100 amino acid long, type I and II units contains 43 and 49 amino acid residues. Additionally, all three modules (type I-III) contains at least two antiparallel β-sheets that fold over to form a central core. Combinations of these modules form distinct structural and functional domains that mediate binding to integrin, heparin, collagen, and fibrin (reviewed in (313–315)). A large number of different integrins, including $\alpha5\beta1$ and $\alpha v\beta3$, bind to Fn. In this regard, the RGD tripeptide sequence in typeIII-10th repeat has been found to be critical for integrin binding. A second site in typeIII-9th repeat, PHSRN, synergizes with RGD sequence to promote specific integrin binding to Fn (320,321). These interactions between Fn and integrin modulate mechano-transduction signaling through FAK-Src and ILK-GSK3 proteins, adhesion dynamics, and cell migration; all of which is essential for embryonic development, immune cell homing, wound healing and angiogenesis. Moreover, dysfunction of Fn-integrin binding has been associated with

several diseases such as RA, fibrosis and cancer. Additionally, Fn has been frequently observed to be citrullinated by PADs 2 and 4 in such diseased patients (312,322–327). Indeed, citrullinated Fn is a hallmark of inflammatory diseases and the presence of antibodies against citrullinated Fn is a well-established and highly-specific biomarker of RA (323,328,329). Nevertheless, the physiological functions of citrullinated Fn remains ill-defined.

Given the scarcity of information about citrullinated fibronectin, and the implications of citrullination on the interaction profile of Fn, the Barker's group decided to investigate citrullination of fibronectin mediated by *in vitro* activity of PADs 2 and 4. In our lab, we identified citrullination of 24 arginine residues, approximately 59% of which were found in regions important for protein-protein interactions such as binding to integrin, fibrin, or heparin. Importantly, 5 citrullines were in the type III 9-10 region involved in cell attachment. Of these sites, one modified arginine (R1410) was in the synergy site (PHSRN) for integrin binding, while another R1434 was proximal to the synergy site. Three additional citrullination sites (R1479, R1476, R1452) were close to the RGD sequence critical for integrin binding. Furthermore, not all arginine residues were equally citrullinated by PADs 2 and 4. Indeed, we found that PAD4 citrullinate Fn more efficiently than PAD2, although a considerable overlap was observed in their site-specificity. Additionally, Stefanelli et. al. showed that citrullination of Fn has prominent impact on its integrin binding specificity with increased preference towards $\alpha 5\beta 1$ integrin. They further showed that this integrin switch to $\alpha 5\beta 1$ subsequently accentuates mechano-transductive signaling through FAK-Src and ILK-GSK3 and the migratory nature of cells. Taken together, we report the comprehensive map of citrullination sites on Fn and its potential to alter cell signaling and behaviors, that can have implications in the pathophysiology of inflammatory diseases, such as RA.

5.3 RESULTS

5.3.1. Identification of citrullination sites on human fibronectin.

Fibronectins (Fn) are large glycoproteins composed of two nearly identical disulphide bonded subunuits; and are present in the extracellular matrix (insoluble form) and the plasma (soluble form) (313–315). Additionally, in humans, as many as 17 isoforms of Fn are generated by the alternative splicing of the pre-mRNA, that play important roles in cell adhesion, migration, growth and differentiation (313–315). Although several studies have linked citrullination of Fn to rheumatoid arthritis, fibrosis, and cancer; little is known about the citrullinated sites on Fn and its impact on the physiological function of Fn (312,323–327).

To this end, we first used LC-MS/MS to map the positions of citrullinated residues in purified plasma Fn, which were subjected to *in vitro* enzymatic citrullination by PAD2, PAD4, or both. Using a combination of complementary in-gel digestion techniques (see methods), we achieved a total of 81% coverage across all samples with more than 25,000 peptide spectral matches (PSMs) spanning across all isoforms of Fn, except isoforms 4 and 16, the unique peptides of which were not detected. Citrullinated sites were identified by searching against a database comprising of all isoforms of Fn and were further confirmed by manual investigation of the peptide spectral patterns. In total, we identified 24 citrullination sites, including the 3 previously reported sites (R1035, R1036, and R2356)(328,329). Figure 1A shows a schematic overview of all the sites mapped on the canonical Fn-1 comprising of a polypeptide of 2,386 amino acids. Of the 24 citrullinated sites identified, 58.3% were located on regions with defined function, such as fibrin and heparin binding, collagen binding, and cell attachment, with maximum citrullination (7 sites) observed in region 1267-1540 involved in cell-attachment (Figure 1B). Interestingly, 3 citrullination sites (R1479, R1476, R1452) were within the $^{9\text{-}10}$Fn-III domain near the

canonical integrin binding tripeptide, RGD (Figure 1C), although the RGD site itself was unmodified. Additionally, the PHSRN synergy site (R1410), important for strengthening α5β1 integrin attachment in coordination with RGD[10], was also found to be citrullinated, along with the nearby R1434 (Figure 1C). In conclusion, our work represents the most detailed mapping of the citrullination sites on Fn. Notably, the robust citrullination sites of Fn, specifically near integrin binding/specificity sites, could reflect a potentially critical role of this PTM in regulating Fn-integrin binding specificity and eventually cell behavior.

A. Fibronectin (P02751)

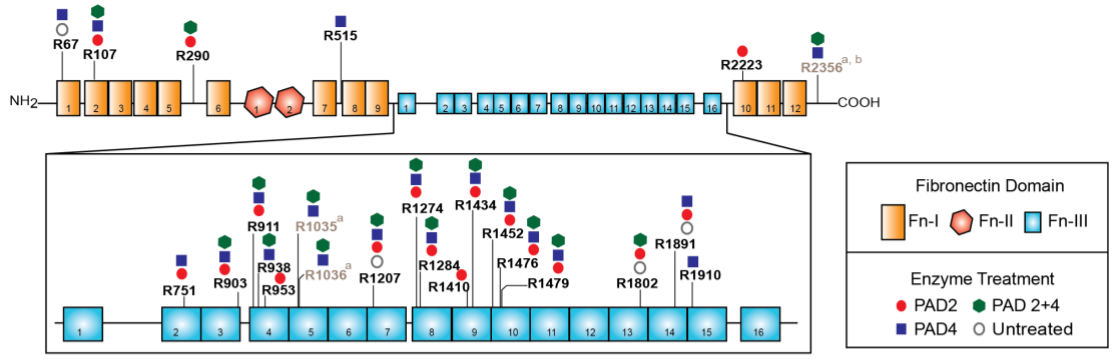

B.

Position(s)	Description of functional region	Citrullination sites identified by MS/MS	Total sites
52 - 272	Fibrin- and heparin-binding 1	67, 107	2
308 - 608	Collagen-binding	515	1
1267 - 1540	Cell-attachment	1274, 1284, 1410, 1434, 1452, 1476, 1479	7
1721 - 1991	Heparin-binding 2	1802, 1891, 1910	3
2206 - 2337	Fibrin-binding 2	2223	1
Other	Undefined	290, 751, 903, 911, 938, 953, 1035, 1036, 1207, 2356	10
		Total citrullinated sites identified by MS/MS	24

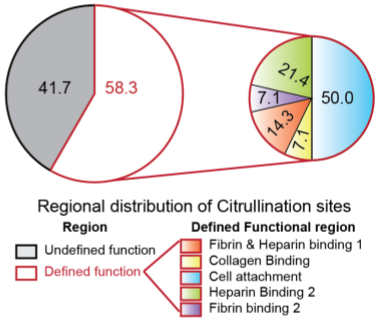

C.

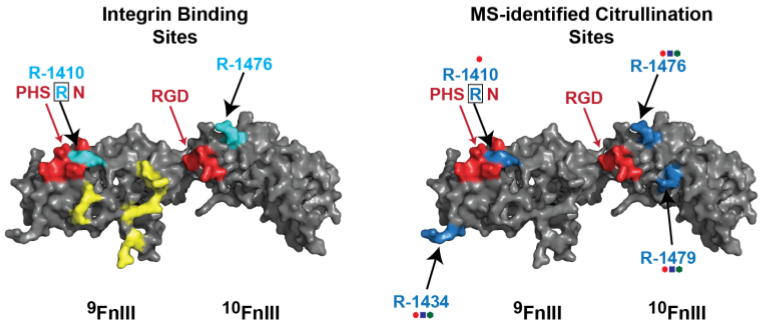

Figure 5.1. Mapping citrullination sites on human fibronectin. (A) Schematic overview of citrullination sites mapped onto human Fn comprised of repetitive units of type I-III domains (depicted in different shapes). Tandem mass spectrometry was used to map the positions of citrullinated residues in purified plasma Fn, which were either untreated or subjected to *in vitro* enzymatic citrullination by PAD2, PAD4, or both. Three previously reported sites (R1035, R1036, and R2356) that were also detected here are shown (residue labeled in brown) ((a) van Beer et. al. 2012; (b) K. Sipila et. al. 2017). (B) Citrullination sites identified in this study were grouped based on location within regions of fibronectin and known physiological function (based on overlap with data compiled by UniProt: (http://www.uniprot.org/uniprot/P02751) (left). Of the 24 citrullinated sites identified, 58.3% were located in regions with defined function, such as fibrin and heparin binding, collagen binding, and cell attachment, with maximum citrullination observed in the region involved in cell-attachment (right). (C) Three-dimensional structure of the 9th and 10th fibronectin type III domain (PDB 4LXO) highlighting residues previously shown to be essential for integrin binding (Redick et al, 2000) (Left). (Red) RGD and PHSRN sequences essential for synergistic integrin binding. (Cyan) residues with the greatest degree of binding influence outside the RGD site (R1410 and R1476). (Yellow) residues that help to facilitate PHSRN interactions. (Right) MS-identified citrullination sites within the $^{9\text{-}10}$FnIII domains showing overlap with integrin binding residues R1410 and R1476, as well as additional sites near the integrin binding interface (R1434, R1479) and R1452 (underneath R1476 and not shown here).

5.3.2. Citrullination of human fibronectin is specific to PAD-activity.

Citrullination is catalyzed by peptidylarginine deiminases (PADs) family of calcium-binding enzyme. To date, five isoenzymes have been identified that differ in their calcium and pH preferences. Moreover, the expression of PADs is tissue-specific, for example, while PAD2 is ubiquitously expressed, PAD4 is specific to neutrophils and eosinophils. Additionally, amongst the 5 isoenzymes, PAD2 and PAD4 are most frequently associated with inflammation and cancer metastasis (reviewed in (311)). However, the extent to which either PAD2 or PAD4 contribute to citrullination of Fn is not known.

To estimate the crude relative efficacy of PAD activity, we relied on the number of sites modified and percent of citrullinated peptide spectral matches (PSMs) normalized to the total PSM in each PAD treated Fn sample. As expected, citrullination of ariginine residues in Fn were specific to the enzymatic activity of PAD, with majority of residues

(84%) citrullinated only in the presence of PAD activity. In contrast, 16% of identified residues, corresponding to 4 arginine residues (R67, R1207, R1802, and R1891) were found citrullinated in plasma Fn in the absence of any PAD treatment *in vitro*. Amongst the remaining 20 sites, 4 sites (R290, R953, R2223, and R1410) and 6 sites (R515, R938, R1035, R1036, R1910, and R2356) were specific to PAD2 and PAD4 activity respectively. Whereas the specificity for 10 sites (R107, R751, R903, R911, R1274, R1284, R1432, R1452, R1476, and R1479) overlapped by both PAD2 and PAD4 (Figure 1A, Figure 2A). Interestingly, the frequency of PAD2 or PAD4 citrullinated PSMs was unique to each residue. Among the 10 sites modified by both PAD2 and PAD4, 7 sites (R751, R903, R911, R1432, R1452, R1476, and R1479) displayed relatively higher frequency of PSMs with PAD4 than PAD2. Moreover, the overall efficacy of *in vitro* citrullination by PAD4 was twice greater than by PAD2, as measured by the percent of PSMs for citrullinated peptides over the total PSMs (Figure 2B-C). Taken together, our data suggests that citrullination of Fn is relatively more efficient by PAD4 than PAD2.

5.3.3. Citrullination of fibronectin enhances cell adhesion and migration

Fibronectin functions *in vivo* as an anchor for cells in the extracellular matrix, and participates in complex interaction with other matrix proteins as well as integrin receptors on cell surface (313–315). The cell attachment activity of fibronectin is mediated via the binding of the RGD motif in $^{9\text{-}10}$Fn-III domain to special $\alpha\beta$ heterodimeric transmembrane receptors – integrins - on cells (330–333). This binding event results in clustering of integrins and other adhesome proteins at the attachment site leading to formation of a focal adhesions (FAs) and organization of the actin cytoskeleton (330–334). Indeed, a switch in the expression profile of two key integrins- $\alpha5\beta1$ and $\alpha v\beta3$ – is critical to modulate

A.

Description of citrullinated sites	Residue Position	Total sites
PAD independent sites	R67, R1207, R1802, R1891	4
PAD2 unique sites	R290, R953, R1410, R2223	4
PAD4 unique sites	R515, R938, R1035, R1036, R1910, R2356	6
Overlapping sites	R107, R751, R903, R911, R1274, R1284, R1434, R1452, R1476, R1479	10

B.

Description	Untreated sample	PAD2	PAD4	PAD2 +4
PSMs	6527	7688	7159	4435
Citr. PSMs	32	90	193	111
% Citr. PSMs	0.49	1.17	2.69	2.50

C.

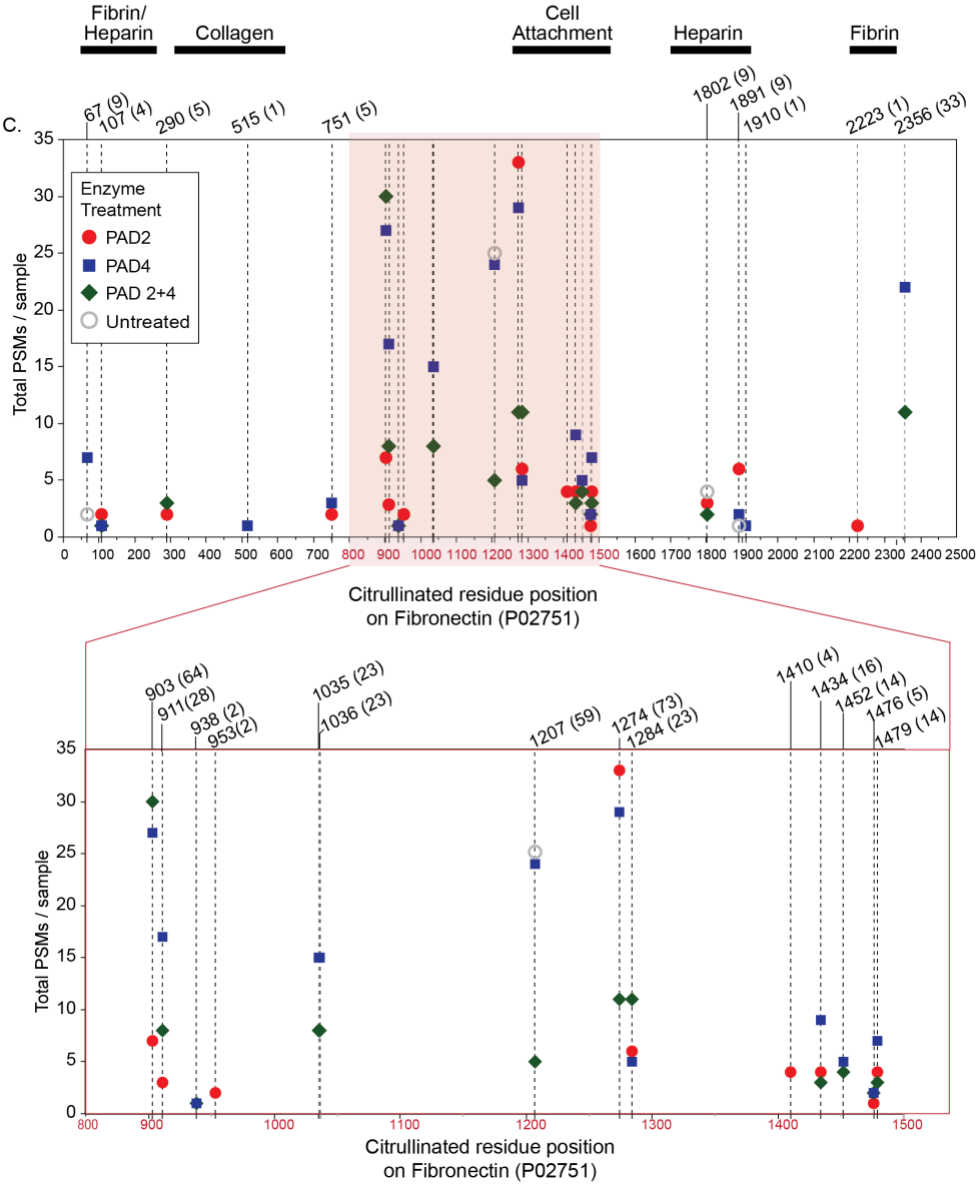

Figure 5.2. Frequency of identified citrullinated sites and peptide spectral matches (PSMs) for human fibronectin. (A) Table linking specific and shared citrullination sites between PAD2 or PAD4. Most sites (41.7%) were citrullinated by both PAD2 and PAD4, followed by PAD4 unique sites (25%). (B)Table showing the number of PSMs observed in each sample. Overall, the efficacy of *in vitro* citrullination by PAD4 was twice greater than by PAD2, as measured by the percent of PSMs for citrullinated peptides over the total PSMs. (B) Plot showing the citrullinated PSMs corresponding to residue position of human fibronectin (UID P02751), with the known functional regions (as in Figure 1.1B) delimited as horizontal bars above the residues. Color codes represents respective enzyme treatment. PAD2 and PAD4 citrullinated some residues more frequently than others. Of the 10 overlapping sites, 6 sites (R751, R903, R911, R1434, R1476, and R1479) were citrullinated by PAD4 more efficiently in comparison to PAD2. The cumulative PSMs for each site (across all experiments/all PADs) is denoted in the parenthesis adjacent to the annotated residue. Comprehensive list of PSMs provided in supplementary table.

cell behavior such as cell adhesion and migration (333,335). Besides cell-matrix adhesion, Fn-integrin binding result in activation of downstream signaling through FAK/Src complex and GSK3 (glycogen synthase kinase 3) (330–334,336). Together, these cell behaviors and signaling are critical for several physiological processes such as wound healing and embryonic morphogenesis. Nevertheless, the implications of citrullination of Fn on controlling cell behaviors is yet to be determined.

Stefanelli et. al. compared the efficiency of citrullinated Fn to unmodified Fn in modulating Fn-integrin binding specificity and the mechano-transduction signaling, which ultimately controls cell adhesion and cell migration. Through a series of biochemical and mechanical experiments, they made several key discoveries- citrullination of Fn lead to (i) integrin switch from $\alpha v\beta 3$ to $\alpha 5\beta 1$, (ii) enhanced FAK/Src activation, (iii) reduced GSK activation, (iv) increased cell adhesion turnover, and (v) increased cell migration (Stefanelli et. al. in review). They showed that citrullinated Fn has reduced affinity for $\alpha v\beta 3$ integrin, an observation consistent with a previous work in the field (328). Furthermore, they proposed that the switch to $\alpha 5\beta 1$ integrin clusters in FA serves to compensate for the diminished $\alpha v\beta 3$ binding and triggers robust cytoskeletal remodeling. Moreover, since citrullination causes irreversible protein structural modifications, Steffanali et al. propose

that citrullinated Fn could act as a memory store of inflammatory attacks (Stefanelli et. al. in submission). Together, Steffanali et. al. showed that citrullination of Fn can serve as extracellular matrix memory by inducing an integrin switch in interacting cells.

5.4 DISCUSSION

5.4.1. Challenges in the identification of citrullination sites on fibronectin

Citrullination, the product of protein arginine deiminase (PAD)- mediated deimination of arginine residues in a protein, has been implicated in several physiological and pathological processes (312,323,337–341). Indeed, citrullination of fibronectin is associated with RA, fibrosis and cancer metastasis. Commercially available anti-citrulline antibodies are often used to detect citrullination of proteins, including Fn. However, detection with antibodies is not optimal due to two key reasons. One, antibodies fail to provide sequence information of citrullines in a protein. Two, anti-citrulline antibodies often display overlap in reactivity and falsely detect carbamylation of lysine as citrullination(342). Currently, the best available method to accurately map citrullination sites is through the combination of high resolution MS and bottom up strategies. Nevertheless, detection of citrullination by MS has few limitations. Unlike arginine, citrulline is resistant to proteolytic cleavage by the protease trypsin- an enzyme that cleaves the C-terminus peptide bonds of arginine and lysine and is routinely used in bottom up approaches to digest proteins to peptides by prior to MS analysis. This elimination of tryptic sites results in larger peptides that are harder to detect and sequence. Furthermore, deamidation of glutamine and asparagine produces monoisotopic mass difference of +0.984016, identical to citrullination of arginine, leading to misidentification of sites. Additionally, the limited number and uneven distribution of lysine and arginine throughout the fibronectin sequence of 2386

amino acids, results in poor sequence coverage by the conventional trypsin-based bottom up MS. Indeed, the maximum reported sequence coverage of Fn till date is approximately 53 percent (329). In this study, we attempt to overcome these challenges by (i) employing multi-protease strategy that capitalizes on different proteolytic enzymes with specific cleavage chemistry to generate a diverse pool of peptides prior to MS analysis, which in turn increases sequence coverage and identification of citrullination sites; and (ii) including deamidation of glutamine and asparagine as dynamic modification parameter in the SEQUEST search algorithm as well as confirming the citrullinated sites by manual annotation.

Indeed, by using three commercially available proteases- trypsin, gluC, and chymotrypsin- either individually or as a mixture (trypsin and gluC) to prepare digested samples for LC-MS analysis, we were able to achieve 81% sequence coverage across all samples. Such results were not attainable by performing multiple technical replicates of a single protease digest. Moreover, the diverse population of peptides generated due to multi-protease approach allowed substantial increase in the identification of citrullination sites, which otherwise would have been missed due to tryptic miscleavage. Indeed, prior to our report, only two groups have investigated *in vivo* citrullination of Fn in inflammatory synovial fluid and determined 7 citrulline sites (R241, R440, R1035, R1036, R1162, R1573, and R2356) (328,329) compared to the 24 sites identified in this study. Of the 7 previously identified sites, 3 citrullination sites (R1035, R1036, and R2356) were also identified in our *in vitro* study; 2 sites (R241 and R440) were not covered by our LC-MS analysis; and the remaining two sites (R1162 and R1573) were covered but not found to be citrullinated. A key difference in our study vs previous studies is the source of citrullinated Fn- while our study is based on *in vitro* citrullinated Fn, previous studies are on *in vivo* citrullinated Fn. Thus, whether the increased number of citrullination sites

identified in this study is due to better sequence coverage of Fn or increased efficiency of PADs to citrullinate *in vitro* is debatable. Indeed, since PAD activity is dependent on calcium concentration, the efficiency of PAD may vary in *in vitro* experiment vs a natural physiological or inflamed microenvironment. Nevertheless, the comprehensive mapping of citrullination modifications on Fn have opened avenues to future studies aimed at determining the functional relevance of these citrullines in development of RA, fibrosis, cancer or other diseases.

5.4.2. Implications of citrullination on fibronectin properties and its significance to disease progression

Fibronectin, a large ECM protein, plays important roles in cell adhesion, migration, growth, and differentiation. Indeed, interactions between Fn and adhesion receptors, especially the members of the integrin family, mediate the anchorage of cells to ECM and orchestrate chemical and mechanical signal transduction critical for controlling cell behavior (314). Furthermore, fibronectin is extensively subjected to citrullination by PADs released by dying granulocytes (343) and has major implications in the pathogenesis of inflammatory diseases and tumor metastasis. Nevertheless, the mechanism by which citrullinated Fn interferes with its physiological functions or orchestrates the deterioration of healthy to pathological tissues remains poorly understood. In this collaborative work, Stefanelli et. al. showed that citrullination of Fn has a uniquely activating effect mediated through an induced switch in integrin profile from $\alpha v\beta 3$ to $\alpha 5\beta 1$ that subsequently enhances mechano-transductive signaling and the migratory nature of stromal cells. Interestingly, $\alpha 5\beta 1$ integrin, unlike $\alpha v\beta 3$, by virtue of its exposed RGD binding pocket and binding ability to the PHSRN synergy site has more affinity to soluble Fn (344–347). Notably, conversion of arginine to citrulline in a protein and the consequential decrease in

net charge, loss of potential ionic bonds, and interference of H-bonds has often been suggested to alter protein structure (348). Indeed, several PAD substrates such as filaggrin, trichohyalin, amyloid β-protein, FET proteins (FUS, EWS, and TAF15), upon citrullination show reduced structural organization and ability to form aggregates (340,341,348). Thus, an interesting but yet answered question is whether citrullination of Fn favors the "soluble" over the "stretched" conformation of Fn and thereby affects the accessibility of the RGD and PHSRN motif which ultimately dictates the preference for specific integrin partner.

Several studies have shown that overexpression of α5β1 coupled with its enhanced engagement with ECM proteins facilitate cancer cell invasion and tumor progression (349–351). Additionally, α5β1 integrin plays significant role during acute inflammatory conditions, including RA, wherein α5β1 induces increased leucocyte migration and protection of synovial cells from apoptosis (352–355). Thus, Stefanelli et al. suggest that the implications of citrullinated Fn in metastasis of cancer and inflammatory diseases could be mediated through the αvβ3 to α5β1 integrin switch and consequent changes in cell signaling and behavior. Furthermore, since citrullination is an irreversible PTM that renders proteins resistant to degradation (356), the impact of citrullinated Fn is long-lived. Thus, our findings further the understanding of the underlying mechanism by which ECM influence cancer metastasis and inflammatory disease progression.

5.5 EXPERIMENTAL PROCEDURES

In-gel Protein Digestion

In-gel protein digestion was conducted as previously described (309), with modifications. Briefly, selected protein bands were excised from the Coomassie-stained gel, diced into small pieces, and then destained with HPLC-grade water (Avantor) and 1:1

acetonitrile (ACN)/ammonium bicarbonate (ABC) (Sigma-Aldrich). The de-stained gel pieces were then dehydrated with multiple ACN washes until rock hard, followed by air drying for ~10 minutes. The gel pieces were rehydrated for 30 minutes with 50mM dithiothreitol (Sigma-Aldrich) to reduce disulfide bonds, followed by replacement with 100mM iodoacetic acid (Sigma-Aldrich) and 45 minutes shaking at 750 rpm in the dark to alkylate the reduced thiols. After reduction/alkylation, the gel pieces were once again washed and dehydrated as before, and then chilled on ice for 10 minutes. In-gel digestion was achieved by rehydrating the gel pieces with either trypsin (40µg/mL, Promega Cat # V511A), gluC (40µg/mL, Calbiochem Cat # 324713), chymotrypsin (50µg/mL, Promega Cat # V1062) or a mixture of trypsin and gluC. In each case, 50µL of the sequencing grade enzyme solution was added to the gel pieces and incubated on ice for 30 minutes. Excess enzyme solution was then removed and replaced with 100µL 50mM ABC and the pieces were incubated overnight at 37°C with shaking at 750 rpm. Resultant proteolytic peptides were extracted by two rounds of dehydration using 100µL ACN and collection of the resulting extract into low-retention microfuge tubes, which were frozen solid at -80°C and then sublimated by centri-vapping. The dried peptides were reconstituted by sonication in 5% ACN/0.1% formic acid and stored at -80°C prior to analysis.

Mass Spectrometry

LC-MS analysis of peptides produced by in-gel digestion was carried out with an UltiMate™ 3000 RSLCnano System UPLC system (Dionex) with Acclaim PepMap RSLC column (75µm x 25cm nanoViper C18 2µm, 100Å) coupled to a Q-Exactive Plus Orbitrap mass spectrometer (Thermo Scientific) run in data-dependent acquisition mode (top-8). Resultant RAW files were analyzed using Proteome Discoverer 2.1 with embedded SEQUEST search algorithm operating with an allowable 1% false-discovery rate, wherein

the human fibronectin (P02751) isoforms 1-17 were used as targets for spectral matching. Mass deviations for precursor ions and fragment ions were set to 10 ppm and 0.6 Da respectively. Besides citrullination (R), other modifications such as deamidation (N, Q), oxidation (M), phosphorylation (S, T, Y), acetylation (protein N-terminus), and caramidomethylation (C) were included in the analysis. Additionally, the citrullinated sites were checked manually.

CHAPTER 6

CONCLUSIONS AND FUTURE DIRECTIONS

6.1 CONCLUSIONS

Fibronectin (Fn), a large extracellular matrix (ECM) protein, mediates various physiological processes through interactions with cell-surface integrin receptors and growth factors (313). Post-translational modification of Fn, specifically citrullination, is intimately involved in the pathogenesis of rheumatoid arthritis (RA), fibrosis and cancer metastasis (327,357). Citrullination is the conversion of peptidylarginine to citrulline catalyzed by peptidylarginine deiminase (PAD) (310). In this collaborative study, we investigated the citrullination of Fn and its implication on modulating the cell behavior. The key findings of this study are listed below.

1. Fn has at least 24 *in-vitro* citrullination sites. Of these, 3 sites were previously reported (328,329), and 21 sites are unique to this study. Thus, our work represents the most detailed mapping of citrullination sites on Fn.
2. Three citrullinated sites (R1452, R1476, R1479) are close to the integrin binding site (RGD) on Fn and 2 sites (R1410, R1434) are in or near the PHSRN synergy site. Collectively, these citrullines could modulate integrin-binding dynamics.
3. Citrullination of Fn altered the integrin-binding dynamics resulting in a switch from $\alpha v\beta 3$ to $\alpha 5\beta 1$ integrin, enhanced mechano-transduction signaling through FAK, Src, and ILC activation, and enhanced cell adhesion and migration.
4. Since citrullination is an irreversible PTM and citrullinated Fn is resistant to degradation, citrullinated Fn influence future cell behaviors for a prolonged time and acts as an ECM memory.

6.2 FUTURE DIRECTIONS

This collaborative study has provided an insight into the mechanism by which citrullination of fibronectin can modulate cell signaling and behaviors, and thereby inspire new approaches to exploit the mechanobiology of ECM in regenerative medicine as well as for diagnostic and therapeutic applications. Furthermore, this study opens up several avenues for future work, some of which are discussed below.

What is the magnitude of citrullination of fibronectin *in vivo* in inflammatory microenvironments?

A key regulator of PADs- enzymes that catalyze citrullination- is calcium. Indeed, different PADs require different calcium ion concentration and pH for their activity. In *in vitro* experiments, citrullination is observed only at very high concentration of calcium (358). However, under physiological conditions, the calcium concentration is in the range of 1 micromolar to 10 nanomolar which is insufficient for PAD activity. Thus, citrullination is only observed during inflammatory disease, such as RA, which is often accompanied by increase in calcium levels in the serum (approximate final concentration of calcium is 2.2- 2.6mM) (359,360). For this study, Fn was citrullinated in a PAD reaction buffer containing final concentrations of 5mM $CaCl_2$- almost double the concentration of calcium within inflammatory microenvironment. Thus, a key question is whether all the 24 citrullination sites identified in this study will be citrullinated *in vivo*. Indeed, only a limited number of citrullination sites (7 sites in total) on Fn extracted from RA patients have been identified till date by using a trypsin-based bottom up MS approach (328,329). An interesting future work will be to utilize the advantage of multi-protease bottom-up MS approach used in this study, to explore citrullination of Fn that has been either extracted from patients (*in vivo*) or subjected to *in vitro* citrullination reaction in a buffer containing a range of calcium concentration that mimics inflamed sera.

Are all citrullination sites functionally equivalent?

In this collaborative study, we identified 24 citrullination sites that spanned the entire length of Fn. Additionally, Stefanalli et.al. described the implications of global citrullination of Fn on cell signaling and behaviors; however site-specific function of citrulline is yet unknown. Thus, an enticing future direction is to determine the contribution of each citrullination site in the altered function of Fn. This question can be tackled by a strategy that couples emerging computational methods with the established biochemical/biomechanical assays in the field. In this unified approach, PTM function prioritization tool will be used to predict a set of high-priority citrullination sites that can be further studied by point mutations to decipher the site-specific function of citrullinated Fn.

Furthermore, this study explored the implications of citrullination of Fn on cell adhesion and migration which is mediated through the interaction of Fn with cell adhesion receptors, integrins. However, Fn is a large protein with multiple functional domains that mediate interactions with not only cell receptors such as integrins, but also bind to other ECM proteins such as heparin and collagen (313). Thus, an extension of this work can be to determine the potential contribution of citrullinated Fn in altering interactions with other ECM proteins, and eventually affecting ECM structure.

Which citrullination sites on fibronectin are immunogenic?

Citrullination involves conversion of arginine to an uncommon amino acid, citrulline, which can act as antigens to provoke immunogenic reaction. Indeed, three citrullinated residues (R1035, R1036, and R2356) on Fn comprise two epitopes recognized by anti-citrullinated protein antibodies (ACPAs) that are routinely used for the diagnosis of RA (329). We have identified a total 24 citrullination sites on Fn, 21 of which are unique to this study and the immunogenic properties of which remains unclear. An interesting study will be to characterize the epitope specificity of the citrullination sites and

its ability to be recognized by ACPAs. This information can further our knowledge about the citrullination of Fn in inflammatory conditions, such as RA, and also provide new diagnostic biomarkers.

CHAPTER 7

BROADER THESIS SIGNIFICANCE- INTRA- VERSUS EXTRACELLULAR PTM-DEPENDENT SIGNALING: NEW PARADIGMS AND PRINCIPLES

With progress towards ever better detection of protein post-translational modifications (PTMs) continues in what appears to be an exponential manner, it becomes more evident that virtually all cellular process and phenotypes are in some way regulated by this understudied layer of the central dogma. However, the exponential rate at which PTMs are detected far surpasses the rate at which we can understand their functional importance. Thus, a significant knowledge gap between these two aspects of any PTM remains extraordinarily large.

Significant biological insight about a PTM can be gleaned through coupling high-resolution mass spectrometry, computational PTM prioritization tools, and biochemical and cellular assays. Through my utilization of such a unified approach has revealed several fascinating implications of PTM on cell signaling and behavior. Perhaps the most intriguing is that PTMs can not only rapidly reprogram cell signaling to elicit an immediate cell response but can also imprint proteins in an irreversible manner that influences future cellular behaviors – analogous to a *memory*. In this thesis I have observed both phenomena. Indeed, I have shown that dynamic regulatory phosphorylation can mediate negative synergistic interactions between G protein γ subunits and a G$\beta\gamma$ effector proteins. Through collaboration with the Barker lab, I have seen that irreversible citrullination of

extracellular matrix (ECM) protein, fibronectin (Fn), is more prevalent than once thought and that these marks can influence the future behavior of cells that must adhere to or migrate through such proteins.

This work also provides a unique perspective on the nature of PTM, particularly in regards to where it can and does occur and how this influences the manner in which one attempts to understand biological function. For example, PTMs of key intracellular or membrane bound proteins in the G-protein signaling pathway, such as phosphorylation of $G\beta\gamma$ effector proteins, dictate the phenotype through processes that are inherently intracellular. This has long been thought to be the realm of PTMs – as components of proteins that occur within a cell. Intriguingly, PTM of extracellular proteins falls outside of this paradigm. Indeed, citrullination of Fn, an inherently extracellular protein, is not intra- but rather extracellular. Thus, at first glance one might not consider the protein to be a target for PTM. I have used mass spec to reveal the largest map of citrullination sites in Fn to date and through collaboration with the Barker lab we have determined that citrullinated Fn can alter the intracellular signaling events of ECM-interacting cells. As such, this work necessitates a refinement of the existing paradigm that PTM regulation is largely an intracellular process. This further requires that principles underlying intracellular PTM will likely need to be readdressed for extracellular proteins, which undergo PTM in a manner that appears to be less well regulated by precise enzyme localization.

Finally, a somewhat understated yet seminal discovery emerging from this work is that PTMs on distinct proteins can co-operate to elicit their regulatory

effects. I have discovered that phosphorylation of G proteins and their effectors, together regulate signaling and phenotypic outcome. To our knowledge, this type of PTM interaction is very rare, likely due to the fact that such a relationship can be difficult to detect given the complexity of the eukaryotic proteome. In the studies described herein, the well-characterized G protein signaling pathway in yeast served as an ideal model system that enabled the discovery of cross-protein PTM interaction/synergy that likely would've been difficult to detect in any other less characterized cell system. Moreover, given the constrained evolutionary phylogeny of G proteins and their effectors, these results may serve as a foundation for predictive models that can be used to identify other similar PTM interactions. These discoveries further serve as a testament to the continued utility of the yeast model system in elucidating novel mechanisms of PTM regulation that pioneer our understanding of regulatory PTM in all eukaryotes.

APPENDIX A

SUPPLEMENTARY INFORMATION FOR CHAPTER 2

Supplemental Experimental Procedures

Yeast strains and plasmids – Standard methods for cell growth, maintenance, and transformation of yeast, and for the manipulation of DNA were used throughout. Strain *BY4741* (*MATa leu2*Δ *met15*Δ *his3*Δ *ura3*Δ) and *BY4741*- derived mutants were used. Details of strains used are listed in Table A.S1. The *fus3*Δ *kss1*Δ double deletion mutant was created by replacing the *KSS1* gene with *LEU2* in the *fus3*Δ background strain obtained from Open Biosysytems. The non-docking mutants of Ste5 ($Ste5^{ND}$; *STE5* Q292A, I294A, Y295A, L307A, P310A, $N315A_{)}$ were created in *HA-STE18*^{WT}, *HA-STE18*^{3A} and *HA-STE18*^{3E} background strains (Dewhurst et al., 2015), using the two-step dellitto perfetto mutagenesis method (Storici and Resnick, 2006). Briefly, a CORE cassette comprising of counter selectable marker and reporter gene was inserted via homologous recombination, in the 829-990 region of *STE5* coding sequence containing the Fus3 docking region on the protein. The CORE cassette was later replaced by oligonucleotides containing the desired mutations and regions of homology to *STE5*. Similarly, GFP-tagged *STE5* strains were constructed by integrating a CORE cassette at the 3-prime end of *STE5* and replacing it with the coding sequence for Green Fluorescent Protein (GFP). Strains were verified at each step by PCR amplification and dideoxy sequencing (Eurofins MWG Operon). LRB341 and LRB345 strains harboring *yck1*Δ and temperature-sensitive *yck2*^{ts} alleles were graciously provided by Dr. Lucy Robinson

(Robinson et al., 1993). Plasmids used in this study for kinase deletion screening (pRS316-*CUP1- HA-STE18*), were graciously provided (gift from T. Chernova).

Yeast cell culture and treatments – Yeast Strains were grown in YPD growth medium (Yeast Extract, Peptone, 2% Dextrose media) unless otherwise noted. Cells were grown at 30C with shaking at 250 rpm and cell culture density was determined by absorbance at 600nm (OD600). All experiments were conducted with log phase cells between OD600 0.75-0.85. Log-phase cells were then treated with α-factor peptide hormone (Genscript) at 3μM final concentration. 10ml aliquots of treated cells were harvested with 0.5ml trichloroacetic acid (TCA) on ice and centrifuged at 3724 x g in Allegra X-14R Beckman Coulter Centrifuge. Cells were then washed with 10ml MiliQ water, followed by transfer to microcentrifuge tubes that were immediately frozen at -80C.

For kinase screening, deletion strains carrying the pRS316-*CUP1-HA-STE18* plasmid were grown in synthetic media lacking uracil and other appropriate amino acids as necessary. An overnight saturated culture was then diluted to OD600 0.05 and allowed to grow until OD600 0.2. Expression of *HA-STE18* was then induced by addition of 100μM copper sulfate. Cells were grown till log-phase (OD 0.75-0.85), followed by treatment with 3μM α-factor for an hour. The cells were harvested with TCA as described earlier. For *yck*^{ts} strains, *HA-STE18* expression was induced as above. At OD600 0.8, each culture was split into two parts: One subjected to pheromone treatment and the other incubated at 37C for 30 minutes prior to stimulation with pheromone.

Cell extracts and Immunoblotting - Protein extracts were resolved by 7.5% or 12.5% SDS-PAGE and immunoblotted with epitope-specific antibodies specific to: the hemagluttinin antigen epitope (HA) (Cell Signaling Technologies, Cat #3724) at 1:5000; activating phosphorylated sites in Fus3 and Kss1 (Phospho-p44/42 MAPK) (Cell Signaling

Technologies, Cat #9101) at 1:500; Fus3 protein (Santa Cruz, anti-Fus3 yC-19, Cat # sc-6773) at 1:350; Kss1 protein (Santa Cruz, anti-Kss1 yC-19, Cat # sc-6775R) at 1:1500; GFP (Invitrogen, Cat# GF28R MA5-1526-HRP) at 1:1000; and glucose-6-phosphate dehydrogenase (loading control; LC) (Sigma-Aldrich, Cat #A9521) at 1:50,000.

Phosphatase Assay – Pheromone-treated cells were harvested as described earlier. The frozen pellets were resuspended in 1x phosphatase buffer mix (New England Biolabs), comprising of 1x PMP buffer (50mM HEPES (pH 7.5), 100mM NaCl, 2 mM DTT, 0.01% Brij 35), 1mM $MnCl_2$, and 1x EDTAfree protease inhibitors (Roche). The resuspended pellet were equally aliquoted into three tubes- Control, AP (Alkaline phosphatase), and AP/I (Alkaline phosphatase Inhibitor). Each resuspended pellet was subjected to glass bead lysis in the absence (Control and AP sample) or presence (AP/I sample) of phosphatase inhibitors (50mM NaF and 1.3mM sodium orthovandate). The lysates were centrifuged at 21.1 x g in Thermo Pico21 centrifuge and the supernatant was collected in a fresh tube. The AP and AP/I samples were treated with phosphatase enzyme (final concentration of 2.25U/µl) for 30 mins at 30C; whereas the control sample was left untreated. The reaction was stopped by addition of 6x SDS loading dye, and the samples were immediately run on SDS-PAGE gel and subjected to immunoblotting.

Phos-tag gel analysis – Protein extracts were resolved by 100µM Mn^{2+}-Phos-tag in 7.5% acrylamide SDS-PAGE as per manufacturer's instructions (Wako Chemicals, Richmond, VA). The gel was run at a constant current of 30 mA per gel till dye ran off. Next, the gel was soaked in transfer buffer (0.125M tris, 0.96M glycine, 20% methanol v/v) containing 1mM EDTA, and later in transfer buffer without EDTA for 30 min each with gentle shaking. This process chelates Mn^{2+} and increases transfer efficiency of both phosphorylated and non-phosphorylated proteins. Wet-tank transfer in buffer containing

0.1% SDS was used to effectively transfer proteins onto nitrocellulose membrane. The proteins were then subjected to immunoblotting.

Morphological response assay – The morphological response of *STE18/STE5* mutants to α-factor was measured as described previously (Coyle et al., 2013; Malleshaiah et al., 2010). Briefly, an overnight culture was washed twice with MilliQ water, and then diluted to an OD600 0.05 in synthetic complete (SC) media. After 4h of growth at 30C with shaking at 250 rpm, the cultures were distributed into separate tubes, and serially diluted pheromone was added to each. The morphology of the cells was determined, 3h post-stimulation, by differential interface contrast (DIC) confocal microscopy using a PerkinElmer UltraVIEW spinning disk confocal microscope. Number of cells with mating projections were counted as a percentage of total.

Ste5-GFP localization assay – Live cells endogenously expressing either Ste5-GFP or Ste5ND-GFP were visualized by microscopy. Log phase cultures (OD 600 0.7-0.8) grown in SC media were briefly sonicated, centrifuged, and resuspended in SC media containing 10μM α-factor. Cells were immediately mounted on a SC agar (2.5%) pad with 30μM a-factor and the GFP fluorescence was monitored for 200 minutes. Cells were visualized by fluorescence microscopy using a PerkinElmer Ultraview VoX spinning disk confocal scanner with a Hamamatsu ORCA FLASH 4 camera on a Nikon Ti-e microscope stand. Photomicrographs were obtained using a 60x NA 1.49 apochromatic objective. The 488nm laser line was set at 10%, image exposure set to 500ms, and the Z-stacks were obtained for 4μm with 0.2μm step-size. A 525nm center, 50nm bandwidth emission filter was used for all fluorescence images. Images were analyzed using Volocity quantitation software (Perkin Elmer). Find object module was used to identify objects with the threshold set to 18.4% for fluorescence intensity. Images were linearly contrast enhanced for

visualization. Quantification was performed on raw data from which integrated pixel intensity was used for all further analyses.

Co-immunoprecipitation – 50 ml cultures of cells expressing different combinations of wild type or mutant HA- STE18 and STE5-GFP were grown to an OD of 0.8 and treated with 10μM pheromone for 20 mins. Cells were then harvested, washed with water, snap-chilled in liquid nitrogen and stored in -80C. Cell pellets were subjected to glass bead lysis in buffer containing 20 mM Tris-HCl (pH 8.0), 150 mM NaCl, 2 mM MgCl2, 0.1% Triton X-100 (Sigma Aldrich), 5% glycerol, 1 mM TCEP, 0.5mM PMSF, and protease and phosphatase inhibitor tablets (Pierce #A32959). The soluble protein extract was then collected in a fresh tube after centrifugation at 21,000xg for 10 min. For immunoprecipitation of Ste5-GFP, anti-GFP mAb-agarose (MBL, #D153-8) pre-equilibrated with the lysis buffer was added to each lysate of fixed concentration and total mass followed by incubation with gentle agitation at 4C for 3 hours. Beads were washed with lysis buffer to reduce non-specifically bound proteins. Washed beads were resuspended in 1x SDS-PAGE buffer and boiled for 3 min to elute bound protein. Eluted proteins were separated by SDS-PAGE and immunoblotting with anti-GFP (Invitrogen, A11122) and anti-HA.

Supplemental References

Coyle, S.M., Flores, J., and Lim, W.A. (2013). Exploitation of latent allostery enables the evolution of new modes of MAP kinase regulation. Cell *154*, 875–887.

Dewhurst, H.M., Choudhury, S., and Torres, M.P. (2015). Structural Analysis of PTM Hotspots (SAPH-ire)--A Quantitative Informatics Method Enabling the Discovery of Novel Regulatory Elements in Protein Families. Mol. Cell. Proteomics *14*, 2285–2297.

Malleshaiah, M.K., Shahrezaei, V., Swain, P.S., and Michnick, S.W. (2010). The scaffold protein Ste5 directly controls a switch-like mating decision in yeast. Nature *465*, 101–105.

Storici, F., and Resnick, M. a (2006). The delitto perfetto approach to in vivo site-directed mutagenesis and chromosome rearrangements with synthetic oligonucleotides in yeast. Methods Enzymol. *409*, 329–345.

Supplemental Data Items

Table A.S1. List of strains used in this study.

Strain	Genotype	Ref
BY4741	*MAT**a** leu2Δ met15Δ his3Δ ura3Δ*	
YMT235	BY4741 HA-STE18 WT	PMID 26070665
YMT236	BY4741 HA-STE18 3A	PMID 26070665
YMT237	BY4741 HA-STE18 3E	PMID 26070665
ste20Δ	BY4741 *ste20::KanMX*	YKO collections from Open Biosystems.
ste11Δ	BY4741 *ste11::KanMX*	YKO collections from Open Biosystems.
ste7Δ	BY4741 *ste7::KanMX*	YKO collections from Open Biosystems.
fus3Δ	BY4741 *fus3::KanMX*	YKO collections from Open Biosystems.
kss1Δ	BY4741 *kss1::KanMX*	YKO collections from Open Biosystems.
ste5Δ	BY4741 *ste5::KanMX*	YKO collections from Open Biosystems.
sst2Δ	BY4741 *sst2::KanMX*	YKO collections from Open Biosystems.
akr1Δ	BY4741 *akr1::KanMX*	YKO collections from Open Biosystems.
YMT286	BY4741 *fus3::KanMX kss1::LEU2*	this study
YMT 491	BY4741 HA-STE18 WT STE5 ND (Q292A, I294A, Y295A, L307A, P310A, N315A) aka WT / ND	this study
YMT 492	BY4741 HA-STE18 3E STE5 ND (Q292A, I294A, Y295A, L307A, P310A, N315A) aka 3A / ND	this study
YMT 501	BY4741 HA-STE18 3A STE5 ND (Q292A, I294A, Y295A, L307A, P310A, N315A) aka 3E / ND	this study
YMT 581	BY4741 HA STE18 WT STE5-GFP	this study
YMT 611	BY4741 HA STE18 3A STE5-GFP	this study
YMT 585	BY4741 HA STE18 3E STE5-GFP	this study
YMT 582	BY4741 HA STE18 WT $STE5^{ND}$-GFP	this study
YMT 583	BY4741 HA STE18 3A $STE5^{ND}$-GFP	this study
YMT 584	BY4741 HA STE18 3E $STE5^{ND}$-GFP	this study
LRB 341	*MATa his3 leu2 ura3-52*	PMID 8474447
LRB 345	*MATa his3 leu2 ura3-52 yck1-Δ yck2-ts*	PMID 8474447

Table A.S2. Synergy tests for independent versus combined mutation of Ste18 phosphosites and Ste5^{FBD}. The independent or combined effects of Ste18/Ste5 phosphorylation on Fus3 peak activation time (F3PAT) and Fus3 mean peak amplitude (F3MPA) was compared as a test for synergistic or additive effects. (A) Summary table of F3PAT and F3MPA raw, relative and integrated data. Red text indicates mutants representing a *Ste18 element off* state (Ste18^{3A}/Ste5^{WT}) or *Ste5 element off* state (Ste18^{WT}/Ste5ND). Blue text indicates the mutant representing *both elements off* (Ste18^{3A}/Ste5ND). (B) Sub-tables showing synergy test results for F3PAT, F3MPA, and Integrated Outcomes. The total integrated rate and amplitude enhancement observed for Fus3 activation in Ste18^{3A}/Ste5^{WT} and Ste18^{WT}/Ste5ND was ~4x lower than that of Ste18^{3A}/Ste5ND cells (compare 5.6 to 21.7) (bottom table). The greatest degree of synergy between Ste18/Ste5 elements were observed for Fus3 peak activation time (top table). In contrast, peak activation amplitude results from additive rather than synergistic effects of the two elements (since the sum of effects for removal of either Ste18 or Ste5 elements alone were nearly equal to the elimination of both elements together) (middle table).

A

Ste18/Ste5	Fus3 Peak Activation Time (F3PAT)	Shift in F3PAT Relative to WT/WT (A)	Fold Rate Enahancement over WT/WT (B)	Fus3 Mean Peak Amplitude	Fold Amplitude Enhancement over WT/WT (C)	Integrated (B) * (C)
WT / WT	30	0	1	100.00	1.0	1.0
3A / WT	15	-15	2	162.57	1.6	3.3
3E / WT	30	0	1	114.60	1.1	1.1
WT / ND	30	0	1	235.01	2.4	2.4
3A / ND	5	-25	6	361.35	3.6	21.7
3E / ND	15	-15	2	210.71	2.1	4.2

B

Synergy Test for Peak Activation Time (Column B)	
Sum of Fold Rate Enhancement for 3A/WT, WT/ND	2
Fold Rate Enhancement for 3A/ND	6

Synergy Test for Peak Amplitude (Column C)	
Sum of Fold Amplitude Enhancement for 3A/WT, WT/ND	4.0
Fold Amplitude Enhancement for 3A/ND	3.6

Synergy Test for Integrated Outcomes [Peak Activation Time * Peak Amplitude]	
Sum of Fold Integrated Enhancement [(B) * (C)] for 3A/WT & WT/ND	5.6
Fold Integrated Enhancement [(B) * (C)] for 3A/ND	21.7

Table A.S3. Best-fit values for pheromone dose-response of independent or combined mutation of Ste18 phosphosites and Ste5^{FBD}. Sigmoidal dose-response curves with variable slope were fit to data shown in Figure 4 to estimate switch or graded morphological responses for each indicated yeast strain. A constraint value of 100 was applied to the top of the curve.

Category	WT	3A	3E	WT / ND	3A / ND	3E / ND
Best-fit values						
Bottom	4.674	5.923	4.646	7.79	12.61	2.151
Top	= 100	= 100	= 100	= 100	= 100	= 100
HillSlope	6.201	6.253	3.681	0.9708	0.8519	2.703
EC50	0.4468	0.6442	0.4677	0.5597	0.2966	0.9898
95% CI (asymptotic)						
Bottom	3.379 to 5.968	4.381 to 7.464	3.04 to 6.251	5.08 to 10.5	7.49 to 17.72	0.6774 to 3.624
HillSlope	5.473 to 6.93	4.908 to 7.597	3.223 to 4.138	0.8652 to 1.076	0.6876 to 1.016	2.292 to 3.114
EC50	0.4379 to 0.4559	0.6031 to 0.6882	0.4532 to 0.4827	0.5009 to 0.6254	0.2394 to 0.3674	0.9331 to 1.05
Goodness of Fit						
Degrees of Freedom	45	42	45	45	45	44
R square	0.9933	0.9875	0.9904	0.9779	0.9362	0.9879
Number of points						
# of X values	48	48	48	48	48	48
# Y values analyzed	48	45	48	48	48	47

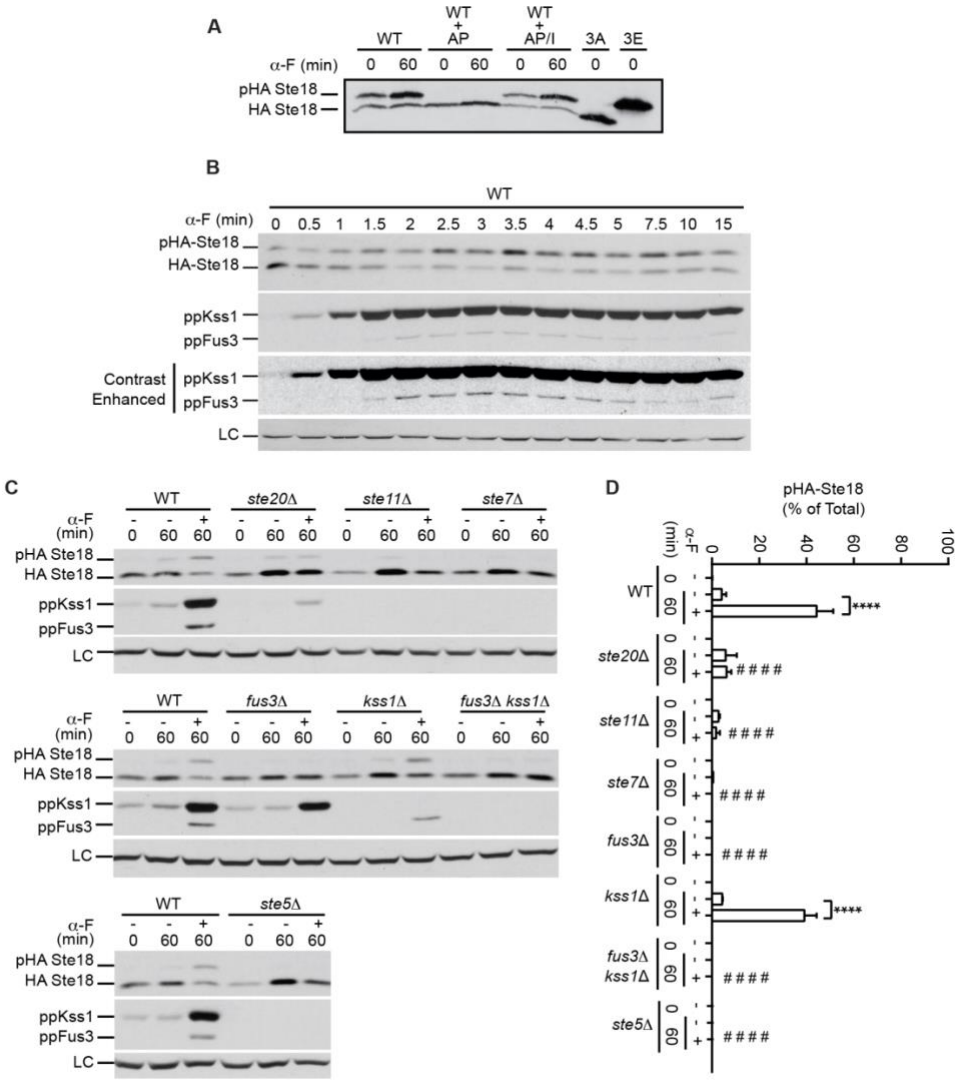

Figure A.S1. Ste18^{Nt} phosphorylation in response to pheromone and dependence on scaffolded MAPKs. The abundance of phosphorylated HA-Ste18 in cells treated with pheromone for the indicated duration was determined by immunoblotting with anti-HA antibody. (A) Protein extracts from pheromone induced wild type cells were subjected to phosphatase treatment in the absence or presence of phosphatase inhibitor, and HA-Ste18 was detected by immunoblotting. (B) Immunoblots showing Ste18-Nt phosphorylation as well as Kss1 and Fus3 activation measured in 30 second intervals within the first 15 minutes of the pheromone response in wild type cells. Immunoblot of activated Kss1 and Fus3 has been contrast enhanced to facilitate visualization, and equivalent loading of lanes in immunoblot is demonstrated by comparable levels of G6PDH (LC). (C-D) Yeast single gene deletion mutants transformed with the *pCUP1-HA-STE18* expression plasmid were stimulated with 3μM pheromone for 1 hour followed by immunoblot analysis of HA-Ste18, activated Kss1 and Fus3, and loading control proteins. The phosphorylation percentage of Ste18 (% of total) was compared between time 0 and

60 minutes with or without pheromone stimulation. (C) Representative immunoblots showing the phosphorylation of Ste18 in cells lacking the indicated kinase, or the MAPK scaffold (*ste5Δ*). Activation of Kss1 and Fus3 were also measured to observe the effect of each mutant on pathway activation. (D) Average percent Ste18 phosphorylation and standard deviation for three independent colonies. Statistical significance determined by 2-way ANOVA: (#) significant difference from the same pheromone treatment in wild type, and (*) significant difference between 60-/60+ pheromone treatment within the same strain. AP: alkaline phosphatase, AP/I : alkaline phosphatase + phosphatase inhibitor.

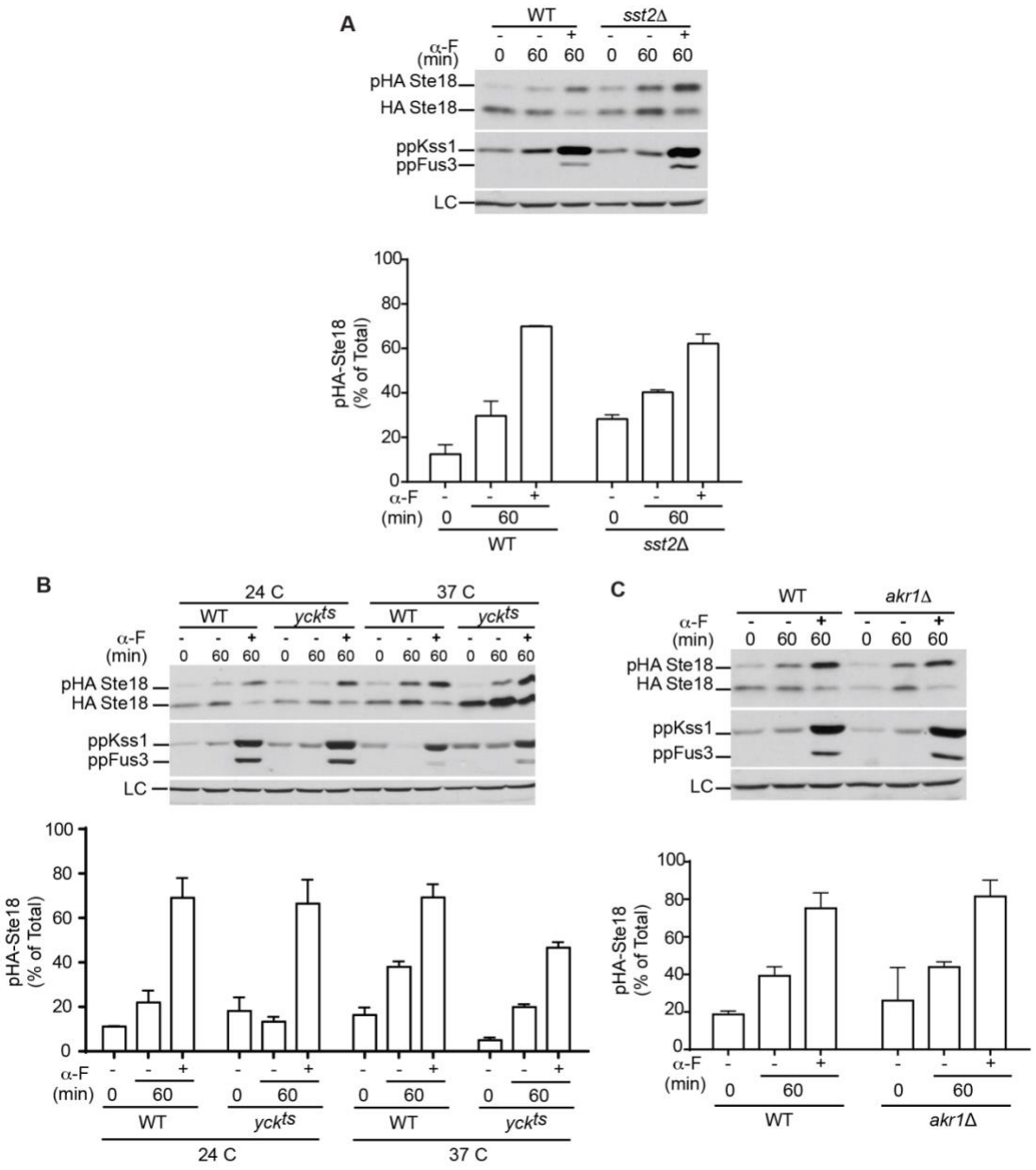

Figure A.S2. Effect of *SST2* and *YCK1/2* on the phosphorylation of Ste18-Nt. Yeast single gene deletion mutants transformed with the *pCUP1-HA-STE18* expression plasmid were stimulated with 3μM pheromone for 1 hour followed by immunoblot analysis of HA-Ste18, activated Kss1 and Fus3, and loading control proteins (as in Figure S1). Representative immunoblots and quantification of Ste18 phosphorylation percentage are shown for three independent colonies with error bars representing standard deviation. Results are shown for yeast lacking: (A) the RGS protein (*sst2Δ*), (B) the yeast casein kinases (*yck1Δ/yck2ts*), and (C) the Yck1/2 palmitoyltransferase (*akr1Δ*).

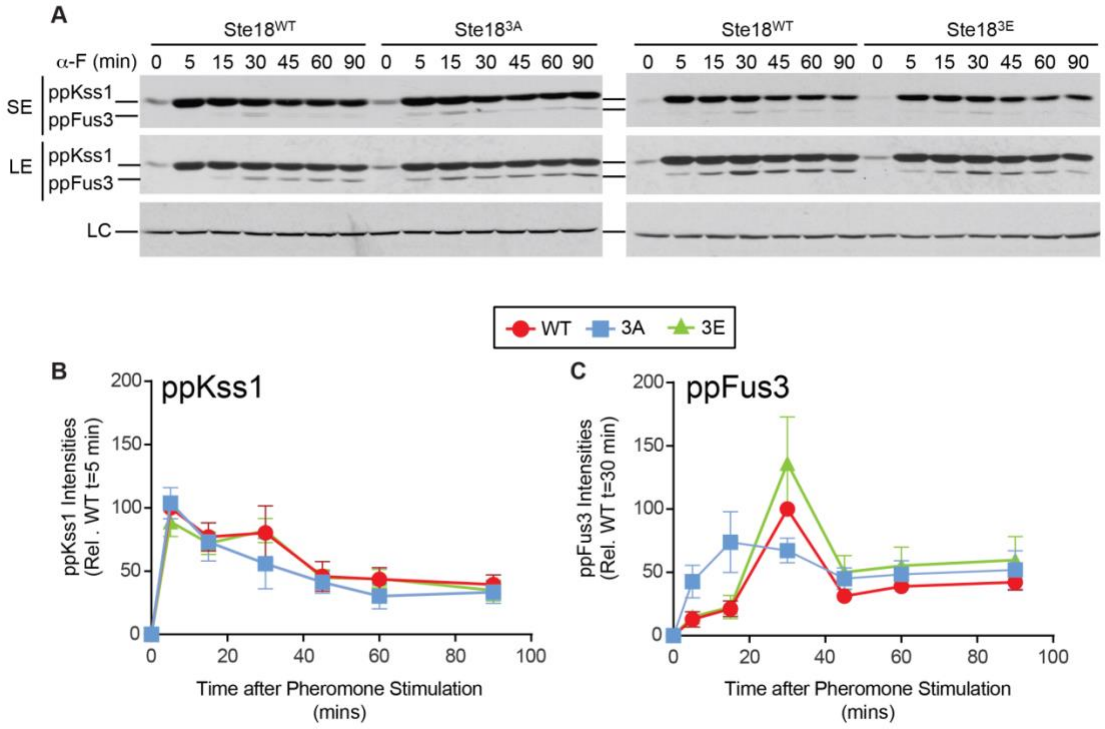

Figure A.S3. N-terminal phosphorylation of Ste18 is required for delayed peak activation of Fus3 in response to pheromone. (A) Yeast strains harboring wild type, phospho-null (3A) or phospho-mimic (3E) versions of HA-Ste18 expressed from the endogenous genomic locus and stimulated with 3μM pheromone for the indicated times followed by immunoblot analysis of pKss1 and pFus3. Both long and short film exposures (LE and SE, respectively) are shown. (B) Quantitative comparison of activated Kss1. (C) Quantitative comparison of activated Fus3. Average and standard error bars are shown for 8 independent colonies in 2 independent experiments.

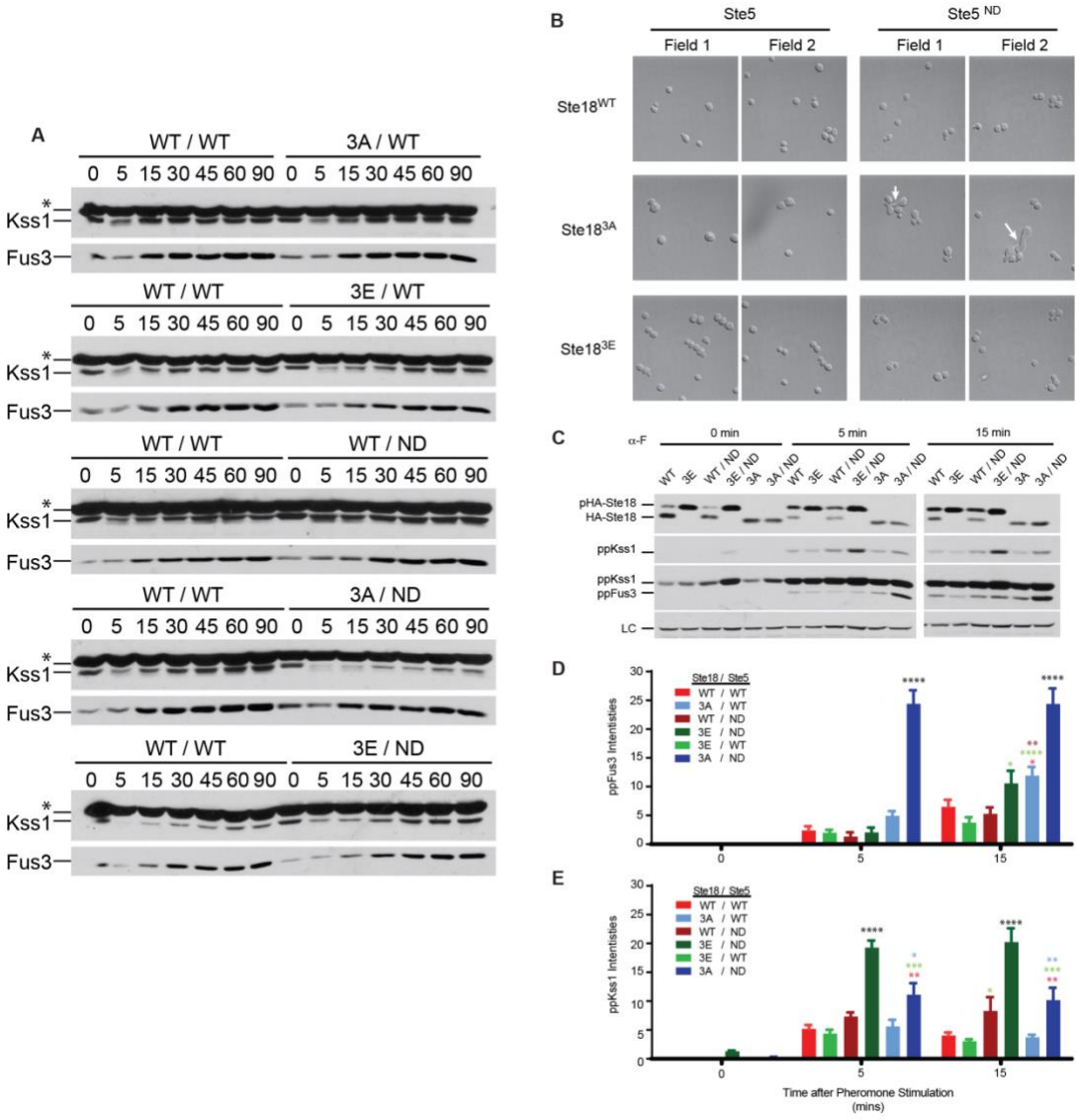

Figure A.S4. Effect of phosphorylation synergy between Ste5 and Ste18 on cell polarization and MAPK activation level in response to GPCR activation. Morphology and MAPK activation profile of cells harboring the indicated combinations of HA-Ste18 and Ste5 were analyzed in the absence or presence of pheromone stimulation respectively. (A) Immunoblots for Fus3 and Kss1 proteins from experiment shown in Figure 3C (B) The different Ste18/Ste5 mutants were visualized by differential interference contrast (DIC) microscopy in the absence of pheromone. Multiple fields are shown to provide additional views of the cell population. White arrows highlight polarized elongated growth that was exclusively observed in $Ste18^{3A}/Ste5^{ND}$ cells. No other signs of similarly extreme morphology could be found in any other cell type. (C-E) Pheromone- dependent activation of Fus3 and Kss1 was measured for the desired amount of time. (C) Representative immunoblots showing the result of endpoint assays for HA-Ste18, activated MAPKs Kss1 and Fus3, and the loading control (LC). (D and E) Graphical representation of the mean ± SD of the activated MAPK levels (Kss1 in C, and Fus3 in D) in wild type and mutant cells. Statistical significance was determined by two-way ANOVA

tests between each strain within a time point and is indicated by ($p<0.05$, *), ($p<0.01$, **), ($p<0.001$, ***), and ($p<0.0001$, ****). Each test result is color matched to each compared strain for which statistically significant differences were observed. Black asterisks indicate significant difference from all other strains within the same time point.

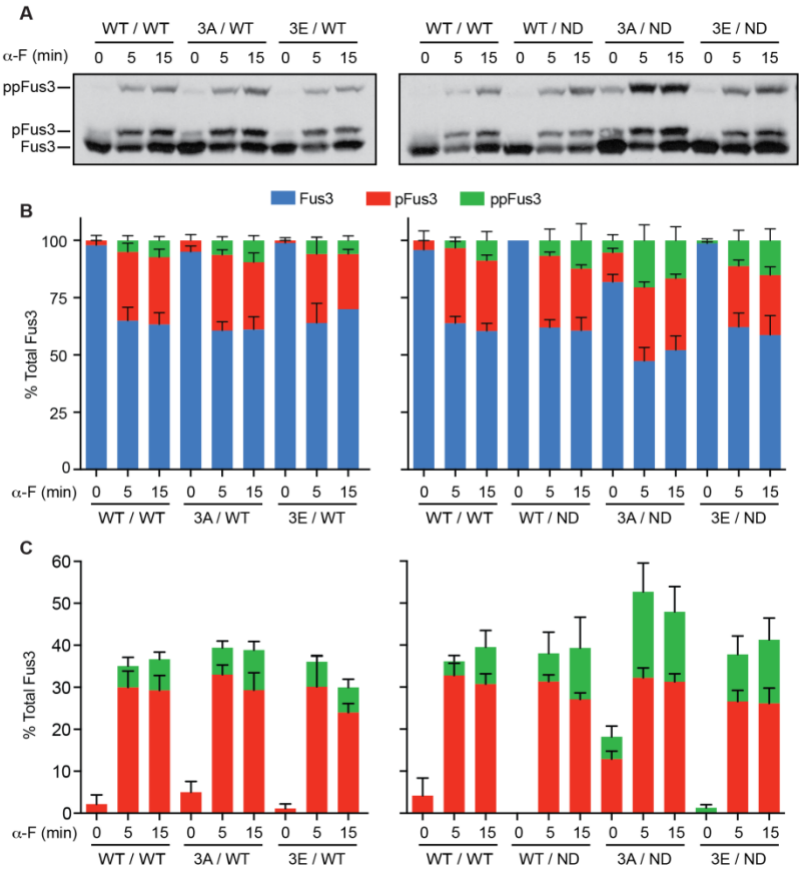

Figure A.S5. Ste18/Ste5 phosphorylation cooperatively impact the mono- and di-phosphorylation of Fus3. Protein extracts from cells treated with 3μM α-factor for the desired duration (same as in Figure S4) were resolved on a phos-tag gel and immunoblotted with anti-Fus3 antibody. (A) Representative immunoblot showing the mono-phosphorylated (pFus3), di-phosphorylated (ppFus3) and non-phosphorylated Fus3 (Fus3). The relative abundance of Fus3 di-phosphorylation (ppFus3) confirms results from di-phospho-specific antibody blots shown in Figures 2 and 3. This same trend was also observed for mono-phosphorylated Fus3 (pFus3). (B) Quantification of the band intensity of ppFus3, pFus3 and Fus3 is denoted as percentage of total Fus3 in each lane. (C) Graphical representation of the percentage of mono- and di-phosphorylated Fus3 from B. Before pheromone stimulation (time 0), neither pFus3 nor ppFus3 are detectable in $Ste18^{WT}/Ste5^{ND}$ cells since the $Ste5^{FBD}$ is needed for allosteric activation and mono-phosphorylation of Fus3. Both pFus3 and ppFus3 are significantly elevated in $Ste18^{3A}/Ste5^{ND}$ cells and moderately elevated in $Ste18^{3A}/Ste5^{WT}$ cells (relative to wild type cells) before the addition of pheromone, suggesting that phosphorylation of both proteins contributes to the inhibition of MAPK activation in the absence of pheromone. Consistent with this conclusion, we found that pFus3 was diminished or completely abolished in wild type or $Ste18^{3E}/Ste5^{ND}$ cells, which mimics partial inhibition. Overall, these data suggest

that either Ste18-Nt phosphorylation or Ste5 phosphorylation (controlled by Fus3 docking on Ste5), can effectively inhibit the aberrant di-phosphorylation of Fus3 in the absence of pheromone. Furthermore, simultaneously preventing phosphorylation on both proteins results in aberrant di-phosphorylation of Fus3 in the absence of pheromone. Data represent the mean ± SD for 3 independent colonies.

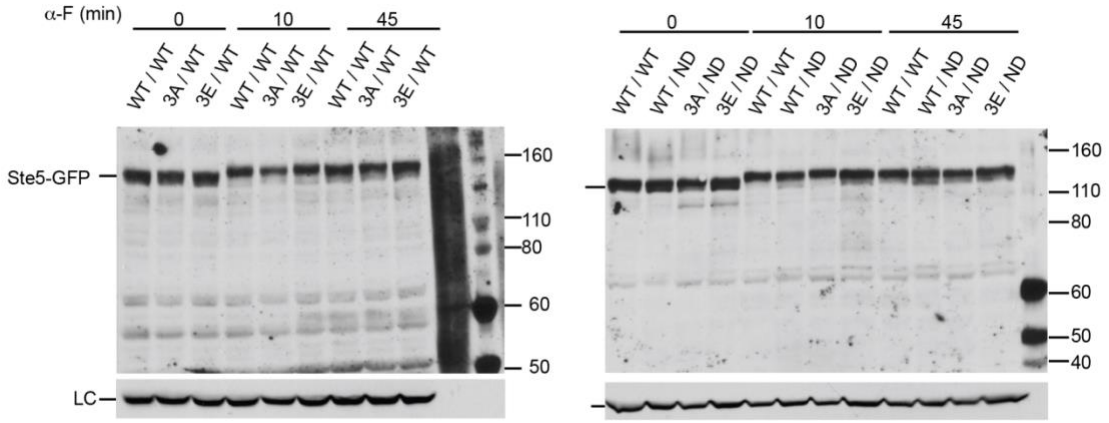

Figure A.S6. The steady state level of Ste5-GFP in cells used for PM translocation experiments. Cells expressing either Ste5-GFP or Ste5ND-GFP along with different phospho-mutants of Ste18 (same cells as used in Figure 3) were treated with 10μM α-factor for the desired time. Protein extracts were separated by 7.5% SDS- PAGE until higher molecular weight markers (110-160kDa markers of the Novex Sharp pre-stained protein standard [LC5800]) were well resolved, which was ~20 minutes after the loading dye ran off of the gel. Ste5-GFP ran at its expected size of approximately 130kDa (Ste5: 102 kDa and GFP: 27kDa). The abundance of Ste5 was probed using anti-GFP antibody. LC: loading control.

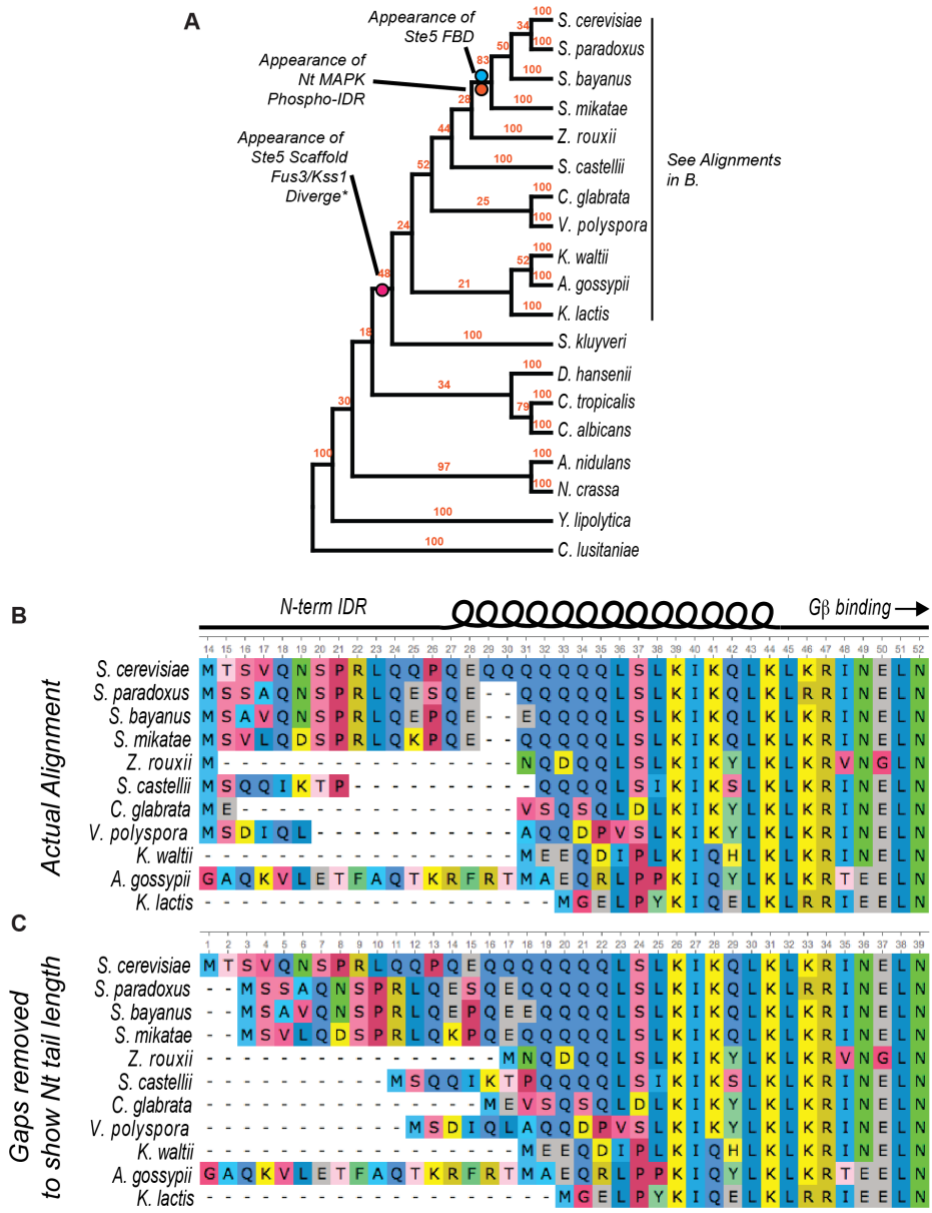

Figure A.S7. Phylogenetic analysis of the Ste18/Ste5 phospho-regulatory system. (A) Bootstrapped phylogenetic tree of Ste18 orthologs with bootstrap replicates conforming to the illustrated phylogenetic tree indicated (out of 100). (B) Multiple sequence alignment of Ste18 yeast orthologs correlated with the predicted secondary structure of Ste18, including the N-terminal intrinsically disordered region (N-term IDR) and alpha helical residues. (C) Alignment from B with all alignment gaps removed to illustrate the lengthening of the N-term IDR in *S. mikatae*, *S. bayanus*, *S. paradoxus*, and *S. cerevisiae* – yeast strains that also harbor Fus3 binding domains (FBD) in their Ste5-orthologous scaffolds. Sequences in the alignment shown are in order of appearance (from top to bottom) in A.

APPENDIX B

SUPPLEMENTARY INFORMATION FOR CHAPTER 3

Supplementary Data Items

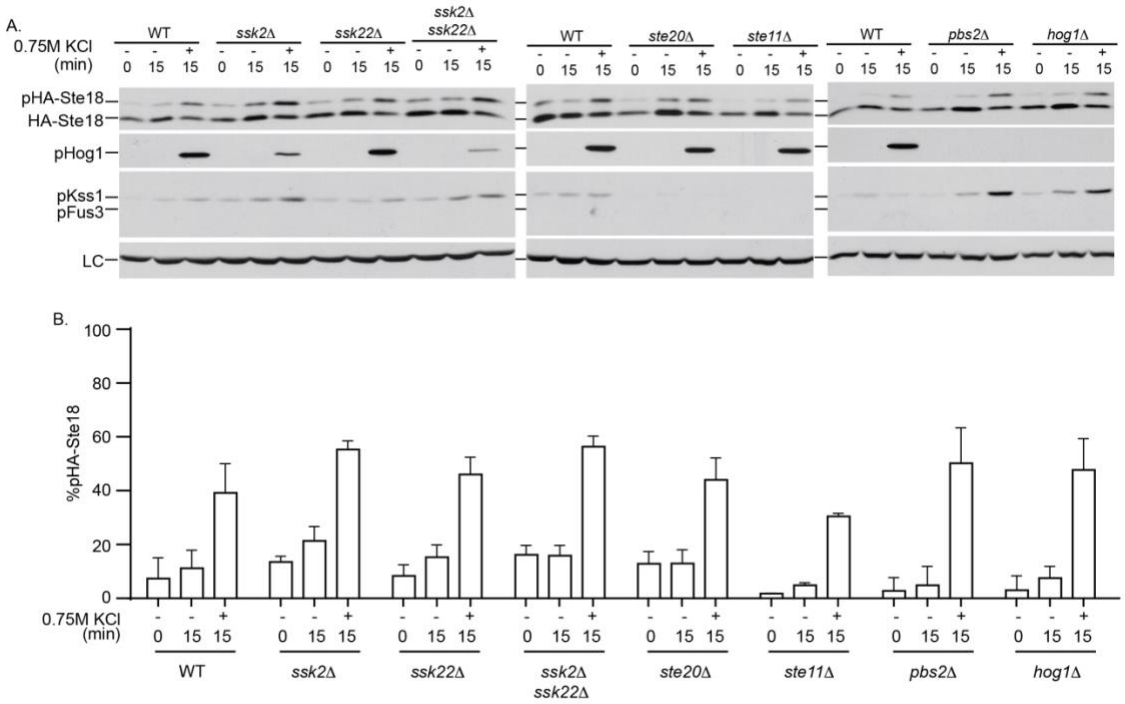

Figure B.S1. Osmotic stress induced phosphorylation of Ste18-Nt is independent of kinases in HOG pathway. Kinase deletion strains harboring the CUP1-HA-Ste18 expression plasmid were stimulated with 0.75 KCl for 15 minutes. The phosphorylation percentage of Ste18 (% of total) was compared between time 0 and 15 minutes with or without stress. (A) Representative immunoblots showing the phosphorylation of Ste18 in cells lacking the indicated kinase. Activated MAPKs (pHog1, pKss1 and pFus3) were also measured. (B) Quantification of average and standard deviation for the HA-Ste18-Nt phosphorylation percentage (% of total) is shown for three independent colonies/experiments for each strain.

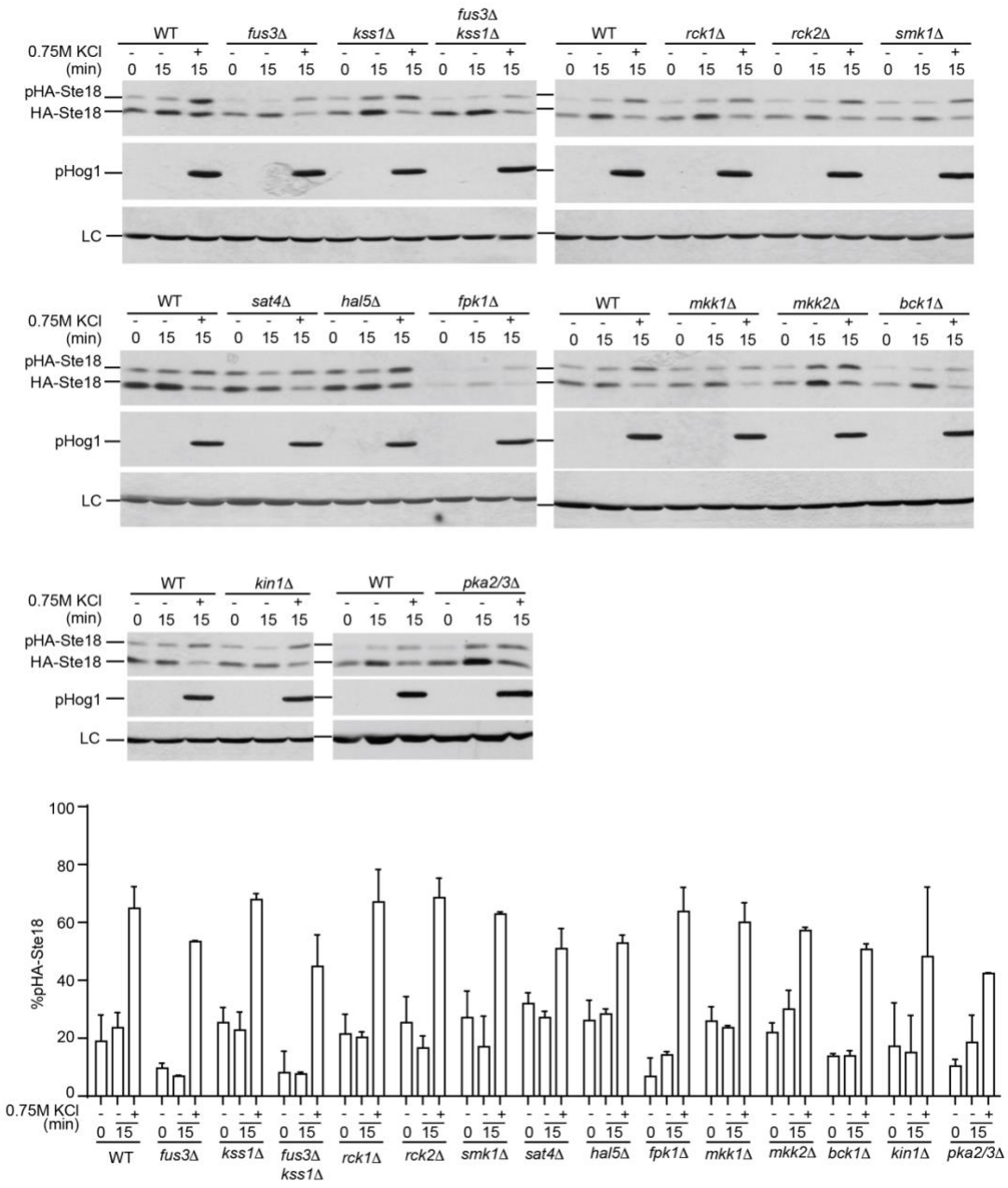

Figure B.S2. None of the kinases screened so far are essential for phosphorylation of Ste18-Nt in response to osmotic stress. Kinase deletion strains harboring the CUP1-HA-Ste18 expression plasmid were stimulated with 0.75 KCl for 15 minutes (same as in Figure B.S1). Representative immunoblots (top) and quantitative graph (below) showing the phosphorylation of Ste18 in cells lacking the indicated kinase. Data shown is mean ± S.D. for three independent experiments for each strain.

APPENDIX C

SUPPLEMENTARY INFORMATION FOR CHAPTER 5

Table C. S1: List of unique citrullinated Fn peptides identified and the corresponding modified residue (r) position in the native protein.

PAD Treatment	Peptide Sequence	PSM	Citrullinated Residue 1	Citrullinated Residue 2
PAD4	QINQQWErTY	7	67	
Untreated	QINQQWErTY	2	67	
PAD2	TGNTYrVGDTY	2	107	
PAD2+4	TGNTYrVGDTY	1	107	
PAD4	TGNTYrVGDTY	1	107	
PAD2	TDVrAAVY	1	290	
PAD2	VrAAVYQPQPHPQPPPYGHcVTD	1	290	
PAD2+4	VrAAVYQPQPHPQPPPYGHcVTD	3	290	
PAD4	SQLrDQcIVDDITY	1	515	
PAD2	ITASSFVVSWVSASDTVSGFrVE	1	751	
PAD4	ITASSFVVSWVSASDTVSGFrVE	3	751	
PAD2	TTPFSPLVATSESVTEITASSFVVSWVSASDTVSGFrVE	1	751	
PAD2	AVEENQESTPVVIQQETTGTPrSDTVPSPRDLQF	1	903	
PAD4	TTGTPrSDTVPSPR	18	903	
PAD2+4	TTGTPrSDTVPSPRD	3	903	
PAD2	TTGTPrSDTVPSPrDLQFVE	1	903	911
PAD2	TTGTPrSDTVPSPRDLQFVE	5	903	
PAD2+4	TTGTPrSDTVPSPrDLQFVE	1	903	911
PAD2+4	TTGTPrSDTVPSPRDLQFVE	26	903	
PAD4	TTGTPrSDTVPSPRDLQFVE	9	903	
PAD2	AVEENQESTPVVIQQETTGTPRSDTVPSPrDLQF	1	911	
PAD4	TTGTPRSDTVPSPr	1	911	
PAD2	TTGTPRSDTVPSPrDLQFVE	1	911	
PAD2+4	TTGTPRSDTVPSPrDLQFVE	7	911	
PAD4	TTGTPrSDTVPSPrDLQFVE	3	911	
PAD4	TTGTPRSDTVPSPrDLQFVE	13	911	
PAD2+4	SAVTGYrVDVIPVNLPGE	1	938	
PAD4	SAVTGYrVDVIPVNLPGE	1	938	
PAD2	RVDVIPVNLPGEHGQrLPISRNTF	2	953	
PAD2+4	LTVGLTrrGQPR	8	1035	1036

PAD Treatment	Peptide Sequence	PSM	Citrullinated Residue 1	Citrullinated Residue 2
PAD4	LTVGLTrrGQPR	15	1035	1036
PAD2	ITGYrITTTPTNGQQGNSLEE	2	1207	
PAD2+4	ITGYrITTTPTNGQQGNSLEE	3	1207	
PAD4	ITGYrITTTPTNGQQGNSLEE	1	1207	
Untreated	ITGYrITTTPTNGQQGNSLEE	1	1207	
PAD2	RSTTPDITGYrITTTPTNGQQGNSLEE	3	1207	
PAD2+4	RSTTPDITGYrITTTPTNGQQGnSLEE	1	1207	
PAD2+4	RSTTPDITGYrITTTPTNGQQGNSLEE	1	1207	
PAD4	RSTTPDITGYrITTTPTNGQQGNSLEE	23	1207	
Untreated	RSTTPDITGYrITTTPTNGQQGNSLEE	24	1207	
PAD2	LrFTNIGPDTMRVtWAPPPSID	13	1274	
PAD2	LrFTNIGPDTMRVTWAPPPsID	11	1274	
PAD2+4	LrFTNIGPDTMRVtWAPPPSID	4	1274	
PAD2+4	LrFTNIGPDTMRVTWAPPPsID	2	1274	
PAD4	LrFTNIGPDTmrVtWAPPPSID	1	1274	1284
PAD4	LrFTNIGPDTmrVTWAPPPsID	1	1274	
PAD4	LrFTNIGPDTMRVtWAPPPSID	10	1274	
PAD4	LrFTNIGPDTMRVTWAPPPsID	11	1274	
PAD2	SVPISDTIIPAVPPPTDLrFTNIGPD	2	1274	
PAD2+4	SVPISDTIIPAVPPPTDLrFTNIGPD	2	1274	
PAD4	SVPISDTIIPAVPPPTDLrFTNIGPD	2	1274	
PAD2	SVPISDTIIPAVPPPTDLrFTNIGPDTmrVTWAPPPSID	3	1274	1284
PAD2	SVPISDTIIPAVPPPTDLrFTNIGPDTmRVTWAPPPSID	1	1274	
PAD2+4	SVPISDTIIPAVPPPTDLrFTNIGPDTmrVTWAPPPSID	1	1274	1284
PAD4	SVPISDTIIPAVPPPTDLrFTNIGPDTmrVTWAPPPSID	3	1274	1284
PAD2	TIIPAVPPPTDLrFTNIGPD	3	1274	
PAD2+4	TIIPAVPPPTDLrFTNIGPD	2	1274	
PAD4	TIIPAVPPPTDLrFTNIGPDTmrVTWAPPPSID	1	1274	1284
PAD2	LRFTNIGPDTMrVTWAPPPsID	2	1284	
PAD2+4	LRFTNIGPDTMrVtWAPPPSID	1	1284	
PAD2+4	LRFTNIGPDTMrVTWAPPPsID	9	1284	
PAD4	LRFTNIGPDTMrVTWAPPPsID	2	1284	
PAD2	DRVPHSrNsITLTNLTPGTEYVVsIVALnGREE	1	1410	
PAD2	DRVPHSrNsITLTNLTPGTEYVVsIVALNGrEE	1	1410	1434
PAD2	DRVPHSrNSItLTNLTPGTEYVVsIVALnGREE	1	1410	
PAD2	DRVPHSrNSItLTNLTPGTEYVVsIVALNGrEE	1	1410	1434
PAD2+4	YVVSIVALNGrE	1	1434	
PAD2+4	YVVSIVALNGrEE	1	1434	
PAD4	YVVSIVALNGrEE	9	1434	

PAD Treatment	Peptide Sequence	PSM	Citrullinated Residue 1	Citrullinated Residue 2
PAD2	YVVSIVALNGrEESPLLIGQQSTVSDVPrDLE	1	1434	1452
PAD2	YVVSIVALNGrEESPLLIGQQSTVSDVPRDLE	1	1434	
PAD2+4	YVVSIVALNGrEESPLLIGQQSTVSDVPrDLE	1	1434	1452
PAD2	ESPLLIGQQSTVSDVPrDLE	4	1452	
PAD2+4	ESPLLIGQQSTVSDVPrDLE	3	1452	
PAD4	ESPLLIGQQSTVSDVPrDLE	5	1452	
PAD2	VVAATPTSLLISWDAPAVTVrYYrITYGE	1	1476	1479
PAD2+4	VVAATPTSLLISWDAPAVTVrYYrITYGE	2	1476	1479
PAD4	VVAATPTSLLISWDAPAVTVrYYrITYGE	2	1476	1479
PAD4	rITYGETGGNSPVQEF	2	1479	
PAD2	VVAATPTSLLISWDAPAVTVRYYrITYGE	3	1479	
PAD2+4	VVAATPTSLLISWDAPAVTVRYYrITYGE	1	1479	
PAD4	VVAATPTSLLISWDAPAVTVRYYrITYGE	3	1479	
PAD2	DTLTSrPAQGVVTTLENVSPPR	1	1802	
PAD2+4	DTLTSrPAQGVVTTLENVSPPR	2	1802	
Untreated	DTLTSrPAQGVVTTLENVSPPR	4	1802	
PAD2	TLTSrPAQGVVTTLE	2	1802	
PAD2	TLNDNArSSPVVIDASTAIDAPSNLRF	6	1891	
PAD4	TLNDNArSSPVVIDASTAIDAPSNLRF	2	1891	
Untreated	TLNDNArSSPVVIDASTAIDAPSNLRF	1	1891	
PAD4	TLNDNARSSPVVIDASTAIDAPSNLrF	1	1910	
PAD2	AVGDEWErmSESGF	1	2223	
PAD4	GTTGQSYNQYSQrYHQR	22	2356	
PAD2+4	RPGGEPSPEGTTGQSYNQYSQrYHQR	11	2356	

Table C. S2: List of citrullinated Fn peptide spectral matches identified by LC-MS/MS.

PAD treatment	Citrullinated Residue 1	Citrullinated Residue 2	Annotated Sequence	Modifications	Charge	Delta Score	DeltaCn	m/z [Da]	MH+ [Da]	DeltaM [ppm]	Deltam/z [Da]	XCorr
Untreated	67		QINQQWErTY	R8(Citrul)	2	0.097	0.000	683.818	1366.629	-7.278	-0.005	1.949
Untreated	67		QINQQWErTY	R8(Citrul)	2	0.025	0.000	683.819	1366.630	-6.653	-0.005	2.029
PAD4	67		QINQQWErTY	R8(Citrul)	2	0.172	0.000	683.817	1366.626	-9.600	-0.007	1.982
PAD4	67		QINQQWErTY	R8(Citrul)	2	0.130	0.000	683.818	1366.629	-7.814	-0.005	2.077
PAD4	67		QINQQWErTY	R8(Citrul)	2	0.071	0.000	683.817	1366.626	-9.600	-0.007	2.238
PAD4	67		QINQQWErTY	R8(Citrul)	2	0.095	0.000	683.820	1366.632	-5.134	-0.004	2.114
PAD4	67		QINQQWErTY	R8(Citrul)	2	0.112	0.000	683.819	1366.630	-7.010	-0.005	2.056
PAD4	67		QINQQWErTY	R8(Citrul)	2	0.022	0.000	683.818	1366.629	-7.725	-0.005	2.292
PAD4	67		QINQQWErTY	R8(Citrul)	2	0.070	0.000	683.819	1366.630	-6.564	-0.004	2.149
PAD2+4	107		TGNTYrVGDTY	R6(Citrul)	2	0.024	0.000	624.278	1247.548	-5.318	-0.003	2.120

PAD2	107	TGNTYrVGDTY	R6(Citrul)	2	0.012	0.000	624.278	1247.549	-4.8029	0.003	3.411
PAD2	107	TGNTYrVGDTY	R6(Citrul)	2	0.010	0.000	624.278	1247.549	-4.3040	0.003	3.174
PAD4	107	TGNTYrVGDTY	R6(Citrul)	2	1.000	0.000	624.277	1247.546	-6.6088	0.004	2.621
PAD2	290	TDVrAAVY	R4(Citrul)	2	1.000	0.000	448.226	895.444	-9.7060	0.004	1.999
PAD2	290	VrAAVYQPQPHPQPPPYGHcVTD	R2(Citrul); C20(Carbamidomethyl)	3	0.126	0.000	872.419	2615.243	-1.428	0.001	3.331
PAD2+4	290	VrAAVYQPQPHPQPPPYGHcVTD	R2(Citrul); C20(Carbamidomethyl)	3	0.066	0.000	872.413	2615.224	-8.7080	0.008	2.713
PAD2+4	290	VrAAVYQPQPHPQPPPYGHcVTD	R2(Citrul); C20(Carbamidomethyl)	3	0.138	0.000	872.415	2615.230	-6.329	0.006	3.692
PAD2+4	290	VrAAVYQPQPHPQPPPYGHcVTD	R2(Citrul); C20(Carbamidomethyl)	3	0.045	0.000	872.415	2615.231	-5.839	0.005	2.450
PAD4	515	SQLrDQcIVDDITY	R4(Citrul); C7(Carbamidomethyl)	2	0.037	0.000	863.902	1726.796	-0.046	0.000	2.182
PAD2	751	ITASSFVVSWVSASDTVSGFrVE	R21(Citrul)	2	1.000	0.000	1216.599	2432.191	-3.012	0.004	5.145
PAD4	751	ITASSFVVSWVSASDTVSGFrVE	R21(Citrul)	2	1.000	0.000	1216.615	2432.222	-9.635	0.012	5.336
PAD4	751	ITASSFVVSWVSASDTVSGFrVE	R21(Citrul)	2	0.991	0.000	1216.599	2432.192	-2.912	0.004	5.800
PAD4	751	ITASSFVVSWVSASDTVSGFrVE	R21(Citrul)	2	1.000	0.000	1216.599	2432.191	-3.113	0.004	3.080
PAD2	751	TTPFSPLVATSESVTEITASSFVVSWVSASDTVSGFrVE	R37(Citrul)	4	1.000	0.000	1020.505	4079.000	-0.630	0.001	2.634

PAD2	903	AVEENQESTPVVIQQETTGTPrSDTVPSPRDLQF	R22(Citrul)	3	0.012	0.000	1252.945	3756.822	0.289	0.000	3.397
PAD4	903	TTGTPrSDTVPSPR	R6(Citrul)	2	0.216	0.000	736.866	1472.725	6.436	0.005	2.274
PAD4	903	TTGTPrSDTVPSPR	R6(Citrul)	2	0.308	0.000	736.868	1472.728	4.612	0.003	1.948
PAD4	903	TTGTPrSDTVPSPR	R6(Citrul)	2	0.163	0.000	736.867	1472.727	5.441	0.004	2.453
PAD4	903	TTGTPrSDTVPSPR	R6(Citrul)	2	0.155	0.000	736.866	1472.725	6.436	0.005	2.517
PAD4	903	TTGTPrSDTVPSPR	R6(Citrul)	3	0.289	0.000	491.579	1472.723	8.206	0.004	2.702
PAD4	903	TTGTPrSDTVPSPR	R6(Citrul)	2	0.302	0.000	736.868	1472.728	4.695	0.003	2.024
PAD4	903	TTGTPrSDTVPSPR	R6(Citrul)	2	0.166	0.000	736.866	1472.725	6.519	0.005	2.471
PAD4	903	TTGTPrSDTVPSPR	R6(Citrul)	2	0.176	0.000	736.867	1472.726	5.690	0.004	2.561
PAD4	903	TTGTPrSDTVPSPR	R6(Citrul)	2	0.088	0.000	736.867	1472.726	5.856	0.004	3.304
PAD4	903	TTGTPrSDTVPSPR	R6(Citrul)	2	0.095	0.000	736.866	1472.724	7.182	0.005	3.360
PAD4	903	TTGTPrSDTVPSPR	R6(Citrul)	3	0.283	0.000	491.579	1472.724	7.460	0.004	3.079
PAD4	903	TTGTPrSDTVPSPR	R6(Citrul)	2	0.094	0.000	736.866	1472.724	7.016	0.005	3.423
PAD4	903	TTGTPrSDTVPSPR	R6(Citrul)	2	0.103	0.000	736.867	1472.727	5.110	0.004	2.825

PAD4	903		TTGTPrSDTVPSPR	R6(Citrul)	2	0.101	0.000	736.868	1472.728	-4.612	-0.003	2.169
PAD4	903		TTGTPrSDTVPSPR	R6(Citrul)	3	0.255	0.000	491.579	1472.723	-7.771	-0.004	3.062
PAD4	903		TTGTPrSDTVPSPR	R6(Citrul)	3	0.304	0.000	491.579	1472.722	-8.704	-0.004	2.930
PAD4	903		TTGTPrSDTVPSPR	R6(Citrul)	2	0.100	0.000	736.865	1472.722	-8.508	-0.006	3.507
PAD4	903		TTGTPrSDTVPSPR	R6(Citrul)	2	0.163	0.000	736.866	1472.724	-7.016	-0.005	2.028
PAD2+4	903		TTGTPrSDTVPSPRD	R6(Citrul)	2	0.118	0.000	794.378	1587.748	-8.639	-0.007	2.383
PAD2+4	903		TTGTPrSDTVPSPRD	R6(Citrul)	2	0.098	0.000	794.377	1587.747	-9.254	-0.007	2.345
PAD2+4	903		TTGTPrSDTVPSPRD	R6(Citrul)	2	0.119	0.000	794.379	1587.751	-6.870	-0.005	2.267
PAD2	903	911	TTGTPrSDTVPSPrDLQFVE	R6(Citrul); R14(Citrul)	2	0.457	0.000	1103.036	2205.065	-1.504	-0.002	2.097
PAD2	903		TTGTPrSDTVPSPRDLQFVE	R6(Citrul)	3	0.250	0.000	735.369	2204.092	-3.638	-0.003	2.362
PAD2	903		TTGTPrSDTVPSPRDLQFVE	R6(Citrul)	2		0.034	1102.537	2204.066	-7.848	-0.009	2.283
PAD2	903		TTGTPrSDTVPSPRDLQFVE	R6(Citrul)	2	0.154	0.000	1102.536	2204.064	-8.955	-0.010	2.149
PAD2	903		TTGTPrSDTVPSPRDLQFVE	R6(Citrul)	3	0.046	0.000	735.368	2204.090	-2.808	-0.002	2.375
PAD2	903		TTGTPrSDTVPSPRDLQFVE	R6(Citrul)	3	0.026	0.000	735.370	2204.095	-5.300	-0.004	2.340

PAD 2+4	903	911	TTGTPrSDTVPSPrDLQFVE	R6(Citrul); R14(Citrul)	2		0.023	1103.035	2205.063	-2.501	-0.003	2.558
PAD 2+4	903		TTGTPrSDTVPSPRDLQFVE	R6(Citrul)	2	0.163	0.000	1102.535	2204.063	-9.620	-0.011	2.094
PAD 2+4	903		TTGTPrSDTVPSPRDLQFVE	R6(Citrul)	2		0.022	1102.535	2204.062	-9.841	-0.011	3.125
PAD 2+4	903		TTGTPrSDTVPSPRDLQFVE	R6(Citrul)	2		0.027	1102.536	2204.064	-9.066	-0.010	3.258
PAD 2+4	903		TTGTPrSDTVPSPRDLQFVE	R6(Citrul)	3	0.212	0.000	735.361	2204.067	-7.411	-0.005	2.693
PAD 2+4	903		TTGTPrSDTVPSPRDLQFVE	R6(Citrul)	3	0.161	0.000	735.359	2204.062	-9.820	-0.007	2.801
PAD 2+4	903		TTGTPrSDTVPSPRDLQFVE	R6(Citrul)	3	0.231	0.000	735.359	2204.064	-9.155	-0.007	2.769
PAD 2+4	903		TTGTPrSDTVPSPRDLQFVE	R6(Citrul)	2	0.003	0.000	1102.538	2204.069	-6.851	-0.008	2.987
PAD 2+4	903		TTGTPrSDTVPSPRDLQFVE	R6(Citrul)	3	0.240	0.000	735.360	2204.065	-8.324	-0.006	2.459
PAD 2+4	903		TTGTPrSDTVPSPRDLQFVE	R6(Citrul)	3	0.009	0.000	735.364	2204.076	-3.423	-0.003	2.364
PAD 2+4	903		TTGTPrSDTVPSPRDLQFVE	R6(Citrul)	3	0.142	0.000	735.361	2204.069	-6.912	-0.005	2.599
PAD 2+4	903		TTGTPrSDTVPSPRDLQFVE	R6(Citrul)	2	0.030	0.000	1102.536	2204.064	-8.844	-0.010	3.327
PAD 2+4	903		TTGTPrSDTVPSPRDLQFVE	R6(Citrul)	2		0.009	1102.535	2204.062	-9.731	-0.011	3.417

PAD2+4	903	TTGTPrSDTVPSPRDLQFVE	R6(Citrul)	3	0.209	0.000	735.364	2204.079	-2.343	0.002	2.338
PAD2+4	903	TTGTPrSDTVPSPRDLQFVE	R6(Citrul)	3	0.155	0.000	735.361	2204.069	-6.580	0.005	2.838
PAD2+4	903	TTGTPrSDTVPSPRDLQFVE	R6(Citrul)	2	0.017	0.000	1102.537	2204.067	-7.515	0.008	3.536
PAD2+4	903	TTGTPrSDTVPSPRDLQFVE	R6(Citrul)	3	0.195	0.000	735.360	2204.067	-7.743	0.006	3.068
PAD2+4	903	TTGTPrSDTVPSPRDLQFVE	R6(Citrul)	2		0.034	1102.538	2204.070	-6.408	0.007	2.569
PAD2+4	903	TTGTPrSDTVPSPRDLQFVE	R6(Citrul)	3	0.226	0.000	735.360	2204.067	-7.826	0.006	3.141
PAD2+4	903	TTGTPrSDTVPSPRDLQFVE	R6(Citrul)	3	0.154	0.000	735.360	2204.066	-7.909	0.006	2.797
PAD2+4	903	TTGTPrSDTVPSPRDLQFVE	R6(Citrul)	2	0.003	0.000	1102.537	2204.068	-7.294	0.008	3.514
PAD2+4	903	TTGTPrSDTVPSPRDLQFVE	R6(Citrul)	3	0.222	0.000	735.362	2204.071	-5.915	0.004	2.930
PAD2+4	903	TTGTPrSDTVPSPRDLQFVE	R6(Citrul)	3	0.167	0.000	735.361	2204.069	-6.497	0.005	2.387
PAD2+4	903	TTGTPrSDTVPSPRDLQFVE	R6(Citrul)	2	0.032	0.000	1102.536	2204.065	-8.623	0.010	3.452
PAD2+4	903	TTGTPrSDTVPSPRDLQFVE	R6(Citrul)	3	0.129	0.000	735.362	2204.070	-6.248	0.005	2.563
PAD2+4	903	TTGTPrSDTVPSPRDLQFVE	R6(Citrul)	3	0.059	0.000	735.362	2204.070	-6.248	0.005	2.529

PAD2+4	903		TTGTPrSDTVPSPRDLQFVE	R6(Citrul)	3	0.130	0.000	735.360	2204.067	-7.743	-0.006	2.466
PAD4	903		TTGTPrSDTVPSPRDLQFVE	R6(Citrul)	2		0.023	1102.538	2204.068	-7.072	-0.008	2.546
PAD4	903		TTGTPrSDTVPSPRDLQFVE	R6(Citrul)	2		0.025	1102.547	2204.086	-1.125	-0.001	2.721
PAD4	903		TTGTPrSDTVPSPRDLQFVE	R6(Citrul)	2	0.018	0.000	1102.536	2204.065	-8.512	-0.009	2.837
PAD4	903		TTGTPrSDTVPSPRDLQFVE	R6(Citrul)	2		0.028	1102.540	2204.073	-4.857	-0.005	3.143
PAD4	903		TTGTPrSDTVPSPRDLQFVE	R6(Citrul)	2		0.030	1102.536	2204.066	-8.180	-0.009	3.222
PAD4	903		TTGTPrSDTVPSPRDLQFVE	R6(Citrul)	2	0.071	0.000	1102.546	2204.085	-0.682	-0.001	2.100
PAD4	903		TTGTPrSDTVPSPRDLQFVE	R6(Citrul)	2	0.028	0.000	1102.538	2204.069	-6.629	-0.007	2.860
PAD4	903		TTGTPrSDTVPSPRDLQFVE	R6(Citrul)	3	0.279	0.000	735.360	2204.066	-7.992	-0.006	2.758
PAD4	903		TTGTPrSDTVPSPRDLQFVE	R6(Citrul)	2		0.003	1102.538	2204.068	-6.961	-0.008	3.144
PAD4	903	911	TTGTPrSDTVPSPrDLQFVE	R6(Citrul); R14(Citrul)	2	0.412	0.000	1103.039	2205.070	-0.599	-0.001	2.326
PAD4	903	911	TTGTPrSDTVPSPrDLQFVE	R6(Citrul); R14(Citrul)	2		0.024	1103.033	2205.058	-4.715	-0.005	2.436
PAD4	903	911	TTGTPrSDTVPSPrDLQFVE	R6(Citrul); R14(Citrul)	2	0.484	0.000	1103.047	2205.088	-8.682	-0.010	2.439
PAD2	911		AVEENQESTPVVIQQETTGTPRSDTVPSPrDLQF	R30(Citrul)	3		0.012	1252.945	3756.822	-0.289	-0.000	3.361
PAD4	911		TTGTPRSDTVPSPr	R14(Citrul)	2		0.045	736.866	1472.725	-6.850	-0.005	3.602

PAD2	911	TTGTPRSDTVPSPrDLQFVE	R14(Citrul)	2	0.034	0.000	1102.537	2204.066	-7.848	-0.009	2.357
PAD2+4	911	TTGTPRSDTVPSPrDLQFVE	R14(Citrul)	2		0.017	1102.538	2204.069	-6.851	-0.008	2.935
PAD2+4	911	TTGTPRSDTVPSPrDLQFVE	R14(Citrul)	2	0.009	0.000	1102.535	2204.062	-9.731	-0.011	3.452
PAD2+4	911	TTGTPRSDTVPSPrDLQFVE	R14(Citrul)	2		0.006	1102.535	2204.062	-9.841	-0.011	3.185
PAD2+4	911	TTGTPRSDTVPSPrDLQFVE	R14(Citrul)	2		0.024	1102.536	2204.064	-9.066	-0.010	3.272
PAD2+4	911	TTGTPRSDTVPSPrDLQFVE	R14(Citrul)	2		0.034	1102.538	2204.070	-6.408	-0.007	2.569
PAD2+4	911	TTGTPRSDTVPSPrDLQFVE	R14(Citrul)	2		0.034	1102.537	2204.067	-7.515	-0.008	3.424
PAD2+4	911	TTGTPRSDTVPSPrDLQFVE	R14(Citrul)	2		0.009	1102.537	2204.068	-7.294	-0.008	3.485
PAD4	911	TTGTPRSDTVPSPrDLQFVE	R14(Citrul)	2		0.022	1102.547	2204.086	-1.125	-0.001	2.728
PAD4	911	TTGTPRSDTVPSPrDLQFVE	R14(Citrul)	2		0.016	1102.540	2204.073	-4.857	-0.005	3.185
PAD4	911	TTGTPRSDTVPSPrDLQFVE	R14(Citrul)	2		0.009	1102.536	2204.066	-8.180	-0.009	3.292
PAD4	911	TTGTPRSDTVPSPrDLQFVE	R14(Citrul)	2		0.031	1102.537	2204.067	-7.515	-0.008	2.514
PAD4	911	TTGTPRSDTVPSPrDLQFVE	R14(Citrul)	2		0.039	1102.536	2204.065	-8.512	-0.009	2.734
PAD4	911	TTGTPRSDTVPSPrDLQFVE	R14(Citrul)	2		0.021	1102.537	2204.066	-7.958	-0.009	2.829

PAD4	911		TTGTPRSDTVPSPrDLQFVE	R14(Citrul)	2	0.114	0.000	1102.552	2204.097	5.9	0.00	2.3
PAD4	911		TTGTPRSDTVPSPrDLQFVE	R14(Citrul)	2	0.053	0.000	1102.543	2204.079	1.9	0.00	2.0
PAD4	911		TTGTPRSDTVPSPrDLQFVE	R14(Citrul)	2		0.023	1102.538	2204.068	7.0	0.00	2.5
PAD4	911		TTGTPRSDTVPSPrDLQFVE	R14(Citrul)	2		0.009	1102.538	2204.069	6.5	0.00	3.2
PAD4	911		TTGTPRSDTVPSPrDLQFVE	R14(Citrul)	2		0.035	1102.538	2204.069	6.6	0.00	2.7
PAD4	911		TTGTPRSDTVPSPrDLQFVE	R14(Citrul)	2		0.013	1102.538	2204.068	6.9	0.00	3.1
PAD4	911		TTGTPRSDTVPSPrDLQFVE	R14(Citrul)	2		0.023	1102.537	2204.067	7.6	0.00	3.0
PAD2+4	938		SAVTGYrVDVIPVNLPGE	R7(Citrul)	2	0.060	0.000	944.004	1887.001	7.8	0.00	2.0
PAD4	938		SAVTGYrVDVIPVNLPGE	R7(Citrul)	2	0.017	0.000	944.000	1886.993	3.3	0.00	2.3
PAD2	953		RVDVIPVNLPGEHGQrLPISRNTF	R16(Citrul)	4	0.022	0.000	679.623	2715.472	0.7	0.00	3.6
PAD2	953		RVDVIPVNLPGEHGQrLPISRNTF	R16(Citrul)	4	0.013	0.000	679.622	2715.464	2.0	0.00	3.0
PAD4	1035	1036	LTVGLTrrGQPR	R7(Citrul); R8(Citrul)	2	0.197	0.000	678.388	1355.768	6.6	0.00	2.6
PAD4	1035	1036	LTVGLTrrGQPR	R7(Citrul); R8(Citrul)	2	0.164	0.000	678.388	1355.768	6.4	0.00	2.6
PAD4	1035	1036	LTVGLTrrGQPR	R7(Citrul); R8(Citrul)	2	0.175	0.000	678.389	1355.770	5.2	0.00	2.1
PAD4	1035	1036	LTVGLTrrGQPR	R7(Citrul); R8(Citrul)	2	0.148	0.000	678.389	1355.771	4.1	0.00	2.6

PAD4	1035	1036	LTVGLTrrGQPR	R7(Citrul); R8(Citrul)	2	0.162	0.000	678.389	1355.770	-5.160	-0.003	2.725
PAD4	1035	1036	LTVGLTrrGQPR	R7(Citrul); R8(Citrul)	2	0.077	0.000	678.388	1355.769	-5.791	-0.004	3.356
PAD4	1035	1036	LTVGLTrrGQPR	R7(Citrul); R8(Citrul)	2	0.060	0.000	678.388	1355.769	-5.971	-0.004	3.492
PAD4	1035	1036	LTVGLTrrGQPR	R7(Citrul); R8(Citrul)	2	0.057	0.000	678.388	1355.769	-5.791	-0.004	3.892
PAD4	1035	1036	LTVGLTrrGQPR	R7(Citrul); R8(Citrul)	2	0.056	0.000	678.388	1355.769	-6.151	-0.004	3.382
PAD4	1035	1036	LTVGLTrrGQPR	R7(Citrul); R8(Citrul)	2	0.076	0.000	678.388	1355.768	-6.511	-0.004	3.016
PAD4	1035	1036	LTVGLTrrGQPR	R7(Citrul); R8(Citrul)	2	0.033	0.000	678.388	1355.769	-5.791	-0.004	2.420
PAD4	1035	1036	LTVGLTrrGQPR	R7(Citrul); R8(Citrul)	2	0.035	0.000	678.389	1355.770	-4.890	-0.003	2.012
PAD4	1035	1036	LTVGLTrrGQPR	R7(Citrul); R8(Citrul)	2	0.087	0.000	678.388	1355.768	-6.331	-0.004	2.070
PAD4	1035	1036	LTVGLTrrGQPR	R7(Citrul); R8(Citrul)	2	0.067	0.000	678.388	1355.769	-5.971	-0.004	3.604
PAD4	1035	1036	LTVGLTrrGQPR	R7(Citrul); R8(Citrul)	2	0.059	0.000	678.388	1355.769	-6.061	-0.004	3.398
PAD2+4	1035	1036	LTVGLTrrGQPR	R7(Citrul); R8(Citrul)	2	0.069	0.000	678.385	1355.764	-9.752	-0.007	3.362
PAD2+4	1035	1036	LTVGLTrrGQPR	R7(Citrul); R8(Citrul)	2	0.050	0.000	678.387	1355.766	-7.861	-0.005	3.430

PAD 2+4	1035	1036	LTVGLTrrGQPR	R7(Citrul); R8(Citrul)	2	0.063	0.00 0	678. 385	1355 .764	-9.7 52	-0.00 7	3.4 69
PAD 2+4	1035	1036	LTVGLTrrGQPR	R7(Citrul); R8(Citrul)	2	0.014	0.00 0	678. 388	1355 .768	-6.5 11	-0.00 4	2.2 31
PAD 2+4	1035	1036	LTVGLTrrGQPR	R7(Citrul); R8(Citrul)	2	0.064	0.00 0	678. 387	1355 .767	-7.5 01	-0.00 5	3.4 56
PAD 2+4	1035	1036	LTVGLTrrGQPR	R7(Citrul); R8(Citrul)	2	0.056	0.00 0	678. 387	1355 .766	-8.2 22	-0.00 6	2.8 41
PAD 2+4	1035	1036	LTVGLTrrGQPR	R7(Citrul); R8(Citrul)	2	0.049	0.00 0	678. 385	1355 .764	-9.8 42	-0.00 7	2.6 85
PAD 2+4	1035	1036	LTVGLTrrGQPR	R7(Citrul); R8(Citrul)	2	0.008	0.00 0	678. 388	1355 .768	-6.3 31	-0.00 4	2.4 26
Untre ated	1207		ITGYrITTTPTNGQQGNSLEE	R5(Citrul)	3	0.026	0.00 0	761. 035	2281 .091	-1.7 29	-0.00 1	3.4 50
PAD 2	1207		ITGYrITTTPTNGQQGNSLEE	R5(Citrul)	2	0.014	0.00 0	1141 .047	2281 .086	-3.9 71	-0.00 5	5.7 15
PAD 2	1207		ITGYrITTTPTNGQQGNSLEE	R5(Citrul)	3	0.032	0.00 0	761. 033	2281 .084	-4.9 40	-0.00 4	4.3 96
PAD 2+4	1207		ITGYrITTTPTNGQQGNSLEE	R5(Citrul)	3	0.004	0.00 0	761. 030	2281 .076	-8.2 31	-0.00 6	2.8 73
PAD 2+4	1207		ITGYrITTTPTNGQQGNSLEE	R5(Citrul)	2	1.000	0.00 0	1141 .063	2281 .118	-9.9 43	-0.01 1	2.1 92
PAD 2+4	1207		ITGYrITTTPTNGQQGNSLEE	R5(Citrul)	3	0.148	0.00 0	761. 032	2281 .080	-6.4 65	-0.00 5	2.7 03
PAD 4	1207		ITGYrITTTPTNGQQGNSLEE	R5(Citrul)	3	0.019	0.00 0	761. 033	2281 .085	-4.5 39	-0.00 3	3.6 43
Untre ated	1207		RSTTPDITGYrITTTPTNGQQG NSLEE	R11(Citrul)	3		0.02 1	980. 137	2938 .395	-2.7 26	-0.00 3	3.8 22

Untreated	1207	RSTTPDITGYrITTTPTNGQQGNSLEE	R11(Citrul)	3		0.018	980.138	2938.399	-1.604	-0.002	4.399
Untreated	1207	RSTTPDITGYrITTTPTNGQQGNSLEE	R11(Citrul)	3		0.031	980.137	2938.397	-2.290	-0.002	4.436
Untreated	1207	RSTTPDITGYrITTTPTNGQQGNSLEE	R11(Citrul)	3		0.013	980.137	2938.395	-2.788	-0.003	4.525
Untreated	1207	RSTTPDITGYrITTTPTNGQQGNSLEE	R11(Citrul)	3		0.045	980.138	2938.398	-1.666	-0.002	4.034
Untreated	1207	RSTTPDITGYrITTTPTNGQQGNSLEE	R11(Citrul)	3		0.045	980.136	2938.392	-3.785	-0.004	2.547
Untreated	1207	RSTTPDITGYrITTTPTNGQQGNSLEE	R11(Citrul)	3		0.032	980.138	2938.398	-1.729	-0.002	3.953
Untreated	1207	RSTTPDITGYrITTTPTNGQQGNSLEE	R11(Citrul)	3		0.042	980.137	2938.396	-2.414	-0.002	4.553
Untreated	1207	RSTTPDITGYrITTTPTNGQQGNSLEE	R11(Citrul)	3	0.002	0.000	980.137	2938.396	-2.601	-0.003	4.367
Untreated	1207	RSTTPDITGYrITTTPTNGQQGNSLEE	R11(Citrul)	3		0.028	980.136	2938.394	-3.037	-0.003	3.459
Untreated	1207	RSTTPDITGYrITTTPTNGQQGNSLEE	R11(Citrul)	3		0.030	980.138	2938.400	-1.043	-0.001	2.549
Untreated	1207	RSTTPDITGYrITTTPTNGQQGNSLEE	R11(Citrul)	3		0.028	980.135	2938.389	-4.845	-0.005	2.430
Untreated	1207	RSTTPDITGYrITTTPTNGQQGNSLEE	R11(Citrul)	3		0.026	980.135	2938.389	-4.782	-0.005	3.064
Untreated	1207	RSTTPDITGYrITTTPTNGQQGNSLEE	R11(Citrul)	3		0.031	980.137	2938.396	-2.414	-0.002	3.791

Untreated	1207	RSTTPDITGYrITTTPTNGQQGNSLEE	R11(Citrul)	3		0.024	980.138	2938.398	-1.7791	-0.002	4.097
Untreated	1207	RSTTPDITGYrITTTPTNGQQGNSLEE	R11(Citrul)	3		0.002	980.137	2938.397	-2.1065	-0.002	4.640
Untreated	1207	RSTTPDITGYrITTTPTNGQQGNSLEE	R11(Citrul)	3		0.015	980.137	2938.396	-2.4777	-0.002	3.991
Untreated	1207	RSTTPDITGYrITTTPTNGQQGNSLEE	R11(Citrul)	3		0.026	980.137	2938.395	-2.726	-0.003	4.094
Untreated	1207	RSTTPDITGYrITTTPTNGQQGNSLEE	R11(Citrul)	3		0.019	980.137	2938.396	-2.539	-0.002	4.128
Untreated	1207	RSTTPDITGYrITTTPTNGQQGNSLEE	R11(Citrul)	3		0.014	980.137	2938.398	-1.9161	-0.002	4.388
Untreated	1207	RSTTPDITGYrITTTPTNGQQGNSLEE	R11(Citrul)	3	0.040	0.000	980.138	2938.399	-1.4171	-0.001	4.501
Untreated	1207	RSTTPDITGYrITTTPTNGQQGNSLEE	R11(Citrul)	3	0.039	0.000	980.137	2938.395	-2.726	-0.003	4.423
Untreated	1207	RSTTPDITGYrITTTPTNGQQGNSLEE	R11(Citrul)	3		0.045	980.137	2938.398	-1.8535	-0.002	4.627
Untreated	1207	RSTTPDITGYrITTTPTNGQQGNSLEE	R11(Citrul)	3		0.029	980.136	2938.393	-3.5363	-0.003	2.970
PAD4	1207	RSTTPDITGYrITTTPTNGQQGNSLEE	R11(Citrul)	3	0.045	0.000	980.136	2938.392	-3.7234	-0.004	5.089
PAD4	1207	RSTTPDITGYrITTTPTNGQQGNSLEE	R11(Citrul)	3	0.015	0.000	980.136	2938.394	-3.0373	-0.003	4.554
PAD4	1207	RSTTPDITGYrITTTPTNGQQGNSLEE	R11(Citrul)	3		0.027	980.136	2938.394	-3.2877	-0.003	4.618

PAD4	1207	RSTTPDITGYrITTTPTNGQQGNSLEE	R11(Citrul)	3		0.004	980.136	2938.394	-3.037	-0.003	5.023
PAD4	1207	RSTTPDITGYrITTTPTNGQQGNSLEE	R11(Citrul)	3		0.019	980.137	2938.396	-2.477	-0.002	4.671
PAD4	1207	RSTTPDITGYrITTTPTNGQQGNSLEE	R11(Citrul)	3		0.038	980.138	2938.399	-1.417	-0.001	4.328
PAD4	1207	RSTTPDITGYrITTTPTNGQQGNSLEE	R11(Citrul)	3		0.037	980.138	2938.399	-1.542	-0.002	3.953
PAD4	1207	RSTTPDITGYrITTTPTNGQQGNSLEE	R11(Citrul)	3		0.027	980.137	2938.397	-2.040	-0.002	3.599
PAD4	1207	RSTTPDITGYrITTTPTNGQQGNSLEE	R11(Citrul)	3		0.007	980.137	2938.398	-1.916	-0.002	4.032
PAD4	1207	RSTTPDITGYrITTTPTNGQQGNSLEE	R11(Citrul)	3	0.040	0.000	980.137	2938.397	-2.103	-0.002	3.526
PAD4	1207	RSTTPDITGYrITTTPTNGQQGNSLEE	R11(Citrul)	3	0.061	0.000	980.134	2938.389	-4.907	-0.005	2.802
PAD4	1207	RSTTPDITGYrITTTPTNGQQGNSLEE	R11(Citrul)	3	0.006	0.000	980.134	2938.388	-5.281	-0.005	3.124
PAD4	1207	RSTTPDITGYrITTTPTNGQQGNSLEE	R11(Citrul)	3	0.079	0.000	980.135	2938.392	-3.972	-0.004	2.654
PAD4	1207	RSTTPDITGYrITTTPTNGQQGNSLEE	R11(Citrul)	3		0.038	980.136	2938.393	-3.474	-0.003	4.797
PAD4	1207	RSTTPDITGYrITTTPTNGQQGNSLEE	R11(Citrul)	3		0.029	980.136	2938.393	-3.598	-0.004	4.755
PAD4	1207	RSTTPDITGYrITTTPTNGQQGNSLEE	R11(Citrul)	3	0.027	0.000	980.138	2938.399	-1.355	-0.001	3.777

PAD4	1207	RSTTPDITGYrITTTPTNGQQGNSLEE	R11(Citrul)	3		0.022	980.136	2938.394	-3.0237	0.003	4.797
PAD4	1207	RSTTPDITGYrITTTPTNGQQGNSLEE	R11(Citrul)	3	0.013	0.000	980.136	2938.394	-3.1003	0.003	4.659
PAD4	1207	RSTTPDITGYrITTTPTNGQQGNSLEE	R11(Citrul)	3		0.022	980.136	2938.392	-3.6061	0.004	4.801
PAD4	1207	RSTTPDITGYrITTTPTNGQQGNSLEE	R11(Citrul)	3	0.021	0.000	980.135	2938.391	-4.0097	0.004	4.366
PAD4	1207	RSTTPDITGYrITTTPTNGQQGNSLEE	R11(Citrul)	3		0.045	980.138	2938.398	-1.7291	0.002	5.046
PAD4	1207	RSTTPDITGYrITTTPTNGQQGNSLEE	R11(Citrul)	3		0.009	980.137	2938.396	-2.4077	0.002	5.455
PAD4	1207	RSTTPDITGYrITTTPTNGQQGNSLEE	R11(Citrul)	3		0.021	980.132	2938.382	-7.0887	0.007	5.549
PAD2	1207	RSTTPDITGYrITTTPTNGQQGNSLEE	R11(Citrul)	3	0.004	0.000	980.145	2938.420	-5.6246	0.006	5.434
PAD2	1207	RSTTPDITGYrITTTPTNGQQGNSLEE	R11(Citrul)	3		0.045	980.136	2938.393	-3.4119	0.003	4.893
PAD2	1207	RSTTPDITGYrITTTPTNGQQGNSLEE	R11(Citrul)	3		0.004	980.142	2938.411	-2.6331	0.003	2.614
PAD2+4	1207	RSTTPDITGYrITTTPTNGQQGnSLEE	R11(Citrul); N23(Deamidation)	3	0.003	0.000	980.468	2939.390	-0.8061	0.001	3.350
PAD2+4	1207	RSTTPDITGYrITTTPTNGQQGNSLEE	R11(Citrul)	3	0.025	0.000	980.136	2938.393	-3.4174	0.003	3.972
PAD2	1274	LrFTNIGPDTMRVtWAPPPSID	R2(Citrul); T14(Phospho)	2		0.008	1283.109	2565.211	-4.2025	0.005	2.437
PAD2	1274	LrFTNIGPDTMRVtWAPPPSID	R2(Citrul); T14(Phospho)	2		0.008	1283.111	2565.215	-2.3943	0.003	2.448

PAD2	1274	LrFTNIGPDTMRVtWAPPPSID	R2(Citrul); T14(Phospho)	2		0.030	1283.106	2565.205	-6.2960	0.008	2.555
PAD2	1274	LrFTNIGPDTMRVtWAPPPSID	R2(Citrul); T14(Phospho)	2		0.020	1283.111	2565.214	-2.8704	0.004	2.485
PAD2	1274	LrFTNIGPDTMRVtWAPPPSID	R2(Citrul); T14(Phospho)	2		0.015	1283.107	2565.207	-5.6307	0.007	2.595
PAD2	1274	LrFTNIGPDTMRVtWAPPPSID	R2(Citrul); T14(Phospho)	2		0.008	1283.108	2565.209	-5.0596	0.006	2.389
PAD2	1274	LrFTNIGPDTMRVtWAPPPSID	R2(Citrul); T14(Phospho)	2		0.012	1283.108	2565.209	-5.0596	0.006	2.572
PAD2	1274	LrFTNIGPDTMRVtWAPPPSID	R2(Citrul); T14(Phospho)	2		0.008	1283.109	2565.210	-4.5083	0.006	2.448
PAD2	1274	LrFTNIGPDTMRVtWAPPPSID	R2(Citrul); T14(Phospho)	2		0.030	1283.109	2565.210	-4.3093	0.006	2.608
PAD2	1274	LrFTNIGPDTMRVtWAPPPSID	R2(Citrul); T14(Phospho)	2		0.025	1283.109	2565.211	-4.2025	0.005	2.336
PAD2	1274	LrFTNIGPDTMRVtWAPPPSID	R2(Citrul); T14(Phospho)	2		0.004	1283.107	2565.207	-5.6307	0.007	2.236
PAD2	1274	LrFTNIGPDTMRVtWAPPPSID	R2(Citrul); T14(Phospho)	2	0.017	0.000	1283.115	2565.222	0.1760	0.000	2.336
PAD2	1274	LrFTNIGPDTMRVtWAPPPSID	R2(Citrul); T14(Phospho)	2		0.025	1283.108	2565.209	-4.7373	0.006	2.378
PAD2	1274	LrFTNIGPDTMRVTWAPPPsID	R2(Citrul); S20(Phospho)	2		0.016	1283.111	2565.215	-2.3943	0.003	2.430
PAD2	1274	LrFTNIGPDTMRVTWAPPPsID	R2(Citrul); S20(Phospho)	2		0.032	1283.111	2565.214	-2.8704	0.004	2.465
PAD2	1274	LrFTNIGPDTMRVTWAPPPsID	R2(Citrul); S20(Phospho)	2		0.023	1283.107	2565.207	-5.6307	0.007	2.582

PAD2	1274	LrFTNIGPDTMRVTWAPPPsID	R2(Citrul); S20(Phospho)	2		0.025	1283.108	2565.209	-5.059	0.006	2.352
PAD2	1274	LrFTNIGPDTMRVTWAPPPsID	R2(Citrul); S20(Phospho)	2		0.029	1283.109	2565.211	-4.202	0.005	2.392
PAD2	1274	LrFTNIGPDTMRVTWAPPPsID	R2(Citrul); S20(Phospho)	2		0.049	1283.108	2565.209	-4.773	0.006	2.320
PAD2	1274	LrFTNIGPDTMRVTWAPPPsID	R2(Citrul); S20(Phospho)	2		0.008	1283.108	2565.209	-5.059	0.006	2.584
PAD2	1274	LrFTNIGPDTMRVTWAPPPsID	R2(Citrul); S20(Phospho)	2		0.031	1283.107	2565.207	-5.630	0.007	2.180
PAD2	1274	LrFTNIGPDTMRVTWAPPPsID	R2(Citrul); S20(Phospho)	2		0.017	1283.115	2565.222	-0.176	0.000	2.298
PAD2	1274	LrFTNIGPDTMRVTWAPPPsID	R2(Citrul); S20(Phospho)	2		0.012	1283.109	2565.210	-4.583	0.006	2.438
PAD2	1274	LrFTNIGPDTMRVTWAPPPsID	R2(Citrul); S20(Phospho)	2		0.017	1283.109	2565.211	-4.202	0.005	2.355
PAD2+4	1274	LrFTNIGPDTMRVtWAPPPSID	R2(Citrul); T14(Phospho)	2		0.025	1283.103	2565.199	-8.675	0.011	2.349
PAD2+4	1274	LrFTNIGPDTMRVtWAPPPSID	R2(Citrul); T14(Phospho)	2		0.021	1283.102	2565.197	-9.627	0.012	2.394
PAD2+4	1274	LrFTNIGPDTMRVtWAPPPSID	R2(Citrul); T14(Phospho)	2		0.014	1283.103	2565.199	-8.961	0.011	2.136
PAD2+4	1274	LrFTNIGPDTMRVTWAPPPsID	R2(Citrul); S20(Phospho)	2		0.012	1283.103	2565.199	-8.675	0.011	2.380
PAD2+4	1274	LrFTNIGPDTMRVTWAPPPsID	R2(Citrul); S20(Phospho)	2	0.021	0.000	1283.102	2565.197	-9.627	0.012	2.438
PAD2+4	1274	LrFTNIGPDTMRVtWAPPPSID	R2(Citrul); T14(Phospho)	2		0.018	1283.102	2565.197	-9.532	0.012	2.245

PAD4	1274	LrFTNIGPDTMRVtWAPPPSID	R2(Citrul); T14(Phospho)	2		0.015	1283.107	2565.208	-5.440	0.007	2.551
PAD4	1274	LrFTNIGPDTMRVtWAPPPSID	R2(Citrul); T14(Phospho)	2		0.016	1283.105	2565.204	-6.962	0.009	2.462
PAD4	1274	LrFTNIGPDTMRVtWAPPPSID	R2(Citrul); T14(Phospho)	2		0.031	1283.107	2565.206	-6.106	0.008	2.186
PAD4	1274	LrFTNIGPDTMRVtWAPPPSID	R2(Citrul); T14(Phospho)	2		0.004	1283.108	2565.208	-5.344	0.007	2.532
PAD4	1274	LrFTNIGPDTMRVtWAPPPSID	R2(Citrul); T14(Phospho)	2		0.008	1283.107	2565.207	-5.820	0.007	2.552
PAD4	1274	LrFTNIGPDTMRVtWAPPPSID	R2(Citrul); T14(Phospho)	2		0.015	1283.103	2565.198	-9.246	0.012	2.703
PAD4	1274	LrFTNIGPDTMRVtWAPPPSID	R2(Citrul); T14(Phospho)	2		0.004	1283.105	2565.203	-7.248	0.009	2.548
PAD4	1274	LrFTNIGPDTMRVtWAPPPSID	R2(Citrul); T14(Phospho)	2		0.020	1283.106	2565.204	-6.772	0.009	2.409
PAD4	1274	LrFTNIGPDTMRVtWAPPPSID	R2(Citrul); T14(Phospho)	2	0.035	0.000	1283.110	2565.213	-3.346	0.004	2.266
PAD4	1274	LrFTNIGPDTMRVtWAPPPSID	R2(Citrul); T14(Phospho)	2		0.008	1283.106	2565.205	-6.296	0.008	2.567
PAD4	1274	LrFTNIGPDTMRVTWAPPPsID	R2(Citrul); S20(Phospho)	2		0.043	1283.107	2565.208	-5.440	0.007	2.476
PAD4	1274	LrFTNIGPDTMRVTWAPPPsID	R2(Citrul); S20(Phospho)	2		0.008	1283.105	2565.203	-7.248	0.009	2.539
PAD4	1274	LrFTNIGPDTMRVTWAPPPsID	R2(Citrul); S20(Phospho)	2		0.032	1283.105	2565.204	-6.962	0.009	2.420

PAD4	1274		LrFTNIGPDTMRVTWAPPPsID	R2(Citrul); S20(Phospho)	2		0.029	1283.103	2565.198	-9.246	-0.012	2.656
PAD4	1274		LrFTNIGPDTMRVTWAPPPsID	R2(Citrul); S20(Phospho)	2		0.035	1283.107	2565.207	-5.820	-0.007	2.478
PAD4	1274		LrFTNIGPDTMRVTWAPPPsID	R2(Citrul); S20(Phospho)	2		0.013	1283.107	2565.206	-6.106	-0.008	2.227
PAD4	1274		LrFTNIGPDTMRVTWAPPPsID	R2(Citrul); S20(Phospho)	2		0.012	1283.108	2565.208	-5.344	-0.007	2.509
PAD4	1274		LrFTNIGPDTMRVTWAPPPsID	R2(Citrul); S20(Phospho)	2		0.040	1283.110	2565.213	-3.346	-0.004	2.178
PAD4	1274		LrFTNIGPDTMRVTWAPPPsID	R2(Citrul); S20(Phospho)	2		0.012	1283.106	2565.205	-6.296	-0.008	2.558
PAD4	1274		LrFTNIGPDTMRVTWAPPPsID	R2(Citrul); S20(Phospho)	2		0.045	1283.106	2565.204	-6.772	-0.009	2.350
PAD4	1274		LrFTNIGPDTMRVTWAPPPsID	R2(Citrul); S20(Phospho)	2		0.036	1283.110	2565.212	-3.726	-0.005	2.424
PAD4	1274	1284	LrFTNIGPDTmrVtWAPPPSID	R2(Citrul); M11(Oxidation); R12(Citrul); T14(Phospho)	3	0.029	0.000	861.411	2582.218	6.323	0.008	2.398
PAD4	1274	1284	LrFTNIGPDTmrVTWAPPPsID	R2(Citrul); M11(Oxidation); R12(Citrul); S20(Phospho)	3		0.029	861.411	2582.218	6.323	0.008	2.329
PAD2	1274		SVPISDTIIPAVPPPTDLrFTNIGPD	R19(Citrul)	2	0.027	0.000	1367.218	2733.428	-2.758	-0.004	4.081
PAD2	1274		SVPISDTIIPAVPPPTDLrFTNIGPD	R19(Citrul)	2	0.052	0.000	1367.227	2733.446	3.940	0.005	2.898
PAD2+4	1274		SVPISDTIIPAVPPPTDLrFTNIGPD	R19(Citrul)	2	0.053	0.000	1367.218	2733.428	-2.580	-0.004	2.467
PAD2+4	1274		SVPISDTIIPAVPPPTDLrFTNIGPD	R19(Citrul)	2	0.044	0.000	1367.223	2733.438	0.993	0.001	2.741
PAD4	1274		SVPISDTIIPAVPPPTDLrFTNIGPD	R19(Citrul)	2	0.037	0.000	1367.234	2733.461	9.389	0.013	4.090

PAD			SVPISDTIIPAVPPPTDLrFTNIG				0.00	1367	2733	0.9	0.00	4.0
4	1274		PD	R19(Citrul)	2	0.032	0	.223	.438	04	1	86
										-	-	
PAD			SVPISDTIIPAVPPPTDLrFTNIG	R19(Citrul); M28(Oxidation);			0.00	1401	4202	6.2	0.00	2.9
2	1274	1284	PDTmrVTWAPPPSID	R29(Citrul)	3	0.072	0	.375	.112	46	9	30
										-	-	
PAD			SVPISDTIIPAVPPPTDLrFTNIG				0.00	1051	4201	1.4	0.00	3.5
2	1274		PDTmRVTWAPPPSID	R19(Citrul); M28(Oxidation)	4	0.008	0	.042	.147	86	2	68
PAD			SVPISDTIIPAVPPPTDLrFTNIG	R19(Citrul); M28(Oxidation);			0.00	1051	4202	3.1	0.00	3.4
2	1274	1284	PDTmrVTWAPPPSID	R29(Citrul)	4	0.200	0	.293	.152	78	3	47
PAD			SVPISDTIIPAVPPPTDLrFTNIG	R19(Citrul); M28(Oxidation);			0.00	1401	4202	1.3	0.00	3.5
2	1274	1284	PDTmrVTWAPPPSID	R29(Citrul)	3	0.108	0	.386	.144	36	2	19
										-	-	
PAD			SVPISDTIIPAVPPPTDLrFTNIG	R19(Citrul); M28(Oxidation);			0.00	1051	4202	4.1	0.00	3.5
2+4	1274	1284	PDTmrVTWAPPPSID	R29(Citrul)	4	0.128	0	.286	.121	43	4	89
										-	-	
PAD			SVPISDTIIPAVPPPTDLrFTNIG	R19(Citrul); M28(Oxidation);			0.00	1401	4202	2.4	0.00	3.3
4	1274	1284	PDTmrVTWAPPPSID	R29(Citrul)	3	0.073	0	.381	.128	11	3	00
										-	-	
PAD			SVPISDTIIPAVPPPTDLrFTNIG	R19(Citrul); M28(Oxidation);			0.00	1401	4202	3.8	0.00	3.5
4	1274	1284	PDTmrVTWAPPPSID	R29(Citrul)	3	0.094	0	.379	.122	93	5	31
										-	-	
PAD			SVPISDTIIPAVPPPTDLrFTNIG	R19(Citrul); M28(Oxidation);			0.00	1051	4202	3.5	0.00	2.9
4	1274	1284	PDTmrVTWAPPPSID	R29(Citrul)	4	0.054	0	.286	.123	62	4	83
PAD							0.00	1068	2135	0.7	0.00	2.5
2	1274		TIIPAVPPPTDLrFTNIGPD	R13(Citrul)	2	1.000	0	.074	.141	46	1	36
										-	-	
PAD							0.00	1068	2135	1.5	0.00	2.1
2	1274		TIIPAVPPPTDLrFTNIGPD	R13(Citrul)	2	1.000	0	.072	.136	41	2	49
PAD							0.00	1068	2135	8.6	0.00	2.0
2	1274		TIIPAVPPPTDLrFTNIGPD	R13(Citrul)	2	1.000	0	.082	.158	35	9	36
PAD							0.00	1068	2135	1.8	0.00	2.5
2+4	1274		TIIPAVPPPTDLrFTNIGPD	R13(Citrul)	2	1.000	0	.075	.143	89	2	97
										-	-	
PAD							0.00	1068	2135	4.4	0.00	2.1
2+4	1274		TIIPAVPPPTDLrFTNIGPD	R13(Citrul)	2	1.000	0	.068	.130	00	5	11
PAD			TIIPAVPPPTDLrFTNIGPDTmrV	R13(Citrul); M22(Oxidation);			0.00	1201	3603	0.6	0.00	2.4
4	1274		TWAPPPSID	R23(Citrul)	3	0.033	0	.953	.844	03	1	09
PAD							0.00	855.	2565	1.0	0.00	2.3
2	1284		LRFTNIGPDTMrVTWAPPPsID	R12(Citrul); S20(Phospho)	3	0.110	0	746	.224	03	1	61

PAD2	1284	LRFTNIGPDTMrVTWAPPPsID	R12(Citrul); S20(Phospho)	3	0.165	0.000	855.747	2565.228	2.502	0.002	2.296
PAD2+4	1284	LRFTNIGPDTMrVtWAPPPSID	R12(Citrul); T14(Phospho)	2		0.037	1283.103	2565.199	8.961	0.011	2.088
PAD2+4	1284	LRFTNIGPDTMrVTWAPPPsID	R12(Citrul); S20(Phospho)	3	0.100	0.000	855.741	2565.209	4.921	0.004	2.404
PAD2+4	1284	LRFTNIGPDTMrVTWAPPPsID	R12(Citrul); S20(Phospho)	3	0.074	0.000	855.743	2565.214	2.994	0.003	2.303
PAD2+4	1284	LRFTNIGPDTMrVTWAPPPsID	R12(Citrul); S20(Phospho)	3	0.137	0.000	855.741	2565.210	4.636	0.004	2.339
PAD2+4	1284	LRFTNIGPDTMrVTWAPPPsID	R12(Citrul); S20(Phospho)	3	0.104	0.000	855.743	2565.216	2.280	0.002	2.314
PAD2+4	1284	LRFTNIGPDTMrVTWAPPPsID	R12(Citrul); S20(Phospho)	3	0.041	0.000	855.744	2565.217	1.923	0.002	2.700
PAD2+4	1284	LRFTNIGPDTMrVTWAPPPsID	R12(Citrul); S20(Phospho)	3	0.125	0.000	855.740	2565.205	6.492	0.006	2.716
PAD2+4	1284	LRFTNIGPDTMrVTWAPPPsID	R12(Citrul); S20(Phospho)	3	0.127	0.000	855.744	2565.218	1.352	0.001	2.520
PAD2+4	1284	LRFTNIGPDTMrVTWAPPPsID	R12(Citrul); S20(Phospho)	3	0.147	0.000	855.746	2565.224	1.003	0.001	2.325
PAD2+4	1284	LRFTNIGPDTMrVTWAPPPsID	R12(Citrul); S20(Phospho)	3	0.124	0.000	855.744	2565.219	1.067	0.001	2.498
PAD4	1284	LRFTNIGPDTMrVTWAPPPsID	R12(Citrul); S20(Phospho)	3	0.082	0.000	855.744	2565.217	1.852	0.002	2.311
PAD4	1284	LRFTNIGPDTMrVTWAPPPsID	R12(Citrul); S20(Phospho)	3	0.150	0.000	855.743	2565.215	2.494	0.002	2.670
PAD2	1410	DRVPHSrNsITLTNLTPGTEYVVsIVALnGREE	R7(Citrul); S9(Phospho); S24(Phospho); N29(Deamidation)	3		0.014	1267.266	3799.785	2.800	0.004	3.449

PAD2	1410	1434	DRVPHSrNsITLTNLTPGTEYVVsIVALNGrEE	R7(Citrul); S9(Phospho); S24(Phospho); R31(Citrul)	3		0.003	1267.266	3799.785	-2.8000	-0.004	3.488
PAD2	1410		DRVPHSrNSItLTNLTPGTEYVVsIVALnGREE	R7(Citrul); T11(Phospho); S24(Phospho); N29(Deamidation)	3		0.011	1267.266	3799.785	-2.8000	-0.004	3.464
PAD2	1410	1434	DRVPHSrNSItLTNLTPGTEYVVsIVALNGrEE	R7(Citrul); T11(Phospho); S24(Phospho); R31(Citrul)	3		0.000	1267.266	3799.785	-2.8000	-0.004	3.503
PAD2+4	1434		YVVSIVALNGrE	R11(Citrul)	2		0.046	660.856	1320.705	-8.670	-0.006	2.482
PAD2+4	1434		YVVSIVALNGrEE	R11(Citrul)	2	1.000	0.000	725.376	1449.745	-9.913	-0.007	2.778
PAD4	1434		YVVSIVALNGrEE	R11(Citrul)	2		0.024	725.378	1449.750	-6.629	-0.005	3.327
PAD4	1434		YVVSIVALNGrEE	R11(Citrul)	2		0.031	725.378	1449.749	-7.302	-0.005	3.172
PAD4	1434		YVVSIVALNGrEE	R11(Citrul)	2		0.037	725.378	1449.749	-6.797	-0.005	3.167
PAD4	1434		YVVSIVALNGrEE	R11(Citrul)	2		0.035	725.378	1449.749	-6.797	-0.005	3.056
PAD4	1434		YVVSIVALNGrEE	R11(Citrul)	2		0.021	725.379	1449.751	-5.787	-0.004	3.265
PAD4	1434		YVVSIVALNGrEE	R11(Citrul)	2		0.038	725.382	1449.756	-2.082	-0.002	3.300
PAD4	1434		YVVSIVALNGrEE	R11(Citrul)	2		0.025	725.378	1449.749	-7.218	-0.005	3.087
PAD4	1434		YVVSIVALNGrEE	R11(Citrul)	2		0.038	725.376	1449.745	-9.660	-0.007	2.559

PAD4	1434		YVVSIVALNGrEE	R11(Citrul)	2		0.021	725.380	1449.752	-4.861	-0.004	3.232
PAD2	1434	1452	YVVSIVALNGrEESPLLIGQQSTVSDVPrDLE	R11(Citrul); R29(Citrul)	3	0.004	0.000	1162.601	3485.789	-3.773	-0.004	6.983
PAD2	1434		YVVSIVALNGrEESPLLIGQQSTVSDVPRDLE	R11(Citrul)	3	0.018	0.000	1162.272	3484.803	-4.282	-0.005	4.884
PAD2+4	1434	1452	YVVSIVALNGrEESPLLIGQQSTVSDVPrDLE	R11(Citrul); R29(Citrul)	3		0.000	1162.608	3485.809	-1.901	-0.002	6.435
PAD2	1452		ESPLLIGQQSTVSDVPrDLE	R17(Citrul)	3	0.003	0.000	728.710	2184.117	-5.942	-0.004	3.678
PAD2	1452		ESPLLIGQQSTVSDVPrDLE	R17(Citrul)	3		0.046	728.702	2184.090	-6.131	-0.004	2.891
PAD2	1452		ESPLLIGQQSTVSDVPrDLE	R17(Citrul)	3		0.014	728.704	2184.097	-3.113	-0.002	3.491
PAD2	1452		ESPLLIGQQSTVSDVPrDLE	R17(Citrul)	3	0.026	0.000	728.710	2184.114	-4.768	-0.003	3.879
PAD2+4	1452		ESPLLIGQQSTVSDVPrDLE	R17(Citrul)	3	0.013	0.000	728.711	2184.119	-6.780	-0.005	3.120
PAD2+4	1452		ESPLLIGQQSTVSDVPrDLE	R17(Citrul)	2		0.000	1092.556	2184.105	-0.331	0.000	5.174
PAD2+4	1452		ESPLLIGQQSTVSDVPrDLE	R17(Citrul)	3		0.030	728.707	2184.105	-0.744	-0.001	2.604
PAD4	1452		ESPLLIGQQSTVSDVPrDLE	R17(Citrul)	3		0.031	728.704	2184.097	-2.945	-0.002	2.829
PAD4	1452		ESPLLIGQQSTVSDVPrDLE	R17(Citrul)	2		0.030	1092.560	2184.113	-4.020	-0.004	4.897
PAD4	1452		ESPLLIGQQSTVSDVPrDLE	R17(Citrul)	2		0.037	1092.564	2184.121	-7.820	-0.009	4.702
PAD4	1452		ESPLLIGQQSTVSDVPrDLE	R17(Citrul)	2		0.032	1092.563	2184.119	-7.149	-0.008	4.821
PAD4	1452		ESPLLIGQQSTVSDVPrDLE	R17(Citrul)	3		0.023	728.704	2184.097	-3.113	-0.002	2.989
PAD2	1476	1479	VVAATPTSLLISWDAPAVTVrYYrITYGE	R21(Citrul); R24(Citrul)	3	1.000	0.000	1072.233	3214.683	-4.610	-0.005	3.534

PAD 2+4	1476	1479	VVAATPTSLLISWDAPAVTVrY YrITYGE	R21(Citrul); R24(Citrul)	3	1.000	0.00 0	1072 .230	3214 .676	2.3 32 -	0.00 2 -	3.2 16
PAD 2+4	1476	1479	VVAATPTSLLISWDAPAVTVrY YrITYGE	R21(Citrul); R24(Citrul)	3	1.000	0.00 0	1072 .223	3214 .654	4.5 04	0.00 5	2.6 09
PAD 4	1476	1479	VVAATPTSLLISWDAPAVTVrY YrITYGE	R21(Citrul); R24(Citrul)	3	1.000	0.00 0	1072 .230	3214 .675	2.1 04	0.00 2	3.2 22
PAD 4	1476	1479	VVAATPTSLLISWDAPAVTVrY YrITYGE	R21(Citrul); R24(Citrul)	3	1.000	0.00 0	1072 .237	3214 .697	8.7 11 -	0.00 9 -	2.7 67
PAD 4	1479		rITYGETGGNSPVQEF	R1(Citrul)	2	1.000	0.00 0	878. 405	1755 .803	9.3 53 -	0.00 8 -	3.2 04
PAD 4	1479		rITYGETGGNSPVQEF	R1(Citrul)	2	1.000	0.00 0	878. 405	1755 .803	9.2 13 -	0.00 8 -	2.8 82
PAD 2	1479		VVAATPTSLLISWDAPAVTVRY YrITYGE	R24(Citrul)	4	0.095	0.00 0	804. 175	3213 .680	1.2 43	0.00 1	3.5 85
PAD 2	1479		VVAATPTSLLISWDAPAVTVRY YrITYGE	R24(Citrul)	3	0.102	0.00 0	1071 .906	3213 .705	6.4 53	0.00 7	2.6 50
PAD 2	1479		VVAATPTSLLISWDAPAVTVRY YrITYGE	R24(Citrul)	3	0.098	0.00 0	1071 .903	3213 .696	3.7 18	0.00 4	2.9 72
PAD 2+4	1479		VVAATPTSLLISWDAPAVTVRY YrITYGE	R24(Citrul)	3	0.131	0.00 0	1071 .901	3213 .690	1.8 95 -	0.00 2 -	2.8 26
PAD 4	1479		VVAATPTSLLISWDAPAVTVRY YrITYGE	R24(Citrul)	3	0.065	0.00 0	1071 .894	3213 .668	4.9 42	0.00 5	2.7 87
PAD 4	1479		VVAATPTSLLISWDAPAVTVRY YrITYGE	R24(Citrul)	3	0.054	0.00 0	1071 .901	3213 .689	1.6 67	0.00 2	3.9 23
PAD 4	1479		VVAATPTSLLISWDAPAVTVRY YrITYGE	R24(Citrul)	3	0.097	0.00 0	1071 .900	3213 .685	0.2 99	0.00 0	2.9 83
PAD 2	1802		DTLTSrPAQGVVTTLENVSPPR	R6(Citrul)	3		0.00 3	780. 412	2339 .222	0.2 90 -	0.00 0 -	3.5 83
Untre ated	1802		DTLTSrPAQGVVTTLENVSPPR	R6(Citrul)	4		0.02 7	585. 559	2339 .214	2.8 46 -	0.00 2 -	4.6 83
Untre ated	1802		DTLTSrPAQGVVTTLENVSPPR	R6(Citrul)	3	0.053	0.00 0	780. 411	2339 .218	1.1 97	0.00 1	6.2 80
Untre ated	1802		DTLTSrPAQGVVTTLENVSPPR	R6(Citrul)	3	0.014	0.00 0	780. 416	2339 .234	5.6 91	0.00 4	4.3 30

Untreated	1802	DTLTSrPAQGVVTTLENVSPPR	R6(Citrul)	3		0.021	780.409	2339.213	-3.4677	0.003	4.616
PAD2+4	1802	DTLTSrPAQGVVTTLENVSPPR	R6(Citrul)	3	0.022	0.000	780.407	2339.206	-6.2075	0.005	2.739
PAD2+4	1802	DTLTSrPAQGVVTTLENVSPPR	R6(Citrul)	3	0.167	0.000	780.412	2339.222	0.369	0.000	2.507
PAD2	1802	TLTSrPAQGVVTTLE	R5(Citrul)	2	0.004	0.000	787.430	1573.853	5.558	0.004	2.660
PAD2	1802	TLTSrPAQGVVTTLE	R5(Citrul)	2		0.047	787.424	1573.841	-1.9662	0.002	3.018
Untreated	1891	TLNDNArSSPVVIDASTAIDAPSNLRF	R7(Citrul)	3		0.018	949.147	2845.428	-2.0312	0.002	6.563
PAD2	1891	TLNDNArSSPVVIDASTAIDAPSNLRF	R7(Citrul)	3		0.003	949.143	2845.413	-7.0507	0.007	3.474
PAD2	1891	TLNDNArSSPVVIDASTAIDAPSNLRF	R7(Citrul)	3	0.366	0.000	949.144	2845.417	-5.6345	0.005	2.434
PAD2	1891	TLNDNArSSPVVIDASTAIDAPSNLRF	R7(Citrul)	3	0.005	0.000	949.149	2845.431	-0.6791	0.001	3.747
PAD2	1891	TLNDNArSSPVVIDASTAIDAPSNLRF	R7(Citrul)	3	0.306	0.000	949.144	2845.419	-5.1919	0.005	2.812
PAD2	1891	TLNDNArSSPVVIDASTAIDAPSNLRF	R7(Citrul)	3	0.021	0.000	949.141	2845.408	-8.7087	0.008	3.291
PAD2	1891	TLNDNArSSPVVIDASTAIDAPSNLRF	R7(Citrul)	3	0.014	0.000	949.143	2845.414	-6.7936	0.006	3.631
PAD4	1891	TLNDNArSSPVVIDASTAIDAPSNLRF	R7(Citrul)	3	0.084	0.000	949.148	2845.429	-1.5161	0.001	2.498
PAD4	1891	TLNDNArSSPVVIDASTAIDAPSNLRF	R7(Citrul)	3	0.125	0.000	949.143	2845.414	-6.9867	0.007	2.325

PAD4	1910	TLNDNARSSPVVIDASTAIDAPSNLrF	R26(Citrul)	3	0.054	0.000	949.146	2845.423	-3.768	0.004	2.394
PAD2	2223	AVGDEWErmSESGF	R8(Citrul); M9(Oxidation)	2	1.000	0.000	808.837	1616.666	-7.392	0.006	2.073
PAD4	2356	GTTGQSYNQYSQrYHQR	R13(Citrul)	3	0.028	0.000	692.314	2074.929	-2.273	0.002	2.530
PAD4	2356	GTTGQSYNQYSQrYHQR	R13(Citrul)	3	0.057	0.000	692.314	2074.927	-3.155	0.002	2.471
PAD4	2356	GTTGQSYNQYSQrYHQR	R13(Citrul)	2	0.020	0.000	1037.967	2074.926	-3.619	0.004	1.965
PAD4	2356	GTTGQSYNQYSQrYHQR	R13(Citrul)	3	0.047	0.000	692.314	2074.927	-2.890	0.002	2.570
PAD4	2356	GTTGQSYNQYSQrYHQR	R13(Citrul)	3	0.008	0.000	692.314	2074.927	-2.979	0.002	2.416
PAD4	2356	GTTGQSYNQYSQrYHQR	R13(Citrul)	3	0.039	0.000	692.313	2074.924	-4.479	0.003	4.603
PAD4	2356	GTTGQSYNQYSQrYHQR	R13(Citrul)	2	0.083	0.000	1037.964	2074.921	-5.855	0.006	3.020
PAD4	2356	GTTGQSYNQYSQrYHQR	R13(Citrul)	3	0.019	0.000	692.312	2074.920	-6.332	0.004	3.755
PAD4	2356	GTTGQSYNQYSQrYHQR	R13(Citrul)	3	0.039	0.000	692.313	2074.925	-4.038	0.003	4.583
PAD4	2356	GTTGQSYNQYSQrYHQR	R13(Citrul)	2	0.032	0.000	1037.961	2074.915	-9.032	0.009	2.825
PAD4	2356	GTTGQSYNQYSQrYHQR	R13(Citrul)	2	0.044	0.000	1037.968	2074.928	-2.678	0.003	2.745
PAD4	2356	GTTGQSYNQYSQrYHQR	R13(Citrul)	3	0.033	0.000	692.313	2074.924	-4.302	0.003	4.509

PAD4	2356	GTTGQSYNQYSQrYHQR	R13(Citrul)	2	0.138	0.000	1037.971	2074.935	0.852	0.001	1.959
PAD4	2356	GTTGQSYNQYSQrYHQR	R13(Citrul)	3	0.042	0.000	692.314	2074.926	3.508	0.002	4.033
PAD4	2356	GTTGQSYNQYSQrYHQR	R13(Citrul)	3	0.004	0.000	692.313	2074.924	4.479	0.003	2.447
PAD4	2356	GTTGQSYNQYSQrYHQR	R13(Citrul)	2	0.040	0.000	1037.968	2074.929	2.207	0.002	3.239
PAD4	2356	GTTGQSYNQYSQrYHQR	R13(Citrul)	3	0.005	0.000	692.311	2074.918	7.567	0.005	3.734
PAD4	2356	GTTGQSYNQYSQrYHQR	R13(Citrul)	3	0.006	0.000	692.311	2074.920	6.597	0.005	3.507
PAD4	2356	GTTGQSYNQYSQrYHQR	R13(Citrul)	3	0.010	0.000	692.311	2074.918	7.303	0.005	2.992
PAD4	2356	GTTGQSYNQYSQrYHQR	R13(Citrul)	3	0.014	0.000	692.312	2074.921	5.802	0.004	2.839
PAD4	2356	GTTGQSYNQYSQrYHQR	R13(Citrul)	3	0.012	0.000	692.311	2074.919	6.773	0.005	3.290
PAD4	2356	GTTGQSYNQYSQrYHQR	R13(Citrul)	2	0.058	0.000	1037.962	2074.917	7.973	0.008	3.100
PAD2+4	2356	RPGGEPSPEGTTGQSYNQYSQrYHQR	R22(Citrul)	4	0.015	0.000	746.088	2981.330	7.519	0.006	5.266
PAD2+4	2356	RPGGEPSPEGTTGQSYNQYSQrYHQR	R22(Citrul)	4	0.025	0.000	746.087	2981.328	8.420	0.006	3.985
PAD2+4	2356	RPGGEPSPEGTTGQSYNQYSQrYHQR	R22(Citrul)	4	0.013	0.000	746.087	2981.328	8.420	0.006	3.008
PAD2+4	2356	RPGGEPSPEGTTGQSYNQYSQrYHQR	R22(Citrul)	4	0.016	0.000	746.087	2981.327	8.584	0.006	4.469

PAD 2+4	2356	RPGGEPSPEGTTGQSYNQYS QrYHQR	R22(Citrul)	3	0.023	0.00 0	994. 461	2981 .370	5.7 10 -	0.00 6 -	5.3 13
PAD 2+4	2356	RPGGEPSPEGTTGQSYNQYS QrYHQR	R22(Citrul)	4	0.011	0.00 0	746. 088	2981 .331	7.3 55 -	0.00 5 -	5.3 42
PAD 2+4	2356	RPGGEPSPEGTTGQSYNQYS QrYHQR	R22(Citrul)	4	0.021	0.00 0	746. 088	2981 .331	7.4 37 -	0.00 6 -	5.8 13
PAD 2+4	2356	RPGGEPSPEGTTGQSYNQYS QrYHQR	R22(Citrul)	3	0.013	0.00 0	994. 461	2981 .369	5.4 65 -	0.00 5 -	7.0 21
PAD 2+4	2356	RPGGEPSPEGTTGQSYNQYS QrYHQR	R22(Citrul)	4	0.008	0.00 0	746. 088	2981 .330	7.5 19 -	0.00 6 -	5.1 10
PAD 2+4	2356	RPGGEPSPEGTTGQSYNQYS QrYHQR	R22(Citrul)	4	0.017	0.00 0	746. 088	2981 .329	8.1 74 -	0.00 6 -	4.5 96
PAD 2+4	2356	RPGGEPSPEGTTGQSYNQYS QrYHQR	R22(Citrul)	4	0.065	0.00 0	746. 092	2981 .345	2.7 70	0.00 2	2.7 60

REFERENCES

1. Heng BC, Aubel D, Fussenegger M. An overview of the diverse roles of G-protein coupled receptors (GPCRs) in the pathophysiology of various human diseases. Biotechnol Adv. 2013;31(8):1676–94.
2. Spiegel AM, Weinstein LS. Inherited Diseases Involving G Proteins and G Protein–Coupled Receptors. Annu Rev Med. 2004;55(1):27–39.
3. Roman DL, Traynor JR. Regulators of G protein signaling (RGS) proteins as drug targets: modulating G-protein-coupled receptor (GPCR) signal transduction. J Med Chem. 2011 Nov 10;54(21):7433–40.
4. Khan SM, Sleno R, Gora S, Zylbergold P, Laverdure J, Labbé J, et al. The Expanding Roles of G bg Subunits in G Protein – Coupled Receptor Signaling and Drug Action. 2013;65(4):545–77.
5. Weinstein LS, Chen M, Xie T, Liu J. Genetic diseases associated with heterotrimeric G proteins. Trends Pharmacol Sci. 2006;27(5):260–6.
6. Cook JL. G Protein–Coupled Receptors as Disease Targets: Emerging Paradigms. Ochsner J. 2010;10(1):2–7.
7. Hanyaloglu AC, Grammatopoulos DK. Pleiotropic GPCR signaling in health and disease. Mol Cell Endocrinol. 2017;449:1–2.
8. El-Haibi CP, Sharma P, Singh R, Gupta P, Taub DD, Singh S, et al. Differential G protein subunit expression by prostate cancer cells and their interaction with CXCR5. Mol Cancer. 2013;12(1):64.
9. Birnbaumer L. The discovery of signal transduction by G proteins: a personal account and an overview of the initial findings and contributions that led to our present understanding. Biochim Biophys Acta. 2007 Apr;1768(4):756–71.

10. McCudden CR, Hains MD, Kimple RJ, Siderovski DP, Willard FS. G-protein signaling: back to the future. Cell Mol Life Sci. 2005;62:551–77.
11. Cabrera-Vera TM, Vanhauwe J, Thomas TO, Medkova M, Preininger A, Mazzoni MR, et al. Insights into G protein structure, function, and regulation. Endocr Rev. 2003;24(6):765–81.
12. Wettschureck N, Offermanns S. Mammalian G Proteins and Their Cell Type Specific Functions. Physilological Rev. 2005;1159–204.
13. Alvaro CG, Thorner J. Heterotrimeric G protein-coupled receptor signaling in yeast mating pheromone response. J Biol Chem. 2016;291(15):7785–98.
14. Yang G, Sau C, Lai W, Cichon J, Li W. Regulation, Signaling and Physiological Functions of G-proteins. 2015;344(6188):1173–8.
15. Jastrzebska B. GPCR: G protein complexes - The fundamental signaling assembly. Amino Acids. 2013;45(6):1303–14.
16. Smrcka A V. G protein beta gamma subunits: Central mediators of G protein-coupled receptor signaling. Cell Mol Life Sci. 2008;65(14):2191–214.
17. Vries L De, Zheng B, Fischer T, Elenko E, Farquhar MG. The regulator of G-protein signaling. Annu Rev Pharmacol Toxicol. 2000;40:235–71.
18. Berman DM, Gilman AG. Mammalian RGS proteins: Barbarians at the gate. J Biol Chem. 1998;273(3):1269–72.
19. Flower DR. Modelling G-protein-coupled receptors for drug design. Biochim Biophys Acta - Rev Biomembr. 1999;1422(3):207–34.
20. Mirzadegan T, Benko G. Sequence Analyses of G-Protein-Coupled Receptors: Simi- larities to Rhodopsin - Corrections. Biochemistry. 2003;42(10):2759–67.
21. Thal DM, Vuckovic Z, Draper-joyce CJ, Liang Y, Glukhova A, Christopoulos A, et al. Recent advances in the determination of G protein-coupled receptor structures. Curr Opin Struct Biol. 2018;51:28–34.

22. Katritch V, Cherezov V, Stevens RC. Structure-function of the G protein-coupled receptor superfamily. Annu Rev Pharmacol Toxicol. 2013;53(39):531–56.
23. Rosenbaum DM, Rasmussen SGF, Kobilka BK. The structure and function of G-protein-coupled receptors Daniel. Nature. 2014;459(7245):356–63.
24. Latek D, Modzelewska A, Trzaskowski B, Krzysztof P, Filipek S. G protein-coupled receptors — recent advances. Acta Biochim Pol. 2012;59(4):515–29.
25. Neves SR. G Protein Pathways. Science (80-). 2002;296(5573):1636–9.
26. Marinissen MJ, Gutkind JS. G-protein-coupled receptors and signaling networks: Emerging paradigms. Trends Pharmacol Sci. 2001;22(7):368–76.
27. Ferguson SS. Evolving concepts in G protein-coupled receptor endocytosis: the role in receptor desensitization and signaling. Pharmacol Rev. 2001;53(1):1–24.
28. Neer EJ, Clapham DE. Roles of G protein subunits in transmembrane signalling. Nature. 1988 May 12;333(6169):129–34.
29. Simon MI, Strathmann MP, Gautam N. Diversity of G proteins in signal transduction. Science (80-). 1991;252(5007):802–8.
30. Milligan G, Kostenis E. Heterotrimeric G-proteins: a short history. Br J Pharmacol. 2006 Jan;147 Suppl:S46-55.
31. Van Eps N, Preininger AM, Alexander N, Kaya AI, Meier S, Meiler J, et al. Interaction of a G protein with an activated receptor opens the interdomain interface in the alpha subunit. Proc Natl Acad Sci U S A. 2011 Jun 7;108(23):9420–4.
32. Westfield GH, Rasmussen SGF, Su M, Dutta S, DeVree BT, Chung KY, et al. Structural flexibility of the Gαs α-helical domain in the β2 -adrenoceptor Gs complex. Proc Natl Acad Sci U S A. 2011;108(38):16086–91.
33. Marrari Y, Crouthamel M, Irannejad R, Wedegaertner PB. Assembly and trafficking of heterotrimeric G proteins. Biochemistry. 2007;46(26):7665–77.

34. Clapham DE, Neer EJ. G PROTEIN βγ SUBUNITS. 1997;167–203.

35. Kisselev O, Ermolaeva M, Gautam N. Efficient interaction with a receptor requires a specific type of prenyl group on the G protein gamma subunit. J Biol Chem. 1995;270(43):25356–8.

36. Schwindinger WF, Betz KS, Giger KE, Sabol A, Bronson SK, Robishaw JD. Loss of G protein γ7 alters behavior and reduces striatal αolf level and cAMP production. J Biol Chem. 2003;278(8):6575–9.

37. Schwindinger WF, Giger KE, Betz KS, Stauffer AM, Sunderlin EM, Sim-Selley LJ, et al. Mice with deficiency of G protein gamma3 are lean and have seizures. Mol Cell Biol. 2004;24(17):7758–68.

38. Lambright DG, Sondek J, Bohm a, Skiba NP, Hamm HE, Sigler PB. The 2.0 A crystal structure of a heterotrimeric G protein. Vol. 379, Nature. 1996. p. 311–9.

39. Sondek J, Bohm A, Lambright DG, Hamm HE, Sigler PB. Crystal structure of a GA protein βγdimer at 2.1 Å resolution. Nature. 1996;379(6563):369–74.

40. Wall M a, Coleman DE, Lee E, Iñiguez-Lluhi J a, Posner B a, Gilman a G, et al. The structure of the G protein heterotrimer Gi alpha 1 beta 1 gamma 2. Cell. 1995;83(6):1047–58.

41. Higgins JB, Casey PJ. The role of prenylation in G-protein assembly and function. Cell Signal. 1996;8(6):433–7.

42. Higgins JB, Casey PJ. In Vitro processing of recombinant G protein γ subunits: Requirements for assembly of an active βγ complex. J Biol Chem. 1994;269(12):9067–73.

43. SUTHERLAND EW, RALL TW. Fractionation and characterization of a cyclic adenine ribonucleotide formed by tissue particles. J Biol Chem. 1958 Jun;232(2):1077–91.

44. Neer EJ. Heterotrimeric C proteins: Organizers of transmembrane signals. Cell.

1995;80(2):249–57.

45. Brand CS, Sadana R, Malik S, Smrcka A V., Dessauer CW. Adenylyl Cyclase 5 Regulation by Gβγ Involves Isoform-Specific Use of Multiple Interaction Sites. Mol Pharmacol. 2015 Oct;88(4):758–67.

46. Pitcher JA, Freedman NJ, Lefkowitz RJ. G Protein – Coupled Receptor Kinases. Annu Rev Biochem. 1998;67:653–92.

47. Gurevich E V, Tesmer JJG, Mushegian A, Gurevich V V. G protein-coupled receptor kinases: more than just kinases and not only for GPCRs. Pharmacol Ther. 2012 Jan;133(1):40–69.

48. Gurevich E V, Premont RT, Gainetdinov RR. G protein-coupled receptor kinases: from molecules to diseases. Faseb J. 2015;29(2):361–4.

49. Dohlman HG, Song J, Ma D, Courchesne WE, Thorner J. Sst2, a negative regulator of pheromone signaling in the yeast Saccharomyces cerevisiae: expression, localization, and genetic interaction and physical association with Gpa1 (the G-protein alpha subunit). Mol Cell Biol. 1996;16(9):5194–209.

50. Tesmer JJG. Chapter 4 Structure and Function of Regulator of G Protein Signaling Homology Domains. 1st ed. Vol. 86, Progress in Molecular Biology and Translational Science. Elsevier Inc.; 2009. 75-113 p.

51. Heximer SP, Watson N, Linder ME, Blumer KJ, Hepler JR. RGS2/G0S8 is a selective inhibitor of Gqalpha function. Proc Natl Acad Sci U S A. 1997;94(26):14389–93.

52. Tesmer JJ, Berman DM, Gilman AG, Sprang SR. Structure of RGS4 bound to AlF4--activated G(i alpha1): stabilization of the transition state for GTP hydrolysis. Cell. 1997;89(2):251–61.

53. Hepler JR, Berman DM, Gilman AG, Kozasa T. RGS4 and GAIP are GTPase-activating proteins for Gq alpha and block activation of phospholipase C beta by

gamma-thio-GTP-Gq alpha. Proc Natl Acad Sci U S A. 1997;94(2):428–32.

54. Johnson EN, Druey KM. Heterotrimeric G protein signaling: Role in asthma and allergic inflammation. J Allergy Clin Immunol. 2002;109(4):592–602.

55. Kirui JK, Xie Y, Wolff DW, Jiang H, Abel PW, Tu Y. G beta gamma Signaling Promotes Breast Cancer Cell Migration and Invasion. J Pharmacol Exp Ther. 2010;333(2):393–403.

56. Dores MR, Trejo J. Ubiquitination of G protein-coupled receptors: functional implications and drug discovery. Mol Pharmacol. 2012 Oct;82(4):563–70.

57. Vazquez-Prado J, Bracho-Valdes I, Cervantes-Villagrana RD, Reyes-Cruz G. G Pathways in Cell Polarity and Migration Linked to Oncogenic GPCR Signaling: Potential Relevance in Tumor Microenvironment. Mol Pharmacol. 2016;90(5):573–86.

58. De Francesco E, Sotgia F, Clarke R, Lisanti M, Maggiolini M. G Protein-Coupled Receptors at the Crossroad between Physiologic and Pathologic Angiogenesis: Old Paradigms and Emerging Concepts. Int J Mol Sci. 2017;18(12):2713.

59. Santos R, Ursu O, Gaulton A, Bento AP, Donadi RS, Bologa CG, et al. A comprehensive map of molecular drug targets. Nat Publ Gr. 2016;16(1):19–34.

60. Rask-Andersen M, Masuram S, Schiöth HB. The druggable genome: Evaluation of drug targets in clinical trials suggests major shifts in molecular class and indication. Annu Rev Pharmacol Toxicol. 2014;54:9–26.

61. Hauser AS, Attwood MM, Rask-Andersen M, Schiöth HB, Gloriam DE. Trends in GPCR drug discovery: New agents, targets and indications. Nat Rev Drug Discov. 2017;16(12):829–42.

62. Belmonte SL, Blaxall BC. G protein coupled receptor kinases as therapeutic targets in cardiovascular disease. Circ Res. 2011;109(3):309–19.

63. Xiong Y, Guo J, Candelore MR, Liang R, Miller C, Dallas-Yang Q, et al. Discovery

of a novel glucagon receptor antagonist N-[(4-{(1S)-1-[3-(3, 5-dichlorophenyl)-5-(6-methoxynaphthalen-2-yl)-1H-pyrazol-1-yl]ethyl}phenyl)carbonyl]-β-alanine (MK-0893) for the treatment of type II diabetes. J Med Chem. 2012 Jul 12;55(13):6137–48.

64. Singh S, Sadanandam A, Nannuru KC, Varney ML, Mayer-Ezell R, Bond R, et al. Small-molecule antagonists for CXCR2 and CXCR1 inhibit human melanoma growth by decreasing tumor cell proliferation, survival, and angiogenesis. Clin Cancer Res. 2009;15(7):2380–6.

65. Ling X, Spaeth E, Chen Y, Shi Y, Zhang W, Schober W, et al. The CXCR4 Antagonist AMD3465 Regulates Oncogenic Signaling and Invasiveness In Vitro and Prevents Breast Cancer Growth and Metastasis In Vivo. PLoS One. 2013;8(3).

66. Rask-Andersen M, Almén MS, Schiöth HB. Trends in the exploitation of novel drug targets. Nat Rev Drug Discov. 2011;10(8):579–90.

67. Garland SL. Are GPCRs still a source of new targets? J Biomol Screen. 2013;18(9):947–66.

68. Hauser AS, Chavali S, Masuho I, Jahn LJ, Martemyanov KA, Gloriam DE, et al. Pharmacogenomics of GPCR Drug Targets. Cell. 2017;172(1–2):41–43.e19.

69. Zhong H, Neubig RR. Regulator of G protein signaling proteins: novel multifunctional drug targets. J Pharmacol Exp Ther. 2001;297(3):837–45.

70. Ayoub MA, Damian M, Gespach C, Ferrandis E, Lavergne O, De Wever O, et al. Inhibition of heterotrimeric G protein signaling by a small molecule acting on Gα subunit. J Biol Chem. 2009;284(42):29136–45.

71. Wang Y, Lee Y, Zhang J, Young KH. Identification of peptides that inhibit regulator of G protein signaling 4 function. Pharmacology. 2008;82(2):97–104.

72. Jin Y, Zhong H, Omnaas JR, Neubig RR, Mosberg HI. Structure-based design,

synthesis, and activity of peptide inhibitors of RGS4 GAP activity. Methods Enzymol. 2004;389:266–77.

73. Roof RA, Sobczyk-Kojiro K, Turbiak AJ, Roman DL, Pogozheva ID, Blazer LL, et al. Novel peptide ligands of RGS4 from a focused one-bead, one-compound library. Chem Biol Drug Des. 2008;72(2):111–9.

74. Kotecha SA, Oak JN, Jackson MF, Perez Y, Orser BA, Van Tol HHM, et al. A D2 class dopamine receptor transactivates a receptor tyrosine kinase to inhibit NMDA receptor transmission. Neuron. 2002;35(6):1111–22.

75. Hamilton MH, Cook L a, McRackan TR, Schey KL, Hildebrandt JD. Gamma 2 subunit of G protein heterotrimer is an N-end rule ubiquitylation substrate. Proc Natl Acad Sci U S A. 2003;100(9):5081–6.

76. Liggett SB. Phosphorylation Barcoding as a Mechanism of Directing GPCR Signaling. Sci Signal. 2011;4(185):pe36.

77. Hislop JN, Von Zastrow M. Role of Ubiquitination in Endocytic Trafficking of G-Protein-Coupled Receptors. Traffic. 2011;12(2):137–48.

78. Zhu M, Torres MP, Kelley JB, Dohlman HG, Wang Y. Pheromone- and RSP5-dependent ubiquitination of the G protein β subunit Ste4 in yeast. J Biol Chem. 2011;286(31):27147–55.

79. Garrison JC, Yasuda H, Lindorfer MA, Myung C-S. Phosphorylation of thh ci protein y12 subunit regulates effector specificity. FASEB J. 1998;12(8):A1315.

80. Clement ST, Dixit G, Dohlman HG. Regulation of yeast G protein signaling by the kinases that activate the AMPK homolog Snf1. Sci Signal. 2013;6(291):ra78.

81. Chishiki K, Kamakura S, Yuzawa S, Hayase J, Sumimoto H. Ubiquitination of the heterotrimeric G protein α subunits Gαi2 and Gαq is prevented by the guanine nucleotide exchange factor Ric-8A. Biochem Biophys Res Commun. 2013;435(3):414–9.

82. Tobin AB. G-protein-coupled receptor phosphorylation: where, when and by whom. Br J Pharmacol. 2008;153 Suppl(December 2007):S167–76.

83. Torres MP, Lee MJ, Ding F, Purbeck C, Kuhlman B, Dokholyan N V., et al. G protein mono-ubiquitination by the Rsp5 ubiquitin ligase. J Biol Chem. 2009;284(13):8940–50.

84. Li X, Létourneau D, Holleran B, Leduc R, Lavigne P, Lavoie C. Gα s protein binds ubiquitin to regulate epidermal growth factor receptor endosomal sorting. Proc Natl Acad Sci. 2017;114(51):13477–82.

85. Parnell SC, Marotti LA, Kiang L, Torres MP, Borchers CH, Dohlman HG. Phosphorylation of the RGS protein Sst2 by the MAP kinase Fus3 and use of Sst2 as a model to analyze determinants of substrate sequence specificity. Biochemistry. 2005 Jun 7;44(22):8159–66.

86. Goddard AD, Watts A. Regulation of G protein-coupled receptors by palmitoylation and cholesterol. BMC Biol. 2012;10:2–4.

87. Isom D, Sridharan V, Baker R, Clement S, Smalley D, Dohlman H. Protons as second messenger regulators of G protein signaling. Mol Cell. 2013;51(4):531–8.

88. Torres MP, Clement ST, Cappell SD, Dohlman HG. Cell cycle-dependent phosphorylation and ubiquitination of a G protein α subunit. J Biol Chem. 2011;286(23):20208–16.

89. Wedegaertner PB, Wilson PT, Bourne HR. Lipid modifications of trimeric G proteins. Vol. 270, Journal of Biological Chemistry. 1995. p. 503–6.

90. Marotti LA, Newitt R, Wang Y, Aebersold R, Dohlman HG. Direct identification of a G protein ubiquitination site by mass spectrometry. Biochemistry. 2002;41(16):5067–74.

91. Morishita R, Nakayama H, Isobe T, Matsuda T, Hashimoto Y, Okano T, et al. Primary structure of a gamma subunit of G protein, gamma 12, and its

phosphorylation by protein kinase C. J Biol Chem. 1995;270(49):29469–75.

92. DeFlorio R, Brett M-E, Waszczak N, Apollinari E, Metodiev M V., Dubrovskyi O, et al. Phosphorylation of G is crucial for efficient chemotropism in yeast. J Cell Sci. 2013;126(14):2997–3009.

93. Chen CA, Manning DR. Regulation of G proteins by covalent modification. Oncogene. 2001 Mar 26;20(13):1643–52.

94. Chuh KN, Batt AR, Pratt MR. Chemical Methods for Encoding and Decoding of Posttranslational Modifications. Cell Chem Biol. 2016;23(1):86–107.

95. Brien PJO, Zatz M. Acylation of Bovine Rhodopsin by [3H] Palmitic Acid *. J Biol Chem. 1984;259(19):5054–7.

96. O'Dowd BF, Hnatowich M, Caron MG, Lefkowitz RJ, Bouvier M. Palmitoylation of the human ??2-adrenergic receptor. Mutation of Cys341 in the carboxyl tail leads to an uncoupled nonpalmitoylated form of the receptor. J Biol Chem. 1989;264(13):7564–9.

97. Hukovic N, Panetta R, Kumar U, Rocheville M, Patel YC. The cytoplasmic tail of the human somatostatin receptor type 5 is crucial for interaction with adenylyl cyclase and in mediating desensitization and internalization. J Biol Chem. 1998;273(33):21416–22.

98. Tanaka K, Nagayama Y, Nishihara E, Namba H, Yamashita S, Niwa M. Palmitoylation of human thyrotropin receptor: slower intracellular trafficking of the palmitoylation-defective mutant. Endocrinology. 1998 Feb;139(2):803–6.

99. Escribá P V., Wedegaertner PB, Goñi FM, Vögler O. Lipid-protein interactions in GPCR-associated signaling. Biochim Biophys Acta - Biomembr. 2007;1768(4):836–52.

100. Lefkowitz RJ. Historical review: A brief history and personal retrospective of seven-transmembrane receptors. Trends Pharmacol Sci. 2004;25(8):413–22.

101. Ohguro H, Palczewski K, Ericsson LH, Walsh KA, Johnson RS. Sequential Phosphorylation of Rhodopsin at Multiple Sites. Biochemistry. 1993;32(21):5718–24.

102. Benovic JL, Pike LJ, Cerione RA, Staniszewski C, Yoshimasa T, Codina J, et al. Phosphorylation of the mammalian β-adrenergic receptor by cyclic AMP-dependent protein kinase. Regulation of the rate of receptor phosphorylation and dephosphorylation by agonist occupancy and effects on coupling of the receptor to the stimulatory guanine. J Biol Chem. 1985;260(11):7094–101.

103. Namkung Y, Sibley DR. Protein kinase C mediates phosphorylation, desensitization, and trafficking of the D2dopamine receptor. J Biol Chem. 2004;279(47):49533–41.

104. Hicke L, Riezman H. Ubiquitination of a yeast plasma membrane receptor signals its ligand-stimulated endocytosis. Cell. 1996;84(2):277–87.

105. Marchese A, Benovic JL. Agonist-promoted Ubiquitination of the G Protein-coupled Receptor CXCR4 Mediates Lysosomal Sorting. J Biol Chem. 2001;276(49):45509–12.

106. Morris AJ, Malbon CC. Physiological regulation of G protein-linked signaling. Physiol Rev. 1999;79(4):1373–430.

107. Naviglio S, Pagano M, Romano M, Sorrentino A, Fusco A, Illiano F, et al. Adenylate cyclase regulation via proteasome-mediated modulation of Gαslevels. Cell Signal. 2004;16(11):1229–37.

108. Tang T, Gao MH, Miyanohara A, Hammond HK. Gαq reduces cAMP production by decreasing Gαs protein abundance. Biochem Biophys Res Commun. 2008;377(2):679–84.

109. Nagai Y, Nishimura A, Tago K, Mizuno N, Itoh H. Ric-8B stabilizes the alpha subunit of stimulatory G protein by inhibiting its ubiquitination. J Biol Chem. 2010

Apr 9;285(15):11114–20.

110. Hollinger S, Hepler JR. Cellular regulation of RGS proteins: modulators and integrators of G protein signaling. Pharmacol Rev. 2002;54(3):527–59.

111. Cunningham ML, Waldo GL, Hollinger S, Hepler JR, Harden TK. Protein Kinase C Phosphorylates RGS2 and Modulates Its Capacity for Negative Regulation of Gα11 Signaling. J Biol Chem. 2001;276(8):5438–44.

112. Chen C, Wang H, Fong CW, Lin SC. Multiple phosphorylation sites in RGS16 differentially modulate its GAP activity. FEBS Lett. 2001;504(1–2):16–22.

113. Ogier-Denis E, Pattingre S, El Benna J, Codogno P. Erk1/2-dependent phosphorylation of Gα-interacting protein stimulates its GTPase accelerating activity and autophagy in human colon cancer cells. J Biol Chem. 2000;275(50):39090–5.

114. Karathia H, Vilaprinyo E, Sorribas A, Alves R. Saccharomyces cerevisiae as a model organism: a comparative study. PLoS One. 2011 Feb 2;6(2):e16015.

115. Wang Y, Chen W, Simpson DM, Elion EA. Cdc24 regulates nuclear shuttling and recruitment of the Ste5 scaffold to a heterotrimeric G protein in Saccharomyces cerevisiae. J Biol Chem. 2005;280(13):13084–96.

116. Coyle SM, Flores J, Lim WA. Exploitation of latent allostery enables the evolution of new modes of MAP kinase regulation. Cell. 2013 Aug 15;154(4):875–87.

117. Shellhammer JP, Morin-Kensicki E, Matson JP, Yin G, Isom DG, Campbell SL, et al. Amino acid metabolites that regulate G protein signaling during osmotic stress. PLoS Genet. 2017;13(5):1–23.

118. Nagiec MJ, Dohlman HG. Checkpoints in a yeast differentiation pathway coordinate signaling during hyperosmotic stress. PLoS Genet. 2012;8(1):e1002437.

119. Hao N, Zeng Y, Elston TC, Dohlman HG. Control of MAPK specificity by feedback

phosphorylation of shared adaptor protein Ste50. J Biol Chem. 2008;283(49):33798–802.

120. Mohammadi S, Saberidokht B, Subramaniam S, Grama A. Scope and limitations of yeast as a model organism for studying human tissue-specific pathways. BMC Syst Biol. 2015;9(1).

121. Dohlman HG, Thorner JW. R EGULATION OF G PROTEIN – INITIATED SIGNAL TRANSDUCTION IN YEAST. Cell. 2001;

122. Bardwell L. A walk-through of the yeast mating pheromone response pathway. Peptides. 2004;25(9):1465–76.

123. Butty AA, Pryciak PM, Huang LS, Herskowitz I, Peter M. The Role of Far1p in linking the heterotrimeric G protein to polarity establishment proteins during yeast mating. Science (80-). 1998;282:1511–6.

124. Nern A, Arkowitz RA. A Cdc24p-Far1p-Gbetagamma protein complex required for yeast orientation during mating. J Cell Biol. 1999 Mar 22;144(6):1187–202.

125. Blondel M, Galan JM, Chi Y, Lafourcade C, Longaretti C, Deshaies RJ, et al. Nuclear-specific degradation of Far1 is controlled by the localization of the F-box protein Cdc4. EMBO J. 2000;19(22):6085–97.

126. Nern a, Arkowitz R a. Nucleocytoplasmic Shuttling of the Cdc42p Exchange\rFactor Cdc24p. 2000;148(6):1115–22.

127. Shimada Y, Gulli MP, Peter M. Nuclear sequestration of the exchange factor Cdc24 by Far1 regulates cell polarity during yeast mating. Nat Cell Biol. 2000 Feb;2(2):117–24.

128. Ash J, Wu C, Larocque R, Jamal M, Stevens W, Osborne M, et al. Genetic analysis of the interface between Cdc42p and the CRIB domain of Ste20p in Saccharomyces cerevisiae. Genetics. 2003;163(1):9–20.

129. Leberer E, Dignard D, Harcus D, Thomas DY, Whiteway M. The protein kinase

homologue Ste20p is required to link the yeast pheromone response G-protein beta gamma subunits to downstream signalling components. EMBO J. 1992 Dec;11(13):4815–24.

130. Leeuw T, Wu C, Schrag JD, Whiteway M, Thomas DY. Interaction of a G protein beta subunit with a conserved sequence in Ste20/PAK family protein kinases. Nature. 1998;4:191–5.

131. Mahanty SK, Wang Y, Farley FW, Elion EA. Nuclear shuttling of yeast scaffold Ste5 is required for its recruitment to the plasma membrane and activation of the mating MAPK cascade. Cell. 1999;98(4):501–12.

132. Garrenton LS, Braunwarth A, Irniger S, Hurt E, Künzler M, Thorner J. Nucleus-specific and cell cycle-regulated degradation of mitogen-activated protein kinase scaffold protein Ste5 contributes to the control of signaling competence. Mol Cell Biol. 2009;29(2):582–601.

133. Hu Z, Wang Y, Yu L, Mahanty SK, Mendoza N, Elion EA. Mapping regions in Ste5 that support Msn5-dependent and -independent nuclear export. Biochem Cell Biol. 2016;94(2):109–28.

134. Winters MJ, Lamson RE, Nakanishi H, Neiman AM, Pryciak PM. A membrane binding domain in the ste5 scaffold synergizes with gbetagamma binding to control localization and signaling in pheromone response. Mol Cell. 2005 Oct 7;20(1):21–32.

135. Pryciak PM, Huntress FA. Membrane recruitment of the kinase cascade scaffold protein Ste5 by the Gbetagamma complex underlies activation of the yeast pheromone response pathway. Genes Dev. 1998 Sep 1;12(17):2684–97.

136. Garrenton LS, Young SL, Thorner J. Function of the MAPK scaffold protein, Ste5, requires a cryptic PH domain. Genes Dev. 2006;20(14):1946–58.

137. Elion EA, Satterberg B, Kranz JE. FUS3 phosphorylates multiple components of

the mating signal transduction cascade: evidence for STE12 and FAR1. Mol Biol Cell. 1993;4(5):495–510.

138. Pope PA, Bhaduri S, Pryciak PM. Regulation of cyclin-substrate docking by a G1 arrest signaling pathway and the Cdk inhibitor far1. Curr Biol. 2014;24(12):1390–6.

139. Mckinney JD, Cross FR. Far1 and the G1 phase specificity of cell-cycle arrest by mating factor in Saccharomyces cerevisiae. Mol Cell Biol. 1995;15(N5):2509–16.

140. Manney TR. Expression of the BAR1 gene in Saccharomyces cerevisiae: induction by the alpha mating pheromone of an activity associated with a secreted protein. J Bacteriol. 1983 Jul;155(1):291–301.

141. MacKay VL, Welch SK, Insley MY, Manney TR, Holly J, Saari GC, et al. The Saccharomyces cerevisiae BAR1 gene encodes an exported protein with homology to pepsin. Proc Natl Acad Sci U S A. 1988 Jan;85(1):55–9.

142. Feng Y, Davis NG. Akr1p and the type I casein kinases act prior to the ubiquitination step of yeast endocytosis: Akr1p is required for kinase localization to the plasma membrane. Mol Cell Biol. 2000;20(14):5350–9.

143. Hicke L, Zanolari B, Riezman H. Cytoplasmic tail phosphorylation of the alpha-factor receptor is required for its ubiquitination and internalization. J Cell Biol. 1998 Apr 20;141(2):349–58.

144. Smith GR, Givan SA, Cullen P, Sprague GF. GTPase-activating proteins for Cdc42. Eukaryot Cell. 2002;1(3):469–80.

145. Zhan XL, Deschenes RJ, Guan KL. Differential regulation of FUS3 MAP kinase by tyrosine-specific phosphatases PTP2/PTP3 and dual-specificity phosphatase MSG5 in Saccharomyces cerevisiae. Genes Dev. 1997 Jul 1;11(13):1690–702.

146. Doi K, Gartner A, Ammerer G, Errede B, Shinkawa H, Sugimoto K, et al. MSG5, a novel protein phosphatase promotes adaptation to pheromone response in S.

cerevisiae. EMBO J. 1994 Jan 1;13(1):61–70.

147. Bhattacharyya RP, Reményi A, Good MC, Bashor CJ, Falick AM, Lim WA. The Ste5 scaffold allosterically modulates signaling output of the yeast mating pathway. Science. 2006;311(5762):822–6.

148. Good M, Tang G, Singleton J, Remenyi A, Lim WA. Scaffold-Assisted Catalysis: A Novel Domain In the Ste5 Scaffold Protein is Required to Unlock the MAPK Fus3 for Phosphorylation by the MAPKK Ste7. Cell. 2009;136(6):1085–97.

149. Malleshaiah MK, Shahrezaei V, Swain PS, Michnick SW. The scaffold protein Ste5 directly controls a switch-like mating decision in yeast. Nature. 2010;465(7294):101–5.

150. Zalatan JG, Coyle SM, Rajan S, Sidhu SS, Lim WA. Conformational control of the Ste5 scaffold protein insulates against MAP kinase misactivation. Science. 2012 Sep;337(6099):1218–22.

151. Takahashi S, Pryciak PM. Membrane localization of scaffold proteins promotes graded signaling in the yeast MAP kinase cascade. Curr Biol. 2008 Aug 26;18(16):1184–91.

152. Wu C, Leeuw T, Leberer E, Thomas DY, Whiteway M. Cell cycle- and Cln2p-Cdc28p-dependent phosphorylation of the yeast Ste20p protein kinase. J Biol Chem. 1998;273(43):28107–15.

153. McKinney JD, Chang F, Heintz N, Cross FR. Negative regulation of FAR1 at the Start of the cell cycle. Genes Dev. 1993;7:833–43.

154. Chen RE, Thorner J. Function and regulation in MAPK signaling pathways: lessons learned from the yeast Saccharomyces cerevisiae. Biochim Biophys Acta. 2007 Aug;1773(8):1311–40.

155. Reed RH, Chudek JA, Foster R, Gadd GM. Osmotic significance of glycerol accumulation in exponentially growing yeasts. Appl Environ Microbiol.

1987;53(9):2119–23.

156. Dihazi H, Kessler R, Eschrich K. High osmolarity glycerol (HOG) pathway-induced phosphorylation and activation of 6-phosphofructo-2-kinase are essential for glycerol accumulation and yeast cell proliferation under hyperosmotic stress. J Biol Chem. 2004;279(23):23961–8.

157. Cullen PJ, Sprague GF. Glucose depletion causes haploid invasive growth in yeast. Proc Natl Acad Sci U S A. 2000;97(25):13619–24.

158. Strickfaden SC, Winters MJ, Ben-Ari G, Lamson RE, Tyers M, Pryciak PM. A mechanism for cell-cycle regulation of MAP kinase signaling in a yeast differentiation pathway. Cell. 2007 Feb 9;128(3):519–31.

159. Oehlen LJWM, Cross FR. G1 cyclins CLN1 and CLN2 repress the mating factor response pathway at start in the yeast cell cycle. Genes Dev. 1994;8(9):1058–70.

160. Dewhurst HM, Choudhury S, Torres MP. Structural Analysis of PTM Hotspots (SAPH-ire) - A quantitative informatics method enabling the discovery of novel regulatory elements in protein families. Mol Cell Proteomics. 2015;14(8).

161. Muntz KH, Sternweis PC, Gilman AG, Mumby SM. Influence of gamma subunit prenylation on association of guanine nucleotide-binding regulatory proteins with membranes. Mol Biol Cell. 1992;3(1):49–61.

162. Cook LA, Schey KL, Wilcox MD, Dingus J, Hildebrandt JD. Heterogeneous processing of a G protein gamma subunit at a site critical for protein and membrane interactions. Biochemistry. 1998;37(35):12280–6.

163. Li E, Cismowski MJ, Stone DE. Phosphorylation of the pheromone-responsive Gbeta protein of Saccharomyces cerevisiae does not affect its mating-specific signaling function. Mol Gen Genet. 1998;258(6):608–18.

164. Wang Y, Dohlman HG. Pheromone-dependent ubiquitination of the mitogen-activated protein kinase kinase Ste7. J Biol Chem. 2002 May;277(18):15766–72.

165. Wettschureck N, Offermanns S. Mammalian G Proteins and Their Cell Type Specific Functions. Physilological Rev. 2005;85 (4):1159–204.

166. Rockman HA, Koch WJ, Lefkowitz RJ. Seven-transmembrane-spanning receptors and heart function. Nature. 2002;415(6868):206–12.

167. Kaul M, Garden GA, Lipton SA. Pathways to neuronal injury and apoptosis in HIV-associated dementia. Nature. 2001;410(6831):988–94.

168. Fan W, Boston BA, Kesterson RA, Hruby VJ, Cone RD. Role of melanocortinergic neurons in feeding and the agouti obesity syndrome. Nature. 1997;385(6612):165–8.

169. Rosenbaum DM, Rasmussen SGF, Kobilka BK. The structure and function of G-protein-coupled receptors. Nature. 2009;459(7245):356–63.

170. Bargmann CI. Comparative chemosensation from receptors to ecology. Nature. 2006;444(7117):295–301.

171. Hauser AS, Attwood MM, Rask-Andersen M, Schiöth HB, Gloriam DE. Trends in GPCR drug discovery: new agents, targets and indications. Nat Rev Drug Discov. 2017 Dec;16(12):829–42.

172. Dohlman H. Model systems for the study of seven-transmembrane-segment receptors. Annu Rev Biochem. 1991;60(1):653–88.

173. Dohlman HG, Thorner JW. Regulation of G-protein initiated signal transduction in yeast: paradigms and principles. Annu Rev Biochem. 2001;70:703–54.

174. Wang Y, Marotti LA, Lee MJ, Dohlman HG. Differential regulation of G protein α subunit trafficking by mono- and polyubiquitination. J Biol Chem. 2005;280(1):284–91.

175. Clement ST, Dixit G, Dohlman HG. Regulation of yeast G protein signaling by the kinases that activate the AMPK homolog Snf1. Sci Signal. 2013;6(291):ra78-ra78.

176. Cappell SD, Baker R, Skowyra D, Dohlman HG. Systematic analysis of essential

genes reveals important regulators of G protein signaling. Mol Cell. 2010;38(5):746–57.

177. Li E, Cismowski MJ, Stone DE. Phosphorylation of the pheromone-responsive Gbeta protein of Saccharomyces cerevisiae does not affect its mating-specific signaling function. Mol Gen Genet. 1998 Jun;258(6):608–18.

178. Deflorio R, Brett M-E, Waszczak N, Apollinari E, Metodiev M V, Dubrovskyi O, et al. Phosphorylation of Gβ is crucial for efficient chemotropism in yeast. J Cell Sci. 2013;126(14):2997–3009.

179. Stone DE, Cole GM, de Barros Lopes M, Goebl M, Reed SI. N-myristoylation is required for function of the pheromone-responsive G alpha protein of yeast: conditional activation of the pheromone response by a temperature-sensitive N-myristoyl transferase. Genes Dev. 1991;5(11):1969–81.

180. Dohlman HG, Thorner JW. Regulation of G protein-initiated signal transduction in yeast: paradigms and principles. Annu Rev Biochem. 2001;70:703–54.

181. Sprang SR. G protein mechanisms: insights from structural analysis. Annu Rev Biochem. 1997;66:639–78.

182. Nern A, Arkowitz RA. A Cdc24p-Far1p-Gbetagamma protein complex required for yeast orientation during mating. J Cell Biol. 1999;144(6):1187–202.

183. Arkowitz R a. Chemical gradients and chemotropism in yeast. Cold Spring Harb Perspect Biol. 2009;1(2).

184. van Drogen F, Stucke VM, Jorritsma G, Peter M. MAP kinase dynamics in response to pheromones in budding yeast. Nat Cell Biol. 2001;3:1051–9.

185. Good M, Tang G, Singleton J, Remenyi A, Lim WA. The Ste5 Scaffold Directs Mating Signaling by Catalytically Unlocking the Fus3 MAP Kinase for Activation. Cell. 2009;136(6):1085–97.

186. Morishita R, Nakayama H, Isobe T, Matsuda T, Hashimoto Y, Okano T, et al.

Primary structure of a gamma subunit of G protein, gamma 12, and its phosphorylation by protein kinase C. J Biol Chem. 1995 Dec;270(49):29469–75.

187. Yasuda H, Lindorfer MA, Myung CS, Garrison JC. Phosphorylation of the G protein gamma12 subunit regulates effector specificity. J Biol Chem. 1998 Aug 21;273(34):21958–65.

188. Dewhurst HM, Choudhury S, Torres MP. Structural Analysis of PTM Hotspots (SAPH-ire) – A Quantitative Informatics Method Enabling the Discovery of Novel Regulatory Elements in Protein Families. Mol Cell Proteomics. 2015;14(8):2285–97.

189. Soufi B, Kelstrup CD, Stoehr G, Fröhlich F, Walther TC, Olsen J V. Global analysis of the yeast osmotic stress response by quantitative proteomics. Mol Biosyst. 2009;5(11):1337–46.

190. Hao N, Nayak S, Behar M, Shanks RH, Nagiec MJ, Errede B, et al. Regulation of cell signaling dynamics by the protein kinase-scaffold Ste5. Mol Cell. 2008 Jun;30(5):649–56.

191. Yu RC, Pesce CG, Colman-Lerner A, Lok L, Pincus D, Serra E, et al. Supplementary- Negative feedback that improves information transmission in yeast signalling. Nature. 2008 Dec 11;456(7223):755–61.

192. Inouye C, Dhillon N, Durfee T, Zambryski PC, Thorner J. Mutational analysis of STE5 in the yeast Saccharomyces cerevisiae: Application of a differential interaction trap assay for examining protein- protein interactions. Genetics. 1997;147(2):479–92.

193. Dowell SJ, Bishop a L, Dyos SL, Brown AJ, Whiteway MS. Mapping of a yeast G protein betagamma signaling interaction. Genetics. 1998 Dec;150(4):1407–17.

194. Strickfaden SC, Winters MJ, Ben-Ari G, Lamson RE, Tyers M, Pryciak PM. A mechanism for cell-cycle regulation of MAP kinase signaling in a yeast

differentiation pathway. Cell. 2007;128(3):519–31.

195. Maeder CI, Hink M a, Kinkhabwala A, Mayr R, Bastiaens PIH, Knop M. Spatial regulation of Fus3 MAP kinase activity through a reaction-diffusion mechanism in yeast pheromone signalling. Nat Cell Biol. 2007 Nov;9(11):1319–26.

196. Yu L, Qi M, Sheff MA, Elion EA. Counteractive control of polarized morphogenesis during mating by mitogen-activated protein kinase Fus3 and G1 cyclin-dependent kinase. Mol Biol Cell. 2008 Apr;19(4):1739–52.

197. Nagiec MJ, McCarter PC, Kelley JB, Dixit G, Elston TC, Dohlman HG. Signal inhibition by a dynamically regulated pool of monophosphorylated MAPK. Mol Biol Cell. 2015;26(18):3359–71.

198. Zhan X, Deschenes RJ, Kun-liang G. Differential regulation of FUS3 MAP kinase by tyrosine-specificphosphatases in Saccharomyces cerevisiae. 1997;1690–702.

199. Storici F, Resnick M a. The delitto perfetto approach to in vivo site-directed mutagenesis and chromosome rearrangements with synthetic oligonucleotides in yeast. Methods Enzymol. 2006 Jan;409(1976):329–45.

200. Robinson LC, Menold MM, Garrett S, Culbertson MR. Casein kinase I-like protein kinases encoded by YCK1 and YCK2 are required for yeast morphogenesis. Mol Cell Biol. 1993;13(5):2870–81.

201. Lee MJ, Dohlman HG. Coactivation of G Protein Signaling by Cell-Surface Receptors and an Intracellular Exchange Factor. Curr Biol. 2008;18:211–5.

202. Schindelin J, Rueden CT, Hiner MC, Eliceiri KW. The ImageJ ecosystem: An open platform for biomedical image analysis. Mol Reprod Dev. 2015;82(7–8):518–529.

203. Edgar RC. MUSCLE: a multiple sequence alignment method with reduced time and space complexity. BMC Bioinformatics. 2004 Aug;5:113.

204. Okonechnikov K, Golosova O, Fursov M. Unipro UGENE: a unified bioinformatics

toolkit. Bioinformatics. 2012 Apr;28(8):1166–7.

205. Choudhury S, Baradaran-Mashinchi P, Torres MP. Negative Feedback Phosphorylation of Gγ Subunit Ste18 and the Ste5 Scaffold Synergistically Regulates MAPK Activation in Yeast. Cell Rep. 2018;

206. Schnabel P, Bohm M. Heterotrimeric G proteins in heart disease. Cell Signal. 1996;8(6):413–23.

207. Hamm HE. The many faces of G protein signaling. J Biol Chem. 1998;(21):5–8.

208. Dohlman HG, Thorner J. RGS proteins and signalling by heterotrimeric G proteins. J Biol Chem. 1997;272:3871–4.

209. Hepler JR. RGS protein and G protein interactions: a little help from their friends. Mol Pharmacol. 2003;64(3):547–9.

210. Hsueh RC, Natarajan M, Fraser I, Pond B, Liu J, Mumby S, et al. Deciphering signaling outcomes from a system of complex networks. Sci Signal. 2009 May 19;2(71):ra22.

211. Janes KA, Gaudet S, Albeck JG, Nielsen UB, Lauffenburger DA, Sorger PK. The Response of Human Epithelial Cells to TNF Involves an Inducible Autocrine Cascade. Cell. 2006;124(6):1225–39.

212. Natarajan M, Lin KM, Hsueh RC, Sternweis PC, Ranganathan R. A global analysis of cross-talk in a mammalian cellular signalling network. Nat Cell Biol. 2006;8(6):571–80.

213. Godoy J a, Rios J a, Zolezzi JM, Braidy N, Inestrosa NC. Signaling pathway cross talk in Alzheimer's disease. Cell Commun Signal. 2014;12:23.

214. Liu ZP, Wang Y, Zhang XS, Chen L. Identifying dysfunctional crosstalk of pathways in various regions of Alzheimer's disease brains. BMC Syst Biol. 2010;4(SUPPL. 2).

215. Thomas SM, Bhola NE, Zhang Q, Contrucci SC, Wentzel AL, Freilino ML, et al.

Cross-talk between G protein-coupled receptor and epidermal growth factor receptor signaling pathways contributes to growth and invasion of head and neck squamous cell carcinoma. Cancer Res. 2006;66(24):11831–9.

216. Almela P, García-Carmona JA, Martínez-Laorden E, Milanés MV, Laorden ML. Crosstalk between G protein-coupled receptors (GPCRs) and tyrosine kinase receptor (TXR) in the heart after morphine withdrawal. Front Pharmacol. 2013;4 DEC(December):1–13.

217. Jenie RI, Nishimura M, Fujino M, Nakaya M, Mizuno N, Tago K, et al. Increased ubiquitination and the crosstalk of G protein signaling in cardiac myocytes: Involvement of Ric-8B in Gs suppression by Gq signal. Genes to Cells. 2013;18(12):1095–106.

218. Peter M, Gartner A, Horecka J, Ammerer G, Herskowitz I. FAR1 links the signal transduction pathway to the cell cycle machinery in yeast. Cell. 1993;73(4):747–60.

219. Wu C, Leeuw T, Leberer E, Thomas DY, Whiteway M. Cell cycle- and Cln2p-Cdc28p-dependent phosphorylation of the yeast Ste20p protein kinase. J Biol Chem. 1998;273(43):28107–15.

220. Chol K-Y, Satterberg B, Lyons DM, Elion EA. Ste5 tethers multiple protein kinases in the MAP kinase cascade required for mating in S. cerevisiae. Cell. 1994;78(3):499–512.

221. Whiteway MS, Wu C, Leeuw T, Clark K, Fourest-Lieuvin A, Thomas DY, et al. Association of the yeast pheromone response G protein beta gamma subunits with the MAP kinase scaffold Ste5p. Science (80-). 1995;269(5230):1572–5.

222. Tedford K, Kim S, Sa D, Stevens K, Tyers M. Regulation of the mating pheromone and invasive growth responses in yeast by two MAP kinase substrates. Curr Biol. 1997;7(4):228–38.

223. Oehlen LJWM, Cross FR. Potential regulation of Ste20 function by the Cln1-Cdc28 and Cln2-Cdc28 cyclin-dependent protein kinases. J Biol Chem. 1998;273(39):25089–97.

224. Fung BKK, Nash CR. Characterization of transducin from bovine retinal rod outer segments. J Biol Chem. 1983;258(17):10503–10.

225. Gilman A. G Proteins: Transducers Of Receptor-Generated Signals. Annu Rev Biochem. 1987;56(1):615–49.

226. Lochrie MA, Simon MI. G protein multiplicity in eukaryotic signal transduction systems. Biochemistry. 1988;27(14):4957–65.

227. Clapham DE, Neer EJ. G Protein Bγ Subunits. Annu Rev Pharmacol Toxicol. 1997;167–203.

228. Clapham DE, Neer EJ. G PROTEIN $β$$γ$ SUBUNITS. 1997;167–203.

229. Clark KL, Dignard D, Thomas DY, Whiteway M, Al CET. Interactions among the subunits of the G Protein involved in Saccharomyces cerevisiae mating. 1993;13(1):1–8.

230. Durán-Avelar MJ, Ongay-Larios L, Zentella-Dehesa a, Coria R. The carboxy-terminal tail of the Ste2 receptor is involved in activation of the G protein in the Saccharomyces cerevisiae alpha-pheromone response pathway. FEMS Microbiol Lett. 2001;197(1):65–71.

231. Feng Y, Song LY, Kincaid E, Mahanty SK, Elion EA. Functional binding between Gbeta and the LIM domain of Ste5 is required to activate the MEKK Ste11. Curr Biol. 1998;8(5):267–78.

232. Simonds WF, Butrynski JE, Gautam N, Unson CG, Spiegel AM. G-protein beta gamma dimers: Membrane targeting requires subunit coexpression and intact gamma C-A-A-X domain. J Biol Chem. 1991;266(9):5363–6.

233. Fukada Y, Matsuda T, Kokame K, Takao T, Shimonishi Y, Akino T, et al. Effects

of carboxyl methylation of photoreceptor G protein gamma-subunit in visual transduction. J Biol Chem. 1994;269(7):5163–70.

234. Lim WK, Myung C-S, Garrison JC, Neubig RR. Receptor−G Protein γ Specificity: γ11 Shows Unique Potency for A 1 Adenosine and 5-HT 1A Receptors. Biochemistry. 2001;40(35):10532–41.

235. Wright PE, Dyson HJ. Intrinsically disordered proteins in cellular signalling and regulation. Nat Rev Mol Cell Biol. 2014;16(1):18–29.

236. Hansen JC, Lu X, Ross ED, Woody RW. Intrinsic protein disorder, amino acid composition, and histone terminal domains. J Biol Chem. 2006;281(4):1853–6.

237. Liggett SB. Phosphorylation barcoding as a mechanism of directing GPCR signaling. Sci Signal. 2011;4(185):pe36.

238. Nishi H, Demir E, Panchenko AR. Crosstalk between signaling pathways provided by single and multiple protein phosphorylation sites. J Mol Biol. 2015;427(2):511–20.

239. Deshaies RJ. Phosphorylation and proteolysis: partners in the regulation of cell division in budding yeast. Curr Opin Genet Dev. 1997;7(1):7–16.

240. Mendenhall MD, Hodge AE. Regulation of Cdc28 cyclin-dependent protein kinase activity during the cell cycle of the yeast Saccharomyces cerevisiae. Microbiol Mol Biol Rev. 1998;62(4):1191–243.

241. Bhaduri S, Pryciak PM. Cyclin-specific docking motifs promote phosphorylation of yeast signaling proteins by G1/S Cdk complexes. Curr Biol. 2011;21(19):1615–23.

242. Uesono Y, Toh-e A. Transient inhibition of translation initiation by osmotic stress. J Biol Chem. 2002;277(16):13848–55.

243. Escoté X, Zapater M, Clotet J, Posas F. Hog1 mediates cell-cycle arrest in G1 phase by the dual targeting of Sic1. Nat Cell Biol. 2004;6(10):997–1002.

244. Clotet J, Escoté X, Adrover MÀ, Yaakov G, Garí E, Aldea M, et al.

Phosphorylation of Hsl1 by Hog1 leads to a G2 arrest essential for cell survival at high osmolarity. EMBO J. 2006;25(11):2338–46.

245. Muzzey D, Gómez-Uribe CA, Mettetal JT, van Oudenaarden A. A systems-level analysis of perfect adaptation in yeast osmoregulation. Cell. 2009;138(1):160–71.

246. Tyers M, Futcher B. Far1 and Fus3 link the mating pheromone signal transduction pathway to three G1-phase Cdc28 kinase complexes. Mol Cell Biol. 1993;13(9):5659–69.

247. Peter M, Gartner A, Horecka J, Ammerer G, Herskowitz I. FAR1 links the signal transduction pathway to the cell cycle machinery in yeast. Cell. 1993;73(4):747–60.

248. Strickfaden SC, Winters MJ, Ben-Ari G, Lamson RE, Tyers M, Pryciak PM. A mechanism for cell-cycle regulation of MAP kinase signaling in a yeast differentiation pathway. Cell. 2007;128(3):519–31.

249. Hao N, Zeng Y, Elston TC, Dohlman HG. Control of MAPK specificity by feedback phosphorylation of shared adaptor protein Ste50. J Biol Chem. 2008;283(49):33798–802.

250. Warmka J, Hanneman J, Lee J, Amin D, Ota I. Ptc1, a Type 2C Ser/Thr Phosphatase, Inactivates the HOG Pathway by Dephosphorylating the Mitogen-Activated Protein Kinase Hog1. Mol Cell Biol. 2001;21(1):51–60.

251. Bhaduri S, Pryciak PM. Cyclin-Specific Docking Motifs Promote Phosphorylation of Yeast Signaling Proteins by G1/S Cdk Complexes. Curr Biol. 2011;21(19):1615–23.

252. Lobanova ES, Finkelstein S, Herrmann R, Chen Y, Michaud NA, Trieu LH, et al. Transducin gamma-subunit sets expression levels of alpha- and beta-subunits and is crucial for rod viability. J Neurosci. 2009;28(13):3510–20.

253. Varga E V, Hosohata K, Borys D, Navratilova E, Nylen A, Vanderah TW, et al.

Antinociception depends on the presence of G protein gamma2-subunits in brain. Eur J Pharmacol. 2005;508(1–3):93–8.

254. Yajima I, Kumasaka MY, Yamanoshita O, Zou C, Li X, Ohgami N, et al. GNG2 inhibits invasion of human malignant melanoma cells with decreased FAK activity. Am J Cancer Res. 2014;4(2):182–8.

255. Ohta M, Mimori K, Fukuyoshi Y, Kita Y, Motoyama K, Yamashita K, et al. Clinical significance of the reduced expression of G protein gamma 7 (GNG7) in oesophageal cancer. Br J Cancer. 2008;98(2):410–7.

256. Torres MP, Clement ST, Cappell SD, Dohlman HG. Cell cycle-dependent phosphorylation and ubiquitination of a G protein alpha subunit. J Biol Chem. 2011;286(23):20208–16.

257. Lee MJ, Dohlman HG. Co-activation of G-Protein Signaling by Cell-Surface Receptors and an Intracellular Exchange-Factor. Curr Biol. 2008;18(3):211–5.

258. McCudden CR, Hains MD, Kimple RJ, Siderovski DP, Willard FS. G-protein signaling: Back to the future. Cell Mol Life Sci. 2005;62(5):551–77.

259. Spiegel AM. Defects in G protein-coupled signal transduction in human disease. Annu Rev Physiol. 1996;58:143–70.

260. Spiegel AM, Weinstein LS. Inherited diseases involving G proteins and G protein-coupled receptors. Annu Rev Med. 2004;55(2):27–39.

261. Deflorio R, Brett M-E, Waszczak N, Apollinari E, Metodiev M V, Dubrovskyi O, et al. Phosphorylation of Gβ is crucial for efficient chemotropism in yeast. J Cell Sci. 2013;126(Pt 14):2997–3009.

262. Burack WR, Shaw AS. Signal transduction: Hanging on a scaffold. Curr Opin Cell Biol. 2000;12(2):211–6.

263. Zalatan JG, Coyle SM, Rajan S, Sidhu SS, Lim WA. Conformational Control of the Ste5 Scaffold Protein Insulates Against MAP Kinase Misactivation. Science (80-).

2012;337(6099):1218–22.

264. Reményi A, Good MC, Bhattacharyya RP, Lim WA. The role of docking interactions in mediating signaling input, output, and discrimination in the yeast MAPK network. Mol Cell. 2005;20(6):951–62.

265. Inouye C. Ste5 RING-H2 Domain: Role in Ste4-Promoted Oligomerization for Yeast Pheromone Signaling. Science (80-). 1997;278(5335):103–6.

266. Mahanty SK, Wang Y, Farley FW, Elion EA. Nuclear shuttling of yeast scaffold Ste5 is required for its recruitment to the plasma membrane and activation of the mating MAPK cascade. Cell. 1999;98(4):501–12.

267. van Drogen F, Stucke VM, Jorritsma G, Peter M. MAP kinase dynamics in response to pheromones in budding yeast. Nat Cell Biol. 2001;3:1051–9.

268. Nagiec MJ, McCarter PC, Kelley JB, Dixit G, Elston TC, Dohlman HG. Signal inhibition by a dynamically regulated pool of monophosphorylated MAPK. Mol Biol Cell. 2015;26(18):3359–71.

269. New DC, Wong YH. Molecular mechanisms mediating the G protein-coupled receptor regulation of cell cycle progression. J Mol Signal. 2007;2:2.

270. Garrenton LS, Braunwarth A, Irniger S, Hurt E, Künzler M, Thorner J. Nucleus-specific and cell cycle-regulated degradation of mitogen-activated protein kinase scaffold protein Ste5 contributes to the control of signaling competence. Mol Cell Biol. 2009;29(2):582–601.

271. Westfall PJ, Patterson JC, Chen RE, Thorner J. Stress resistance and signal fidelity independent of nuclear MAPK function. 2008;2008.

272. Rourke SMO, Herskowitz I. The Hog1 MAPK prevents cross talk between the HOG and pheromone response MAPK pathways in Saccharomyces cerevisiae The Hog1 MAPK prevents cross talk between the HOG and pheromone response MAPK pathways in Saccharomyces cerevisiae. Genes Dev. 1998;12:2874–86.

273. Wassmann K, Ammerer G. Overexpression of the G1-cyclin gene CLN2 represses the mating pathway in Saccharomyces cerevisiae at the level of the MEKK Ste11. J Biol Chem. 1997;272(20):13180–8.

274. Hall JP, Cherkasova V, Elion E, Gustin MC, Winter E. The osmoregulatory pathway represses mating pathway activity in Saccharomyces cerevisiae: isolation of a FUS3 mutant that is insensitive to the repression mechanism. Mol Cell Biol. 1996;16(12):6715–23.

275. Smrcka a. V. G protein βγ subunits: central mediators of G protein-coupled receptor signaling. Cell Mol Life Sci. 2008 Jul;65(14):2191–214.

276. McCudden CR, Hains MD, Kimple RJ, Siderovski DP, Willard FS. G-protein signaling: Back to the future. Cell Mol Life Sci. 2005;62(5):551–77.

277. Robillard L, Ethier N, Lachance M, Hébert TE. Gβγ subunit combinations differentially modulate receptor and effector coupling in vivo. Cell Signal. 2000;12(9–10):673–82.

278. Schmidt CJ, Thomas TC, Levine MA, Neer EJ. Specificity of G protein beta and gamma subunit interactions. J Biol Chem. 1992;267(20):13807–10.

279. Bonacci TM, Ghosh M, Malik S, Smrcka A V. Regulatory interactions between the amino terminus of G-protein betagamma subunits and the catalytic domain of phospholipase Cbeta2. J Biol Chem. 2005 Mar 18;280(11):10174–81.

280. Yan K, Gautam N. A domain on the G protein beta subunit interacts with both adenylyl cyclase 2 and the muscarinic\ratrial potassium channel. J Biol Chem. 1996;271(20):17597–600.

281. Herskowitz JH, Seyfried NT, Duong DM, Xia Q, Rees HD, Gearing M, et al. Phosphoproteomic analysis reveals site-specific changes in GFAP and NDRG2 phosphorylation in frontotemporal lobar degeneration. J Proteome Res. 2010 Dec 3;9(12):6368–79.

282. Stuart SA, Houel S, Lee T, Wang N, Old WM, Ahn NG. A Phosphoproteomic Comparison of B-RAF V600E and MKK1/2 Inhibitors in Melanoma Cells. Mol Cell Proteomics. 2015;14(6):1599–615.

283. Mertins P, Yang F, Liu T, Mani DR, Petyuk VA, Gillette MA, et al. Ischemia in Tumors Induces Early and Sustained Phosphorylation Changes in Stress Kinase Pathways but Does Not Affect Global Protein Levels. Mol Cell Proteomics. 2014;13(7):1690–704.

284. Mertins P, Mani DR, Ruggles K V, Gillette MA, Clauser KR, Wang P, et al. Proteogenomics connects somatic mutations to signalling in breast cancer. Nature. 2016;534(7605):55–62.

285. Schweppe DK, Rigas JR, Gerber SA. Quantitative Phosphoproteomic Profiling of Human Non-Small Cell Lung Cancer Tumors. J Proteomics. 2014;91:1–21.

286. Britton D, Zen Y, Quaglia A, Selzer S, Mitra V, Löbner C, et al. Quantification of pancreatic cancer proteome and phosphorylome: Indicates molecular events likely contributing to cancer and activity of drug targets. PLoS One. 2014;9(3).

287. Verano-Braga T, Schwämmle V, Sylvester M, Passos-Silva DG, Peluso AAB, Etelvino GM, et al. Time-Resolved quantitative phosphoproteomics: New insights into angiotensin-(1-7) signaling networks in human endothelial cells. J Proteome Res. 2012;11(6):3370–81.

288. Myung C-S, Lim WK, DeFilippo JM, Yasuda H, Neubig RR, Garrison JC. Regions in the G protein gamma subunit important for interaction with receptors and effectors. Mol Pharmacol. 2006;69(3):877–87.

289. Azpiazu I, Gautam N. G Protein γ Subunit Interaction with a Receptor Regulates Receptor-stimulated Nucleotide Exchange. J Biol Chem. 2001;276(45):41742–7.

290. Scott JK, Huang SF, Gangadhar BP, Samoriski GM, Clapp P, Gross RA, et al. Evidence that a protein-protein interaction “hot spot” on heterotrimeric G protein

βγ subunits is used for recognition of a subclass of effectors. EMBO J. 2001;20(4):767–76.

291. Iwami G, Kawabe JI, Ebina T, Cannon PJ, Homcy CJ, Ishikawa Y. Regulation of adenylyl cyclase by protein kinase A. Vol. 270, Journal of Biological Chemistry. 1995. p. 12481–4.

292. Wei J, Wayman G, Storm DR. Phosphorylation and inhibition of type III adenylyl cyclase by calmodulin-dependent protein kinase II in vivo . J Biol Chem. 1996;271(39):24231–5.

293. Johnson H, White FM. Quantitative analysis of signaling networks across differentially embedded tumors highlights interpatient heterogeneity in human glioblastoma. J Proteome Res. 2014 Nov 7;13(11):4581–93.

294. Shen JX, Wachten S, Halls ML, Everett KL, Cooper DMF. Muscarinic receptors stimulate AC2 by novel phosphorylation sites, whereas Gβγ subunits exert opposing effects depending on the G-protein source. Biochem J. 2012;447(3):393–405.

295. Diel S, Klass K, Wittig B, Kleuss C. Gbetagamma activation site in adenylyl cyclase type II. Adenylyl cyclase type III is inhibited by Gbetagamma. J Biol Chem. 2006 Jan 6;281(1):288–94.

296. Esteban V, Heringer-Walther S, Sterner-Kock A, de Bruin R, van den Engel S, Wang Y, et al. Angiotensin-(1-7) and the G protein-coupled receptor Mas are key players in renal inflammation. PLoS One. 2009;4(4).

297. Lothrop AP, Torres MP, Fuchs SM. Deciphering post-translational modification codes. FEBS Lett. 2013;587(8):1247–57.

298. Babu MM. The rules of disorder or why disorder rules. Biophysics (Oxf). 2009;1–10.

299. Cumberworth A, Lamour G, Babu MM, Gsponer J. Promiscuity as a functional

trait: intrinsically disordered regions as central players of interactomes. Biochem J. 2013;454(3):361–9.

300. Orosz F, Ovádi J. Proteins without 3D structure: definition, detection and beyond. Bioinformatics. 2011;27(11):1449–54.

301. Wright PE, Dyson HJ. Intrinsically disordered proteins in cellular signalling and regulation. Nat Rev Mol Cell Biol. 2014;16(1):18–29.

302. Walsh CT, Garneau-Tsodikova S, Gatto GJ. Protein posttranslational modifications: The chemistry of proteome diversifications. Angew Chemie - Int Ed. 2005;44(45):7342–72.

303. Deribe YL, Pawson T, Dikic I. Post-translational modifications in signal integration. Nat Struct Mol Biol. 2010 Jun;17(6):666–72.

304. Lothrop AP, Torres MP, Fuchs SM. Deciphering post-translational modification codes. FEBS Lett. 2013 Feb 10;1–11.

305. Silva AMN, Vitorino R, Domingues MRM, Spickett CM, Domingues P. Post-translational modifications and mass spectrometry detection. Free Radic Biol Med. 2013;65:925–41.

306. Yates JR, Ruse CI, Nakorchevsky A. Proteomics by mass spectrometry: approaches, advances, and applications. Annu Rev Biomed Eng. 2009 Jan;11:49–79.

307. Witze E, Old W, Resing K, Ahn N. Mapping protein post-translational modifications with mass spectrometry. Nat Methods. 2007;4(10).

308. Swaney DL, Villén J. Proteomic analysis of protein posttranslational modifications by mass spectrometry. Cold Spring Harb Protoc. 2016;2016(3):207–9.

309. Shevchenko A, Tomas H, Havlis J, Olsen J V, Mann M. In-gel digestion for mass spectrometric characterization of proteins and proteomes. Nat Protoc. 2006 Jan;1(6):2856–60.

310. Wang S, Wang Y. Peptidylarginine deiminases in citrullination, gene regulation, health and pathogenesis. Biochim Biophys Acta. 2013 Oct;1829(10):1126–35.

311. Bicker KL, Thompson PR. The protein arginine deiminases: Structure, function, inhibition, and disease. Biopolymers. 2013 Feb;99(2):155–63.

312. Venrooij WJ Van. How citrullination invaded rheumatoid arthritis. 2014;1–5.

313. Hynes RO, Yamada KM. Fibronectins: Multifunctional modular glycoproteins. J Cell Biol. 1982;95(2):369–77.

314. Pankov R, Kenneth M. Fibronectin at a glance. 2002;3861–3.

315. Proctor RA. Fibronectin: a brief overview of its structure, function, and physiology. Rev Infect Dis. 2018;9 Suppl 4(May):S317-21.

316. Maurer LM, Ma W, Mosher DF. Dynamic structure of plasma fibronectin. Crit Rev Biochem Mol Biol. 2016;51(4):213–27.

317. Pierschbacher MD, Ruoslahti E, Sundelin J, Lind P, Peterson PA. The cell attachment domain of fibronectin. Determination of the primary structure. J Biol Chem. 1982;257(16):9593–7.

318. Wierzbicka-Patynowski I. The ins and outs of fibronectin matrix assembly. J Cell Sci. 2003;116(16):3269–76.

319. Millard CJ, College L. Structural and functional characterisation of the collagen binding domain of fibronectin. 2007;

320. van der Walle CF, Altroff H, Mardon HJ. Novel mutant human fibronectin FIII9-10 domain pair with increased conformational stability and biological activity. Protein Eng. 2002;15(12):1021–4.

321. Redick SD, Settles DL, Briscoe G, Erickson HP. Defining Fibronectin's cell adhesion synergy site by site-directed mutagenesis. J Cell Biol. 2000;149(2):521–7.

322. Luban S, Li Z. Citrullinated peptide and its relevance to rheumatoid arthritis : an

update. 2010;284–7.

323. Kimura E, Kanzaki T, Tahara K, Hayashi H, Suzuki A, Yamada R, et al. Identification of citrullinated cellular fibronectin in synovial fluid from patients with rheumatoid arthritis Identifi cation of citrullinated cellular fi bronectin in synovial fl uid from patients with rheumatoid arthritis. 2014;7595(September 2017).

324. Chang X, Yamada R, Suzuki A, Kochi Y, Sawada T, Yamamoto K. Citrullination of fibronectin in rheumatoid arthritis synovial tissue. 2017;(May 2005):1374–82.

325. Kristensen JH, Karsdal MA, Genovese F, Johnson S, Svensson B, Jacobsen S, et al. The role of extracellular matrix quality in pulmonary fibrosis. Respiration. 2014;88(6):487–99.

326. Bawadekar M, Gendron-Fitzpatrick A, Rebernick R, Shim D, Warner TF, Nicholas AP, et al. Tumor necrosis factor alpha, citrullination, and peptidylarginine deiminase 4 in lung and joint inflammation. Arthritis Res Ther. 2016;18(1):1–9.

327. Jiang Z, Cui Y, Wang L, Zhao Y, Yan S, Chang X. Investigating citrullinated proteins in tumour cell lines. World J Surg Oncol. 2013;11(1):1.

328. Sipilä KH, Ranga V, Rappu P, Mali M, Pirilä L, Heino I, et al. Joint inflammation related citrullination of functional arginines in extracellular proteins. Sci Rep. 2017;7(1):1–12.

329. van Beers JJBC, Willemze A, Stammen-Vogelzangs J, Drijfhout JW, Toes REM, M Pruijn GJ. Anti-citrullinated fibronectin antibodies in rheumatoid arthritis are associated with human leukocyte antigen-DRB1 shared epitope alleles. Arthritis Res Ther. 2012;14(1):R35.

330. Plow EF, Haas TA, Zhang L, Loftus J, Smith JW. Ligand binding to integrins. J Biol Chem. 2000;275(29):21785–8.

331. Bachman H, Nicosia J, Dysart M, Barker TH. Utilizing Fibronectin Integrin-Binding Specificity to Control Cellular Responses. Adv Wound Care. 2015;4(8):501–11.

332. Huveneers S, Truong H, Fassler R, Sonnenberg A, Danen EHJ. Binding of soluble fibronectin to integrin 5 1 - link to focal adhesion redistribution and contractile shape. J Cell Sci. 2008;121(15):2452–62.

333. Schaufler V, Czichos-Medda H, Hirschfeld-Warnecken V, Neubauer S, Rechenmacher F, Medda R, et al. Selective binding and lateral clustering of α5β1 and αvβ3 integrins: Unraveling the spatial requirements for cell spreading and focal adhesion assembly. Cell Adhes Migr. 2016;10(5):505–15.

334. Balcioglu HE, van Hoorn H, Donato DM, Schmidt T, Danen EHJ. The integrin expression profile modulates orientation and dynamics of force transmission at cell-matrix adhesions. J Cell Sci. 2015;128(7):1316–26.

335. Truong H, Danen EHJ. Integrin switching modulates adhesion dynamics and cell migration. Cell Adhes Migr. 2009;3(2):179–81.

336. Sun T, Rodriguez M, Kim L. Glycogen synthase kinase 3 in the world of cell migration. Dev Growth Differ. 2009;51(9):735–42.

337. Christophorou MA, Castelo-Branco G, Halley-Stott RP, Oliveira CS, Loos R, Radzisheuskaya A, et al. Citrullination regulates pluripotency and histone H1 binding to chromatin. Nature. 2014 Mar 6;507(7490):104–8.

338. Wang HY, Zhou J, Zhu K, Riker AI, Marincola FM, Wang R-F. Identification of a Mutated Fibronectin As a Tumor Antigen Recognized by CD4 + T Cells. J Exp Med. 2002;195(11):1397–406.

339. Ordóñez A, Martínez-Martínez I, Corrales FJ, Miqueo C, Miñano A, Vicente V, et al. Effect of citrullination on the function and conformation of antithrombin. FEBS J. 2009;276(22):6763–72.

340. Tanikawa C, Ueda K, Suzuki A, Iida A, Nakamura R, Atsuta N, et al. Citrullination of RGG Motifs in FET Proteins by PAD4 Regulates Protein Aggregation and ALS Susceptibility. Cell Rep. 2018;22(6):1473–83.

341. Osaki D, Hiramatsu H. Citrullination and deamidation affect aggregation properties of amyloid β-proteins. Amyloid. 2016;23(4):234–41.

342. Verheul MK, van Veelen PA, van Delft MAM, de Ru A, Janssen GMC, Rispens T, et al. Pitfalls in the detection of citrullination and carbamylation. Autoimmun Rev. 2017;17:136–41.

343. Zhou Y, Chen B, Mittereder N, Chaerkady R, Strain M, An LL, et al. Spontaneous secretion of the citrullination enzyme PAD2 and cell surface exposure of PAD4 by neutrophils. Front Immunol. 2017;8(SEP):1–16.

344. Altroff H, Schlinkert R, Van Der Walle CF, Bernini A, Campbell ID, Werner JM, et al. Interdomain tilt angle determines integrin-dependent function of the ninth and tenth FIII domains of human fibronectin. J Biol Chem. 2004;279(53):55995–6003.

345. Aota SI, Nomizu M, Yamada KM. The short amino acid sequence Pro-His-Ser-Arg-Asn in human fibronectin enhances cell-adhesive function. J Biol Chem. 1994;269(40):24756–61.

346. Danen EHJ, Aota S, Kraats A Van, Yamada KM, Dirk J, Muijen GNP Van, et al. Cell Biology and Metabolism : Requirement for the Synergy Site for Cell Adhesion to Fibronectin Depends on the Activation State of Integrin α 5 β 1 Requirement for the Synergy Site for Cell Adhesion to Fibronectin Depends on the Activation State of Integr. 1995;270(37):1–8.

347. Bowditch RD, Hariharan M, Tominna EF, Smith JW, Yamada KM, Getzoff ED, et al. Identification of a novel integrin binding site in fibronectin: Differential utilization by ??3 integrins. J Biol Chem. 1994;269(14):10856–63.

348. Tarcsa E, Marekov LN, Mei G, Melino G, Lee S-C, Steinert PM. Protein Unfolding by Peptidylarginine Deiminase. J Biol Chem. 1996;271(48):30709–16.

349. Mierke CT, Frey B, Fellner M, Herrmann M, Fabry B. Integrin α5β1 facilitates cancer cell invasion through enhanced contractile forces. J Cell Sci. 2011 Feb

1;124(Pt 3):369–83.

350. Roman J, Ritzenthaler JD, Roser-Page S, Sun XJ, Han SW. A5B1-Integrin Expression Is Essential for Tumor Progression in Experimental Lung Cancer. Am J Respir Cell Mol Biol. 2010;43(6):684–91.

351. Lowrie AG, Salter DM, Ross JA. Latent effects of fibronectin, α5β1 integrin, αVβ5 integrin and the cytoskeleton regulate pancreatic carcinoma cell IL-8 secretion. Br J Cancer. 2004;91(7):1327–34.

352. Kitagawa A, Miura Y, Saura R, Mitani M, Ishikawa H, Hashiramoto A, et al. Anchorage on fibronectin via VLA-5 (α5β1 integrin) protects rheumatoid synovial cells from Fas-induced apoptosis. Ann Rheum Dis. 2006;65(6):721–7.

353. Rinaldi N, Schwarz-Eywill M, Weis D, Leppelmann-Jansen P, Lukoschek M, Keilholz U, et al. Increased expression of integrins on fibroblast-like synoviocytes from rheumatoid arthritis in vitro correlates with enhanced binding to extracellular matrix proteins. Ann Rheum Dis. 1997;56(1):45–51.

354. Yurdagul A, Green J, Albert P, McInnis MC, Mazar AP, Orr AW. α5β1 integrin signaling mediates oxidized low-density lipoprotein-induced inflammation and early atherosclerosis. Arterioscler Thromb Vasc Biol. 2014 Jul;34(7):1362–73.

355. Sampaio ALF, Zahn G, Leoni G, Vossmeyer D, Christner C, Marshall JF, et al. Inflammation-dependent alpha 5 beta 1 (very late antigen-5) expression on leukocytes reveals a functional role for this integrin in acute peritonitis. J Leukoc Biol. 2010;87(5):877–84.

356. Sebbag M, Moinard N, Auger I, Clavel C, Arnaud J, Nogueira L, et al. Epitopes of human fibrin recognized by the rheumatoid arthritis-specific autoantibodies to citrullinated proteins. Eur J Immunol. 2006;36(8):2250–63.

357. Beers JJBC Van, Willemze A, Stammen-vogelzangs J, Drijfhout JW, Toes REM. Anti-citrullinated fibronectin antibodies in rheumatoid arthritis are associated with

human leukocyte antigen- DRB1 shared epitope alleles. 2012;1–16.

358. Méchin MC, Enji M, Nachat R, Chavanas S, Charveron M, Ishida-Yamamoto A, et al. The peptidylarginine deiminases expressed in human epidermis differ in their substrate specificities and subcellular locations. Cell Mol Life Sci. 2005;62(17):1984–95.

359. Scott DL, Farr M, Hawkins CF, Wilkinson R, Bold AM. Serum calcium levels in rheumatoid arthritis. Ann Rheum Dis. 1981;40(6):580–3.

360. Kennedy AC, Allam BF, Rooney PJ, Watson ME, Fairney A, Buchanan KD, et al. Hypercalcaemia in rheumatoid arthritis: investigation of its causes and implications. Ann Rheum Dis. 1979;38:401–12.

PUBLICATIONS

CHAPTER 2

Choudhury S, Baradaran-Mashinchi P, Torres MP. Negative feedback phosphorylation of Gγ subunit Ste18 and the Ste5 scaffold synergistically regulates MAPK activation in yeast. Cell Reports. 2018 (PMID: 29719261)

CHAPTER 5

Stefanelli VL, Choudhury S, Yeh V, Chambers DM, Pesson K, Torres MP, Barker TH. Persistent immuno-stromal signaling through extracellular matrix memory. In submission.

Others

Aluru M, McKinney T, Love AK, Choudhury S, Torres MP. Functional mitogen-activated protein kinases are essential regulators of chronological aging in yeast. Aging.2017 (PMID: 29273704)

Dewhurst HM, Choudhury S, Torres MP. Structural Analysis of PTM Hotspots (SAPH-ire) - A Quantitative Informatics Method Enabling the Discovery of Novel Regulatory Elements in Protein Families. Mol. Cell. Proteomics. 2015. (PMID: 26070665)

Saini N, Zhang Y, Nishida Y, Sheng Z, Choudhury S, Mieczkowski P, Lobachev KS. Fragile DNA motifs trigger mutagenesis at distant chromosomal loci in *Saccharomyces cerevisiae*. PLoS Genet. 2013. (PMID: 23785298)